University at Buffalo
The State University of New York

Multiscale Study of Reinforced Concrete Shear Walls Subjected to Elevated Temperatures

by

Alok A. Deshpande and Andrew S. Whittaker

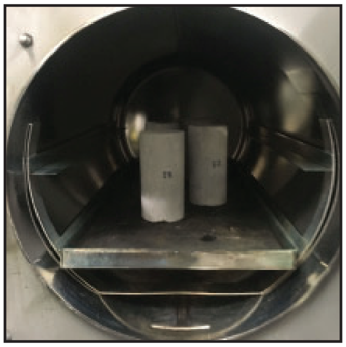

Technical Report MCEER-20-0001

June 26, 2020

MCEER: Earthquake Engineering to Extreme Events

A Multiscale Study of Reinforced Concrete Shear Walls Subjected to Elevated Temperatures

by

Alok A. Deshpande[1] and Andrew S. Whittaker[2]

Publication Date: June 26, 2020
Submittal Date: February 9, 2020

Technical Report MCEER-20-0001

1. Project Consultant, Simpson, Gumpertz and Heger; former Graduate Student, Department of Civil, Structural and Environmental Engineering, University at Buffalo, The State University of New York
2 SUNY Distinguished Professor and MCEER Director, Department of Civil, Structural and Environmental Engineering, University at Buffalo, The State University of New York

MCEER: Earthquake Engineering to Extreme Events
University at Buffalo, The State University of New York
212 Ketter Hall, Buffalo, NY 14260
mceer@buffalo.edu; *buffalo.edu/mceer*

Preface

MCEER is a national center of excellence dedicated to the discovery and development of new knowledge, tools and technologies that equip communities to become more disaster resilient in the face of earthquakes and other extreme events. MCEER accomplishes this through a system of multidisciplinary, multi-hazard research, in tandem with complimentary education and outreach initiatives.

Headquartered at the University at Buffalo, The State University of New York, MCEER was originally established by the National Science Foundation in 1986, as the first National Center for Earthquake Engineering Research (NCEER). In 1998, it became known as the Multidisciplinary Center for Earthquake Engineering Research (MCEER), from which the current name, MCEER, evolved.

Comprising a consortium of researchers and industry partners from numerous disciplines and institutions throughout the United States, MCEER's mission has expanded from its original focus on earthquake engineering to one which addresses the technical and socio-economic impacts of a variety of hazards, both natural and man-made, on critical infrastructure, facilities, and society.

MCEER investigators derive support from the State of New York, National Science Foundation, Federal Highway Administration, National Institute of Standards and Technology, Department of Energy, Nuclear Regulatory Commission, Department of Homeland Security/Federal Emergency Management Agency, other state governments, academic institutions, foreign governments and private industry.

Loss of coolant accidents in containment structures in nuclear power plants could result in internal temperatures of up to 300°F [149°C]. This report presents results of experimental studies on the seismic behavior of low aspect ratio Reinforced Concrete (RC) walls at elevated temperatures. Four large-scale RC walls were subjected to reversed cyclic, inelastic loading after exposure to elevated temperatures of up to 450°F [232°C] in the heated and residual conditions to determine possible changes in initial stiffness and peak shear strength. Materials-level tests were performed to support the component-level testing program and a) characterize the effects of elevated temperature on the behavior of concrete of the type used to cast the walls, b) characterize the effects of elevated temperature on the behavior of mechanically damaged normal strength concrete, and c) investigate the combined effects of moisture condition and elevated temperature on the behavior of normal strength concrete. Results of the experimental studies are used to make recommendations for analysis, design and assessment of low aspect ratio RC walls in nuclear power plants.

ABSTRACT

Low aspect ratio, shear-critical, reinforced concrete walls are used in nuclear power plants to resist gravity and lateral forces, and some serve a containment function. Beyond design basis earthquake shaking has the potential to rupture reactor coolant pipes in containment structures in nuclear power plants, resulting in Loss of Coolant Accidents (LOCA). Design control documents filed with the United States Nuclear Regulatory Commission (NRC) indicate that a LOCA in a containment structure in a new large light water reactor could result in internal temperatures of up to 300°F [149°C]. Accordingly, it is important to understand whether the lateral stiffness and/or peak shear strength of reinforced concrete walls in reactor buildings are meaningfully affected by exposure to LOCA-related temperatures, which will help determine fitness for reactor re-start or the need for extensive, expensive repair or replacement.

The seismic behavior of reinforced concrete walls at elevated temperatures was investigated through a first-of-a-kind experimental study. Four low-aspect ratio, reinforced concrete planar walls were subjected to reversed cyclic, inelastic loading after exposure to elevated temperatures of up to 450°F [232°C] in the heated and residual conditions. Details of the experimental program and results are presented. Materials-level tests were performed to a) characterize the effects of elevated temperature on the behavior of concrete of the type used to cast the walls, b) characterize the effects of elevated temperature on the behavior of mechanically damaged, normal strength concrete; and c) investigate the combined effects of moisture condition (unsealed, sealed and steamed) and elevated temperature on the behavior of normal strength concrete.

Six recommendations are made for analysis and design of low aspect ratio, reinforced concrete walls, namely, 1) at levels of lateral force smaller than 30% of peak strength, the maximum reduction in initial stiffness of a wall due to exposure to temperature of 450°F [232°C] is approximately 30%, 2) at levels of lateral force greater than 30% of peak strength, any reduction in lateral stiffness due to exposure to temperature of 450°F [232°C] is masked by mechanical damage, 3) peak lateral strength is not affected by exposure to temperature of 450°F [232°C], 4) the cyclic backbone curve for a low aspect ratio wall exposed to temperature of 450°F [232°C] can be approximated by the piecewise linear relationship of ASCE 41-17, with linear response to peak

strength, with co-ordinates given in NIST-GCR-17-917-45, 5) the effect of moisture condition (i.e., unsealed, sealed, or steamed) on the mechanical properties of concrete cylinders exposed to temperature of 450°F [232°C] for 90 minutes is negligible, and 6) the ACI 349-13 short-term temperature limit for concrete of 350° [177°C] in Section E.4.2 should be increased to 450°F [232°C].

ACKNOWLEDGMENTS

This research project was funded in part by the United States Department of Energy (DOE). The DOE contract was with Purdue University and the University at Buffalo served as a subcontractor for the tests on reinforced concrete walls. Professor Amit Varma, Dr. Saahastaranshu Bhardwaj and the staff at Bowen Laboratory of Purdue University contributed in a significant way to the execution of the experiments at Purdue University. These contributions are gratefully acknowledged.

Irving Materials Incorporated (IMI) and Buffalo Crushed Stone provided the aggregates, and LafargeHolcim provided the cement, used in the materials studies reported in this research. Their support is gratefully acknowledged. The authors thank Dr. Ravi Ranade of the Department of Civil, Structural and Environmental Engineering at the University at Buffalo for guidance on the execution of the materials tests. The authors also thank the staff of the Structural Engineering and Earthquake Simulation Laboratory at the University at Buffalo, undergraduate intern Elliot Whittaker and graduate student Dhanendra Kumar for their assistance with the materials tests.

TABLE OF CONTENTS

TABLE OF CONTENTS (CONTD.)

TABLE OF CONTENTS (CONTD.)

LIST OF ILLUSTRATIONS

LIST OF ILLUSTRATIONS (CONTD.)

LIST OF ILLUSTRATIONS (CONTD.)

LIST OF ILLUSTRATIONS (CONTD.)

LIST OF ILLUSTRATIONS (CONTD.)

LIST OF TABLES

CHAPTER 1
INTRODUCTION

1.1 General

Concrete structures are subjected to a wide variety of hazards, some of which are natural (e.g., earthquake, tsunami, flood and high winds) and others are human-induced (e.g., fire, blast, impact). Hazards like fires impose thermal loads on structures, involving temperatures as high as 1300°C (Maraveas and Vrakas, 2014). Concrete, unlike other construction materials such as steel and timber, is well suited for high-temperature applications since it is non-combustible, does not emit smoke and has a relatively low value of thermal conductivity (CEB, 2008). However, the mechanical properties of concrete deteriorate at high temperatures (Khoury, 2000; Schneider, 1988), similar to other construction materials. Knowledge of the effects of thermal loading is needed at the material and component levels to assess the safety of a concrete structure during and after exposure to high temperature.

Design standards and codes, such as ACI 216.1-14 (ACI, 2014b) and Eurocode 2 (CEN, 2004), respectively, enable evaluation of the effects of high temperature on the mechanical properties of concrete and steel reinforcement (also known as rebar): the components of reinforced concrete. The provisions in these documents are based on data collected from physical tests performed over several decades. However, there are no standard test protocols for measuring the effects of high temperature on concrete, which contributes to the large scatter observed in reported experimental results (Naus, 2010). Controlled experiments are needed to predict the behavior of concrete and reinforced concrete components and structures at high temperatures. This report contributes to the literature by presenting experimental results performed on concrete and reinforced concrete structures at elevated temperatures.

1.2 Range of temperature considered and motivation

This section identifies the range of elevated temperature expected in nuclear power plants after a thermal accident, and the motivation to study particular topics in concrete and reinforced concrete structures at these elevated temperatures. This section introduces two types of large light water nuclear reactors and the range of elevated temperatures expected in large light water reactor buildings after a Loss of Coolant Accident (LOCA). The motivation to study the seismic behavior of reinforced concrete (RC) walls at elevated temperatures is presented. The motivation to study effects of elevated temperatures on the behavior of concrete is also presented.

1.2.1 Loss of Coolant Accidents (LOCA) in nuclear power plants

The International Atomic Energy Agency reported in May 2019 that there were 451 operational nuclear reactors worldwide, with another 54 reactors under construction. Of the operational reactors, 299 were Pressurized Water Reactors (PWRs), 73 were Boiling Water Reactors (BWRs) and 49 were Pressurized Heavy-Water Reactors (PHWR). Of the 451 operational reactors worldwide, 98 were in the United States (65 PWR and 33 BWR) and another 2 (PWR) were under construction. The two reactors under construction as of May 2019 are at the Vogtle Electric Generating Plant in Waynesboro, Georgia.

In a BWR, heat is generated in the reactor core, which is the portion of the nuclear reactor containing the nuclear fuel and where fission takes place. Water, which is the coolant in this type of reactor, moves upward through the core, absorbing the generated heat. The water in the coolant loop is maintained at a pressure of about 7.6 MPa (1100 psi) so that it boils in the reactor core at about 285°C (545°F). The heat converts the water into a steam-water mixture, which exits the top of the reactor core and is piped to a moisture separation unit, which removes the water droplets from the mixture. The steam is then piped to the turbines to generate electricity. The used steam is then condensed into water and pumped back to the bottom of the core, completing the loop, which is termed the primary coolant loop (NRC, 2018a). Figure 1-1 (a) is a schematic of a typical BWR, showing its main components and the primary coolant loop.

In a PWR, similar to a BWR, heat is generated in the reactor core as a result of nuclear fission. Water, which is the coolant in this type of reactor, absorbs and transports the generated heat to steam generators. The water is maintained at a pressure of about 15.5 MPa (2250 psi), so unlike a BWR, boiling does not occur in the reactor. The hot pressurized water transfers heat to water in the steam generators and is then pumped back to the nuclear reactor, completing the loop (called the primary coolant loop). The water that is heated in the steam generators is vaporized to steam, which is then piped to the power turbines that generate electricity. The used steam is condensed into water and pumped back to the steam generator, completing the loop (called the secondary coolant loop). The water in the primary and secondary coolant loops do not mix. (NRC, 2018d). There are often 2 to 4 primary coolant loops in a nuclear power plant, one per steam generator. Figure 1-1 (b) is a schematic of a typical PWR, showing its main components and the primary and secondary coolant loops.

Loss of Coolant Accidents (LOCA) in nuclear power plants are defined as "*those postulated accidents that result in a loss of reactor coolant at a rate in excess of the capability of the reactor makeup system from breaks in the reactor coolant pressure boundary, up to and including a break equivalent in size to the double-ended rupture of the largest pipe of the reactor coolant system*" (NRC, 2018e). In a LOCA, high-temperature, high-pressure steam would be released into the air-tight containment vessel and would pressurize it. The containment structure is designed to withstand the resultant maximum pressure. But as steam and water partially fill the containment, heat energy is transferred to the surrounding steel and concrete surfaces through convection and conduction, thereby heating the structure (Dai et al., 2014).

Two important documents provide guidance in regard to the expected temperature in the containment structure from thermal accidents: ACI 349-13, Code for the Design of Safety-Related Nuclear Structures (ACI, 2013); and Design Control Documents, which are a repository of information submitted by the Nuclear Steam System Supplier (or reactor manufacturer) to the nuclear regulator for design certification. The range of elevated temperatures identified in these documents is discussed below.

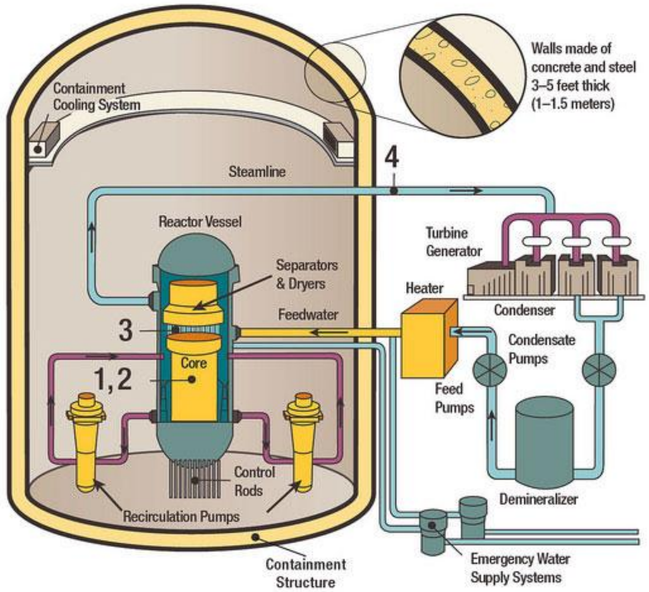

(a) Boiling Water Reactor (BWR)

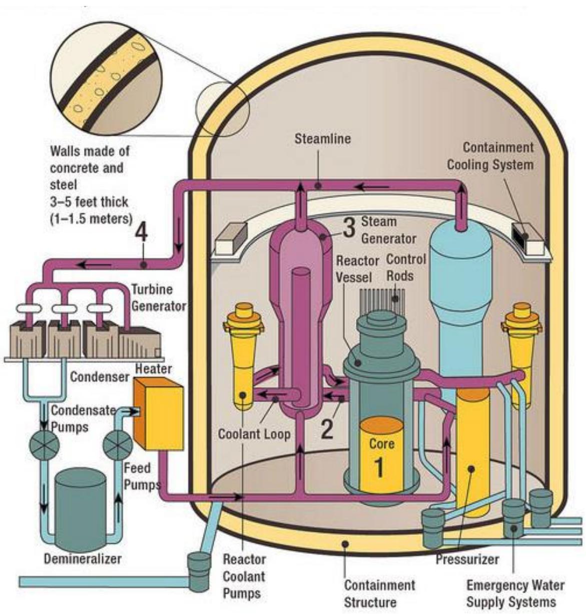

(b) Pressurized Water Reactor (PWR)

Figure 1-1: Schematic diagram of typical NPP reactors (NRC, 2018c)

1.2.1.1 Thermal time series provided by Design Control Documents

The United States Nuclear Regulatory Commission (NRC) approves the design of a nuclear power plant by issuing a design certification, which is based on the Design Control Documents (DCD) submitted by the applicant. As of April 2018, the NRC had issued design certifications for six nuclear power plant designs: (a) Advanced Boiling Water Reactor (ABWR) submitted by

General Electric Nuclear Energy (GENE), (b) ABWR Design Certification Rule (DCR) Amendment submitted by South Texas Project Nuclear Operating Company, (c) System 80+ submitted by Westinghouse Electric Company (WEC), (d) Advanced Passive 600 (AP600) submitted by WEC, (e) Advanced Passive 1000 (AP1000) submitted by WEC, and (f) Economic Simplified Boiling-Water Reactor (ESBWR) submitted by GE-Hitachi Nuclear Energy (GEH). An additional four designs are under review (NRC, 2018b): (a) US Advanced Pressurized-Water Reactor (US-APWR) submitted by Mitsubishi Heavy Industries, (b) ABWR Design Certification Renewal submitted by GEH, (c) Advanced Power Reactor 1400 (APR1400) submitted by Korea Electric Power Corporation and Korea Hydro and Nuclear Company, and (d) NuScale Small Modular Reactor submitted by NuScale Power. The NRC website provides DCDs for three of the six NPP certified designs. The LOCA-related temperatures provided in these three DCDs are introduced below.

Advanced Boiling Water Reactor (ABWR)

The ABWR is a single-cycle, forced-circulation, boiling-water reactor designed by General Electric Nuclear Energy (GENE). It has a rated reactor core thermal power output of 3,926 MWt and a net electrical power output of 1,300 MWe (GENE, 1997). A schematic of the ABWR NPP is shown in Figure 1-2.

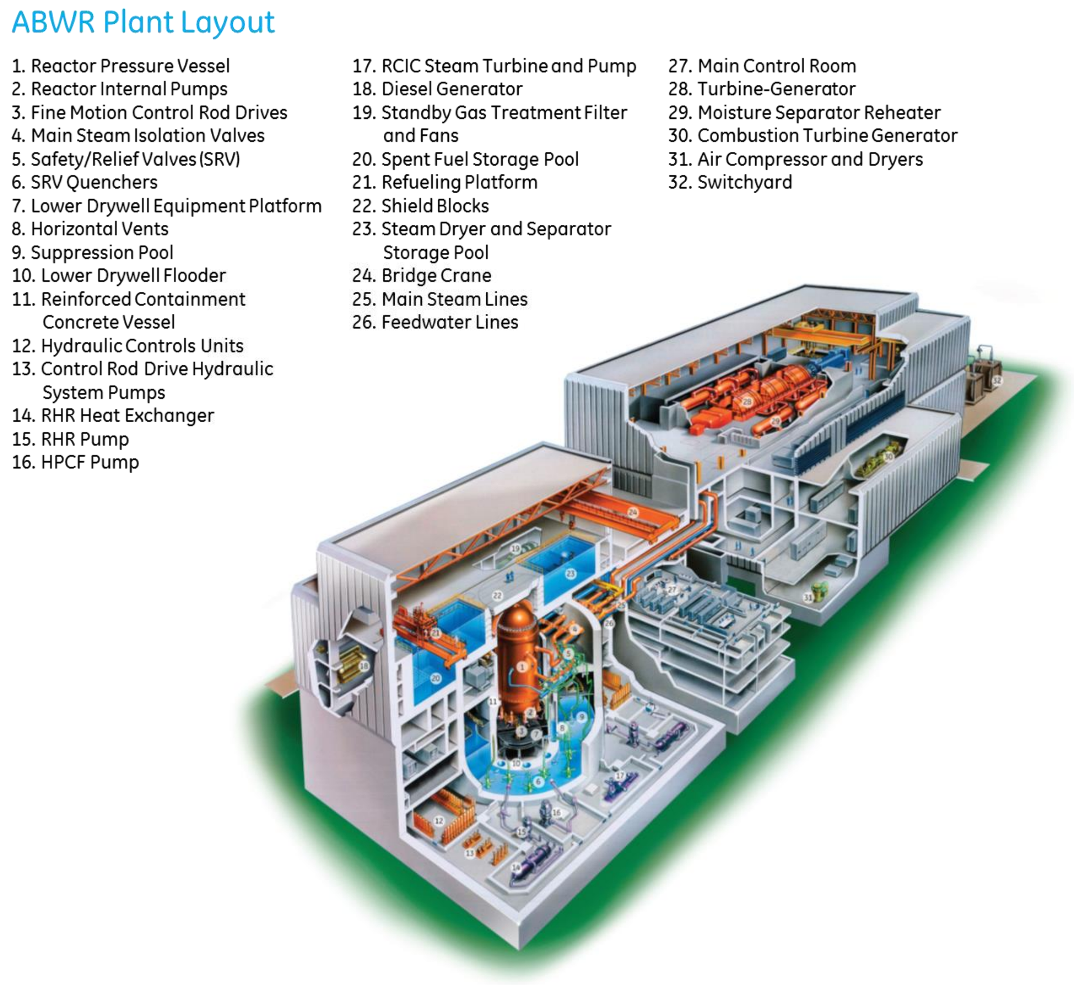

Figure 1-2: Advanced Boiling Water Reactor (ABWR) nuclear power plant (GENE, 1997)

The containment for an ABWR consists of three major components: drywell, wetwell, and steel liner. The drywell is a volume surrounding the reactor pressure vessel and houses the steam and feedwater lines, safety valves, reactor internal pumps and servicing equipment. The wetwell, similar to the drywell, is a volume surrounding the reactor pressure vessel and is placed below the drywell. It is comprised of an air volume and a water-filled suppression pool. The water is placed in the suppression pool to condense steam in case of a LOCA. A steel liner is provided on the inside surface of the reinforced concrete containment structure (#11 in Figure 1-2) and acts as a vapor barrier to prevent gas from escaping through cracks that may develop in the backing reinforced concrete, thereby reducing or eliminating leakage of fission products.

The pipe that transports condensed water to the bottom of the reactor is called the feedwater line and the pipe carrying the steam from the moisture separation unit to the turbine is called the steamline. The DCD for the ABWR provides temperature-time series that were generated by the applicant by performing hygrothermal studies for a postulated pipe-break scenario. The temperature-time results in the drywell, wetwell and suppression pool expected after a feedwater line break are reproduced in Figure 1-3. The maximum pressure expected to occur after a feedwater line break is about 270 kPa (36 psi) in the drywell. The wetwell is expected to attain a maximum temperature of 97°C (207°F) after about 4 hours following a feedwater line break.

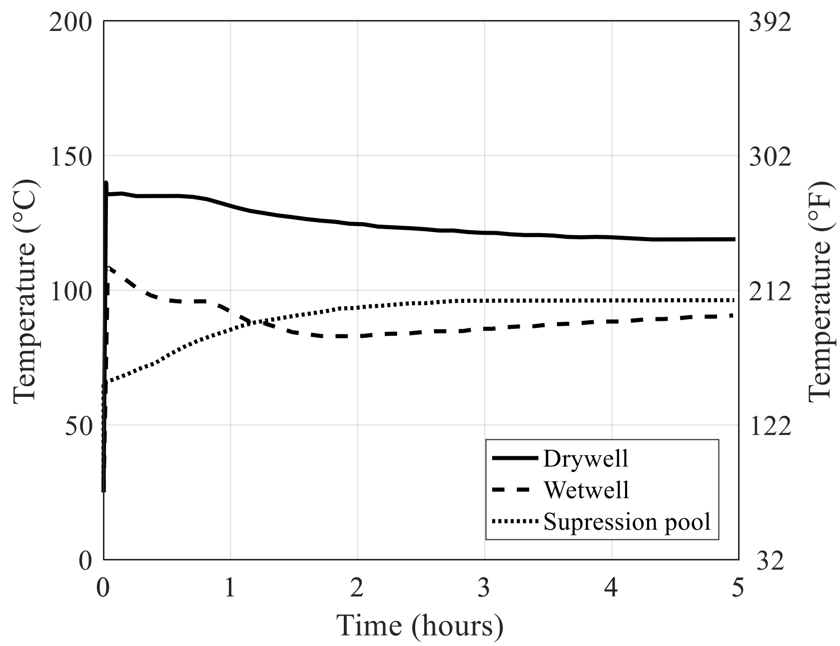

Figure 1-3: Containment temperature-time series after a feedwater line break in ABWR [reproduced from Figure 6.2-8 of the ABWR DCD]

Similar time series are not provided for a steamline break but the maximum expected temperature in the drywell is approximately 170°C (338°F).

Advanced Passive 1000 (AP1000)

The AP1000 is a Pressurized Water Reactor (PWR) designed by the Westinghouse Electric Company (WEC). It has a rated reactor core thermal power output of 3,400 MWt and an electrical power output of 1,100 MWe (WEC, 2011). A schematic of the AP1000 NPP is shown in Figure 1-4.

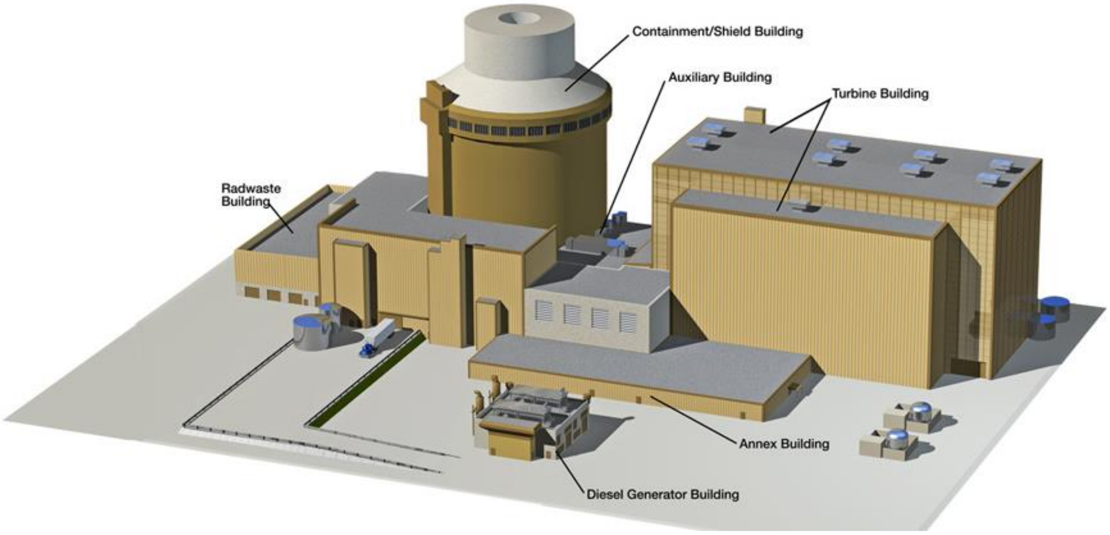

Figure 1-4: Advanced Passive 1000 (AP1000) nuclear power plant (WEC, 2018)

The pressure and temperature time series results from WEC hygrothermal calculations for a Main Steam Line Break (MSLB) accident are provided in the DCD. The containment temperature time series after a double-ended guillotine break in the cold leg of the reactor coolant system, which brings the reactor coolant from the condenser back to the reactor vessel, is reproduced in Figure 1-5. The calculated peak temperature is 141°C (285°F), but the sustained temperature in the following few days is expected to be approximately 110°C (230°F). Similar long-term temperature time series results are not provided for the case of a break in the hot leg (pipes that carry heated coolant from the reactor to the steam generator) of the reactor coolant system.

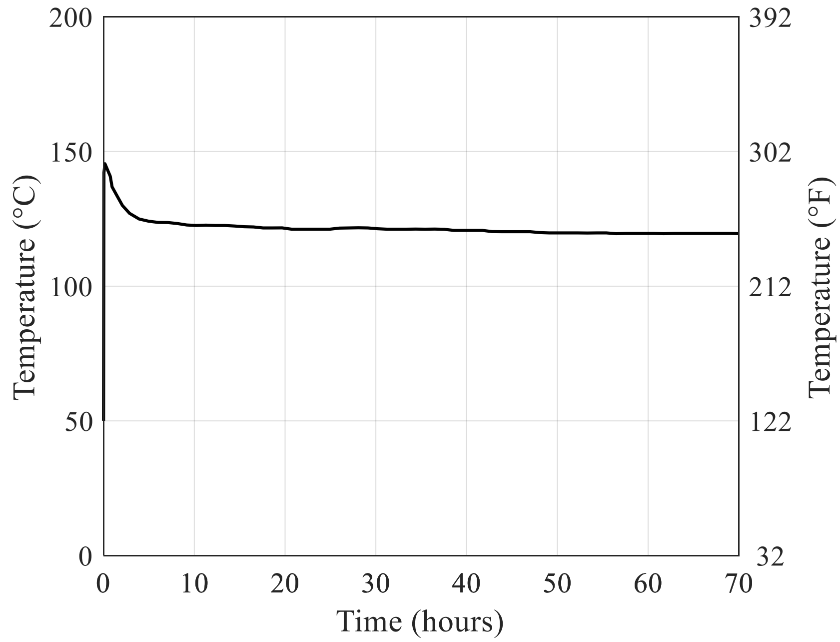

Figure 1-5: Containment temperature-time series after a double-ended cold-leg guillotine LOCA in AP1000 [reproduced from Figure 6.2.1.1-8 of the AP1000 DCD]

Economic Simplified Boiling-Water Reactor (ESBWR)

The ESBWR, manufactured by GE-Hitachi Nuclear Energy (GEH), is a single-cycle boiling-water reactor. It has a rated reactor core thermal power output of 4,500 MWt and a net electrical power output of approximately 1,535 MWe (GEH, 2014). A schematic of the ESBWR NPP is presented in Figure 1-6.

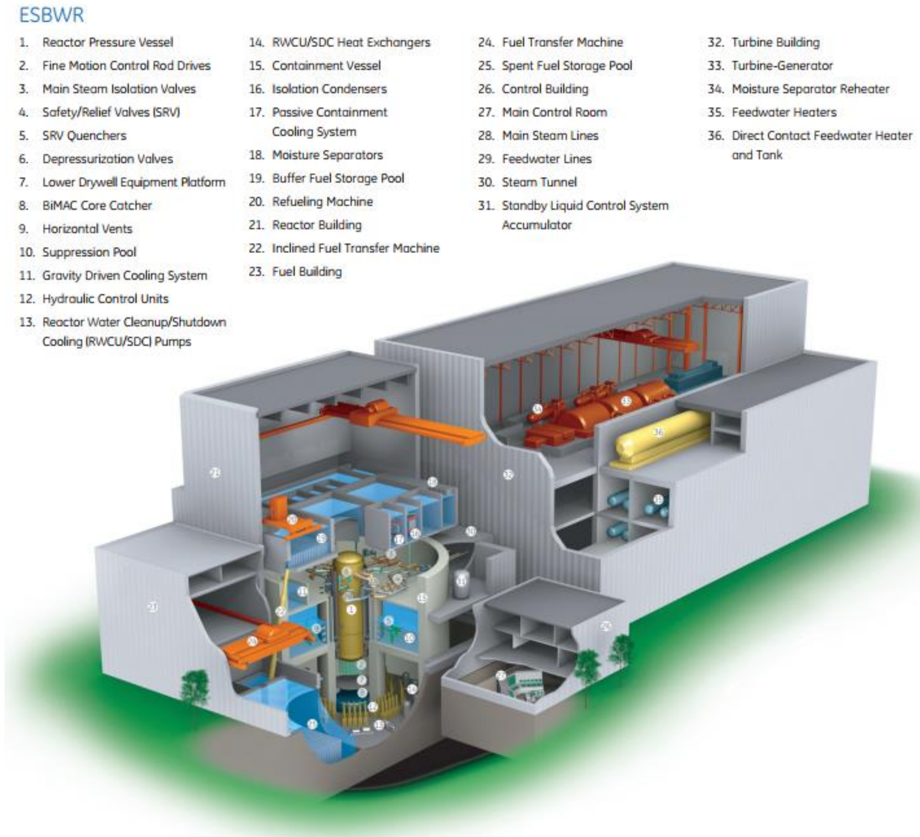

Figure 1-6: Economic Simplified Boiling-Water Reactor (ESBWR) (GEH, 2018)

The temperature-time series from the GEH hygrothermal calculations for a feedwater line break are reproduced in Figure 1-7. Time series are not provided for a steamline break, but the maximum pressures and temperatures expected after such a break are reported. The maximum sustained temperatures in the drywell and wetwell are 143°C (289°F) and 130°C (266°F), respectively. The drywell is a cylindrical reinforced concrete structure, surrounding the reactor vessel. The wetwell is a cylindrical reinforced concrete structure surrounding the reactor vessel and is located below the drywell. The wetwell has a water-filled suppression pool and a volume of air. The maximum expected pressure in the drywell after a steamline break is 295 kPa (43 psi).

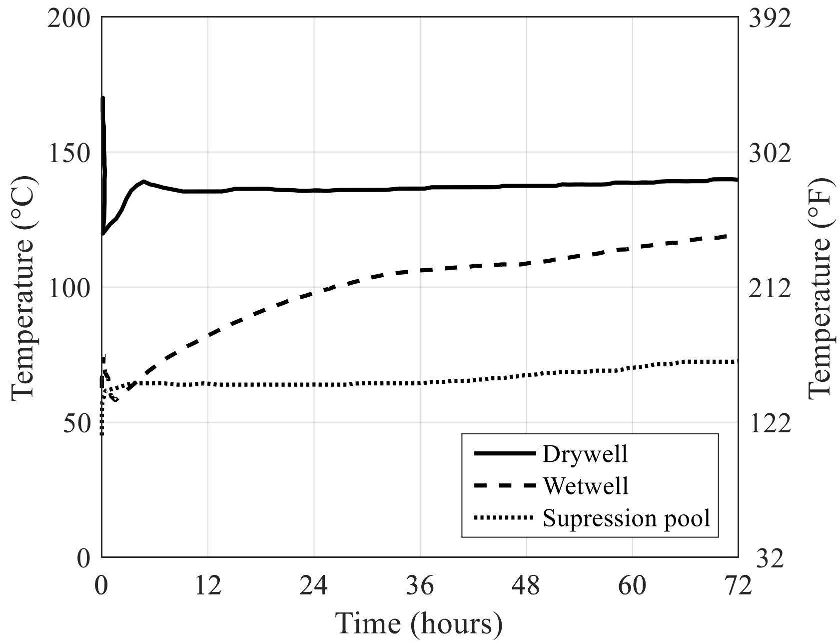

Figure 1-7: Containment temperature-time series after feedwater line break in ESBWR [reproduced from Figure 6.2-9b1 of ESBWR DCD]

Summary

Based on the thermal histories provided in the three DCDs, a maximum temperature of approximately 300°F [149°C] is expected after a LOCA in the containment structure of a large light water nuclear reactor.

1.2.1.2 ACI 349-13 requirements for thermal loading

Appendix E of ACI 349-13, Code Requirements for Nuclear Safety-Related Concrete Structures (ACI, 2013), presents requirements for the design of nuclear safety-related concrete structures subjected to thermal loadings. The thermal loadings could result from either normal operating and shutdown conditions or accidents generated by postulated pipe breaks, as introduced above. The standard notes that structural members near high-energy piping systems might be subjected to a steam environment and a water/steam jet, resulting from the release of high temperature steam or high pressure, high temperature water in the piping systems. This steam environment can be of a long duration, lasting a few days, in the case of containment structures, since venting of the steam to atmosphere should not occur.

For normal operation, the standard states that the maximum concrete temperature shall not exceed 66°C (150°F) or 93°C (200°F) for general surfaces and local areas (such as around penetrations), respectively. These temperature limits are increased to 82°C (180°F) and 110°C (230°F) for general surfaces and local areas, respectively, if the tested concrete strength is equal to or greater than 115 percent of the specified 28-day compressive strength. This increase is permitted presumably because the expected loss in concrete compressive strength exposed to these temperatures is less than the strength gain beyond 28 days. In case of thermal accidents, the temperature limits are increased to 177°C (350°F) and 343°C (650°F) for general concrete surfaces and local areas (such as those impinged by steam or water jets). However, after exposure to these temperatures, the standard requires that the serviceability of the structure be assessed by a licensed professional. The standard states that temperatures higher than the limits for thermal accidents (stated above) are allowed if the reduction in concrete strength is applied to design allowables. Additional 'evidence' that verifies that the increased temperature does not cause deterioration of concrete must also be provided, but the standard does not provide guidance on how this is to be accomplished.

1.2.2 Seismic behavior of RC walls at elevated temperatures

Reinforced concrete walls are used in nuclear power plants to resist gravity and lateral forces, and to serve a confinement function. For design calculations, such walls are typically modeled as linear elements for deformations less than those associated with peak strength. Analysis for beyond design basis loadings could utilize the force – drift ratio model of Figure 1-8 (ASCE, 2017), in which point F is used for shear critical walls only. In Figure 1-8, shear resistance, Q, is normalized by peak shear strength, Q_y, and lateral deformation, Δ, is normalized by story height, h, to get the drift ratio. Parameters, g, d and e, represent yield drift ratio, drift ratio corresponding to the onset of loss of shear strength and ultimate drift ratio respectively. Parameters f and c are associated with the onset of cracking in the wall and residual strength of the wall, respectively.

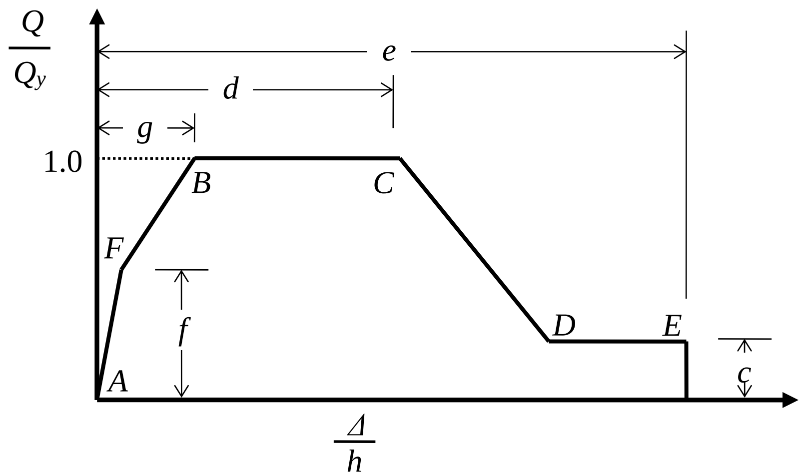

Figure 1-8: Force – drift ratio relationship for reinforced concrete shear walls (ASCE, 2017)

Thermal accidents like a LOCA, could result in temperatures substantially higher than ambient in the containment structure for a few days, as described in Section 1.2.1. It is therefore important to assess the effects of elevated temperature on the stiffness and strength of RC walls, to aid either initial design or a post-accident investigation.

Beyond design basis earthquake shaking has the potential to rupture reactor coolant pipes, resulting in LOCA. This poses an additional challenge because a nuclear power plant with ruptured coolant lines could experience aftershocks as intense as design basis shaking. If the aftershocks occur while temperatures are elevated or before the reinforced concrete structure has cooled, the containment structure and its internal walls will be required to perform a safety-related function at temperatures above ambient. Consequently, it is important to determine the effects, if meaningful, of exposure to elevated temperature on the strength and stiffness of reinforced concrete shear walls.

Pipe breaks can also result from causes other than earthquakes, such as fatigue (Simonen et al., 2001) and thermal aging (Lv et al., 2014). In such cases, questions will be asked by a regulator about whether the seismic robustness of the reactor building has been compromised by the resulting elevated temperature. Section E.4.2 of ACI 349 requires an assessment of the extent of the resulting damage, if any, and its effect on the serviceability of the structure (ACI, 2013).

This research presents the results obtained from a first-of-a-kind experimental study of the seismic behavior of RC walls at elevated temperatures. Experimental results are interpreted to provide guidance to engineers tasked with assessing the impact of thermal loadings on the stiffness and strength of RC shear walls.

1.2.3 Concrete material behavior at high temperatures

Design standards and codes such as the ACI 216.1-14, Code Requirements for Determining Fire Resistance of Concrete and Masonry Construction Assemblies (ACI, 2014b), and EN 1992-1-2:2004, Eurocode 2: Design of Concrete Structures - General Rules - Structural Fire Design (CEN, 2004), respectively, provide guidance on the design of concrete structures to resist the effects of fires. However, the effects of elevated temperature on the mechanical behavior of concrete are not yet fully understood (CEB, 2008).

Materials level testing of concrete is usually performed on virgin concrete specimens that have not been stressed previously. However, concrete structures in service are expected to have pre-existing cracks due to shrinkage and mechanical loading. There is very limited knowledge of the effects of heating on concrete that is cracked prior to heating. Badr (2009) indicates that the presence of prior cracks might exacerbate damage caused by heating. Results from an experimental study performed to study the effects of prior cracking on the mechanical behavior of concrete at high temperatures are presented in this report.

Tests to characterize mechanical behavior have usually been performed in hot-air environments, in which the moisture in the concrete is allowed to escape, commonly referred to as *unsealed* tests. However, concrete deep within a structural element during a fire experiences conditions that are closer to *sealed* heating, wherein moisture is not permitted to escape. Data from experiments performed to study the mechanical behavior of concrete heated in a sealed condition is scarce (Bertero and Polivka, 1972; Willam et al., 2009), but results indicate that the sealed condition is more severe, in terms of reduced strength and stiffness, than the unsealed condition. Results from an experimental study performed on normal strength concrete heated in sealed and unsealed conditions are presented in this report. Additionally, tests are performed in a high-pressure steam environment, as might be expected following a steam pipe-break accident in a nuclear power plant and results are reported.

1.3 Research objectives

The two main objectives of this research are to study a) the effects of elevated temperatures on the seismic behavior of RC walls, and b) the effects of elevated temperatures on the behavior of concrete. Specifically, this research:

1. Documents the design, construction, instrumentation and testing of four RC walls that were subjected to temperatures up to 450°F [232°C] and fully reversed, inelastic cyclic loading.

2. Interprets the results of the materials and component-testing programs to characterize the effects of elevated temperatures, up to 450°F [232°C], on the stiffness, flexural strength and shear strength of RC walls.

3. Characterizes the effects of temperatures up to 752°F [400°C] on the mechanical behavior of normal strength concrete that has been *damaged* prior to heating.

4. Characterizes the mechanical behavior of conventional, normal strength concrete at temperatures of up to 300°F (149°C) in dry-air, sealed and steam conditions.

5. Proposes revisions to Section E.4.2 of ACI 349-13.

1.4 Report organization

This report is organized into four parts, composed of a total of seven chapters, a list of references and an appendix. Part 1 contains two chapters. Chapter 1 introduces the report and presents background, motivation and research objectives. A review of topics related to the effects of high temperatures on the properties of concrete, steel reinforcement (or rebar) and concrete-rebar bond is presented in Chapter 2.

Part 2 describes the testing program performed to study the seismic behavior of four RC walls at elevated temperatures. The experimental program, including the construction of specimens, the instrumentation and test fixture are discussed in Chapter 3. Chapter 4 summarizes the results obtained from these tests.

Part 3 of this report describes the materials-level experiments performed on concrete at elevated temperatures. Chapter 5 presents the effects of high temperatures on the mechanical properties of concrete cracked prior to heating. Chapter 6 presents the effects of high temperatures in the presence of different moisture conditions on the mechanical properties of concrete.

Chapter 7 is Part 4 of this report. It summarizes the research, provides conclusions and offers recommendations for future work. Details of a numerical study performed to calculate the thermal responses of RC walls subjected to pipe-break accidents in NPPs are presented in Appendix A.

CHAPTER 2
LITERATURE REVIEW

2.1 Introduction

The effects of high temperatures on the thermal and mechanical properties of concrete, steel reinforcement (rebar) and rebar-concrete bond, as reported in the literature, are presented in this chapter. The effects of high temperatures on properties of concrete and steel reinforcement are presented in Section 2.2 and Section 2.3, respectively. The effects of elevated temperatures on rebar-concrete bond are discussed in Section 2.4.

2.2 Effects of elevated temperature on concrete

The behavior of concrete at elevated temperatures has been studied for several decades. Important articles and reports include Schneider (1988), Khoury (2000), Willam et al. (2009) and Naus (2010). Key points from these articles and reports are reported in this section.

Aggregates constitute 65 to 70% of the volume of normal strength concrete and hence have a significant effect on the thermal and mechanical properties of concrete. The properties of concrete at elevated temperatures have therefore been classified on the basis of aggregate type. Design codes such as ACI 216.1-14 (ACI, 2014b) and Eurocode 2 (CEN, 2004) provide material relationships for concretes made with calcareous and siliceous aggregates.

The hydration products of cement are responsible for the eventual hardening of concrete. The two primary hydration products are calcium silicate hydrate (CSH) and calcium hydroxide. Mature cement paste consists of about 80% layered CSH gel and about 20% calcium hydroxide and other compounds (Mindess et al., 2003). Testing of concrete at elevated temperatures is usually conducted for unsealed specimens and the rapid drying of the hydrated cement paste with increasing temperature has been recognized as the primary cause for the changes in mechanical properties (Schneider, 1988). The loss of water (chemically and physically adsorbed) from products of cement hydration leads to changes in the volume and stiffness of the gel structure (Willam et al., 2009). These changes are accompanied by changes in the pore structure distribution, generally increasing the size and number of voids and cracks in the cement paste. These changes at the microscopic level manifest as changes in the thermal and mechanical properties at the macroscopic level.

2.2.1 Thermal properties

The thermal properties of interest in this study are density, thermal conductivity (i.e., the rate of heat transfer through a unit thickness of the material per unit area per unit temperature difference (Cengel, 1998)) and specific heat capacity (i.e., the energy required to raise the temperature of a unit mass of a substance by one degree (Cengel, 1998)), as values for these three parameters are needed to calculate heat transfer and thermal gradients in concrete members subjected to elevated temperatures.

2.2.1.1 Density

The variation of density with temperature is small and is primarily a result of loss of moisture (Schneider, 1988). This moisture loss is from evaporable water for temperatures up to about 150°C (302°F) and is followed by the loss of chemically bound water at temperatures of 200°C (392°F) and greater. The variation in density of concrete with temperature, normalized by the density at room temperature, as recommended by Eurocode 2 and for concrete mixes with different aggregates reported by Schneider (1988) and Shin et al. (2002) are presented in Figure 2-1. Eurocode 2 recommends a reduction of 10% in the density at a temperature of 1000°C (1832°F).

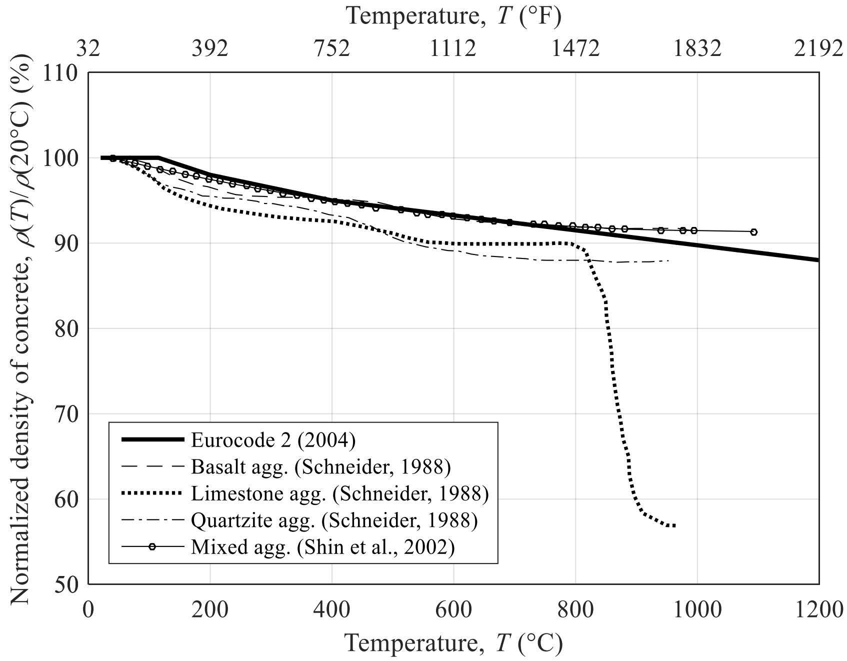

Figure 2-1. Variation in density of concrete with temperature

2.2.1.2 Thermal conductivity

Concrete is a heterogeneous material and its thermal conductivity depends on the conductivities of its constituents (Schneider, 1988). The constituents, listed in descending order of thermal conductivities are aggregate, cement, water and air (Khoury, 2000). The variation in thermal conductivity of concrete with temperature, as recommended by Eurocode 2, and for mixes reported by Harada et al. (1972), Schneider (1988), and Shin et al. (2002) are presented in Figure 2-2.

Thermal conductivity reduces with increasing temperature, which has been attributed to the loss of moisture with increasing temperature (ElMohandes, 2013). With increasing temperature, water evaporates and is replaced by air, which has a significantly lower thermal conductivity. The formation and propagation of cracks in the concrete, regardless of source, increase air gaps, thereby further lowering conductivity.

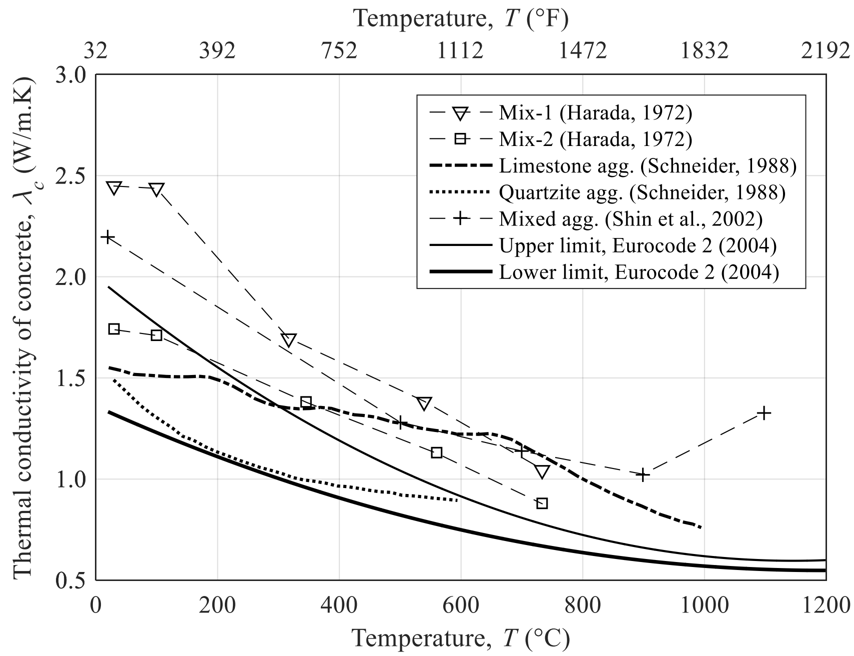

Figure 2-2. Variation in thermal conductivity of concrete with temperature

2.2.1.3 Specific heat capacity

The variation in specific heat capacity with temperature as recommended by Eurocode 2 and reported by Schneider (1988) and Shin et al. (2002) is presented in Figure 2-3.

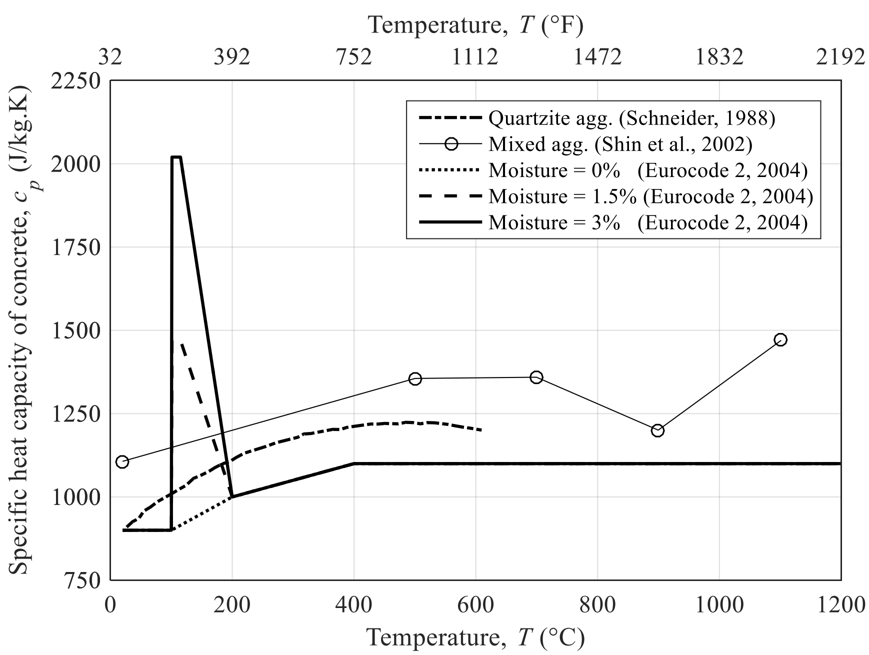

Figure 2-3. Variation in specific heat capacity of concrete with temperature

The type of aggregate has little influence on heat capacity for temperatures below 800°C (1472°F). The specific heat capacity for dry concrete ranges between 800 and 1000 J/kg.K at 20°C (68°F) and increases to about 1100 to 1300 J/kg.K at 400°C (752°F) (Schneider, 1988). Moisture content plays a very important role at temperatures below 200°C (392°F). At 100°C (212°F) (the boiling point of water), Eurocode 2 recommends an increase in the specific heat capacity by a factor of 2.2 and 1.6, for concrete with a moisture content of 1.5% and 3%, respectively.

2.2.2 Mechanical properties

The testing methods commonly used for studying the strength and stiffness of concrete at elevated temperatures have been classified with respect to their heating and loading histories as (1) stressed test, (2) unstressed test, and (3) unstressed residual test (Willam et al., 2009). Schematic diagrams of the temperature and stress histories in these three tests are presented in Figure 2-4.

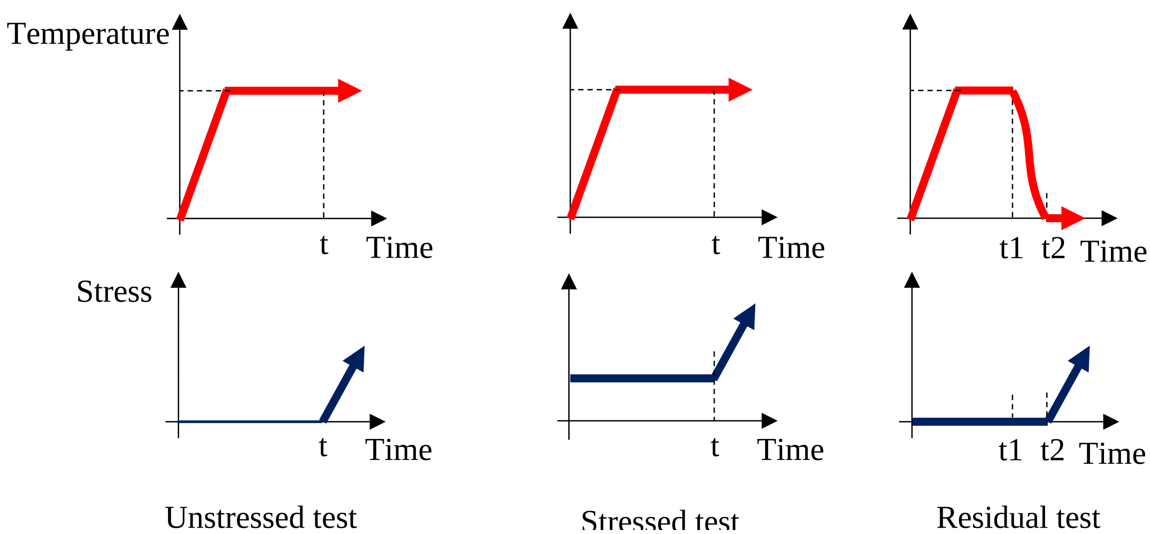

Figure 2-4. Schematics of temperature and loading histories for mechanical testing of concrete subjected to elevated temperatures
[adapted from Willam et al. (2009)]

In the *unstressed* test, the concrete specimen is heated to a particular temperature and kept at that temperature for mechanical testing. The *stressed* test is similar to the *unstressed* test, with the only difference being that a pre-determined stress is maintained during the heating phase. In the *residual* test, the concrete specimen is allowed to cool back to the room temperature after heating and before testing.

Concrete that is exposed to elevated temperatures undergoes physicochemical changes at the microscale, leading to deterioration in mechanical properties. The deterioration of the mechanical properties of concrete has been attributed primarily to three damage mechanisms (Willam et al., 2009): (1) physicochemical changes in the aggregates, (2) physicochemical changes in the cement paste, and (3) thermal incompatibility between aggregates and cement paste.

Concrete, when subjected to elevated temperatures, may also spall, reducing the section size (Khoury, 2000). Spalling is defined as "…the violent or non-violent breaking-off of layers or pieces of concrete from the surface of a structural element, during or after it is exposed to high and rapidly rising temperatures…" (Khoury, 2000; Klingsch, 2014). The resulting loss in cross-sectional area reduces the member strength in addition to exposing the reinforcement and further accelerating damage.

The spalling phenomenon has been explained by two different mechanisms (Mindeguia et al., 2010). The first is thermomechanical in nature, and is a result of the high thermal gradients near the concrete surface that induce local compressive stresses that can exceed concrete strength. The second mechanism is thermohygral, and is a result of the formation of a 'moisture clog', which results from the flow of moisture in the (porous) concrete, particularly in the inner zones (away from the surface). The formation of this 'clog' can cause the pore pressure to exceed the concrete tensile strength, thereby initiating spalling. This is more of a concern for higher strength concretes, which tend to be denser and have limited pore connectivity.

2.2.2.1 Compressive properties

<u>Strength</u>

Experiments conducted to obtain the compressive strength of concrete at elevated temperatures have shown a clear trend of reduction in strength with increasing temperature for temperatures higher than about 250°C (482°F) (Naus, 2010). The trend for temperatures less than 250°C (482°F) is not as clear. In many cases, tests have shown that the strength measured at elevated temperatures, compared to that measured at room temperature, reduces with increasing temperature, then increases and then reduces. Khoury (2000) has suggested that compressive strength achieves a minimum at 80°C (176°F) due to the weakening of the Van der Waal's forces as the expanding water molecules push the CSH layers further apart. Khoury (2000) also reported that strength may increase to a maximum between 200°C (392°F) and 300°C (572°F). However, there is no widely accepted and experimentally validated theory for this "first down, then up and further down trend" in compressive strength at elevated temperatures (Willam et al., 2009). Concrete design codes such as ACI 216.1-14 and Eurocode 2 do not consider any strength gain and instead recommend a monotonic reduction in strength with increasing temperature.

Figure 2-5 presents the variation in compressive strength of concrete with temperature, normalized by the compressive strength at room temperature, as recommended by ACI 216.1-14 (ACI, 2014b), Eurocode 2 (CEN, 2004) and CEB Bulletin No. 208 (CEB, 1991). The compressive strength of concrete made with siliceous aggregate deteriorates faster at elevated temperatures than concrete made with calcareous aggregate (Schneider, 1988). The Eurocode 2 recommended reduction in concrete strength at 200°C (392°F) is 5% and 2% for concretes made with siliceous and calcareous aggregates, respectively.

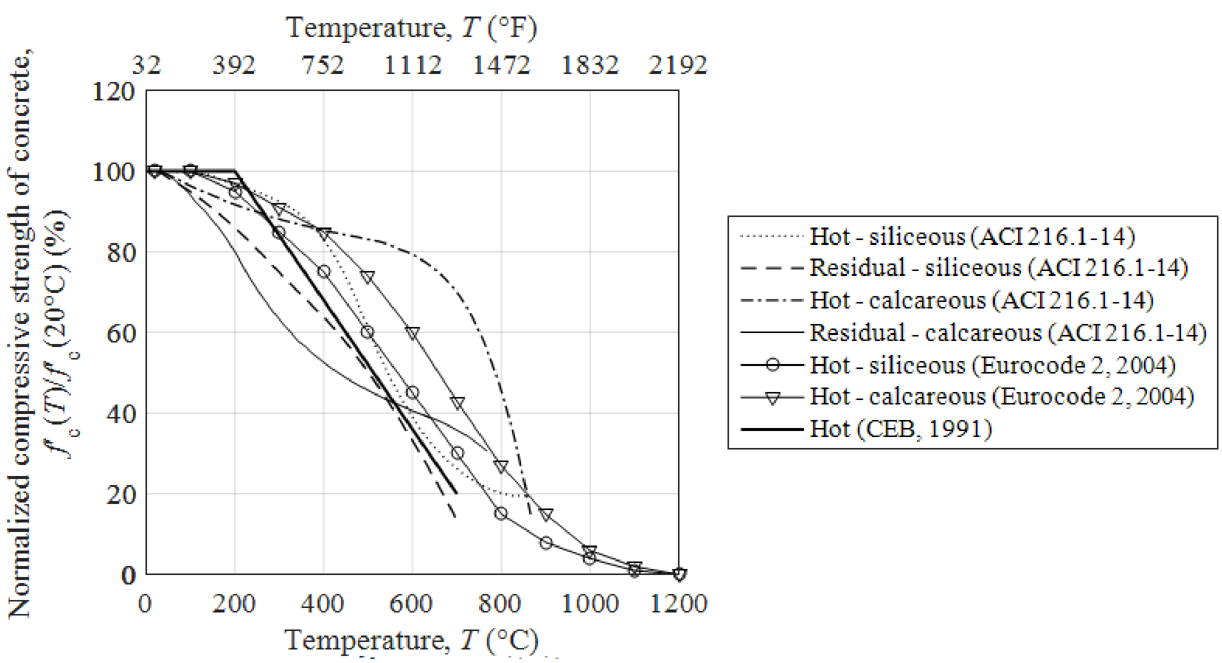

Figure 2-5. Variation in compressive strength of concrete with temperature

The compressive strength of concrete tested in the residual condition is lower than if tested at an elevated temperature (Schneider, 1988). For example, ACI 216.1-14 recommends a reduction of about 20% for calcareous concrete subjected to a temperature of 200°C (392°F) and tested in the residual condition. The corresponding reduction is about 8% for calcareous concrete subjected to the same temperature and tested at elevated temperature.

Tests have generally been performed on unsealed specimens, where moisture in the concrete is allowed to escape. For sealed specimens, where moisture cannot, as may be the case for concrete deep within a structural member, a larger reduction in strength may result from the generation of high pore water pressures (Willam et al., 2009).

Initial modulus of elasticity

Figure 2-6 presents the variation in modulus of elasticity of concrete with temperature, normalized by the modulus at room temperature, as recommended by Eurocode 2, CEB Bulletin No. 208, and experimental results reported by Harada et al. (1972) and Schneider (1988). The variation in modulus recommended by Eurocode 2 is calculated using the parameters provided to plot the stress-strain relationship of concrete at high temperatures.

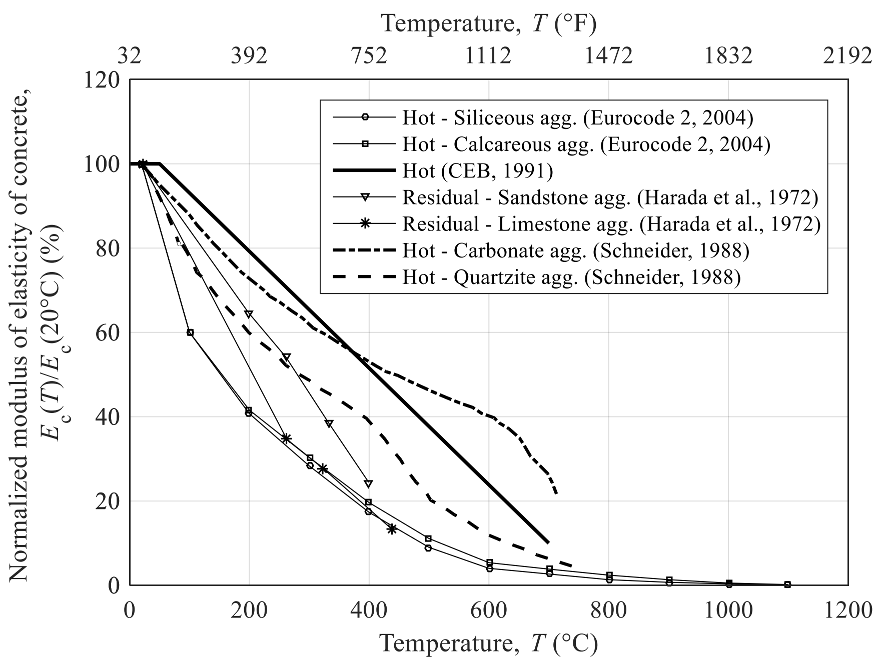

Figure 2-6. Variation in modulus of elasticity of concrete with temperature

The percentage decrease in the modulus of elasticity with increasing temperature exceeds that for compressive strength (Schneider, 1988). Data from tests compiled by Naus (2010) shows that the modulus of elasticity reduces for temperatures exceeding about 100°C (212°F). CEB Bulletin No. 208 (CEB, 1991) recommends a 20% reduction in modulus at 200°C (392°F) with respect to the value at 20°C (75°F). This recommendation matches well with the experimental data for concrete tested at elevated temperatures but underestimates the data from residual tests (Naus, 2010).

2.2.2.2 Tensile properties

Strength

There is limited experimental data on the relationship between tensile strength of concrete and elevated temperature. Figure 2-7 presents the variation in concrete tensile strength with temperature as recommended by Eurocode 2 and CEB and reported from tests performed by Harada et al. (1972) and Thelandersson (1972). The available data shows that tensile strength reduces with increasing temperature and more rapidly than compressive strength (Naus, 2010).

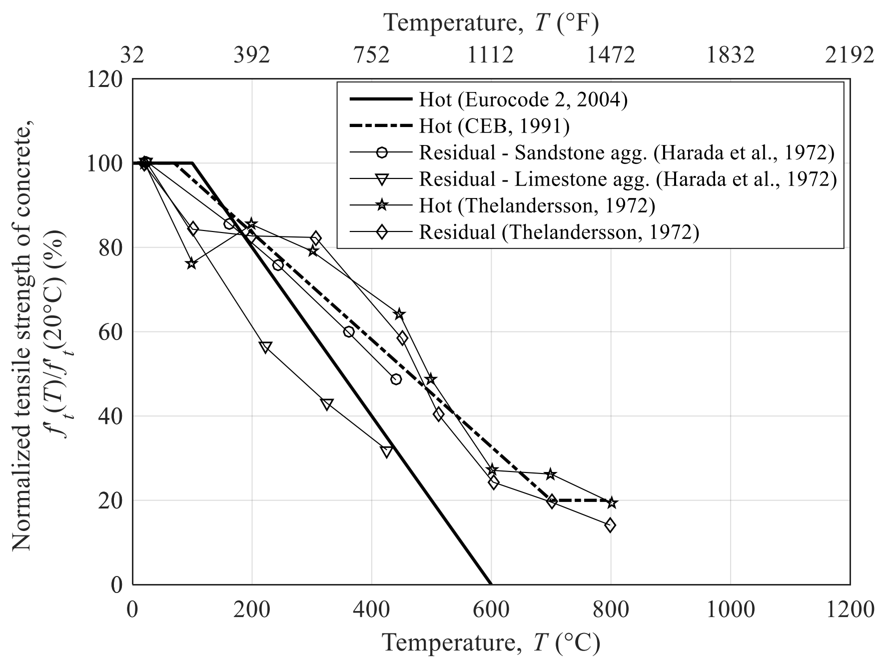

Figure 2-7. Variation in tensile strength of concrete with temperature

Fracture energy

The fracture energy of concrete reduces with temperature (Bazant and Prat, 1988). Figure 2-8 presents the variation in fracture energy that was observed and predicted from experiments, normalized by the fracture energy measured in the dry condition at room temperature. The normalized fracture energy at room temperature is slightly greater than one, because the fracture energy at room temperature (used to normalize the results) and curves presented in Figure 2-8 are obtained from a linear regression of results obtained from tests performed on different types of samples. The percentage loss in fracture energy is higher for concrete tested in a steam environment than a dry environment for the same temperature. Although this observation was made for temperatures lower than 100°C (212°F), the authors reported that the trend was clear and was expected to hold at higher temperatures.

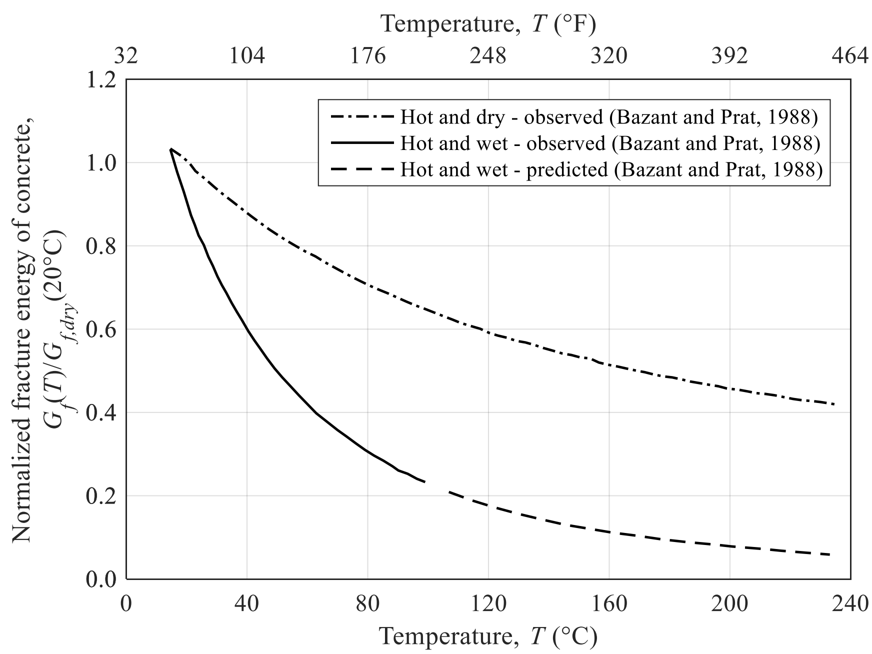

Figure 2-8. Variation in fracture energy of concrete with temperature

2.2.2.3 Thermal expansion

The coefficient of thermal expansion of concrete varies with the type of aggregate used. Willam et al. (2009) report values of 6.8x10^{-6}/°C and 11.9x10^{-6}/°C at a temperature of 75°F (24°C) for concretes made with limestone (calcareous) and quartz (siliceous) aggregate alone, respectively. These values increase with temperature. Figure 2-9 presents the variation of thermal expansion strain of concrete with temperature as recommended by Eurocode 2 and from experiments reported by Harada et al. (1972) and Schneider (1988). The thermal expansion strain, $\varepsilon_c(T)$, is calculated by multiplying the coefficient of thermal expansion by temperature.

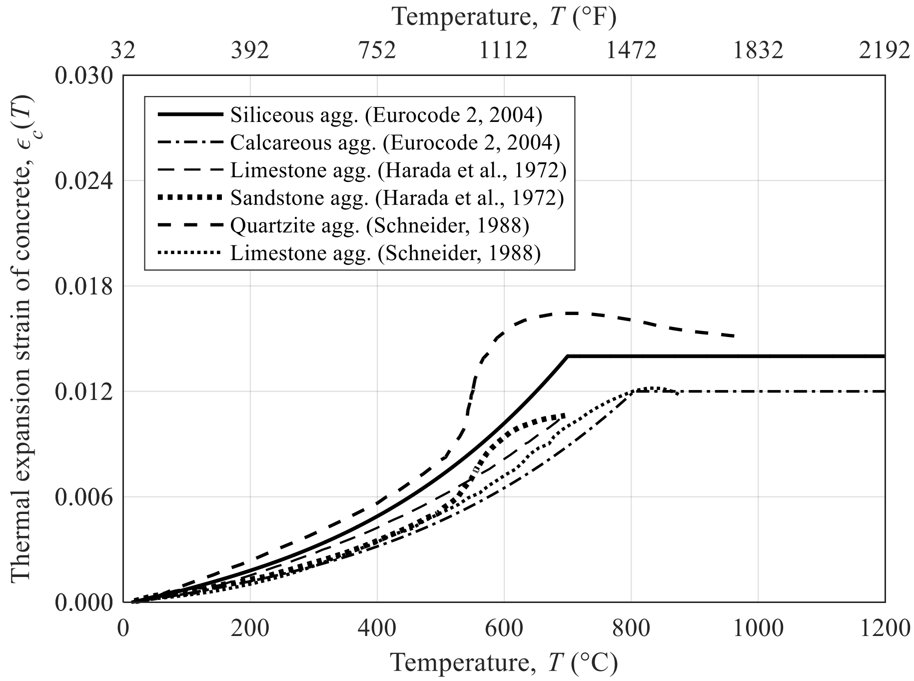

Figure 2-9. Variation in thermal expansion strain of concrete with temperature

2.3 Effects of elevated temperature on steel reinforcement

2.3.1 Modulus of elasticity

The modulus of elasticity of steel reinforcement (rebar) reduces with increasing temperature. Figure 2-10 presents the variation of modulus of elasticity with temperature reported by Schneider et al. (1982), and Takeuchi et al. (1993), and as recommended by Eurocode 2. Eurocode 2 reports a 13% reduction in modulus at 392°F (200°C) for cold-worked reinforcement. Although very limited data are available, exposure to temperatures as high as 1472°F (800°C) does not lead to a reduction in residual modulus of elasticity. Residual modulus of elasticity for steel reinforcement is measured at room temperature after it has been exposed to high temperature.

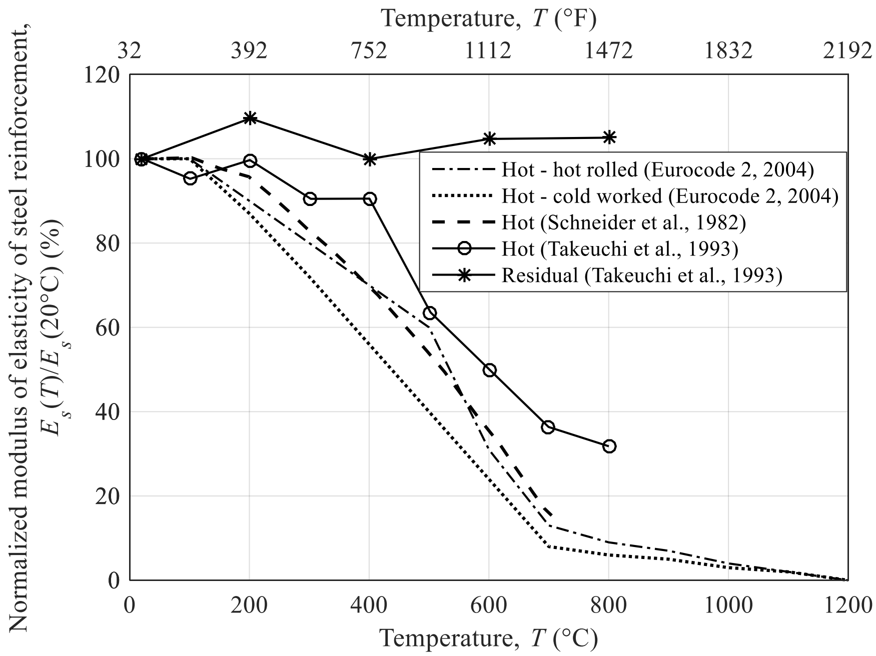

Figure 2-10. Variation in modulus of elasticity of steel reinforcement with temperature

2.3.2 Strength

Figure 2-11 (a) presents the change in yield strength or proportional limit with temperature, normalized by their respective strengths at room temperature, as recommended by Eurocode 2 [proportional limit], and reported from experiments by Schneider et al. (1982), Edwards and Gamble (1986) and Takeuchi et al. (1993) [yield strength]. Figure 2-11 (b) presents companion data for ultimate strength.

There is little variation in the yield and ultimate (tensile) strength of steel reinforcement for temperatures of up to about 300°C (572°F). At higher temperatures, the yield and ultimate strengths reduce with increasing temperature. Although the data is limited, the residual yield and ultimate strengths show a reduction above 500°C (932°F) and 600°C (1112°F), respectively.

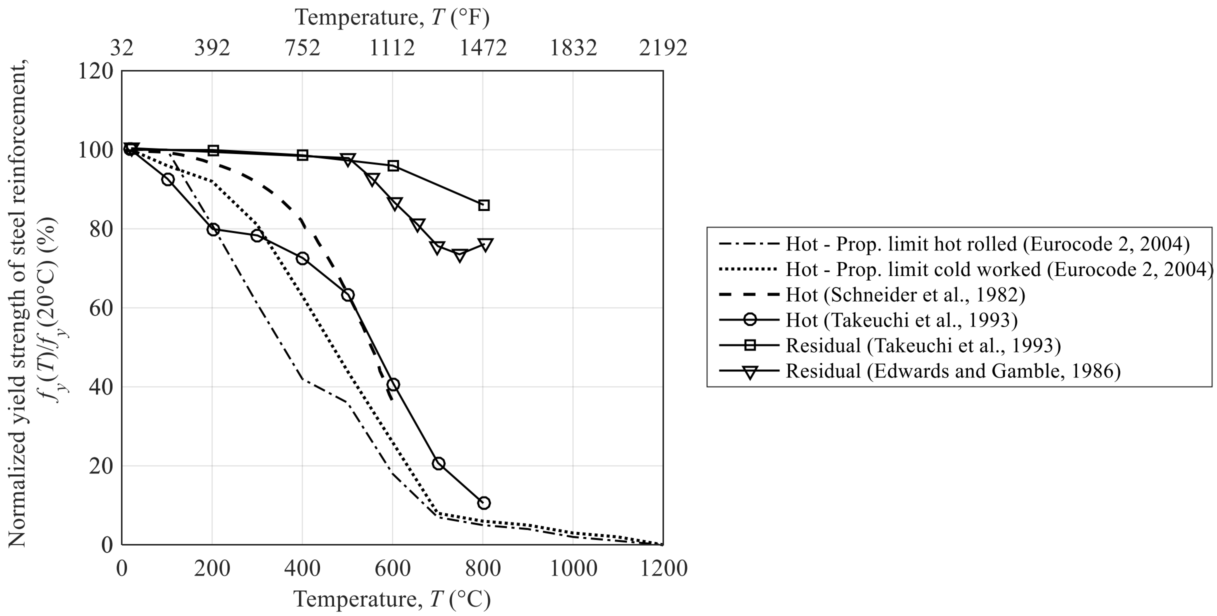

(a) Yield strength or proportional limit

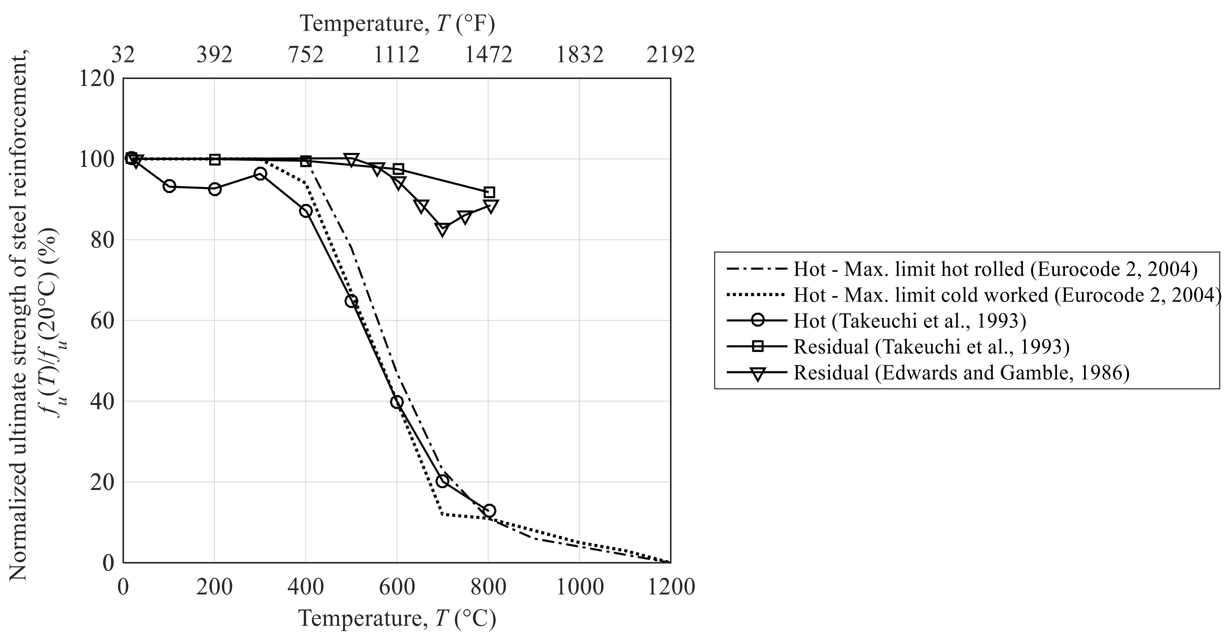

(b) Ultimate strength

Figure 2-11. Change in strength of steel reinforcement with temperature

2.3.3 Thermal expansion

The coefficient of thermal expansion of steel reinforcement is 12×10^{-6}/°C at 75°F (24°C) and the value increases with temperature. At 300°F (149°C) the coefficient is about 10% greater than the value at 75°F (24°C) (Willam et al., 2009). Figure 2-12 presents the variation in the thermal expansion strain of steel reinforcement, as recommended by Eurocode 2 and Schneider et al. (1982) and reported from experimental tests by Takeuchi et al. (1993). The thermal expansion strain, $\varepsilon_s(T)$, is calculated by multiplying the coefficient of thermal expansion by temperature.

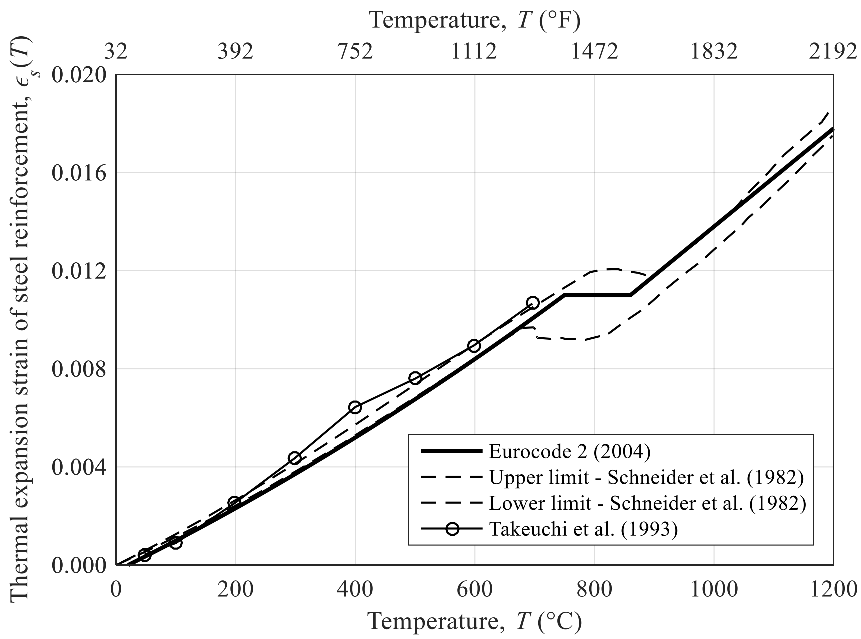

Figure 2-12. Variation in the thermal expansion strain of steel reinforcement with temperature

2.4 Effects of elevated temperature on steel reinforcement-concrete bond

A compilation of experimental test results for the variation in bond strength of steel reinforcement to concrete is presented in Figure 2-13. Data has been obtained from tests performed by Diederichs and Schneider (1981), Hertz (1982), Morley and Royles (1983) and Hlavička (2017). The data are normalized by the bond strength measured at room temperature. The data in Figure 2-13 were obtained from samples in the hot condition (i.e., test was performed when the specimen was at high temperature) and residual conditions (i.e., test was performed at room temperature after the specimen exposed to high temperature had cooled down).

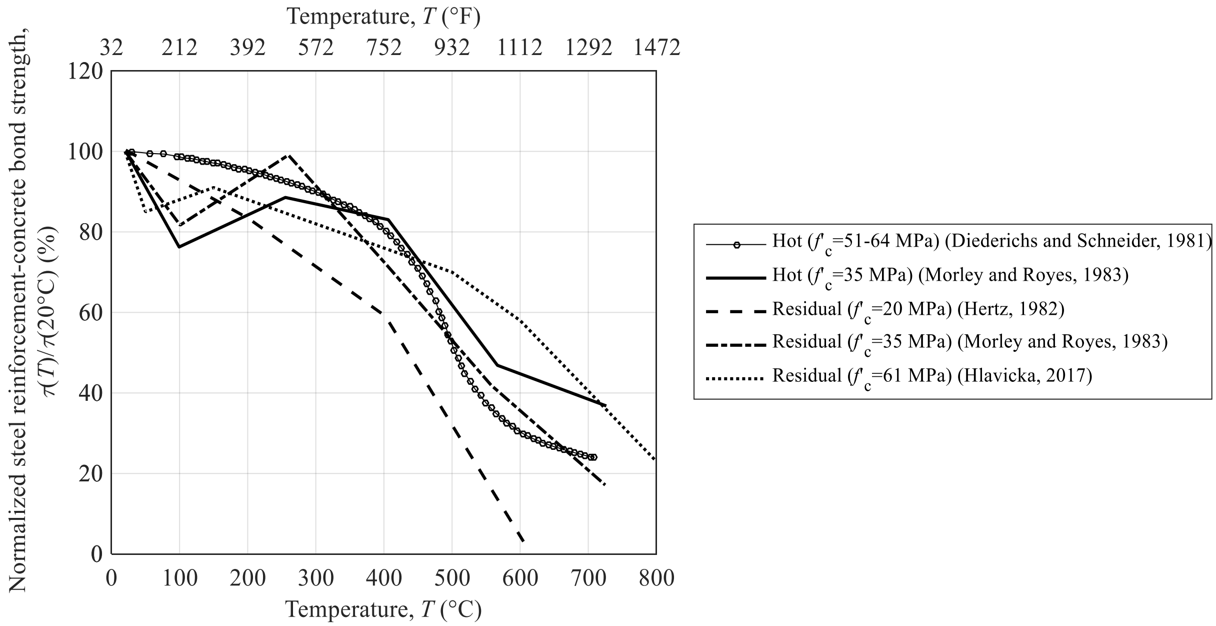

Figure 2-13. Variation of steel reinforcement-concrete bond strength with temperature

Figure 2-13 shows that the bond strength deteriorates with increasing temperature. The primary cause of this deterioration is the difference in the rates of thermal expansion of the reinforcement and the surrounding concrete (Willam et al., 2009). The geometric properties of the reinforcement such as diameter and rib height for deformed bars (beyond a minimum) do not significantly affect the bond behavior with temperature (Willam et al., 2009). The loss in bond strength up to 400°C (752°F) does not show a clear trend but is in the range of about 20 to 30%. The rate of loss of bond strength increases at temperatures greater than 400°C (752°F).

CHAPTER 3
EXPERIMENTAL PROGRAM FOR RC WALL TESTS

3.1 Introduction

This chapter discusses the program for testing of four reinforced concrete structural walls subjected to elevated temperature and reversed cyclic mechanical loading. The wall specimens are described in Section 3.2. Section 3.3 presents the pre-test numerical analysis performed to estimate the peak lateral strength of the four walls. The construction of the specimens is discussed in Section 3.4. The loading and heating apparatus are presented in Sections 3.5 and 3.6, respectively. The mechanical properties of steel rebar and concrete used in the construction of the specimens, including the effects of elevated temperature on the mechanical properties of concrete, are presented in Section 3.7. The test setup, instrumentation and loading protocols are discussed in Sections 3.8, 3.9 and 3.10, respectively.

3.2 Specimen details

Four low-aspect ratio, rectangular, reinforced concrete (RC) structural wall specimens were built and tested in the Robert L. and Terry L. Bowen Laboratory for Large-Scale Civil Engineering Research at Purdue University. The walls are denoted Wall 1 to Wall 4. The aspect ratio, h_w/l_w, for the walls was 0.62, where h_w is the distance from the top of the foundation to the centerline of loading and l_w is the length of the wall. The thickness and the length of the four walls was 10 in. [254 mm] and 60 in. [1524 mm], respectively.

Conventional normal weight concrete was used for all foundations and wall specimens. The same concrete mix design was specified for all specimens, but since they were cast and tested at different times, differences in the compressive strength and related properties were observed (and expected). The reinforcement was spaced at approximately 4 inches [102 mm] in both directions on both faces (i.e., two curtains) in all specimens. The reinforcement in Wall 1 and Wall 4 was #4 bars (0.5 in. [12.7 mm] nominal diameter), each way each face, for a rebar ratio of 0.93%

in both directions. The reinforcement provided in Wall 2 and Wall 3 was #6 bars (0.75 in. [19 mm] nominal diameter) each way each face, for a rebar ratio of 2% in both directions. The rebar was specified to be ASTM A706 Grade 60 (ASTM, 2016b). The rebar in Wall 1 and Wall 4 were from one heat and the rebar in Wall 2 and Wall 3 were from a different heat.

Axial loads were not applied to the specimens. In-plane forces and displacements were applied using a pair of hydraulic cylinder units. Out-of-plane movement of the wall specimen was not restrained but was measured at the top of the wall.

3.3 Pre-test numerical analysis

The peak lateral strengths of the specimens were estimated to aid the design of the foundation and the loading apparatus. Calculations were performed using conservative estimates of material strengths and the assumed wall geometry introduced previously. Codified expressions for nominal strength, equations for peak shear strength in the published literature, and numerical analysis using finite element tools were used for calculations. A concrete uniaxial compressive strength of 6 ksi [41 MPa], 50% greater than the proposed specified value of 4 ksi [28 MPa], and a rebar yield strength of 78 ksi [538 MPa], 30% greater than the minimum specified value of 60 ksi [414 MPa], was used in all these calculations. The different methods are described in this section.

3.3.1 Flexural strength

The nominal flexural strengths of the walls were estimated based on the assumptions provided in Chapter 22 of ACI 318-14 (ACI, 2014a), namely, plane sections remain plane, a maximum compression strain of 0.0030, a rectangular stress block for concrete in compression, and elastic perfectly plastic behavior for the reinforcement.

The lateral load associated with the flexural strength was calculated by dividing the moment by the height of the wall, measured from the top of the foundation to the centerline of loading. This calculation assumed that the wall could be treated as a cantilever with a fixed base. The peak lateral loads associated with flexural strengths for Wall 1 (0.93% web reinforcement ratio) and Wall 2 (2.0% web reinforcement ratio) were 307 kips [1366 kN] and 589 kips [2620 kN], respectively.

3.3.2 Shear strength

Different empirical and mechanics-based expressions are available in the literature to predict the nominal shear strength of RC walls. This section presents five of these expressions, two of which are adopted in ACI 318-14.

3.3.2.1 ACI 318-14 Chapter 11

Section 11.5 of ACI 318-14 (ACI, 2014a) provides the expression to calculate nominal shear strength, V_n, for resistance to non-seismic loadings as:

$$V_n = V_c + V_s \leq 10\sqrt{f_c'}hd \text{ ... in U.S. customary units} \quad (3.1)$$

$$\left[V_n = V_c + V_s \leq 0.83\sqrt{f_c'}hd \text{ ... in SI units}\right]$$

where V_c is the nominal shear strength provided by concrete, V_s is the nominal shear strength provided by the horizontal shear reinforcement, f_c' is the concrete compressive strength, h is the thickness of the wall, and d is the distance from the extreme compression fiber to the centroid of longitudinal tension reinforcement, specified to be taken equal to $0.8l_w$, where l_w is the length of the wall. The nominal shear strength provided by the concrete, V_c, is given as:

$$V_c = \min\left\{\begin{matrix} 3.3\lambda\sqrt{f_c'}hd + \dfrac{N_u d}{4l_w} \\ \left[0.6\lambda\sqrt{f_c'} + \dfrac{l_w\left(1.25\lambda\sqrt{f_c'} + \dfrac{0.2N_u}{l_w h}\right)}{\dfrac{M_u}{V_u} - \dfrac{l_w}{2}}\right]hd \end{matrix}\right\} \text{ ... in U.S. customary units} \quad (3.2)$$

$$\left[V_c = \min \left\{ \begin{array}{c} 0.27\lambda\sqrt{f_c'}hd + \dfrac{N_u d}{4l_w} \\ \left[0.05\lambda\sqrt{f_c'} + \dfrac{l_w\left(0.1\lambda\sqrt{f_c'} + \dfrac{0.2N_u}{l_w h}\right)}{\dfrac{M_u}{V_u} - \dfrac{l_w}{2}} \right] hd \end{array} \right\} \text{... in SI units} \right]$$

where $\lambda = 1$ for normal-weight concrete, N_u is the factored axial compressive force, M_u is the factored moment, and V_u is the factored shear force. The nominal shear strength provided by reinforcement, V_s, is calculated as:

$$V_s = \frac{A_v f_{yt} d}{s} \tag{3.3}$$

where A_v is the area of horizontal reinforcement within distance s, f_{yt} is the specified yield strength of the horizontal reinforcement, and s is the center-to-center spacing of the horizontal reinforcement. The upper limit of $10\sqrt{f_c'}hd$ [$0.83\sqrt{f_c'}hd$ in SI units] is intended to prevent diagonal compression failure.

3.3.2.2 ACI 318-14 Chapter 18

The nominal shear strength to resist seismic loadings, V_n, is calculated per Section 18.10.4 of ACI 318-14 (ACI, 2014a), as:

$$V_n = A_{cv}\left(\alpha_c \lambda \sqrt{f_c'} + \rho_t f_y\right) \le 8A_{cv}\sqrt{f_c'} \text{ ... in U.S. customary units} \tag{3.4}$$

$$\left[V_n = A_{cv}\left(\alpha_c \lambda \sqrt{f_c'} + \rho_t f_y\right) \le 0.66A_{cv}\sqrt{f_c'} \text{ ... in SI units} \right]$$

where A_{cv} is the gross area of the concrete wall bounded by web thickness and length of section. Coefficient α_c is 3.0 for $h_w/l_w \le 1.5$, is 2.0 for $h_w/l_w \ge 2.0$, and varies linearly between 3.0 and 2.0 for h_w/l_w between 1.5 and 2.0; $\lambda = 1.0$ for normal weight concrete; f_c' is the compressive strength of concrete; ρ_t is the horizontal reinforcement ratio; and f_y is the reinforcement yield strength. The upper limit of $8A_{cv}\sqrt{f_c^{'}}$ [$0.66A_{cv}\sqrt{f_c^{'}}$ in SI units] is intended to prevent diagonal compression failure, and is functionally identical to the Chapter 11 limit if $h = 0.8l_w$.

3.3.2.3 Wood (1990)

Wood's (1990) equation for peak average shear stress is:

$$6\sqrt{f_c^{'}} \leq \frac{A_v f_{yv}}{4A_{cv}} \leq 10\sqrt{f_c^{'}} \text{ ... in U.S. customary units} \tag{3.5}$$

$$\left[0.50\sqrt{f_c^{'}} \leq \frac{A_v f_{yv}}{4A_{cv}} \leq 0.83\sqrt{f_c^{'}} \text{ ... in SI units}\right]$$

where $f_c^{'}$ is the compressive strength of concrete, A_{cv} is the effective wall area equal to the product of the wall length and web thickness, A_v is the total area of vertical reinforcement in the wall, and f_{yv} is the yield stress of the vertical reinforcement.

3.3.2.4 Gulec and Whittaker (2011)

The Gulec and Whittaker (2011) empirical expression for peak shear strength of a rectangular wall, V_n, is:

$$V_n = \frac{1.5\sqrt{f_c^{'}}A_w + 0.25F_{vw} + 0.20F_{vbe} + 0.40P}{\sqrt{h_w/l_w}} \leq 10\sqrt{f_c^{'}}A_w \text{ ... in U.S. customary units} \tag{3.6}$$

$$\left[V_n = \frac{0.12\sqrt{f_c^{'}}A_w + 0.25F_{vw} + 0.20F_{vbe} + 0.40P}{\sqrt{h_w/l_w}} \leq 0.83\sqrt{f_c^{'}}A_w \text{ ... in SI units}\right]$$

where $f_c^{'}$ is the compressive strength of concrete, A_w is the area of the wall, F_{vw} is the force attributed to the vertical web reinforcement, F_{vbe} is the force attributed to the boundary reinforcement, P is the axial compressive force, h_w is the height of the wall, and l_w is the length of the wall.

3.3.2.5 Luna (2016)

Luna performed reversed cyclic tests on 12 low aspect ratio walls and proposed a mechanics-based expression (Luna, 2016; Luna et al., 2018) for peak shear strength based on the flow of forces of through the wall. The nominal shear strength of a rectangular, low-aspect ratio RC wall without boundary elements is calculated as:

$$V_n = 1.2\left(\rho_l A_{cv} f_{\bar{y}} + p l_w\right)\left(1 - 0.7\frac{h_w}{l_w} - \frac{c}{l_w}\right) + 0.25\rho_t \frac{h_w}{l_w} A_{cv} f_y + 0.5pc \le 10\sqrt{f_c^{'}} A_{cv} \text{ ... in U.S. customary units} \tag{3.7}$$

$$\left[V_n = 1.2\left(\rho_l A_{cv} f_{\bar{y}} + p l_w\right)\left(1 - 0.7\frac{h_w}{l_w} - \frac{c}{l_w}\right) + 0.25\rho_t \frac{h_w}{l_w} A_{cv} f_y + 0.5pc \le 0.83\sqrt{f_c^{'}} A_{cv} \text{ ... in SI units}\right]$$

where ρ_l is the vertical reinforcement ratio, A_{cv} is the effective wall area equal to the product of the wall length and thickness, $f_{\bar{y}}$ is set equal to $1.25 f_y$, f_y is the reinforcement yield strength, p is the axial load per unit length at the centerline of loading, l_w is the length of the wall, h_w is the height of the wall, ρ_t is the transverse reinforcement ratio, and c is the distance from the toe of the wall in compression to the bottom of the nearest diagonal crack. The variable c is given as:

$$c = \frac{\left(\rho_l t_w f_{\bar{y}} + p\right)\left(\frac{h_w}{\tan\theta}\right)}{f_c t_w + p} \tag{3.8}$$

where t_w is the thickness of the wall, θ is the crack angle with respect to the horizontal, taken to be equal to 40°, and f_c is the axial stress in the diagonal compression strut, taken equal to 80% of the compressive strength.

3.3.3 Nonlinear static analysis

3.3.3.1 VecTor2

VecTor2 (Wong et al., 2013) is a nonlinear finite element program for the analysis of two-dimensional RC membrane structures subjected to quasi-static load conditions and utilizes the Modified Compression Field Theory and the Disturbed Stress Field Model. Four-node quadrilateral elements with smeared reinforcement in both directions and a mesh size of 1×1 inch [25.4×25.4 mm] were used for all models. The uniaxial compressive strength of concrete was assumed to be 6,000 psi [41 MPa] and yield strength of steel was assumed to be 78,000 psi [54 MPa]. All other material parameters were set to the default values.

3.3.3.2 LS-DYNA

LS-DYNA is a general-purpose finite element program (LSTC, 2016). The wall was modeled using 8-noded solid elements with a mesh size of 1×1×1 in. [25.4×25.4×25.4 mm]. Reinforcement was modeled using 1 in. [25.4 mm] frame elements to match the mesh adopted for the concrete. Perfect bond between the concrete and the reinforcement was assumed. The smeared crack Winfrith material model (MAT085) was used to model the concrete. The values of the parameters assigned to this material model are summarized in Table 3-1. The Plastic Kinematic model (MAT003) was used to model the reinforcement; the values assigned to the parameters for this material model are summarized in Table 3-2.

Table 3-1. MAT085 property assignments in LS-DYNA

Parameter	Value	Units
Density	0.09 [2,500]	lb/in^3 [kg/m^3]
Tangent modulus	4,410 [30,406]	ksi [MPa]
Poisson's ratio	0.18	-
Uniaxial compressive strength	6 [41.4]	ksi [MPa]
Uniaxial tensile strength	0.6 [4.1]	ksi [MPa]
Fracture energy	0.0014	-
Aggregate size	0.1875 [4.76]	in. [mm]
Strain rate effects	OFF	-

Table 3-2. MAT003 property assignments in LS-DYNA

Parameter	Value	Unit
Density	0.28 [7,800]	lb/in^3 [kg/m^3]
Young's modulus	29,000 [200,000]	ksi [MPa]
Poisson's ratio	0.3	-
Yield Stress	78 [538]	ksi [MPa]
Tangent modulus	580 [4,000]	ksi [MPa]

3.3.4 Summary

Table 3-3 summarizes the lateral strengths calculated using the predictive equations and analysis of the finite element models for web reinforcement ratios of 0.93% and 2% in both directions. Flexure was expected to control the lateral strength of Walls 1 and 4. Shear was expected to control the lateral strength of Walls 2 and 3. The maximum expected lateral strength of Walls 1 and 4 was 307 kips [1366 kN]; and the maximum expected lateral strength of Walls 2 and 3 was 505 kips [2246 kN]. The maximum lateral forces were increased by 20%, a significant margin, for design of the foundation assembly and test fixture.

Table 3-3. Estimated lateral strengths of walls, in kips [kN], with 0.93% and 2% reinforcement in both directions, f_c' = 6 ksi [41 MPa] and f_y =78 ksi [538 MPa]

Type	Method	Web rebar ratio kips [kN]	
		0.93%	**2%**
Flexure	ACI 318-14 Chapter 22	307 [1,366]	589 [2,621]
Shear	ACI 318-14 Chapter 11	372 [1,655]	372 [1,655]
	ACI 318-14 Chapter 18	372 [1,655]	372 [1,655]
	Wood (1990)	279 [1,242]	279 [1,242]
	Gulec and Whittaker (2011)	241 [1,072]	400 [1,780]
	Luna (2016)	376 [1,673]	465 [2,069]
Nonlinear static analysis	VecTor2	292 [1,299]	456 [2,029]
	LS-DYNA	300 [1,335]	505 [2,247]

3.4 Construction of walls

The foundation assembly for each wall specimen was assembled from three pieces, two of which were reused for all four specimens. The third piece was cast integrally with the wall. The two reusable pieces, hereafter referred to as wing foundation beams, were designed to provide additional sliding and overturning resistance to the wall and its foundation. Details of the wall and foundation assemblies are presented in Figure 3-1. The wing foundations were clamped to the sides of the wall foundation using 1.75-inch diameter Dywidag bars that were each stressed to a load of 240 kips. A bed of 0.5-inch thick grout was provided below the foundation to provide uniform bearing on the strong floor. The eighteen vertical 1.75-inch Dywidag bars identified in Figure 3-1, each stressed to a load of 240 kips, provided resistance to sliding and overturning. The coefficient of sliding friction between the wall foundation and the wing beams, and the foundation and the strong floor, was assumed to be 0.2, based on past experience in the Bowen Laboratory.

The foundation assembly was designed to resist a maximum lateral force of 450 and 600 kips applied at the centerline of loading, for the walls with 0.93% and 2% wall reinforcement in both directions, respectively. The foundation below the wall was designed using strut-and-tie procedures to resist the total overturning moment and a fraction of the lateral force. The wing foundation beams were used to resist the remainder of the lateral force via sliding friction on the strong floor. The reinforcement in these beams met the minimum requirements of ACI 318-14 for flexure and shear reinforcement. Additional bursting reinforcement was provided around the holes provided for the post-tensioning bars in the wall foundation and the wing foundation beams. The reinforcement in the wing foundation beams is described in Figure 3-2. The reinforcement in the walls and their integral foundations are presented in Figure 3-6.

The formwork for casting the wing foundation beams and the wall specimens was built using phenolic film coated plywood that was supported by two-by-four inch timber studs. All four walls were cast using the same formwork.

Each wall and its foundation were cast horizontally. The concrete was supplied by a local batching plant and placed in the form using a concrete bucket and an overhead gantry crane. The foundation and the wall part of the specimen were cast at the same time with no cold or construction joint at the interface of the wall and its foundation. The thickness of the wall and its foundation were 10 and 18 inches, respectively. The lower 4-inch offset between the faces of the wall and the foundation was achieved by raising the formwork. The upper 4-inch offset was achieved through formwork and by leveling the wet concrete with an aluminum flat plane and trowels, using the sides of the forms for reference. The slump of the concrete was small enough so as not to generate significant bulging in the wall thickness at the wall-foundation junction.

Needle vibrators were used to compact the concrete. Cylinders for material testing were cast at the same time as the wall. The casting operation for a given wall took about 60 minutes. The top surface was finished using trowels 60 minutes after completion of casting to achieve a smooth surface finish. Burlap was laid on the specimen, which was then covered with a polythene sheet. The burlap was sprayed with water, twice a day, for seven days. The formwork was removed after seven days. Cylinders were tested before the formwork was removed to ensure that concrete had reached a compressive strength of 4 ksi.

The horizontal and vertical reinforcement was strain gaged before the rebar cages were tied. Additional information about the strain gages and the procedure for attaching them to the rebar is presented in Section 3.9.

Twenty thermocouples, in four sets of five, were installed in each wall specimen. These thermocouples measured temperature through the wall thickness at four locations in the wall. Additional information on the thermocouples is provided in Section 3.9. The thermocouples were attached to a 10-inch long, sacrificial steel rod using electrical tape. Figure 3-7 shows one set of five thermocouples prior to placement in a wall. This assembly was placed in the rebar cage before pouring concrete and held in place using rebar tie wires. The lead wires for all strain gages and thermocouples were brought through the top of the wall. Figure 3-8 to Figure 3-11 present photographs of a rebar cage, a finished concrete surface, and the burlap and polythene covers.

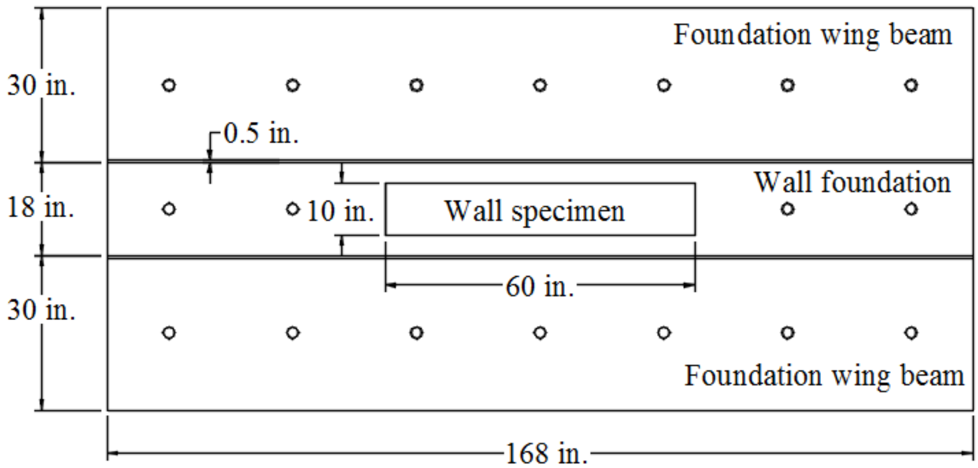

(a) Plan view

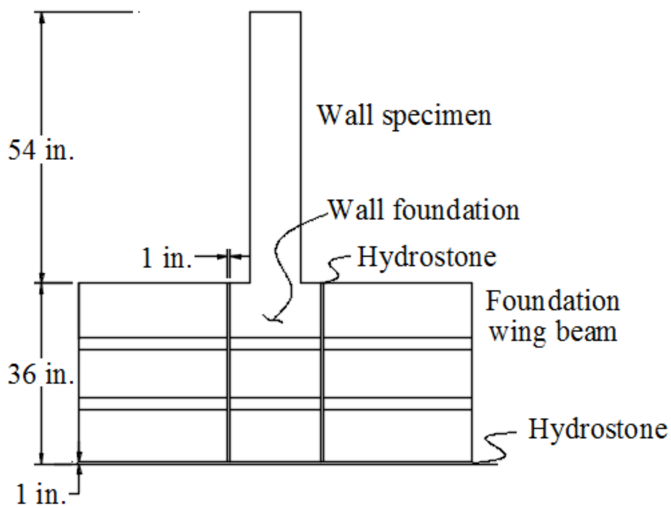

(b) Section view

Figure 3-1. Wall and foundation assembly (Note: 1 in. = 25.4 mm)

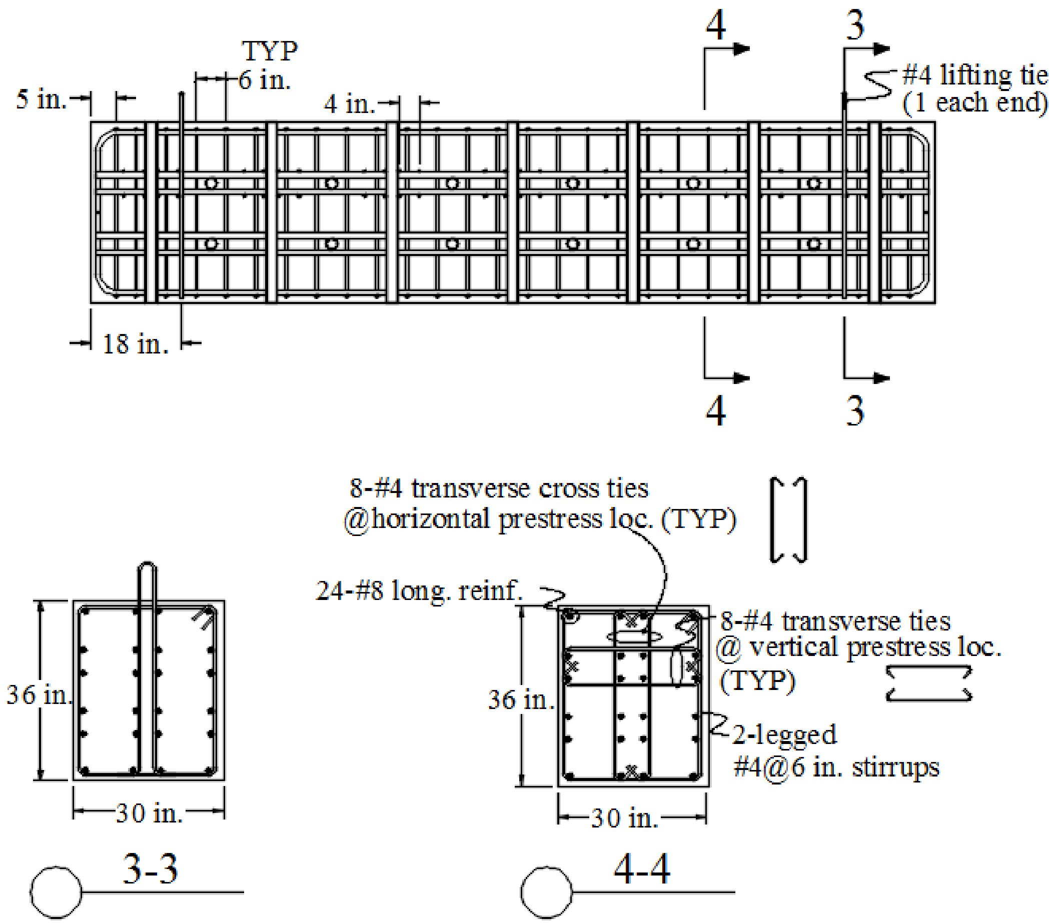

Figure 3-2. Reinforcement details for a wing foundation beam (Note: 1 in. = 25.4 mm)

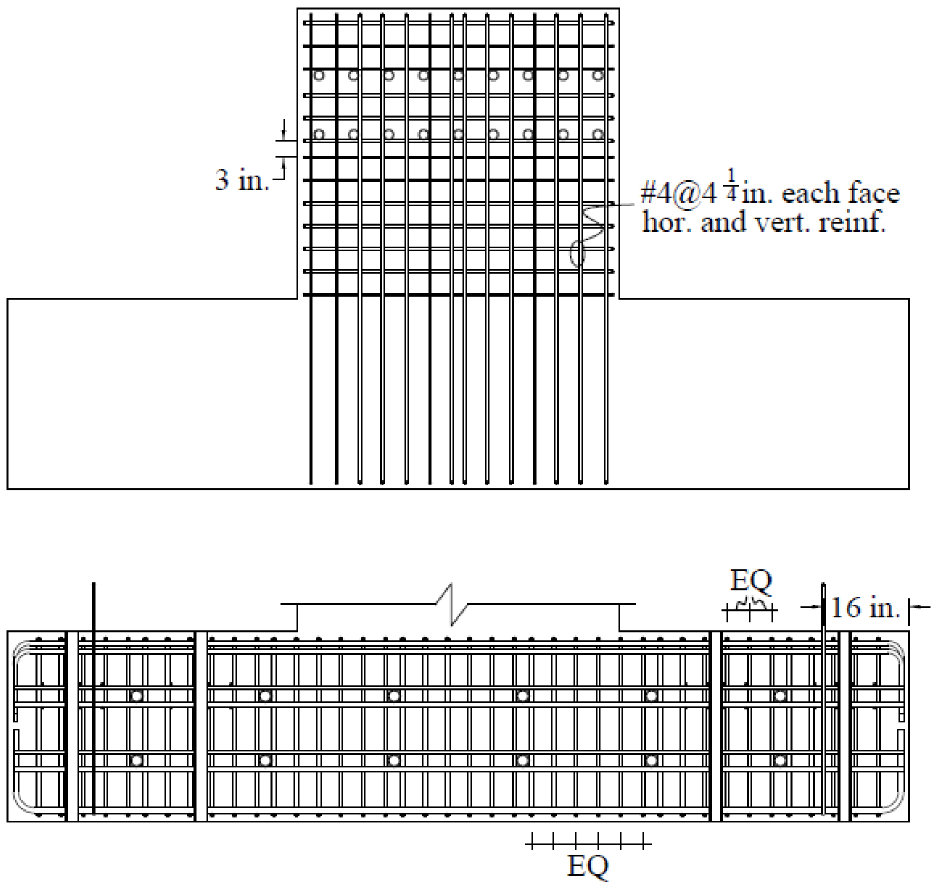

Figure 3-3. Rebar layout for specimen with 0.93% web reinforcement (Walls 1 and 4)
(Note: 1 in. = 25.4 mm)

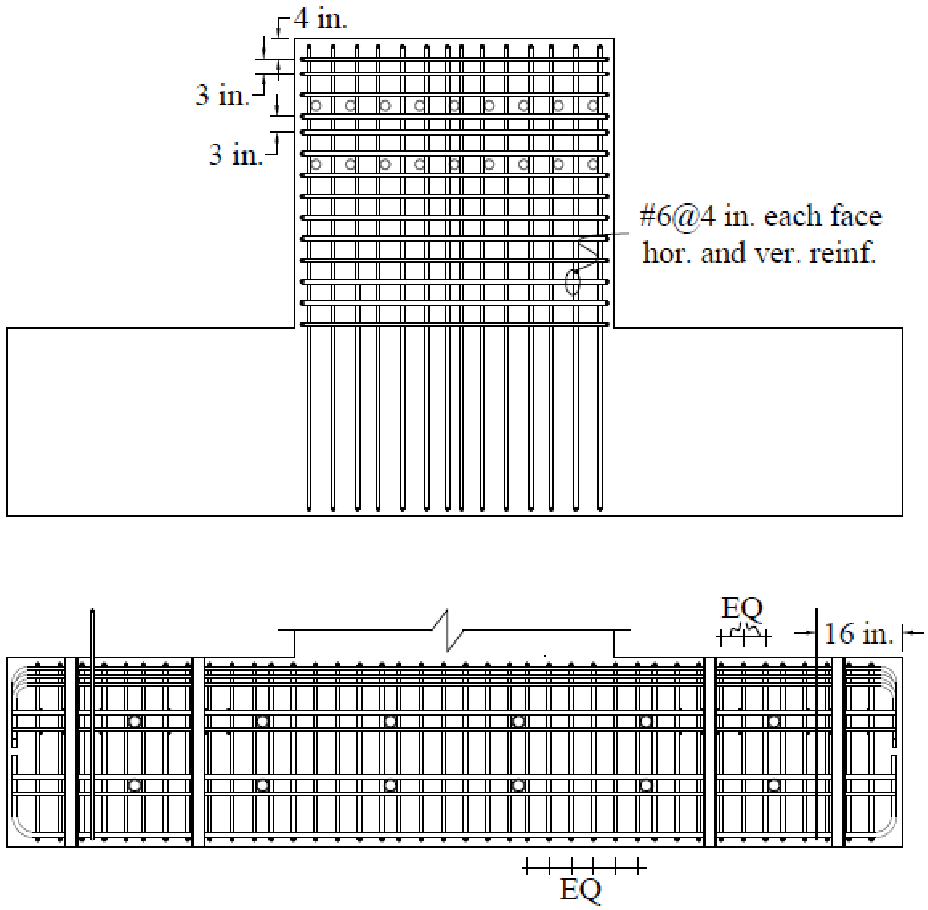

Figure 3-4. Rebar layout for specimen with 2% web reinforcement (Walls 2 and 3)
(Note: 1 in. = 25.4 mm)

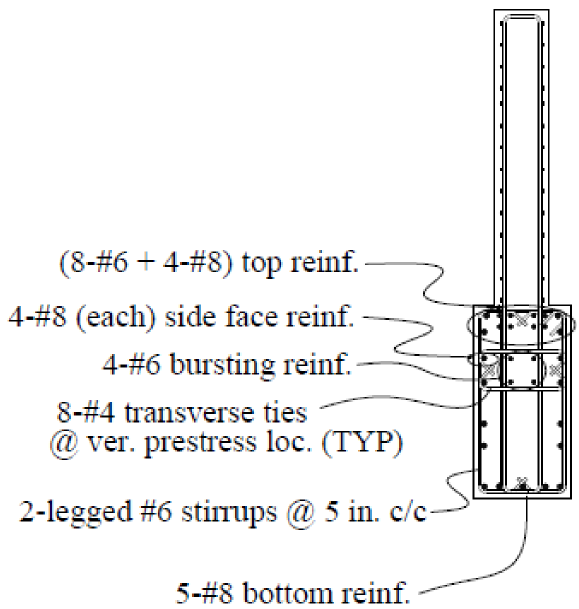

Figure 3-5. Section details for wall and foundation (Walls 1 and 4)

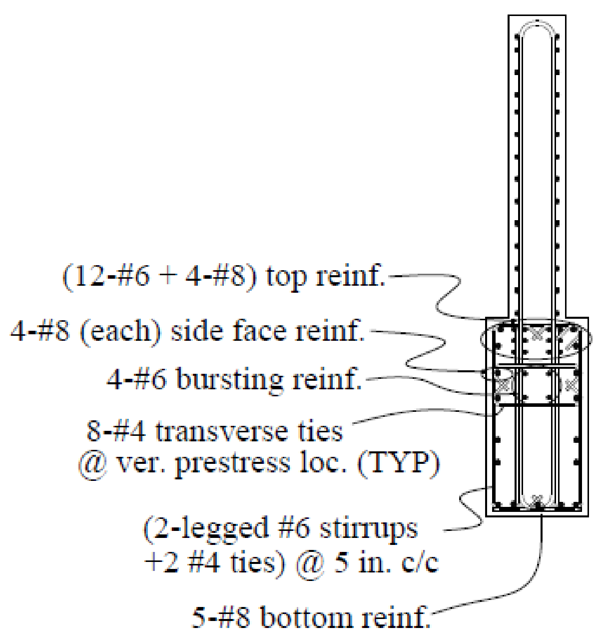

Figure 3-6. Section details for wall and foundation (Walls 2 and 3)

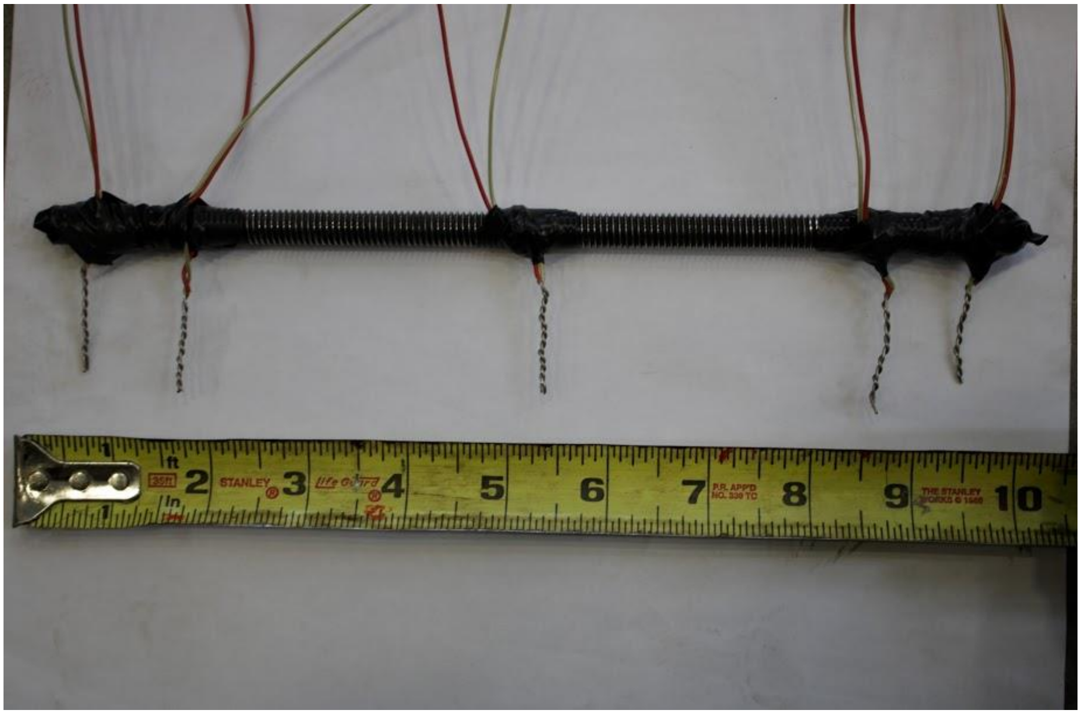

Figure 3-7. One set of five thermocouples

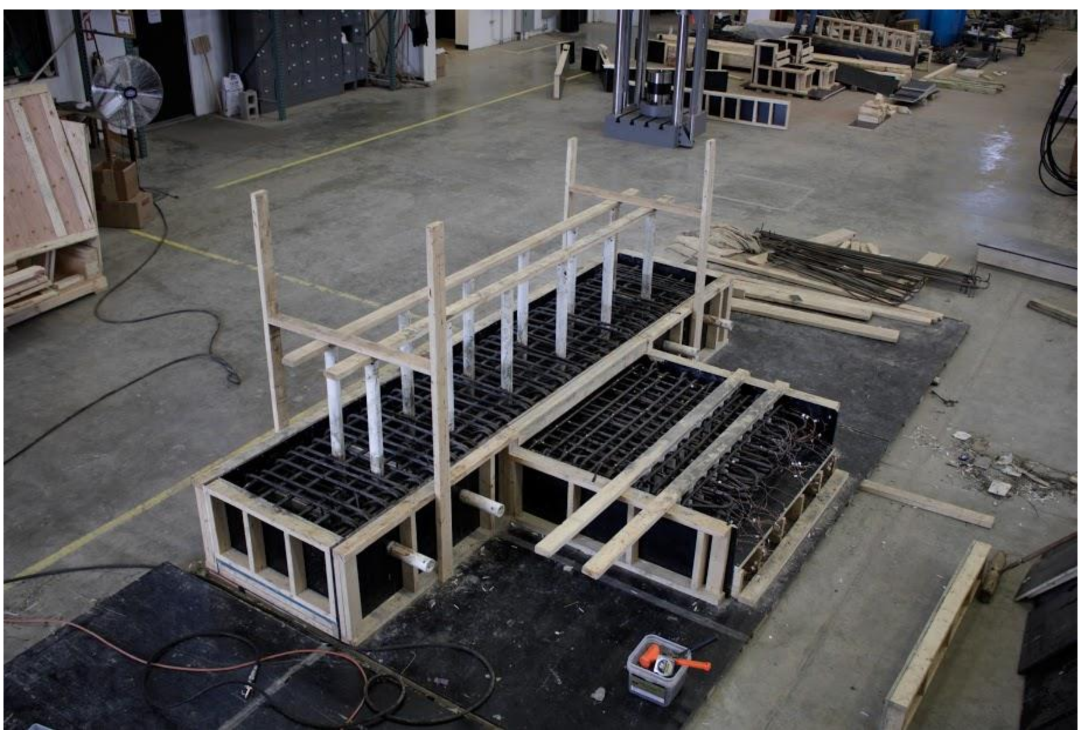

Figure 3-8. Wall and foundation rebar cage before casting

Figure 3-9. Finished concrete surface of a wall and its foundation

Figure 3-10. Burlap cover

Figure 3-11. Polythene cover placed over specimen for curing period

3.5 Loading apparatus

The loading apparatus consisted of two I-shaped structural steel sections. Two rows of 9 holes each were drilled in the I-sections, through which 1.75-inch [44.5 mm] diameter bolts were passed. The I-sections were held in place using temporary cribbing such that there was a gap of about 0.5 inch [12.7 mm] between the wall and the flange of the steel section. A spirit level was used to ensure that the I-section flanges were vertical. A strip of window-sealant foam was attached to the bottom and vertical edges of the flanges adjacent to the wall. A strip of silicone was then applied to the foam to make the gap between the I-section and wall watertight. Hydrostone was then placed in the gap between the steel section and concrete wall surface. Hot glue was used to attach foam cutouts to the concrete wall, prior to pouring hydrostone, at the location of each hole to prevent the hydrostone from flowing into the hole. The hydrostone was allowed to set for 24 hours after which the nuts on the bolts were tightened using an impact wrench until the nuts would not turn further. The temporary cribbing below the I-sections was then removed.

3.6 Heating apparatus

The walls were heated with radiant heating panels, manufactured by Watlow (http://www.watlow.com). Two pairs of four heaters were used for heating the wall from both sides. Sixteen thermocouples were installed on the wall surface, eight each on the East and West faces. Two thermocouples were used for every heater, one provided feedback for controlling the heater and the other for data acquisition. The layout of the heaters and surface thermocouples is presented in Figure 3-12. One pair of surface-mounted thermocouples is shown in Figure 3-13. Figure 3-14 is a photograph of the heater controller and its display. Figure 3-15 shows the front side and back side of one heater assembly. The middle two panels (H2, H3, H5 and H6) each required a 480V supply but the side panels (H1 and H4) operated at 240V and were connected in series. Each panel was rated at 6 kW. The heaters were controlled using a manufacturer-supplied control system. The target temperatures were manually input to the heater controls and monitored for the duration of the test. Figure 3-16 is a photograph of an installed heater assembly. Fiberglass insulation, as seen below the heaters in Figure 3-16, was placed to protect the lead wires for the sensors and surface thermocouples from excessive heat.

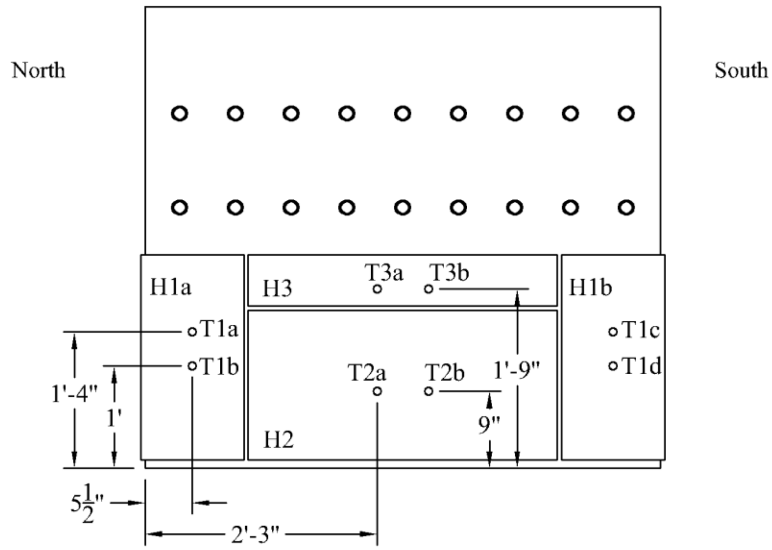

(a) West face

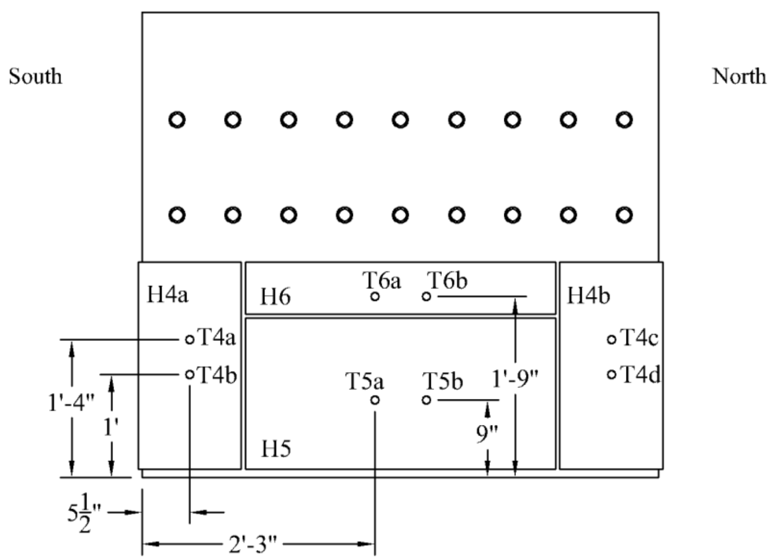

(b) East face

Figure 3-12. Heater and surface thermocouple layout

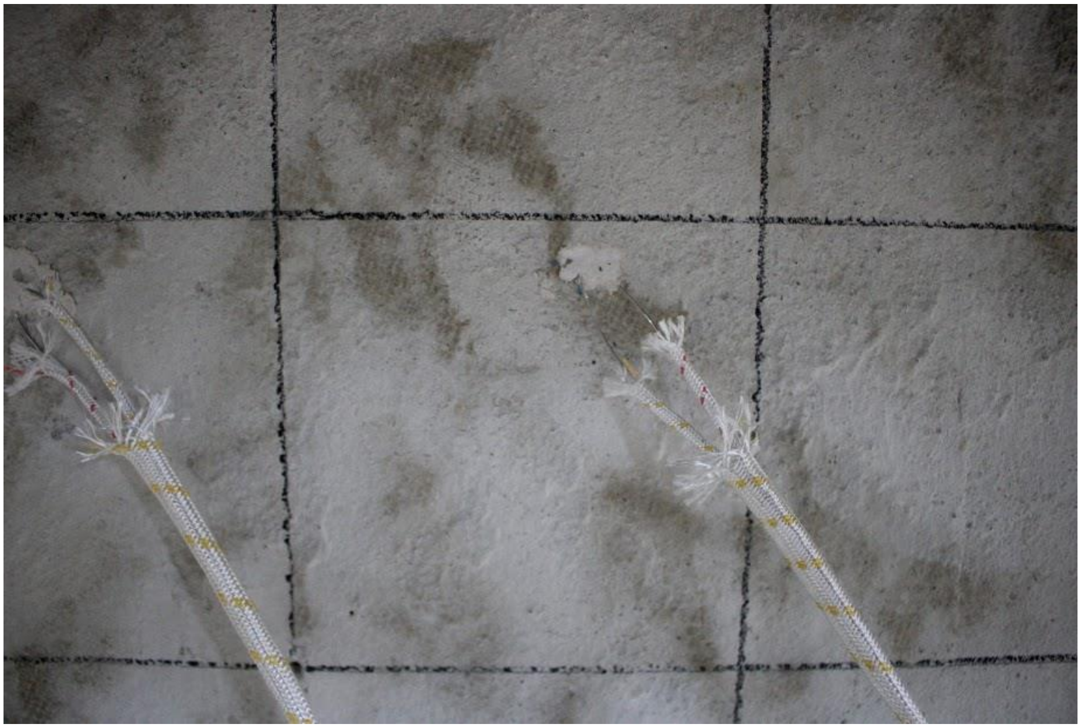

Figure 3-13. Thermocouples for measuring surface temperature

Figure 3-14. Heating control system and display

(a) Front side

(b) Back side

Figure 3-15. One heater assembly

Figure 3-16. Heaters installed on wall specimen

3.7 Mechanical properties of rebar and concrete

This section presents material properties for the concrete and rebar used in the experimental program. Coupons were taken at random from the rebar provided for the walls. Cylinders were cast at the same time as the corresponding wall and foundation and then cured under the same conditions.

3.7.1 Rebar

The rebar used in the walls was specified to conform to ASTM A706 Grade 60 (ASTM, 2016b). The rebar for the two 0.93% and two 2% reinforced walls was each specified to be from the same heat. Uniaxial tension tests were performed on rebar coupons in the laboratory at the University at Buffalo. Stress-strain data were collected from tests of rebar coupons. Five #4 and five #6 bars were tested. Yield and ultimate strengths are reported in Table 3-4. Average yield strengths, standard deviations (SD) and coefficients of variations (CoV) are also reported although the number of data points used for the calculations of standard deviation are small.

Table 3-4. Mechanical characteristics of rebar

Bar dia.	Sample	f_y (ksi)[a]	f_u (ksi)[a]	f_u / f_y	Avg. f_y (ksi)[a] [MPa]	Std. dev. f_y (ksi)[a] [MPa]	CoV
#4	1	68.1	92.3	1.36	63.8 [440]	2.6 [18]	4%
	2	64.9	87.9	1.35			
	3	62.6	89.4	1.43			
	4	62.8	89.5	1.43			
	5	60.4	83.3	1.38			
#6	1	67.5	92.2	1.37	66.5 [459]	2.2 [15]	3%
	2	69.5	94.3	1.36			
	3	64.9	89.7	1.38			
	4	63.2	88.2	1.40			
	5	67.3	92.5	1.37			

[a] 1 ksi = 6.89 MPa

3.7.2 Concrete

The concrete used in all the specimens and the foundation wing beams was sourced from a batching plant near Purdue University. The minimum specified compressive strength for all placed concrete was 4 ksi. The mix proportions, which were the same for all specimens, are listed in Table 3-5. Limestone sourced from a quarry near West Lafayette, Indiana, was used as the coarse aggregate and river sand sourced from a river near West Lafayette, Indiana, was used as fine aggregate. The cement used was Type I (ASTM, 2017a) . The casting dates and concrete slump for the 4 walls are provided in Table 3-6.

Table 3-5. Mix proportion (by weight) of concrete used in all specimens

Constituent	Weight proportion
Cement	1
Water	0.45
Coarse aggregate	3.28
Fine aggregate	2.62

Table 3-6. Casting dates and concrete slump

Specimen	Casting date	Slump (in.) [mm]
Wall 1	April 5, 2017	Not available
Wall 2	June 5, 2017	3.5 [89]
Wall 3	June 22, 2017	6.5 [165]
Wall 4	July 6, 2017	6.5 [165]

3.7.2.1 Uniaxial compressive strength

Cylinders, 4 in. [101.6 mm] in diameter and 8 in. [203.2 mm] in height, were used for testing for uniaxial compressive strength. Tests were performed in accordance with ASTM C39 (ASTM, 2017c) . Results are presented in Table 3-7. Strength is presented in terms of average stress. The calculated standard deviation and coefficient of variation (CoV) are based on the tests performed on that particular day and are based on a very limited number of data points. A small standard deviation, or CoV, provides additional confidence in the calculated means.

Table 3-7. Concrete compressive strength results

Specimen	Age (days)	Sample	Strength (psi)[a]	Average (psi) [MPa]	Std. dev (psi) [MPa]	CoV
Wall 1	5	1	4,080	4,109 [28]	33 [0.2]	1%
		2	4,155			
		3	4,092			
	28	1	6,344	6,418 [44]	52 [0.4]	1%
		2	6,450			
		3	6,460			
	85	1	6,456	6,469 [45]	70 [0.5]	1%
		2	6,561			
		3	6,390			
	97	1	6,348	6,231 [43]	84 [0.6]	1%
		2	6,188			
		3	6,157			
	100	1	5,984	6,192 [43]	172 [1.2]	3%
		2	6,186			
		3	6,406			
Wall 2	16	1	5,865	5,680 [39]	418 [2.9]	7%
		2	5,102			
		3	6,074			
	30	1	5,719	5,801 [40]	61 [0.4]	1%
		2	5,822			
		3	5,863			
	56	1	5,961	5,955 [41]	71 [0.5]	1%
		2	5,865			
		3	6,039			
	143	1	6,007	6,099 [42]	77 [0.5]	1%
		2	6,094			
		3	6,195			

[a] 1 psi = 0.00689 MPa

Table 3-7 (continued): Concrete compressive strength results

Specimen	Age (days)	Sample	Strength (psi)[a]	Average (psi) [MPa]	Std. dev (psi) [MPa]	CoV
Wall 3	5	1	4,150	4,205 [29]	149 [1.0]	4%
		2	4,056			
		3	4,408			
	13	1	5,026	5,049 [35]	61 [0.4]	1%
		2	5,132			
		3	4,989			
	19	1	5,434	5,362 [37]	117 [0.8]	2%
		2	5,197			
		3	5,456			
	126	1	5,557	5,619 [39]	130 [0.9]	2%
		2	5,800			
		3	5,499			
Wall 4	5	1	4,314	4,303 [30]	118 [0.8]	3%
		2	4,153			
		3	4,441			
	36	1	5,932	5,863 [40]	57 [0.4]	1%
		2	5,864			
		3	5,792			
	112	1	6,447	6,527 [45]	171 [1.2]	3%
		2	6,688			
		3	6,486			
		4	6,566			
		5	6,851			
		6	6,524			
		7	6,402			
		8	6,248			

[a] 1 psi = 0.00689 MPa

3.7.2.2 Modulus of elasticity

The modulus of elasticity of concrete in compression was measured using cylinders, 6 inches in diameter and 12 inches in height, and tested in accordance with ASTM C469 (ASTM, 2014b) . The secant stiffness, calculated at 40% of the concrete strength, is reported in Table 3-8. The tests were performed at the University at Buffalo no more than 14 days after completing the tests of their respective walls.

Table 3-8. Modulus of elasticity for concrete used in walls

Specimen	Sample	Modulus (ksi)[a]	Average (ksi) [MPa]	Std. dev. (ksi) [MPa]	CoV
Wall 2	1	3,971	3,863 [26,634]	76 [524]	2%
	2	3,810			
	3	3,808			
Wall 3	1	3,360	3,500 [24,132]	166 [1,145]	5%
	2	3,733			
	3	3,405			
Wall 4	1	3,379	3,645 [25,131]	220 [1,517]	6%
	2	3,918			
	3	3,639			

[a] 1 ksi = 6.89 MPa

3.7.2.3 Modulus of rupture

The modulus of rupture of concrete was measured using 3×3×12 in. [76×76×305 mm] beams. The beams were tested using third-point loading in accordance with ASTM C78 (ASTM, 2016a). The moduli of rupture of the beams is reported in Table 3-9. The tests were performed at the University at Buffalo no more than 14 days after completing the tests of their respective walls. Only two beams were tested for each wall.

Table 3-9. Modulus of rupture for concrete used in walls

Specimen	Sample	Modulus (ksi) [MPa]
Wall 2	1	2.11 [14.5]
	2	1.99 [13.7]
Wall 3	1	1.87 [12.9]
	2	1.71 [11.8]
Wall 4	1	1.64 [11.3]
	2	1.83 [12.6]

3.7.2.4 Effects of temperature on concrete properties

As discussed in Chapter 2, there is large scatter in the data for variation of concrete properties as a function of temperature. The large scatter has been attributed (Schneider, 1988) to incomplete descriptions of tests, different types of concretes, sizes of test articles, and differences in test equipment and procedures. Hence, a series of materials tests were performed on the concrete used to construct the walls tested at Purdue University to help interpret the results of those experiments.

The materials studies were executed after the component tests at Purdue had been completed, using coarse and fine aggregates obtained from the source that supplied materials for casting the walls. Type-I cement conforming to ASTM C150 (ASTM, 2017a) was used in the mix, as was the case for the wall specimens. The mixture proportions for the materials tests are listed in Table 3-5. Twenty-four 3-in. [76-mm] diameter, 6-in. [152-mm] long cylinders were cast for uniaxial compression tests, and twenty-four 4-in. [102-mm] diameter, 8-in. [203 mm] long cylinders were cast for split-cylinder tension tests. The specimens were covered with wet hessian and polythene sheets for 5 days after casting and then demolded and stored at 70°F [21°C] for 30 days, on average, before testing.

Control specimens were maintained and tested at room temperature. The remaining cylinders were tested at room temperature after being heated either to 212°F [100°C], 250°F [121°C], 300°F [149°C], 450°F [232°C] or 600°F [316°C]. These cylinders were heated in a box furnace at a rate of 7°F/min [4°C/min] till they reached the target temperature, were kept at that temperature for 90 minutes, allowed to cool naturally to room temperature in the furnace, and tested approximately 24 hours later. Cylinders were tested in the residual condition because the residual strength is expected to be lower than the equivalent high temperature strength (Schneider, 1988): enabling a lower bound to be established for the strength of the concrete in the tested walls. The compression tests and split-cylinder tension tests were performed in accordance with ASTM C39 (ASTM, 2017c) and ASTM C496 (ASTM, 2017d), respectively.

The dynamic modulus of elasticity was measured before and after heating for all of the cylinders: the ambient and residual conditions, respectively. This modulus was calculated in accordance with ASTM C215 (ASTM, 2014a). The specimen was struck with a small impactor (hammer) and its response was measured by an accelerometer. The fundamental frequency of the specimen was calculated from the acceleration response, and equations in ASTM C215 were used to calculate the corresponding dynamic modulus. The dynamic modulus was measured instead of the static modulus because the test is nondestructive and could measure the effect of elevated temperature alone on concrete stiffness. The data of Phan and Carino (2002) make clear that the percentage reduction in dynamic modulus with increasing temperature in the residual condition is similar to the reduction in static modulus of elasticity in both heated and residual conditions. Accordingly, the reductions observed in dynamic modulus with increasing temperature are deemed to apply to the static modulus used to assess the lateral stiffness of the walls.

The average uniaxial compressive strength and split-cylinder tensile strength at ambient temperature were 5.3 ksi [37 MPa] and 0.7 ksi [5 MPa], respectively. This split-cylinder tension strength corresponds to approximately $9.6\sqrt{f_c}$ [$0.8\sqrt{f_c}$], where f_c is the uniaxial compressive strength in psi [MPa] units. The average dynamic modulus of elasticity at ambient temperature was 5,300 ksi [36,500 MPa], which corresponds to approximately $72,000\sqrt{f_c}$ [$6,000\sqrt{f_c}$], and is approximately 25% greater than the ACI 318-14 value of $57,000\sqrt{f_c}$ [$4,700\sqrt{f_c}$] for the static modulus of elasticity, which is in the range of 20% to 30% identified by Mindess et al. (2003). (The dynamic modulus is greater than the static modulus because the stress-strain relationship for concrete is nonlinear, the static modulus is traditionally measured at a stress level of approximately 40% of ultimate compressive stress, and the dynamic modulus, which is the initial tangent modulus, is measured at an infinitesimally small stress (Mindess et al., 2003).)

The variation in weight loss, compression strength, split-cylinder tension strength, and dynamic modulus of elasticity with temperature are presented in Figure 3-17, Figure 3-18, Figure 3-19 and Figure 3-20, respectively. For the concrete used in this study, at 300°F [149°C], there is reduction of approximately 10%, 10% and 20% in the residual (measured at room temperature after cooling) compressive strength, split-cylinder tensile strength and the dynamic modulus of elasticity, respectively. These percentage reductions are greater than those expected in the heated condition because cooling after heating generates additional damage due to rehydration of the cement paste (Willam et al., 2009). The corresponding percentage reductions at 450°F [232°C] are 10%, 10%, and 30%.

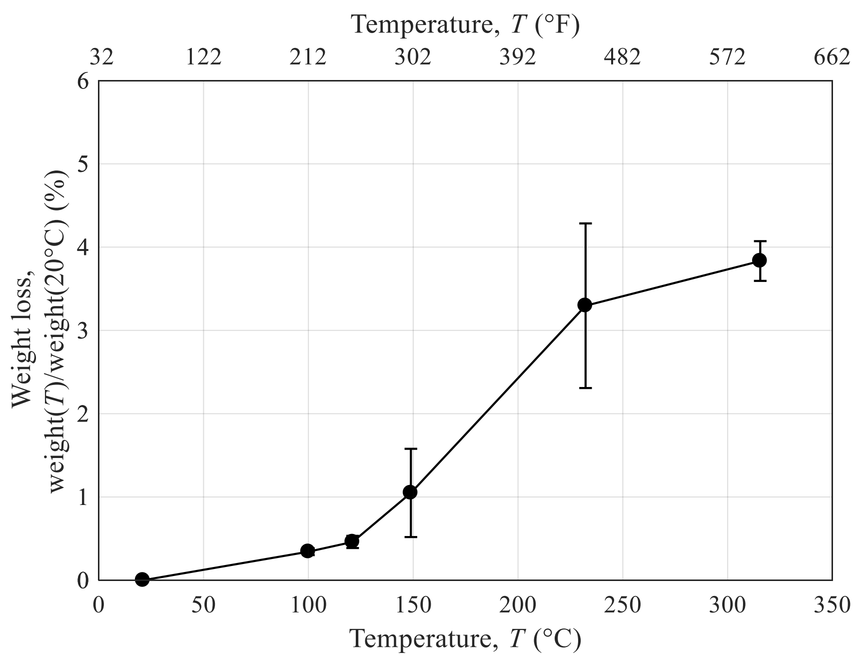

Figure 3-17. Variation in concrete weight loss with temperature

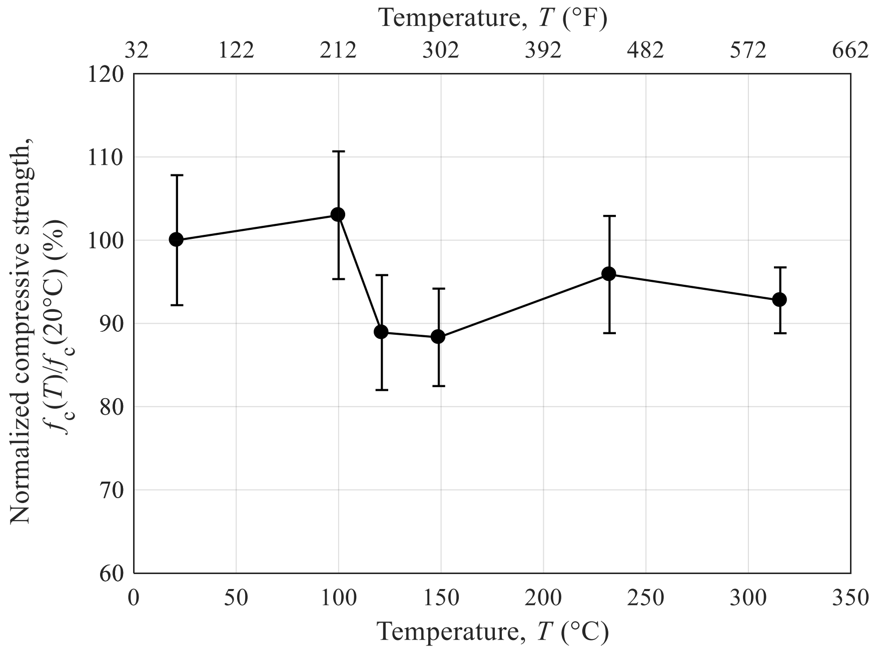

Figure 3-18. Variation in concrete compressive strength with temperature

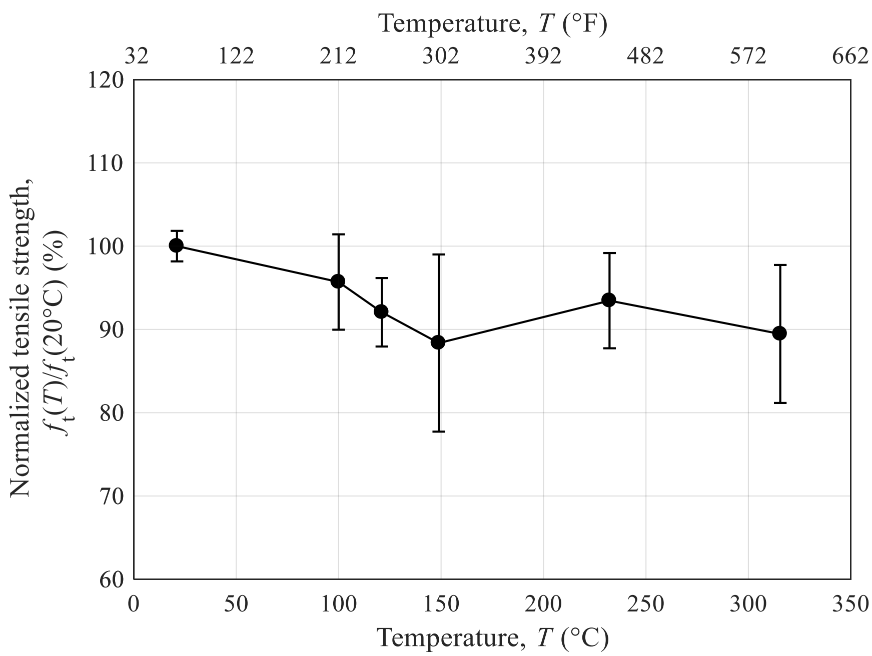

Figure 3-19. Variation in concrete split-cylinder tensile strength with temperature

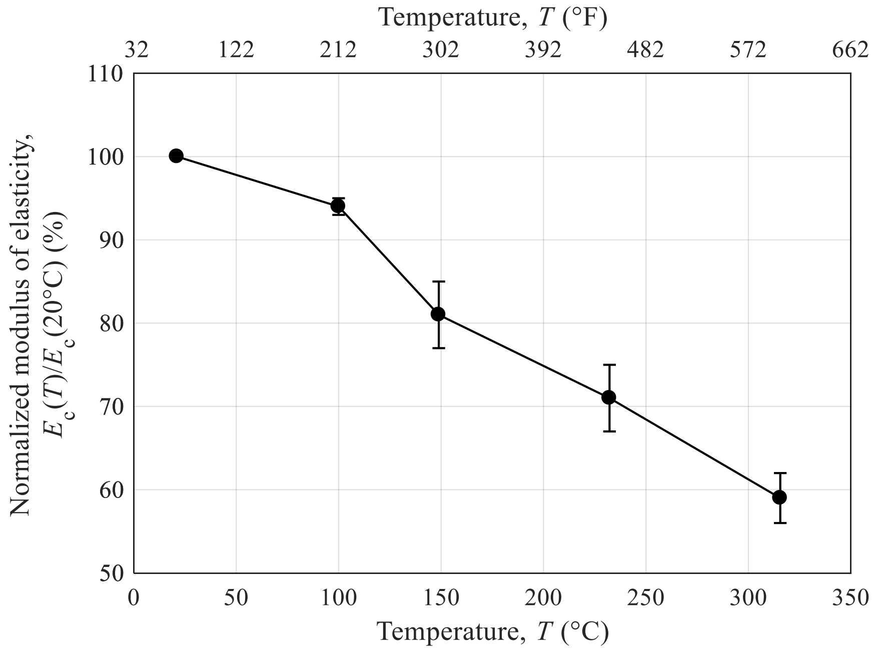

Figure 3-20. Variation in concrete dynamic modulus of elasticity with temperature

3.8 Wall test setup

The steps involved in each wall test at Purdue University involved the following activities: 1) wall surface preparation, 2) positioning the wing foundation beams and the wall specimen, 3) horizontal post-tensioning of the three foundations, 4) vertical post-tensioning of the foundation assembly to the strong floor, 5) attachment of the loading assembly, and 6) installation of the instrumentation. The heater assembly and surface thermocouples were installed only for the heated cycles and were removed after the heated cycles had been completed. Details and a photograph of the test set-up are shown in Figure 3-21 and Figure 3-22, respectively.

The wall specimens were cast with PVC pipes at locations where Dywidag bars or bolts were designated to pass. The PVC pipes were coated with grease before casting and were extracted after removing the formwork. Surface irregularities near the hole locations and edges were eliminated with the use of a concrete grinder to provide a relatively flat surface.

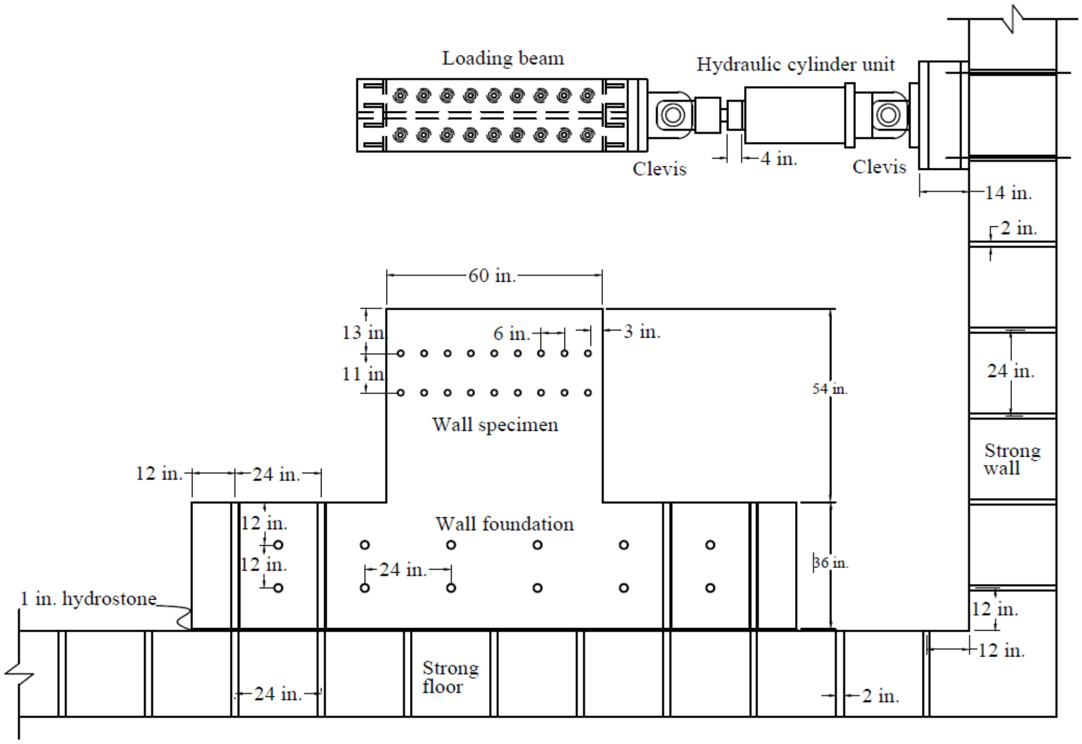

Figure 3-21. Side view of the test set-up
(Note: 1 in. = 25.4 mm; Thickness of strong wall and floor not to scale)

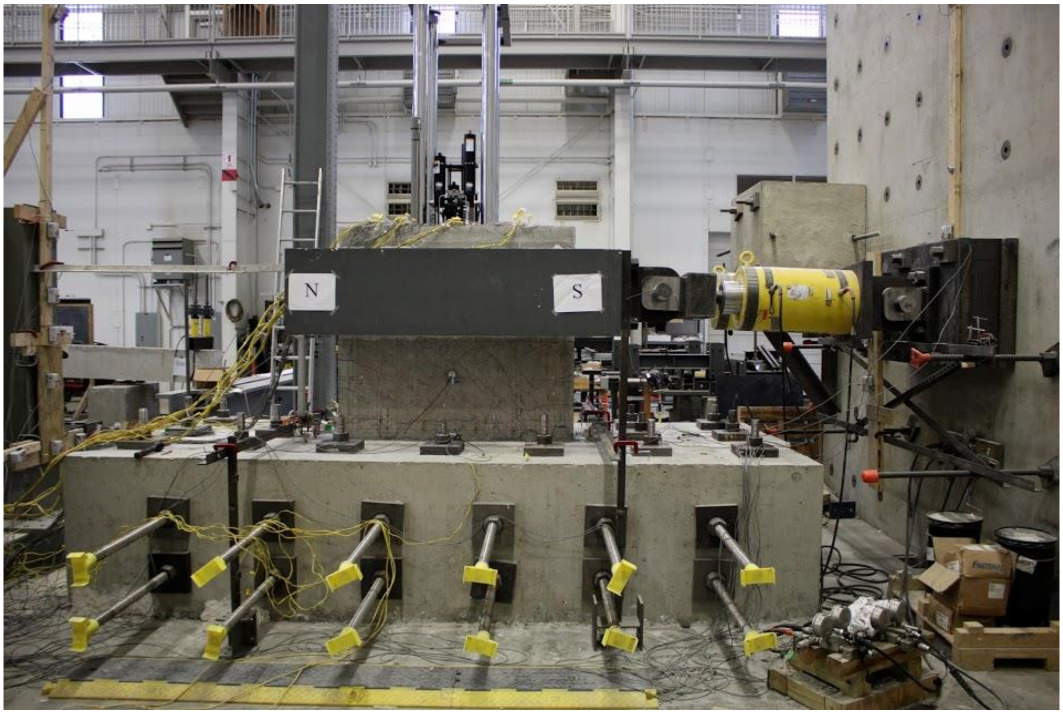

Figure 3-22. Side view of Wall 3 during testing

Hydrostone was placed around the holes in the strong floor that were to be used to engage the foundation assembly. The two wing foundation beams and wall specimen (with its own foundation) were then placed together and aligned with the holes in the strong floor. Hydrostone paste was placed along the edge of the vertical gap between the wall foundation and the wing foundation beams and allowed to set for about 30 minutes. Thinner hydrostone was then poured into the two horizontal gaps between the three foundation parts from the top of the foundation and allowed to set for approximately 24 hours.

The loading beams were then attached to the wall specimen as discussed in Section 3.5. Hydraulic cylinder units were then attached to the loading beam and the strong wall. Each unit had a clevis attached at both ends through which it was connected to the loading beam and to the strong wall using pins.

The formwork for the wall foundations was built 0.5 inch [12.7 mm] higher than specified. The PVC pipes used for the thru-holes for later installation of the loading apparatus were placed 1 in. [25.4 mm] higher in the formwork than specified. These errors resulted in the loading centerline being 1.5 in. [38 mm] higher than designed and the hydraulic cylinders were therefore angled at approximately 1.5° to the horizontal.

3.9 Instrumentation

The instrumentation for measuring deformations and displacements of the wall consisted of strain gages (attached to wall rebar), string potentiometers, linear potentiometers, and inclinometers. Temperatures on the wall surface and insides were measured using Type-K thermocouples. The instrumentation was the same for all wall specimens.

Type ZFLA strain gages, manufactured by Tokyo Sokki Kenkyujo Co. Ltd. (http://www.tml.jp/e) were used to measure the axial strain in the rebar. These gages are designed for use at temperatures up to 572°F [300°C] and can record strains of up to 15%. The manufacturer’s recommendations were followed for attaching the gages. The rebar surface was prepared by grinding using a #36 grit disc, mechanical sanding using a #120 sandpaper and finished using a #220 sandpaper. The surface was then cleaned using denatured alcohol followed by M-Prep Conditioner A and M-Prep Neutralizer 5A. The strain gages were glued to the prepared rebar surface using NP-50B, supplied by Texas Measurements: a two-part adhesive designed for use in high-temperature applications. The gages were then covered with a silicone compound designed for high-temperature use, for waterproofing. The lead wires were taped to the rebar.

String potentiometers and linear potentiometers were used to measure the in-plane and out-of-plane displacements of the wall. The layout of the string potentiometers is shown in Figure 3-23. Two pairs of inclinometers were used to measure in-plane wall rotations at two locations, 2 and 15 inches from the top of the foundation, with one pair each on the west and east faces. The inclinometers measured the rotation of the wall with respect to the vertical. The two inclinometers attached to the base of the wall recorded data for the duration of the test, but the pair attached 15 in. [381 mm] above the base had to be removed for the heated cycles to accommodate the heaters. String potentiometers were also used to measure the in-plane slip of the foundation assembly with respect to the strong floor. Two sets of three linear potentiometers, one for each foundation block, were used to measure the uplift of the foundation assembly, 2 in. [50.8 mm] from the toe of the wall, with respect to the strong floor. Strain gages were attached to the wall rebar prior to assembling the rebar cages, as described previously. Thirty-eight strain gages were attached to rebar in each wall. The locations and numbering of the gages are identified in Figure 3-24.

Each thermocouple was a Type-K, conforming to ASTM E230 (ASTM, 2017b), and was prepared by twisting together a strand of nickel-chromium alloy (chromel) with a strand of nickel-aluminum alloy (alumel). The alloy strands were manufactured by Omega Engineering (https://www.omega.com/). The thermocouples were capable of measuring temperatures up to 2462°F [1350°C].

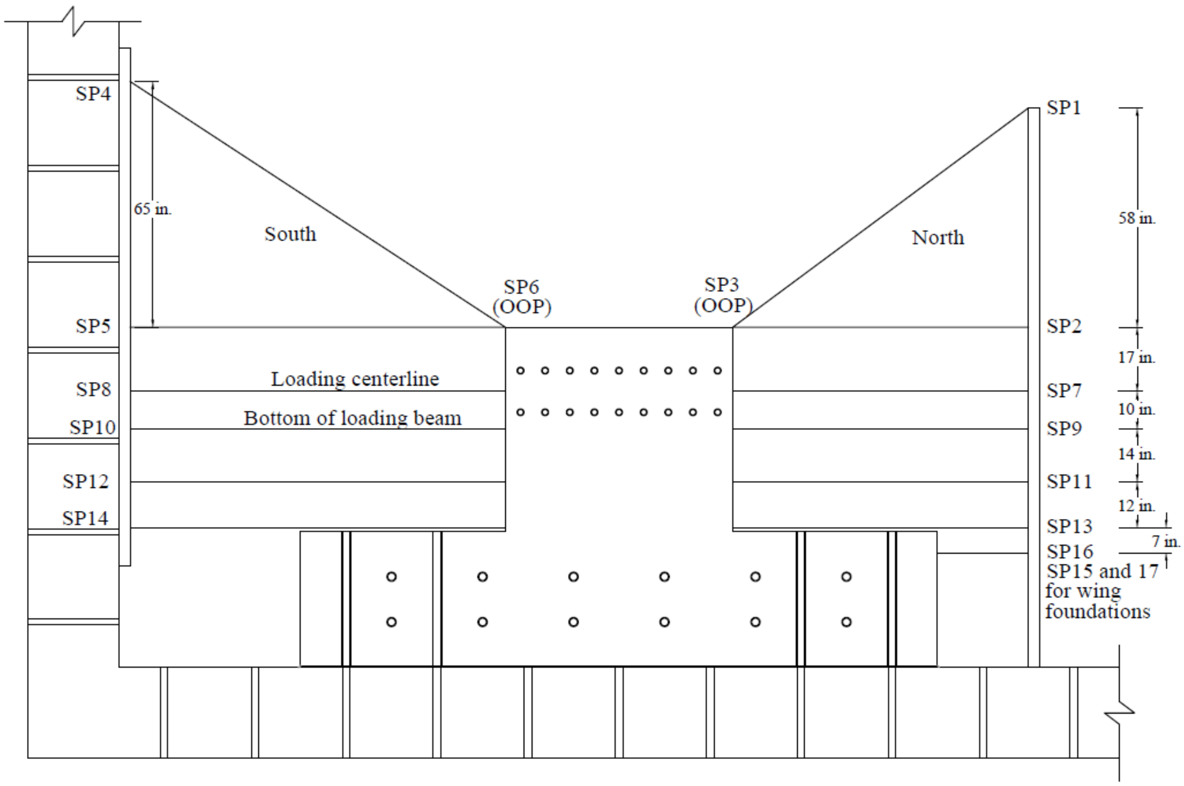

Figure 3-23. String potentiometer layout for all wall specimens

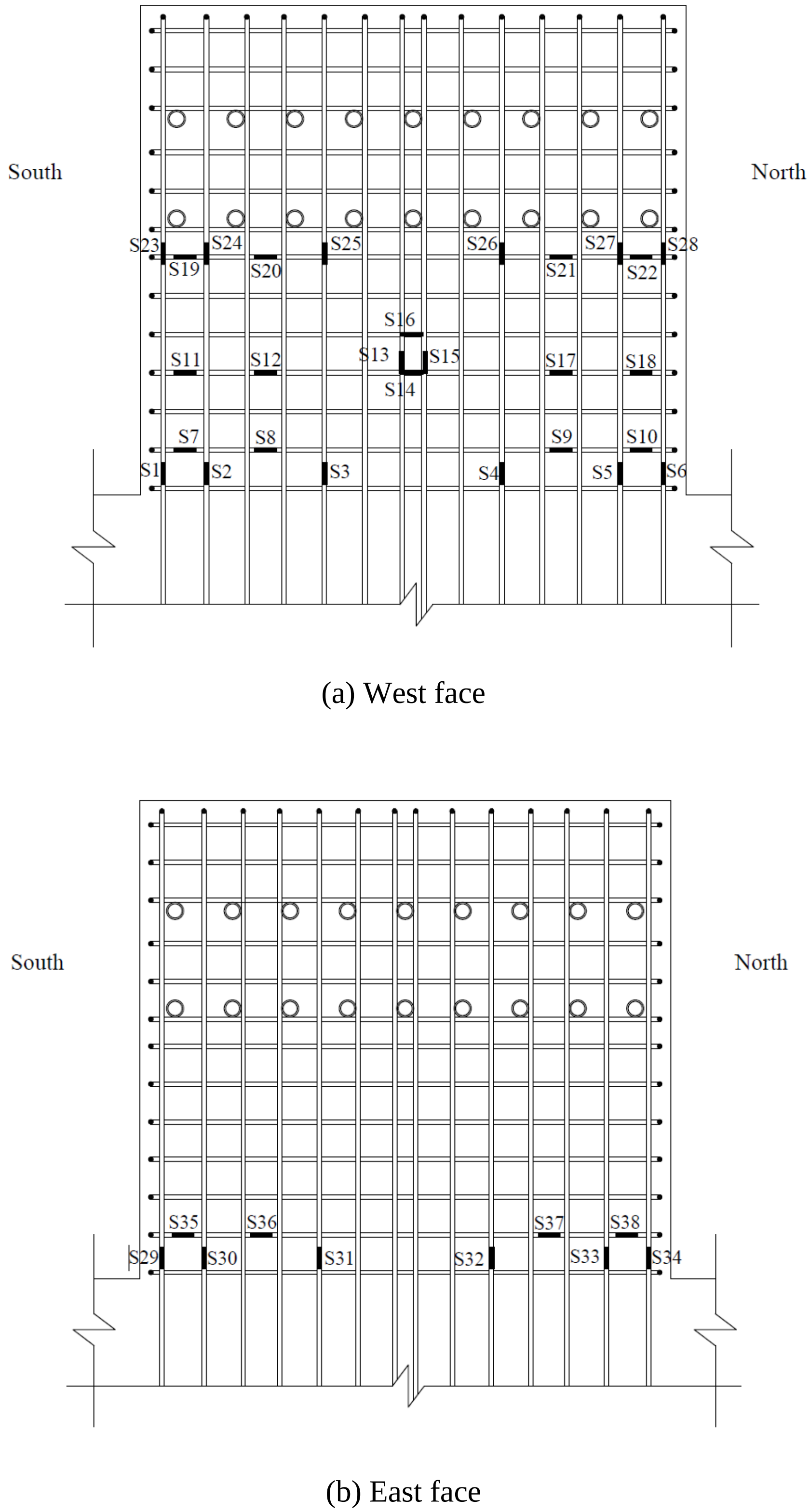

(a) West face

(b) East face

Figure 3-24. Strain gage layout for all walls

In-plane lateral loads were applied to the wall specimen by two Enerpac hydraulic cylinder units. Each unit had a capacity of 1,148 kips [5,109 kN] in compression and 638 kips [2,839 kN] in tension and a stroke of 12 in. [304.8 mm]. One oil pump pressurized both units. The oil hose from the pump was split using a valve into hoses that were attached to individual units. Transducers were installed downstream of the valve to measure the pressure in each of the four hoses. The force in each hydraulic unit was calculated by multiplying the measured pressure by the piston area. Transducers measuring the in-plane displacement of the wall were used to control the stroke of the hydraulic unit.

A National Instruments data acquisition system (or DAQ) was used to collect and process the collected data. A LabVIEW (NI, 2017) script was used to control the imposed forces and displacements. The same script also collected data from the sensors during a test. Raw data was collected from all the sensors at a frequency of 10 Hz. This raw data was then averaged over 10 consecutive measurements and recorded in the data files. The effective frequency of data collection was, therefore, 1 Hz.

3.10 Loading protocols

The walls were subjected to unique mechanical and thermal loading protocols, designed to maximize the output from the tests of a limited number of specimens. Two peak temperatures were used for the thermal loadings: 300°F [149°C] and 450°F [232°C]. Displacements or forces were applied in directions denoted push and pull. The push direction was south to north per Figure 3-22. The pull direction was north to south.

Lateral stiffness was calculated at forces of approximately 25% of the estimated peak lateral strength, at ambient temperature, for each wall. This calculation was repeated in the heated condition to characterize the effect of elevated temperature.

The peak lateral strength of each wall was recorded in a heated condition. The strength was assumed to have been captured when substantially increasing the wall drift did not result in an increase in the resisting force. The specimen was then allowed to cool to ambient temperature and strength was then measured again. Subsequent cycles were performed till the wall resistance dropped to less than 75% of the peak lateral strength. The test was then terminated.

The loading protocols for each wall are discussed in detail in the Chapter 4.

CHAPTER 4
PROTOCOL AND RESULTS OF RC WALL TESTS

4.1 Introduction

This chapter presents the loading protocols for and results of analysis of data from the reversed cyclic testing of the four structural walls introduced in Chapter 3. The specimens were tested between June and October 2017. Procedures used to process the raw data are described in Section 4.2. The test protocol, results and observations for Wall 1, Wall 2, Wall 3 and Wall 4 are presented in Sections 4.3, 4.4, 4.5 and 4.6, respectively.

4.2 Data processing

The displacement reported in the global force-displacement relations in this chapter was measured at the centerline of loading, which was 940 mm [37 in.] above the top of the foundation. Minor in-plane sliding movement of the foundation assembly was observed in some of the load cycles. This movement was less than 5% of the displacement recorded at the loading centerline for that load cycle. The displacements reported in this chapter were corrected by subtracting this foundation movement.

The reported lateral force was calculated as the sum of the axial forces applied by the Enerpac (https://www.enerpac.com/en-us/) hydraulic units, without correction for the angle of inclination of the units to the horizontal. Out-of-plane (OOP) displacements were measured at the top of the wall using two string potentiometers. These displacements were small and so are not discussed further in this chapter.

Heating expanded the walls and so it was expected that prior to mechanical loadings the sensors at the north and south ends would record equal but opposite displacements. However, this was not observed in any of heating phases. The sensors at the north and south ends indicated that the walls displaced in their plane, in one direction, due to heating. This was confirmed by the rotation sensors attached to the base of the walls, which indicated that there were small rotations at the base of the walls associated with heating, producing a crack at the base of each wall. The rotations were measured at a point that was located at mid-length of the wall and about 51 mm [2 in.] above the foundation. The corresponding displacement, of the order of 0.25 mm [0.01 in.], at the centerline of loading was used to correct the lateral force-displacement relationships associated with the mechanical loading.

The secant stiffness for all load cycles and all walls was estimated using two methods. In the first method, designated as I quad hereafter, a point on the force-displacement relationship near the maximum push force was chosen and the stiffness calculated using the origin as a reference. In the second method, designated as I-III quads hereafter, two points on the force-displacement relationship were chosen, and the slope of the line joining these two points was used to calculate the secant stiffness. Two methods were employed to estimate secant stiffness because of spurious displacement readings in some of the load cycles and apparent drifting of some sensors under sustained loadings. An example calculation is illustrated in Figure 4-1.

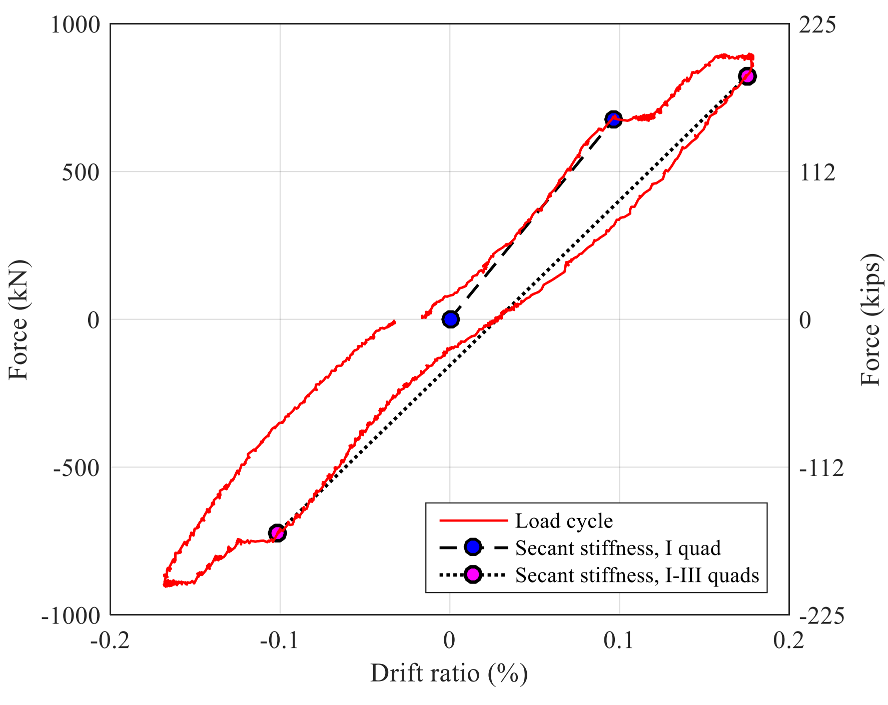

Figure 4-1. Calculations of secant stiffness for LC4 of Wall 2

4.3 Wall 1

Wall 1 was tested between June 30, 2017 and July 12, 2017. The average uniaxial compressive strength of the concrete was 43 MPa [6.3 ksi], based on tests performed during the testing phase. The age of the wall at the start of testing was 86 days. Wall 1 was reinforced with two curtains of #4 bars spaced vertically and horizontally at 102 mm [4 in.] for a reinforcement ratio of 0.93% in each direction. The lateral strength of Wall 1 was expected to be limited by moment capacity to approximately 1224 kN [275 kips], based on the provided reinforcement and day-of-test concrete strength.

4.3.1 Protocol

Two loading cycles (LC1 and LC2) were performed at ambient temperature, at lateral forces corresponding to approximately 25% and 40% of the estimated peak lateral strength. The wall was heated to a target surface temperature of 300°F [149°C] after LC2, and the two load cycles of LC1 and LC2 were repeated, designated as LC3 and LC4. The displacement at the centerline of loading at peak lateral resistance in LC4 was designated as the reference displacement, d*, and further cycles were applied in increments of d*. Two cycles were performed at each target displacement until the strength of the wall in the heated condition had been reached, which occurred in LC15.

The heaters were switched off after LC15 and removed, and the wall cooled to room temperature, after which additional cycles of loading were applied. Most of the subsequent cycles were imposed in increments of d*, starting at the displacement at which testing was stopped in the heated condition. One cycle was performed at each level and loading was continued till the wall *failed*. The loading protocol for Wall 1 is summarized in Table 4-1.

.

Table 4-1: Loading protocol for Wall 1

Load cycle	Time after test start (days)	Surface temperature (°F[a])	Heating duration at start of cycle (min)	Load target	Amplitude
LC1	0	Ambient	-	Force	75 kips[a]
LC2	6	Ambient	-	Force	120 kips
LC3	10	300	15	Force	75 kips
LC4	10	300	27	Force	120 kips[b]
LC5	10	300	45	Displacement	1.5d*
LC6	10	300	69	Displacement	1.5d*
LC7	10	300	106	Displacement	2d*
LC8	10	300	130	Displacement	2d*
LC9	10	300	153	Displacement	3d*
LC10	10	300	181	Displacement	3d*
LC11	10	300	209	Displacement	4d*
LC12	10	300	236	Displacement	4d*
LC13	10	300	257	Displacement	5d*
LC14	10	300	283	Displacement	6d*
LC15	10	300	308	Displacement	7d*
LC16	12	Ambient	-	Force	75 kips
LC17	12	Ambient	-	Force	120 kips
LC18	12	Ambient	-	Force	240 kips
LC19	12	Ambient	-	Disp.	8.3d*
LC20	12	Ambient	-	Disp.	10d*
LC21	12	Ambient	-	Disp.	12d*
LC22	12	Ambient	-	Disp.	14d*
LC23	12	Ambient	-	Disp.	16.7d*
LC24	12	Ambient	-	Disp.	18.3d*
LC25	12	Ambient	-	Disp.	21.7d*

[a] °F = °C×1.8 + 32; 1 kip = 4.45 kN

[b] Displacement measured in this cycle designated as the reference displacement, d*

4.3.2 Results

The global force-drift ratio relationship for all cycles of loading performed on Wall 1 is presented in Figure 4-2. The maximum forces, displacements (measured at loading centerline) and secant stiffness recorded in each cycle are summarized in Table 4-2. The values of secant stiffness reported in Table 4-2 are calculated using the methods described in Section 4.2, and have been normalized by the theoretical value of secant stiffness, k_t, calculated using strength of mechanics formulation and day-of-test uniaxial compressive strength of concrete.

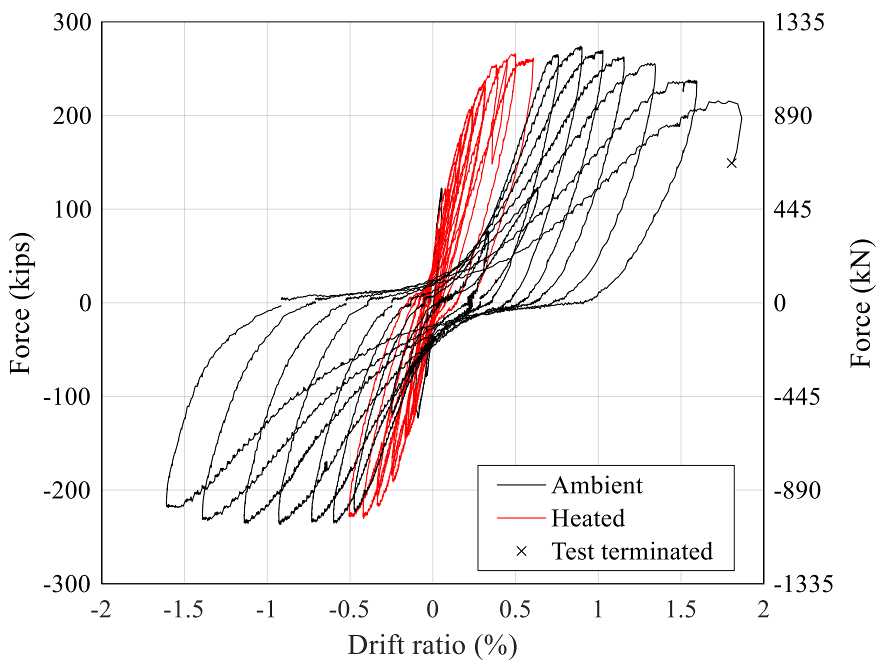

Figure 4-2. Global force-drift ratio relationship for Wall 1

The locations of the thermocouples (identified by CT) embedded in the wall and the temperatures at the start of each heated load cycle are shown in Figure 4-3 and Figure 4-4, respectively. Figure 4-4 (e) provides a legend for Figure 4-4 (a) through (d). The surfaces of the wall were maintained at the target temperature of 300°F [149°C] for all heated cycles; the surface temperatures are not plotted in Figure 4-4. The temperature in the center of the wall was about 100°F [38°C] at the start of the first heated cycle (LC3) and reached about 230°F [110°C] at the start of the last heated cycle (LC15), about 5 hours later, as shown in Figure 4-4.

The secant stiffness in the load cycle performed to a force level of about 40% of the peak strength, at elevated temperature (LC4) was about 20% less than in the corresponding cycle at room temperature (LC2). No significant reduction in lateral stiffness was observed in the load cycles performed to the same displacement in subsequent cycles. Accordingly, the loss of stiffness from LC2 to LC4 is attributed to cracking due to thermal effects and not due to mechanical damage resulting from cyclic loading. The pattern of cracking on a surface of the wall after LC2 is presented in Figure 4-5. Only a few flexure and flexure-shear cracks are evident. (A corresponding photograph after LC4 is not available because the heaters prevented a photograph being taken of the surfaces of the wall.)

The peak lateral strength at 300°F [149°C] was approximately 1179 kN [265 kips]. The pattern of cracks on the East face of Wall 1 after cycling at elevated temperature is presented in Figure 4-6. The peak lateral strength in the residual condition (i.e., at room temperature after the wall was allowed to cool naturally) was approximately 1201 kN [270 kips]. (Both values are within 5% of the estimated lateral strength at room temperature per Table 2.) The secant stiffness and strength of the wall deteriorated in subsequent cycles (LC22 to LC25) to greater displacements. The wall failed in LC25 at a drift ratio of approximately 1.8%. The damage sustained by the wall is shown in Figure 4-7.

Table 4-2: Summary of results for Wall 1

Load cycle	Surface temperature (°F[a])	IP displacement (in[a])		IP force (kips[a])		Secant stiffness[b], I quad		Secant stiffness[b], I-III quad	
		max	min	max	min	k_s (kips/in[a])	$\frac{k_s}{k_t}$	k_s (kips/in[a])	$\frac{k_s}{k_t}$
LC1	Ambient	NA[c]	NA[c]	79	-79	NA[c]	NA[c]	NA[c]	NA[c]
LC2	Ambient	0.020	-0.033	122	-123	6,300	0.33	4,100	0.22
LC3	300	0.012	-0.023	79	-75	6,300	0.33	4,300	0.23
LC4	300	0.028	-0.044	122	-120	4,200	0.22	3,300	0.17
LC5	300	0.050	-0.055	150	-141	3,300	0.17	2,500	0.13
LC6	300	0.036	-0.061	121	-148	3,300	0.17	2,600	0.14
LC7	300	0.063	-0.059	180	-144	3,000	0.16	2,500	0.13
LC8	300	0.061	-0.060	169	-145	2,700	0.14	2,600	0.14
LC9	300	0.088	-0.089	210	-191	2,600	0.14	2,100	0.11
LC10	300	0.088	-0.092	207	-184	2,400	0.13	2,000	0.11
LC11	300	0.116	-0.121	237	-217	2,200	0.12	1,800	0.10
LC12	300	0.114	-0.124	228	-208	2,000	0.11	1,800	0.10
LC13	300	0.142	-0.155	254	-230	2,000	0.11	1,500	0.08
LC14	300	0.183	-0.186	266	-229	1,600	0.08	1,300	0.07
LC15	300	0.225	-0.056	261	-	1,400	0.07	NA[d]	NA[d]
LC16	Ambient	0.124	-0.051	77	-78	600	0.03	900	0.05
LC17	Ambient	0.233	-0.091	122	-119	1,000	0.05	1,100	0.06
LC18	Ambient	0.106	-0.174	-	-223	NA[d]	NA[d]	NA[d]	NA[d]
LC19	Ambient	0.279	-0.221	265	-235	1,000	0.05	1,000	0.05
LC20	Ambient	0.331	-0.270	274	-234	900	0.05	800	0.04
LC21	Ambient	0.380	-0.340	269	-237	800	0.04	700	0.04
LC22	Ambient	0.426	-0.413	263	-236	700	0.04	600	0.03
LC23	Ambient	0.487	-0.503	256	-233	600	0.03	500	0.03
LC24	Ambient	0.572	-0.570	238	-219	500	0.03	400	0.02
LC25	Ambient	0.638	-0.321	216	-	300	0.02	NA[d]	NA[d]

[a] °F = °C*1.8+32; 1 kip = 4.45 kN; 1 in. = 25.4 mm

[b] Calculated value and normalized by k_t (= 18,900 kips/in)

[c] Unequal positive and negative displacements recorded

[d] Fully reversed cyclic loading not applied

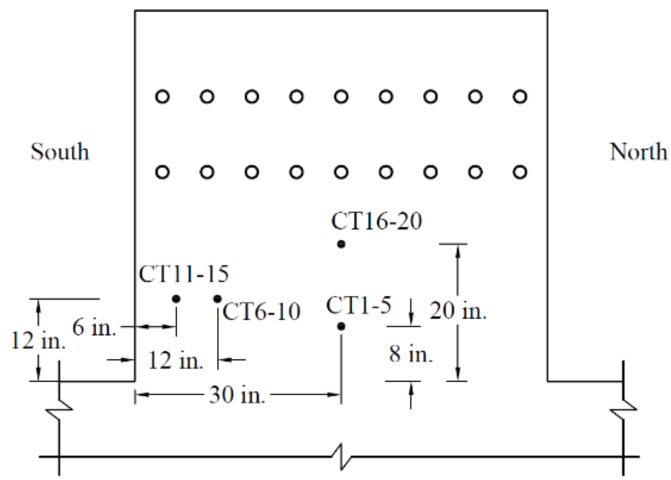

Figure 4-3. Locations of embedded thermocouples in Wall 1

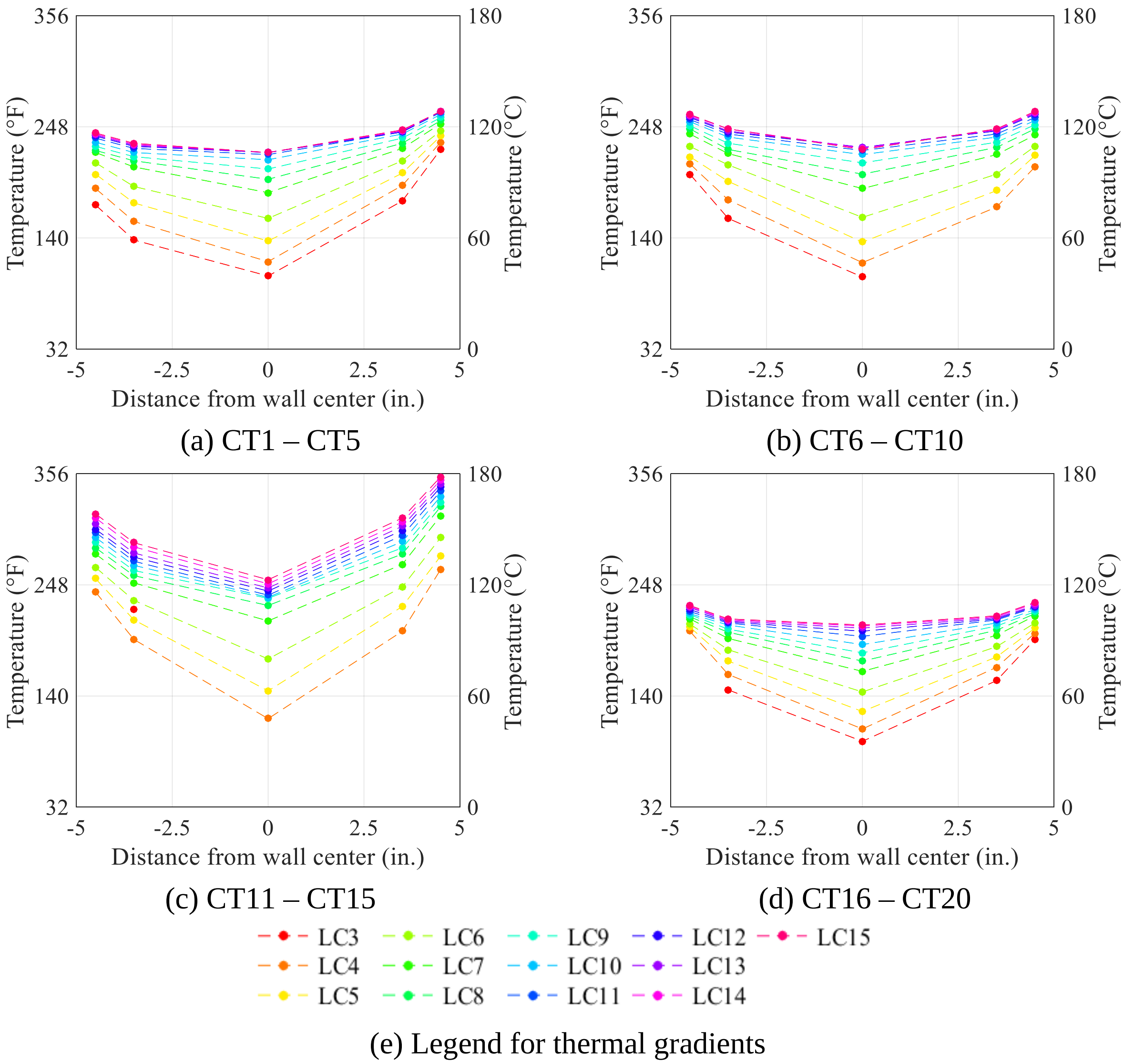

Figure 4-4. Thermal gradients at the start of all heated cycles for Wall 1 [Note: 1 in. = 25.4 mm]

Figure 4-5. Crack pattern on East face of Wall 1 after LC2

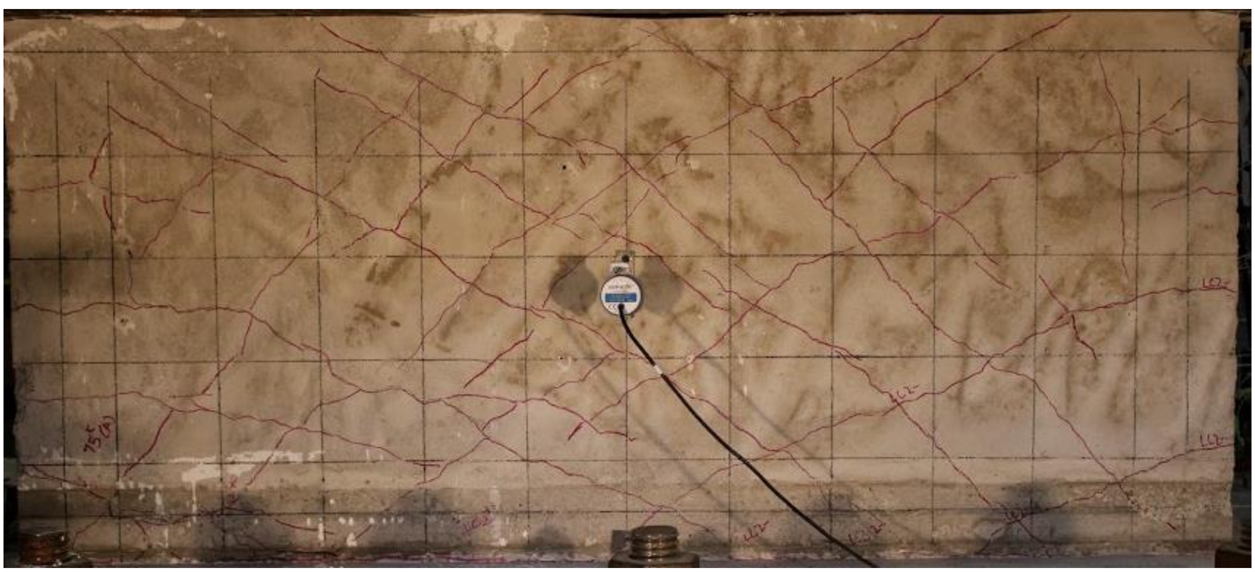

Figure 4-6. Crack pattern on East face of Wall 1 after LC15

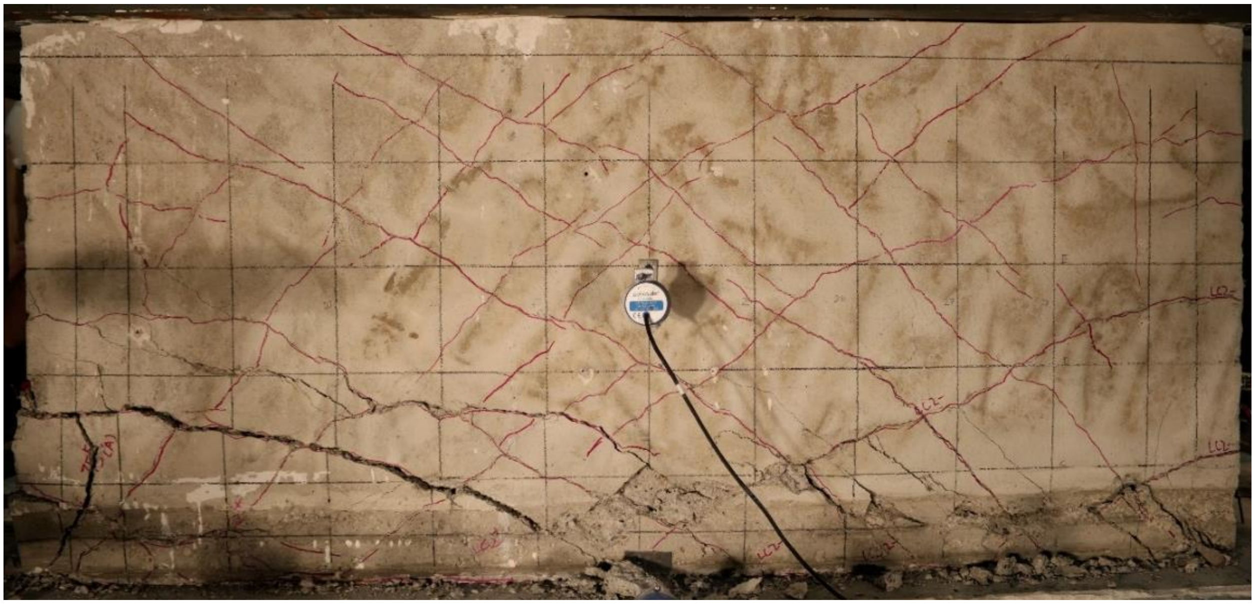

Figure 4-7. Damage to Wall 1 at the end of testing

4.4 Wall 2

Wall 2 was tested between July 27, 2017 and August 9, 2017. The average uniaxial compressive strength of the concrete was 41 MPa [6 ksi], based on tests performed during the testing phase. The age of the wall at the start of testing was 52 days. Wall 2 was reinforced with two curtains of #6 bars spaced vertically and horizontally at 102 mm [4 inches] for a reinforcement ratio of 2% in each direction. The lateral strength of Wall 2 was expected to be limited by shear capacity to approximately 2047 kN [460 kips], based on the provided reinforcement and day-of-test concrete strength.

4.4.1 Test protocol

Four loading cycles (LC1 to LC4) were performed at room temperature, at lateral forces corresponding to approximately 15%, 25%, 25% and 40% of the estimated peak lateral strength. The wall was heated to a target surface temperature of 450°F [232°C] after LC4. Cycles were performed at same force level as that applied for LC4 after two periods of heating: 15 minutes for LC5 and 120 minutes for LC6. The surfaces of the wall were maintained at 450°F [232°C] between cycles LC5 and LC6. The displacement at the centerline of loading at the peak lateral resistance in LC6 was 0.065 inch [1.65 mm] and this was designated as the reference displacement, d*, for this test. The heaters were removed after LC6 and wall cooled naturally to room temperature. This procedure was repeated for displacements of 1.5d* (LC7 and LC8), 2d* (LC9 and LC10), 3d* (LC11 and LC12), 4d* (LC13 and LC14), and 5d* (LC15 and LC16). The odd-numbered and even-numbered cycles were performed after 15 minutes and 120 minutes of heating, respectively. The strength of the wall at a surface temperature of 450°F [232°C] was reached in LC16. One subsequent cycle of loading was applied at a displacement of 5d* in the residual condition (i.e., after wall had cooled to ambient), during which the wall *failed*.

Table 4-3: Loading protocol for Wall 2

Load cycle	Time after test start (days)	Surface temperature (°F[a])	Heating duration at start of cycle (min)	Load target	Amplitude
LC1	0	Ambient	-	Force	75 kips[a]
LC2	0	Ambient	-	Force	120 kips
LC3	1	Ambient	-	Force	120 kips
LC4	1	Ambient	-	Force	200 kips
LC5	4	450	15	Force	200 kips
LC6	4	450	120	Force	200 kips[b]
LC7	6	450	15	Displacement	1.5d*
LC8	6	450	120	Displacement	1.5d*
LC9	8	450	15	Displacement	2d*
LC10	8	450	120	Displacement	2d*
LC11	9	450	15	Displacement	3d*
LC12	9	450	120	Displacement	3d*
LC13	11	450	15	Displacement	4d*
LC14	11	450	120	Displacement	4d*
LC15	12	450	15	Displacement	5d*
LC16	12	450	120	Displacement	5d*
LC17	13	Ambient	-	Displacement	5d*

[a] °F = °C×1.8 + 32; 1 kip = 4.45 kN

[b] Displacement measured in this cycle designated as the reference displacement, d*

4.4.2 Test results

The global force-drift ratio relationship for all cycles of loading performed on Wall 2 is presented in Figure 4-8. The maximum forces, displacements (measured at loading centerline) and secant stiffness recorded in each cycle are summarized in Table 4-4. The values of secant stiffness reported in Table 4-4 are calculated using the methods described in Section 4.2, and have been normalized by the theoretical value of secant stiffness, k_t, calculated using strength of mechanics equations and day-of-test uniaxial compressive strength of concrete.

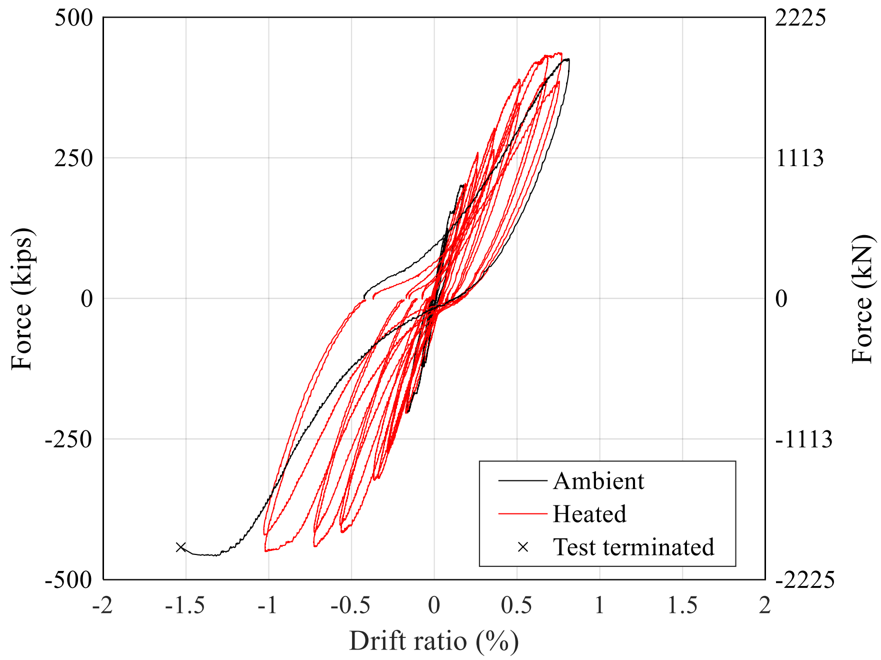

Figure 4-8. Global force-drift ratio relationship for Wall 2

The locations of the thermocouples (CT) embedded in the wall and the temperatures at the start of each heated load cycle are shown in Figure 4-9 and Figure 4-10, respectively. Figure 4-10 (e) provides a legend for Figure 4-10 (a) through (d). The surfaces of the wall were maintained at the target temperature of 450°F [232°C] for all heated cycles; the surface temperatures are not plotted in Figure 4-10. The temperature in the center of the wall was approximately 100°F [38°C] and 230°F [110°C] for all cycles performed after 15 minutes (LC5, LC7, LC9, LC11, LC13 and LC15) and 120 minutes (LC6, LC8, LC10, LC12, LC14 and LC16) of heating, respectively, as shown in Figure 4-10. The thermocouples embedded near the centerline of loading (CT11 to CT15) did not record temperatures higher than about 95°F [35°C] because the surfaces of the wall at this height were covered by the loading beams and not heated directly.

No significant differences in stiffness are observed in the loading cycles performed at a displacement of d*. At greater displacements, loading cycles performed at 120 minutes show a reduction in stiffness, but no greater than 10%, with respect to the cycles performed after 15 minutes of heating. This reduction of stiffness was likely due to mechanical damage resulting from cyclic loading and not from cracking due to thermal loadings.

The pattern of cracks on the West face of the wall after LC4, and prior to heating, is shown in Figure 4-11. Flexure and flexure-shear cracks are visible across the surface of the wall. The patterns of cracks at the end of LC8 (performed at 1.5d*), LC14 (performed at 4d*), and LC16 (performed at 5d*) are presented in Figure 4-12, Figure 4-13 and Figure 4-14, respectively. The number and length of the cracks increase with increasing displacements, which is consistent with fully reversed inelastic cyclic loading.

The peak lateral strength at ambient temperature (LC17) was 2046 kN [460 kips] and within 5% of the peak strength of 2003 kN [450 kips] measured in an earlier heated cycle (LC15). The wall *failed* in shear at a drift ratio of approximately 1.4%. The damage to the wall after all cycles of loading is shown in Figure 4-15.

Table 4-4: Summary of results for Wall 2

Load cycle	Surface temperature (°F[a])	IP displacement (in[a])		IP force (kips[a])		Secant stiffness[b],			
						I quad		I-III quad	
		max	min	max	min	k_s (kips/in)	$\frac{k_s}{k_t}$	k_s (kips/in)	$\frac{k_s}{k_t}$
LC1	Ambient	0.015	-0.011	80	-78	5,300	0.29	5,400	0.29
LC2	Ambient	0.030	-0.023	124	-122	4,900	0.27	4,700	0.25
LC3	Ambient	0.029	-0.028	125	-121	4,400	0.24	4,200	0.23
LC4	Ambient	0.065	-0.062	202	-203	4,300	0.23	3,400	0.18
LC5	450	0.070	-0.060	205	-204	2,900	0.16	3,100	0.17
LC6	450	0.069	-0.063	203	-205	2,900	0.16	3,000	0.16
LC7	450	0.097	-0.101	260	-272	2,600	0.14	2,700	0.15
LC8	450	0.095	-0.105	230	-274	2,400	0.13	2,500	0.14
LC9	450	0.134	-0.124	303	-320	2,300	0.12	2,400	0.13
LC10	450	0.132	-0.134	265	-323	2,000	0.11	2,200	0.12
LC11	450	0.189	-0.205	390	-417	2,100	0.11	2,100	0.11
LC12	450	0.190	-0.209	347	-404	1,800	0.10	1,900	0.10
LC13	450	0.248	-0.266	432	-442	1,900	0.10	1,700	0.09
LC14	450	0.249	-0.267	392	-416	1,600	0.09	1,600	0.09
LC15	450	0.277	-0.376	437	-450	1,700	0.09	1,400	0.08
LC16	450	0.279	-0.380	386	-421	1,400	0.08	1,200	0.07
LC17	Ambient	0.298	-0.487	426	-458	1,400	0.08	NA[c]	NA[c]

[a] °F = °C*1.8+32; 1 kip = 4.45 kN; 1 in. = 25.4 mm

[b] Calculated value and normalized by k_t (= 18,450 kips/in)

[c] Fully reversed cyclic loading not applied

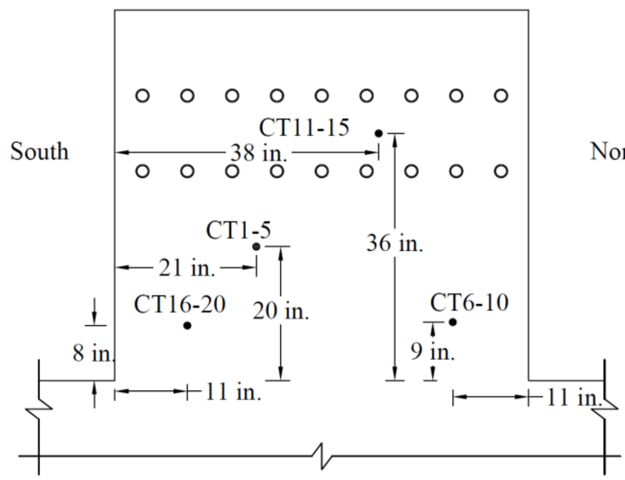

Figure 4-9. Locations of embedded thermocouples in Wall 2
[Note: 1 in. = 25.4 mm]

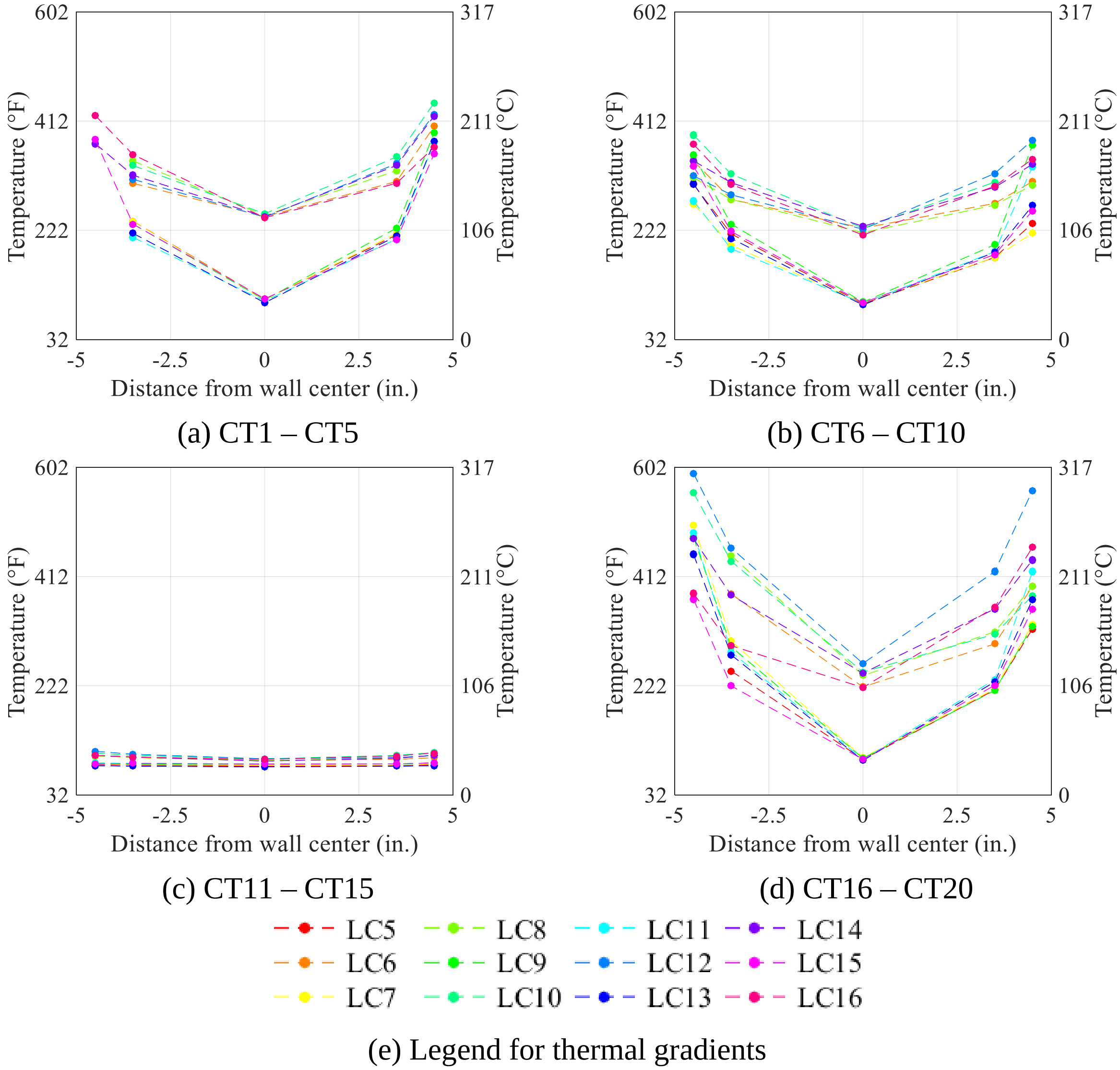

Figure 4-10. Thermal gradients at the start of all heated cycles for Wall 2 [Note: 1 in. = 25.4 mm]

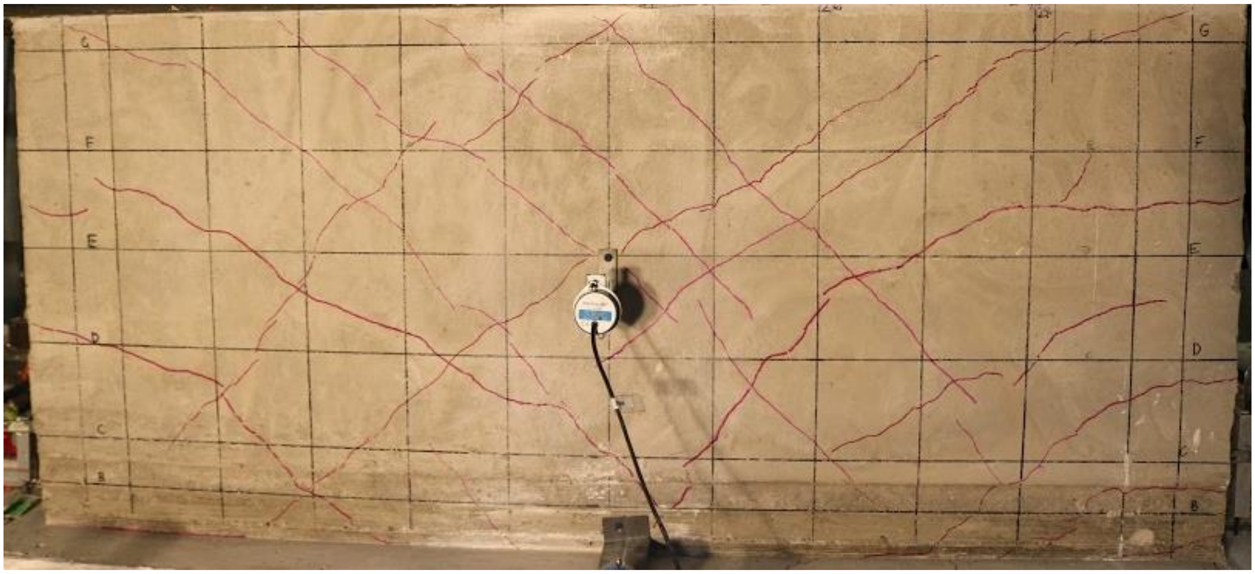

Figure 4-11. Crack pattern on West face of Wall 2 after LC4

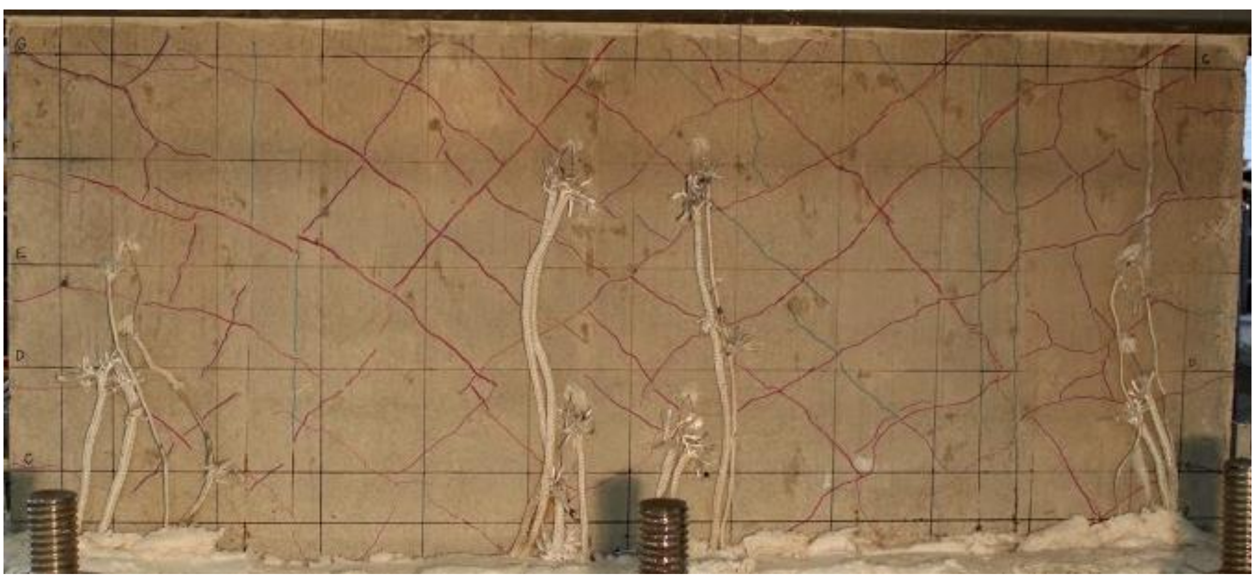

Figure 4-12. Crack pattern on West face of Wall 2 after LC8

Figure 4-13. Crack pattern on West face of Wall 2 after LC14

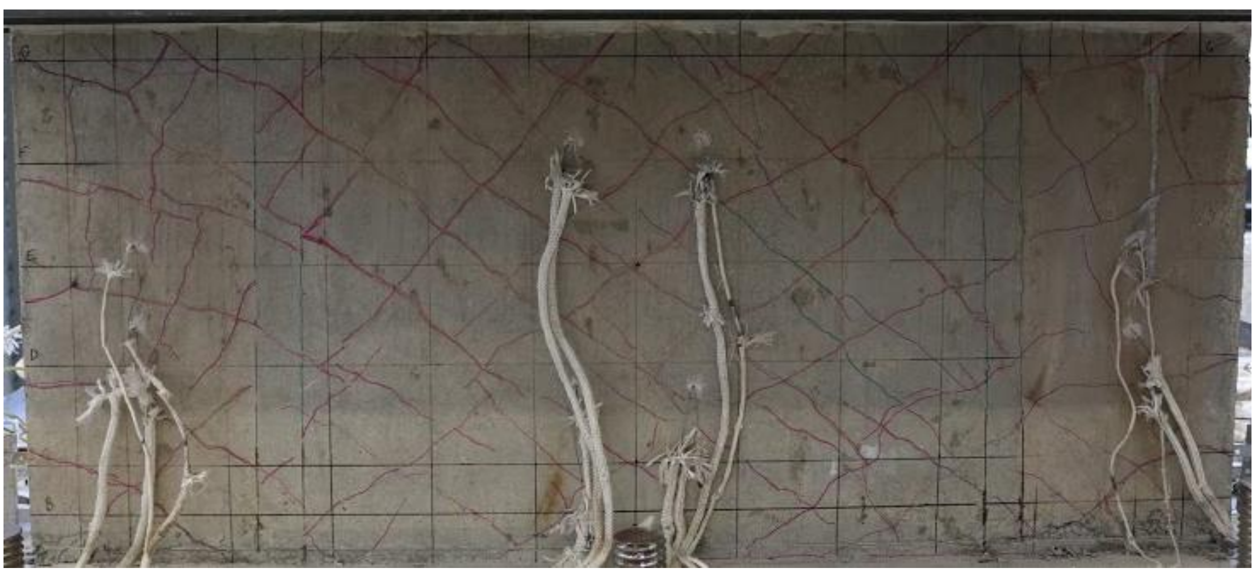

Figure 4-14. Crack pattern on West face of Wall 2 after LC16

Figure 4-15. Damage to Wall 2 at the end of testing

4.5 Wall 3

Wall 3 was tested between October 8, 2017 and October 14, 2017. The average uniaxial compressive strength of the concrete was 39 MPa [5.6 ksi], based on tests performed during the testing phase. The age of the wall at the start of testing was 108 days. Wall 3 was reinforced with two curtains of #6 bars spaced vertically and horizontally at 102 mm [4 inches] for a reinforcement ratio of 2% in each direction. The lateral strength of Wall 3 was expected to be limited by shear capacity to approximately 1958 kN [440 kips], based on the provided reinforcement and day-of-test concrete strength.

4.5.1 Test protocol

Two cycles (LC1 and LC2) were performed at ambient temperature, at forces corresponding to approximately 15% and 25% of the estimated lateral strength. After LC2, the wall was heated to a target surface temperature of 300°F [149°C] and one load cycle (LC3) was performed to the same maximum force of LC2, 15 minutes after the surface of the wall had reached the target temperature. The heaters were then removed and the wall cooled naturally to room temperature. One load cycle (LC4) was then performed to a force corresponding to approximately 40% of the estimated peak lateral strength. Load cycles LC5 and LC6 were performed to the same force level as LC4 but with surface temperatures of 300°F [149°C] and 450°F [232°C], respectively. Load cycles 5 and 6 were performed 15 minutes after the surface temperature reached the target value. The heaters were removed after LC5 and heating for LC6 began after wall had cooled naturally to room temperature. The displacement in LC6 was designated as d* and subsequent cycles were performed in increasing increments of d*. Two cycles were performed at each level till strength of the wall was reached in the heated condition. One cycle was performed at this level. The heaters were then switched off and the wall cooled naturally to room temperature. Additional cycles were performed in increasing increments of d* until the wall *failed*.

Table 4-5: Loading protocol for Wall 3

Load cycle	Time after test start (days)	Surface temperature (°F[a])	Heating duration at start of cycle (min)	Load target	Amplitude
LC1	0	Ambient	-	Force	75 kips[a]
LC2	0	Ambient	-	Force	120 kips
LC3	2	300	15	Force	120 kips
LC4	3	Ambient	-	Force	200 kips
LC5	3	300	15	Force	200 kips
LC6	4	450	15	Force	200 kips[b]
LC7	4	450	50	Displacement	1.6d*
LC8	4	450	89	Displacement	1.6d*
LC9	4	450	116	Displacement	2d*
LC10	4	450	148	Displacement	2d*
LC11	4	450	175	Displacement	3d*
LC12	4	450	215	Displacement	3d*
LC13	4	450	254	Displacement	4d*
LC14	4	450	307	Displacement	4d*
LC15	4	450	342	Displacement	5d*
LC16	5	Ambient	-	Displacement	5d*
LC17	5	Ambient	-	Displacement	6d*
LC18	5	Ambient	-	Displacement	7d*
LC19	6	Ambient	-	Force	120 kips
LC20	6	Ambient	-	Displacement	8d*
LC21	6	Ambient	-	Displacement	9d*

[a] °F = °C×1.8 + 32; 1 kip = 4.45 kN

[b] Displacement measured in this cycle designated as the reference displacement, d*

4.5.2 Test results

The global force-drift ratio relationship for all cycles of loading performed on Wall 3 is presented in Figure 4-16. The maximum forces, displacements (measured at loading centerline) and secant stiffness recorded in each cycle are summarized in Table 4-6. The values of secant stiffness reported in Table 4-6 are calculated using the methods described in Section 4.2, and have been normalized by the theoretical value of secant stiffness, k_t, calculated using strength of mechanics equations and day-of-test uniaxial compressive strength of concrete.

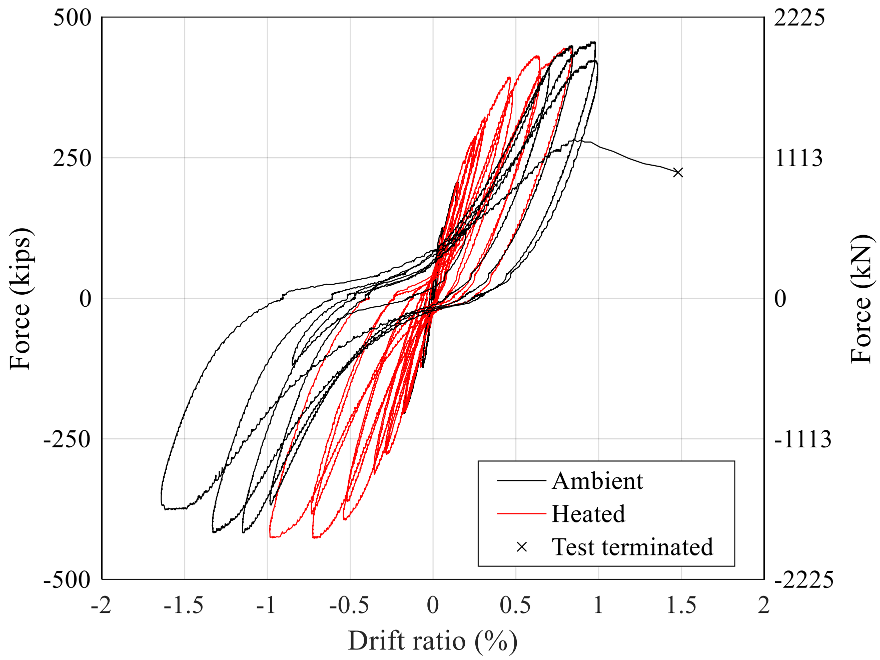

Figure 4-16. Global force-drift ratio relationship for Wall 3

The locations of the thermocouples (CT) embedded in the wall and the temperatures recorded at the start of each heated load cycle are shown in Figure 4-17 and Figure 4-18, respectively. The surfaces of the wall were maintained at the target temperature of 450°F [232°C] for all heated cycles except for LC3 and LC5 for which the target temperature was 300°F [149°C]; the surface temperatures are not plotted in Figure 4-18.

The lateral stiffness of the wall in first heated load cycle (LC3), performed 15 minutes after the surfaces of the wall had reached 300°F [149°C], was approximately 20% less than that in LC2, conducted at room temperature to the same amplitude of force, namely, 25% of the estimated lateral strength per Chapter 3. No significant reduction in lateral stiffness was observed in the load cycles performed to the same displacement in subsequent cycles. Accordingly, the loss in stiffness from LC2 to LC3 is attributed to cracking due to thermal effects and not due to mechanical damage resulting from cyclic loading. The patterns of cracks on one surface of the wall after LC2 and LC3 are shown in Figure 4-19 and Figure 4-20, respectively.

The peak lateral strength at room temperature (in LC18) was 2025 kN [455 kips] and within 5% of the peak value of 1980 kN [445 kips] measured in an earlier heated cycle (LC15). The patterns of cracks on one surface of the wall after LC15 is shown in Figure 4-21. The secant stiffness and strength of the wall deteriorated in subsequent cycles (LC19 to LC21) to greater displacements. The wall *failed* in shear at a drift ratio of approximately 1.5%. The wall *failed* in shear. Figure 4-22 shows cracking and other damage to the wall at the conclusion of testing.

Table 4-6: Summary of results for Wall 3

Load cycle	Surface temperature (°F[a])	IP displacement (in[a])		IP force (kips[a])		Secant stiffness[b],			
						I quad		I-III quad	
		max	min	max	min	k_s (kips/in)	$\frac{k_s}{k_t}$	k_s (kips/in)	$\frac{k_s}{k_t}$
LC1	Ambient	0.010	-0.011	83	-77	8,400	0.47	7,100	0.40
LC2	Ambient	0.020	-0.023	125	-123	7,700	0.43	5,600	0.31
LC3	300	0.023	-0.027	126	-122	5,900	0.33	4,800	0.27
LC4	Ambient	0.055	-0.065	207	-205	4,000	0.22	3,400	0.19
LC5	300	0.055	-0.062	205	-202	3,600	0.20	3,400	0.19
LC6	450	0.055	-0.067	205	-204	3,700	0.21	3,400	0.19
LC7	450	0.094	-0.103	288	-277	3,000	0.17	2,800	0.16
LC8	450	0.092	-0.107	278	-275	3,000	0.17	2,800	0.16
LC9	450	0.116	-0.131	322	-313	2,800	0.16	2,600	0.15
LC10	450	0.111	-0.130	304	-298	2,700	0.15	2,500	0.14
LC11	450	0.171	-0.196	393	-394	2,300	0.13	2,100	0.12
LC12	450	0.176	-0.192	369	-362	2,100	0.12	2,000	0.11
LC13	450	0.232	-0.265	432	-427	1,800	0.10	1,700	0.10
LC14	450	0.238	-0.271	395	-384	1,600	0.09	1,500	0.08
LC15	450	0.303	-0.359	445	-426	1,600	0.09	1,300	0.07
LC16	Ambient	0.259	-0.362	411	-368	1,600	0.09	1,200	0.07
LC17	Ambient	0.310	-0.424	449	-417	1,600	0.09	1,100	0.06
LC18	Ambient	0.353	-0.489	457	-417	1,400	0.08	1,000	0.06
LC19	Ambient	-	-0.313	-	-214	NA[c]	NA[c]	NA[c]	NA[c]
LC20	Ambient	0.360	-0.599	423	-376	1,300	0.07	800	0.04
LC21	Ambient	0.316	-	282	-	NA[d]	NA[d]	-	-

[a] °F = °C*1.8+32; 1 kip = 4.45 kN; 1 in. = 25.4 mm

[b] Calculated value and normalized by k_t (= 17,820 kips/in)

[c] Consistent displacements not recorded

[d] Fully reversed cyclic loading not applied

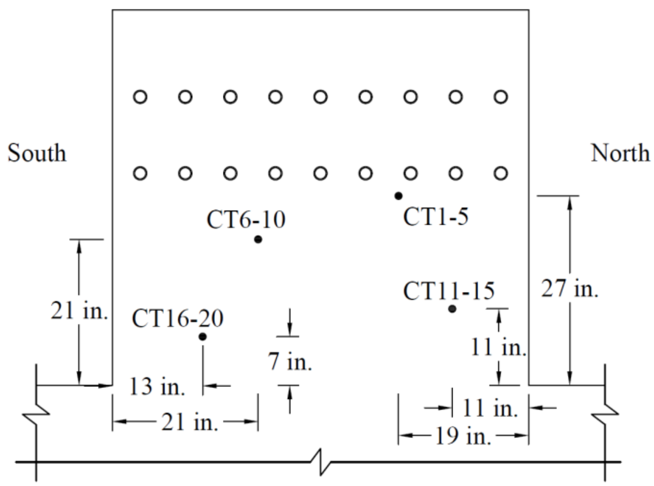

Figure 4-17. Locations of embedded thermocouples in Wall 3
[Note: 1 in. = 25.4 mm]

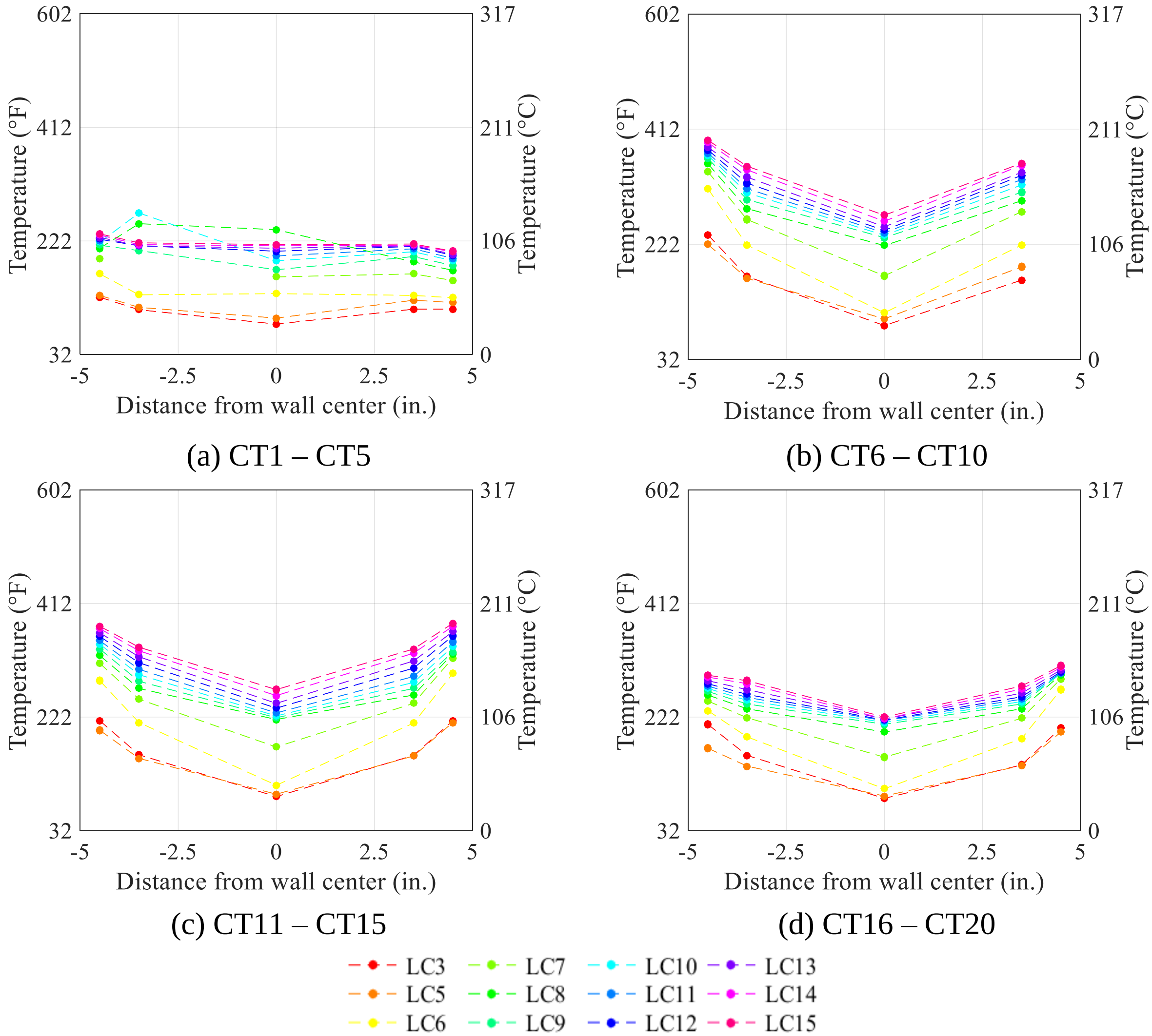

(a) CT1 – CT5

(b) CT6 – CT10

(c) CT11 – CT15

(d) CT16 – CT20

(e) Legend

Figure 4-18. Thermal gradients at the start of all heated cycles for Wall 3
[Note: 1 in. = 25.4 mm]

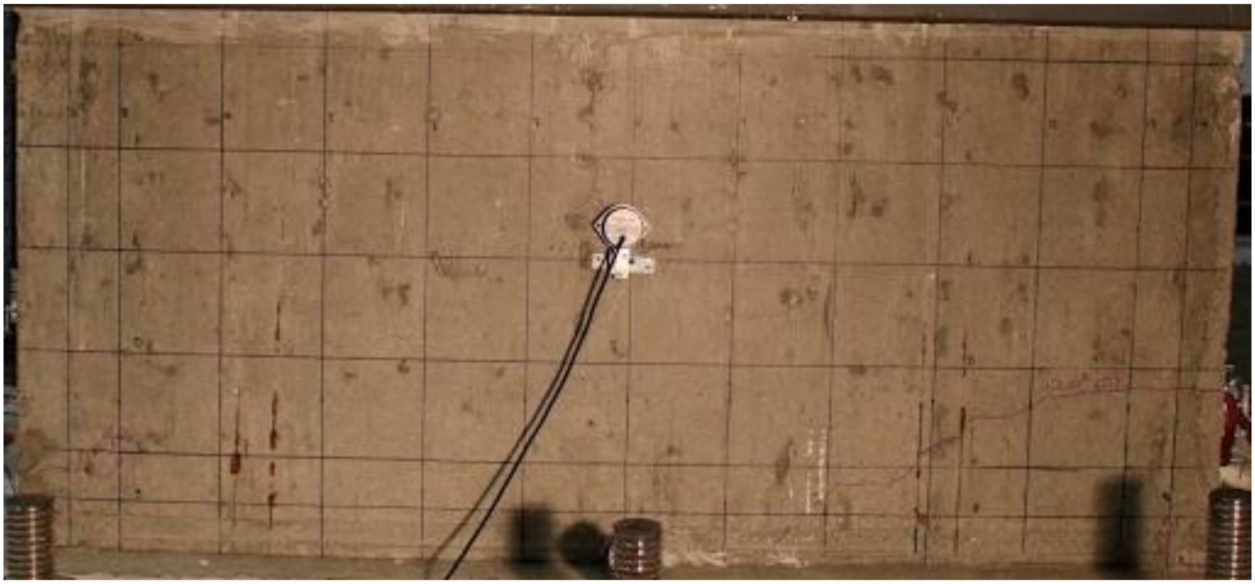

Figure 4-19. Crack pattern on West face of Wall 3 after LC2

Figure 4-20. Crack pattern on West face of Wall 3 after LC3

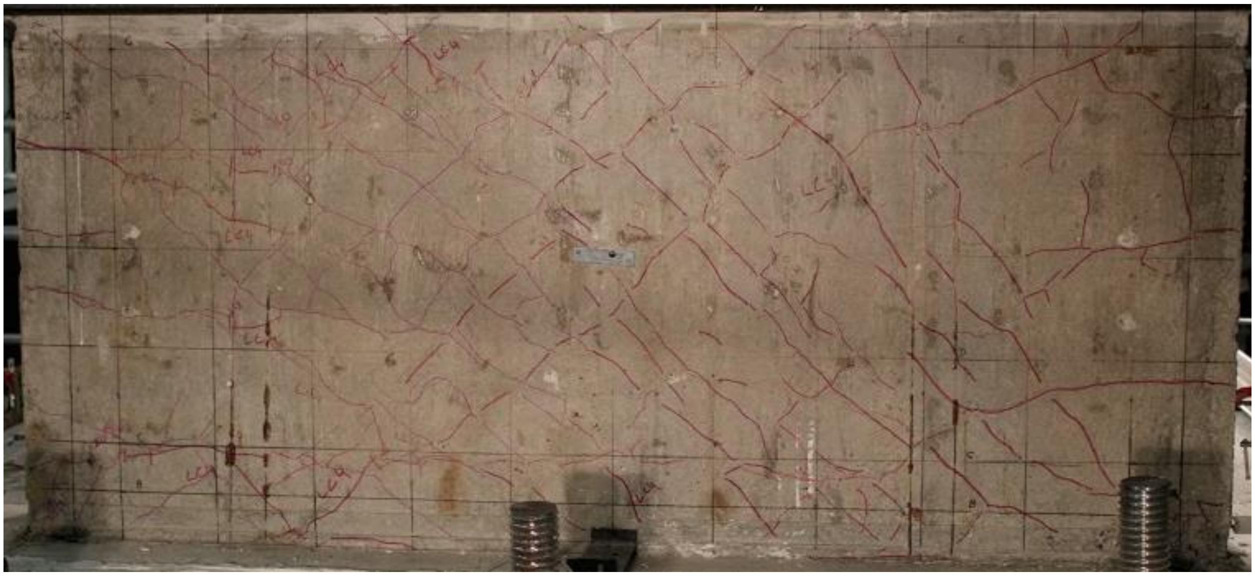

Figure 4-21. Crack pattern on West face of Wall 3 after LC15

Figure 4-22. Damage to Wall 3 at the end of testing

4.6 Wall 4

Wall 4 was tested between October 23, 2017 and October 26, 2017. The average uniaxial compressive strength of concrete was 45 MPa [6.5 ksi], based on tests performed during the testing phase. The age of the wall at the start of testing was 109 days. Wall 4 was reinforced with two curtains of #4 bars spaced vertically and horizontally at 102 mm [4 inches] for a reinforcement ratio of 0.93% in each direction. The lateral strength of Wall 4 was expected to be limited by moment capacity to approximately 1224 kN [275 kips], based on the provided reinforcement and day-of-test concrete strength.

4.6.1 Test protocol

One load cycle (LC1) was performed at room temperature at a lateral force corresponding to approximately 25% of estimated peak lateral strength. After LC1, the wall was heated to a target surface temperature of 450°F [232°C]. Cycles were performed to a force corresponding LC1, 15 minutes (LC2) and 120 minutes (LC3) after the surfaces of the wall had reached 232°C. The temperature of the surfaces of the wall was maintained at 232°C between LC2 and LC3. The heaters were removed after LC3 and the wall cooled naturally to room temperature. Load cycles 4 to 6 repeated the thermal loadings of load cycles 1 to 3, at a force level corresponding to 40% of estimated peak lateral strength. The displacement at the centerline of loading at peak resistance in LC6 was designated as d* and subsequent cycles were applied in increments of d* until strength of wall had been reached in heated conditions. The heaters were not removed after LC6 and testing was continued. The heaters were removed after the strength had been reached in LC15 and the wall was then allowed to cool naturally to room temperature. Additional cycles were performed in increasing increments of d* until the wall failed.

Table 4-7: Loading protocol for Wall 4

Load cycle	Time after test start (days)	Surface temperature (°F[a])	Heating duration at start of cycle (min)	Load target	Amplitude
LC1	0	Ambient	-	Force	75 kips[a]
LC2	0	450	15	Force	75 kips
LC3	0	450	120	Force	75 kips
LC4	2	Ambient	-	Force	120 kips
LC5	2	450	15	Force	120 kips
LC6	2	450	120	Force	120 kips[b]
LC7	2	450	157	Displacement	1.5d*
LC8	2	450	178	Displacement	1.5d*
LC9	2	450	196	Displacement	2d*
LC10	2	450	220	Displacement	2d*
LC11	2	450	239	Displacement	3d*
LC12	2	450	260	Displacement	3d*
LC13	2	450	282	Displacement	4d*
LC14	2	450	327	Displacement	4d*
LC15	2	450	349	Displacement	5d*
LC16	3	Ambient	-	Displacement	5d*
LC17	3	Ambient	-	Displacement	6d*
LC18	3	Ambient	-	Displacement	7d*
LC19	3	Ambient	-	Displacement	8d*
LC20	3	Ambient	-	Displacement	9d*
LC21	3	Ambient	-	Displacement	10d*
LC22	3	Ambient	-	Displacement	11d*
LC23	3	Ambient	-	Displacement	12d*
LC24	3	Ambient	-	Displacement	13d*
LC25	3	Ambient	-	Displacement	14d*
LC26	3	Ambient	-	Displacement	15d*
LC27	3	Ambient	-	Displacement	17d*

[a] °F = °C×1.8 + 32; 1 kip = 4.45 kN

[b] Displacement measured in this cycle designated as the reference displacement, d*

4.6.2 Test results

The global force-drift ratio relationship for all cycles of loading performed on Wall 4 is presented in Figure 4-23. The maximum forces, displacements (measured at loading centerline) and secant stiffness recorded in each cycle are presented in Table 4-8. The values of secant stiffness reported in Table 4-8 are based on the two methods described in Section 4.2, and have been normalized by the theoretical value of secant stiffness, k_t, calculated using strength of mechanics equations and day-of-test uniaxial compressive strength of concrete.

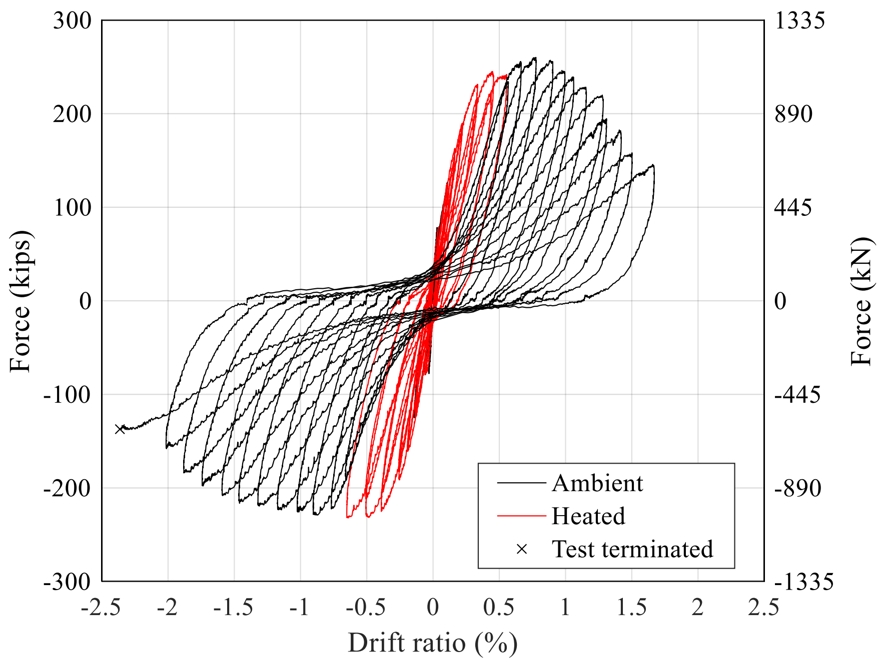

Figure 4-23. Global force-drift ratio relationship for Wall 4

The location of the thermocouples (CT) embedded in the wall and the temperatures recorded at the start of each heated load cycle are shown in Figure 4-24 and Figure 4-25, respectively. The temperature of the surfaces of the wall was maintained at the target value of 450°F [232°C] for all heated cycles; the surface temperatures are not plotted in Figure 4-25.

The lateral stiffness of the wall at elevated temperature in LC2, performed to a force level of approximately 25% of the peak strength, was approximately 30% less than that in LC1, conducted at room temperature to the same amplitude of force. No significant reduction in lateral stiffness was observed in the load cycles performed to the same displacement in subsequent cycles.

Accordingly, the loss of stiffness from LC1 to LC2 is attributed to cracking due to thermal effects and not due to mechanical damage resulting from cyclic loading. The patterns of cracking on the West face of the wall surface after LC1 and LC3 are presented in Figure 4-26 and Figure 4-27, respectively. The effect of elevated temperature on cracking is made clear by Figure 4-27 because there are many more and longer cracks evident in this photograph than are seen on walls tested to a similar lateral force at ambient temperature (e.g., see Figure 4-5).

The peak lateral strength at room temperature (LC18) was 1157 kN [260 kips] and within 5% of the peak strength of 1090 kN [245 kips] measured in an earlier heated cycle (LC13). The pattern of cracking on the West face of the wall after the last heated cycle (LC15) is presented in Figure 4-28. The secant stiffness and strength of the wall deteriorated in subsequent cycles (LC19 to LC27) to greater displacements. The wall *failed* at a drift ratio of approximately 2%. The damage sustained by the wall is shown in Figure 4-29.

Table 4-8: Summary of results for Wall 4

Load cycle	Surface temperature (°F[a])	IP displacement (in[a])		IP force (kips)		Secant stiffness[b],			
						I quad		I-III quad	
		max	min	max	min	k_s (kips/in)	$\frac{k_s}{k_t}$	k_s (kips/in)	$\frac{k_s}{k_t}$
LC1	Ambient	0.011	-0.012	78	-78	6,800	0.35	6,400	0.33
LC2	450	0.016	-0.018	79	-77	5,400	0.28	4,700	0.24
LC3	450	0.014	-0.023	77	-79	5,300	0.28	4,200	0.22
LC4	Ambient	0.040	-0.053	126	-125	3,200	0.17	2,700	0.14
LC5	450	0.041	-0.049	125	-124	3,100	0.16	2,700	0.14
LC6	450	0.040	-0.047	124	-123	3,100	0.16	2,700	0.14
LC7	450	0.061	-0.071	163	-161	2,600	0.14	2,500	0.13
LC8	450	0.060	-0.071	155	-159	2,600	0.14	2,400	0.13
LC9	450	0.081	-0.094	189	-191	2,400	0.13	2,100	0.11
LC10	450	0.080	-0.094	186	-183	2,300	0.12	2,100	0.11
LC11	450	0.124	-0.145	231	-225	1,800	0.09	1,700	0.09
LC12	450	0.123	-0.142	217	-204	1,700	0.09	1,600	0.08
LC13	450	0.166	-0.179	245	-231	1,500	0.08	1,300	0.07
LC14	450	0.161	-0.187	223	-213	1,400	0.07	1,200	0.06
LC15	450	0.205	-0.237	242	-232	1,400	0.07	1,000	0.05
LC16	Ambient	0.210	-0.243	234	-192	1,100	0.06	900	0.05
LC17	Ambient	0.245	-0.284	256	-222	1,100	0.06	900	0.05
LC18	Ambient	0.287	-0.325	260	-229	1,000	0.05	800	0.04
LC19	Ambient	0.328	-0.375	257	-226	800	0.04	700	0.04
LC20	Ambient	0.360	-0.423	246	-223	700	0.04	600	0.03
LC21	Ambient	0.390	-0.485	239	-219	600	0.03	500	0.03

[a] °F = °C*1.8+32; 1 kip = 4.45 kN; 1 in. = 25.4 mm

[b] Calculated value and normalized by k_t (= 19,200 kips/in)

[c] Fully reversed cyclic loading not applied

Table 4-8 (cont.): Summary of results for Wall 4

Load cycle	Surface temperature (°F[a])	IP displacement (in[a])		IP force (kips)		Secant stiffness[b],			
						I quad		I-III quad	
		max	min	max	min	k_s (kips/in)	$\frac{k_s}{k_t}$	k_s (kips/in)	$\frac{k_s}{k_t}$
LC22	Ambient	0.427	-0.540	228	-216	600	0.03	400	0.02
LC23	Ambient	0.473	-0.587	220	-208	500	0.03	400	0.02
LC24	Ambient	0.484	-0.642	195	-198	400	0.02	300	0.02
LC25	Ambient	0.520	-0.696	183	-184	300	0.02	300	0.02
LC26	Ambient	0.556	-0.744	158	-158	300	0.02	200	0.01
LC27	Ambient	0.613	-	146	-	200	0.01	NA[c]	NA[c]

[a] °F = °C*1.8+32; 1 kip = 4.45 kN; 1 in. = 25.4 mm

[b] Calculated value and normalized by k_t (= 19,200 kips/in)

[c] Fully reversed cyclic loading not applied

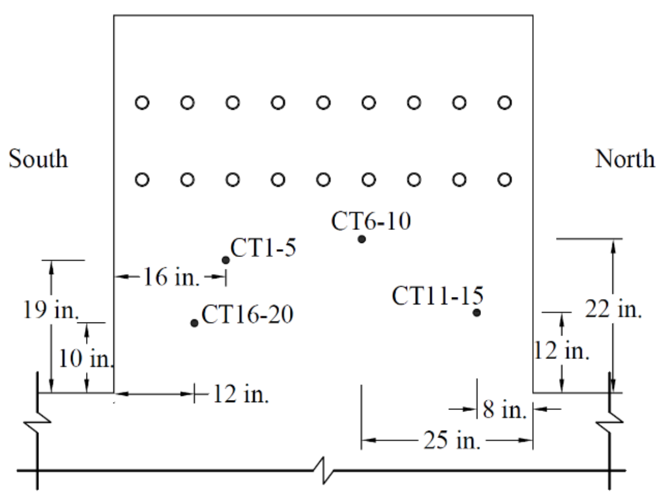

Figure 4-24. Locations of embedded thermocouples in Wall 4
[Note: 1 in. = 25.4 mm]

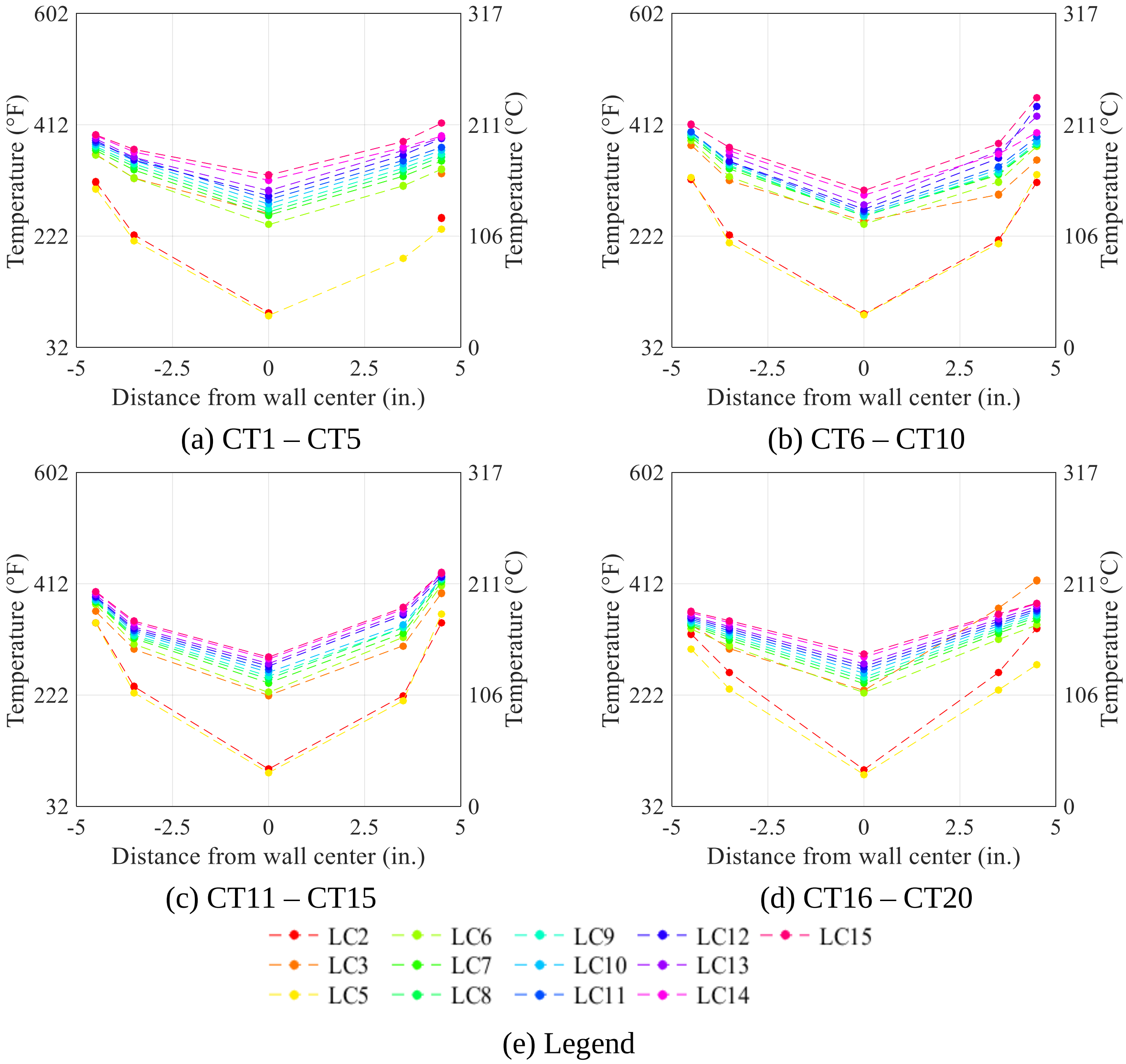

Figure 4-25. Thermal gradients at the start of all heated cycles for Wall 4 [Note: 1 in. = 25.4 mm]

Figure 4-26. Crack pattern on west face of Wall 4 after LC1

Figure 4-27. Crack pattern on west face of Wall 4 after LC3

Figure 4-28. Crack pattern on west face of Wall 4 after LC15

Figure 4-29. Damage to Wall 4 at the end of testing

CHAPTER 5
EFFECTS OF HIGH TEMPERATURE ON DAMAGED CONCRETE

5.1 Introduction

This chapter characterizes the behavior of mechanically *damaged* concrete subjected to high temperatures. Details of the experimental program are presented in Section 5.2. The concrete materials used in this program are described in Section 5.3. Details of the testing program are provided in Section 5.4. Results obtained from the experimental program are presented and discussed in Section 5.5.

5.2 Experimental program

The reinforced concrete walls (details and results presented in Chapters 3 and 4, respectively) were simultaneously subjected to elevated temperatures and mechanical loading. As noted in Chapter 4, shrinkage-induced cracks existed in the walls at the start of testing and additional cracks formed during testing due to mechanical loading and thermal exposure. The materials-level tests reported for the concrete used in the walls, which characterized the effects of elevated temperature on mechanical properties, were performed on virgin (or *undamaged*) cylinders. Because the effects of elevated temperature on damaged concrete are not known, experiments were conducted on mechanically *damaged* concrete cylinders, and results are described below.

Three conventional concretes of different compressive strengths were studied in this experimental program. The materials, designated as Con-4, Con-8 and Con-9, had uniaxial compressive strengths at the time of testing of 4.1 ksi [28.3 MPa], 8.1 ksi [55.8 MPa] and 8.5 ksi [58.6 MPa], respectively. Concrete cylinders, 3 inches [76 mm] in diameter and 6 inches [152 mm] in length were tested.

Defects in the form of microcracks and air voids exist in hardened concrete (Li, 1992). Loading of concrete cylinders in axial compression results in stress concentrations at the locations of voids, which leads to the growth of microcracks in the direction of loading: the strategy used here to induce *damage* albeit by the growth of microcracks and not macro-cracks as observed in the tests of the walls. The *damage* in the concrete cylinders due to microcracking was not visible but was inferred by comparing the dynamic moduli measured before and after testing. The *damaged* cylinders were heated, cooled and tested in the residual condition (i.e., at room temperature) to measure the effects of temperature on mechanical properties in compression. The properties studied in the experimental program are weight, modulus of elasticity in compression and uniaxial compressive strength.

5.3 Materials

All cylinders of a given concrete (i.e., Con-4, Con-8 and Con-9) were cast at the same time from concrete mixed in one batch. Type-I cement conforming to ASTM C150 (ASTM, 2017a) was used in all three concretes. Con-4 was supplied by a local batching plant and used coarse and fine limestone aggregate. Con-8 and Con-9 were prepared using a concrete gravity mixer at the University at Buffalo. The coarse and fine aggregate used in Con-8 and Con-9 were sourced from a limestone quarry near Buffalo. The coarse aggregate had a nominal maximum aggregate size of 0.75 inch [19 mm]. The fine aggregate had a fineness modulus of three. Con-4 had small quantities of an air-entraining admixture and mid-range water-reducing admixture. The mix proportions of the concretes are listed in Table 5-1.

Table 5-1. Mix proportion (by weight) of concretes used in the *damaged concrete* experimental program

Constituent	Con-4	Con-8	Con-9
Cement	1	1	1
Water	0.28	0.39	0.43
Fine aggregate	5.03	1.36	1.74
Coarse aggregate	2.76	1.93	1.83
Air-entraining admixture	0.0007	-	-
Mid-range water-reducing admixture	0.0037	-	-

All concretes had a slump of 4 inches at the time of casting. Concrete placed in the cylinders was compacted by placing the molds on a vibrating table for approximately one minute. The cylinders for Con-8 and Con-9 were demolded 24 hours after casting, cured under water for 21 days and then stored at room temperature (20°C) until testing. Cylinders for Con-4 were demolded five days after casting and stored at room temperature (20°C) until testing. Figure 5-1 shows the cylinders cast for Con-8.

Figure 5-1. Cylinders cast for Con-8

5.4 Testing procedure

Cylinders for Con-4, Con-8 and Con-9 were tested at ages of approximately 95, 140 and 170 days, respectively. The long time between casting and testing ensured that concrete was dry at the time of heating and the effects of moisture (during heating) would be minimal. The weight and dimensions of each cylinder were measured at the start of testing.

To benchmark results of tests of *damaged* cylinders, the uniaxial compressive strength, f_c, of Con-4, Con-8 and Con-9 was measured first by testing cylinders in accordance with ASTM C39 (ASTM, 2017c): three for Con-4, eight for Con-8, and five for Con-9, as shown in Table 5-2 by the combination of 20°C and Virgin. For a given concrete, the average value of uniaxial compressive strength was adopted as the benchmark.

Three protocols were used to induce *damage* in the concrete cylinders. The number of cylinders tested in the experimental program (using different *damage* protocols and at different temperatures) are presented in Table 5-2. For Con-8, the concrete cylinders were grouped into four batches, denoted as Virgin, L1-70, L3-70 and L1-85. Cylinders in the batch denoted as L1-70 were loaded to 70% of the benchmark compressive strength and then unloaded. Cylinders in the batch denoted as L3-70 were loaded and unloaded thrice to 70% of the benchmark compressive strength. Cylinders in the batch denoted as L1-85 were loaded to 85% of the benchmark compressive strength and then unloaded. Based on results obtained for Con-8, cylinders for Con-9 were not subjected to the L1-70 loading protocol and cylinders for Con-4 were subjected to L3-85 only. All batches for a particular temperature were heated at the same time. Cylinders in batches denoted by Virgin and a temperature of 100°C, 200°C, or 400°C were heated to the target value, allowed to cool to room temperature, and then tested monotonically to failure per ASTM C39.

Table 5-2. Number of cylinders tested for the *damaged concrete* experimental program

Temp.	**Con-4**				**Con-8**				**Con-9**			
	Virgin	L1-70	L3-70	L1-85	Virgin	L1-70	L3-70	L1-85	Virgin	L1-70	L3-70	L1-85
20°C	3	-	-	3	8	5	5	3	5	-	3	3
100°C	3	-	-	3	5	5	5	3	3	-	3	3
200°C	3	-	-	3	5	5	5	3	3	-	3	3
400°C	3	-	-	2	3	3	3	3	3	-	3	3

All cylinders were capped at both ends before testing using a sulfur mortar in accordance with ASTM C617 (ASTM, 2015). Capping was performed to provide plane bearing surfaces, perpendicular to the longitudinal axis. For cylinders in which *damage* was induced, the caps at both ends were removed using a chisel and a hammer after completing the *damage* loading protocol and before measuring the dynamic modulus.

The dynamic modulus of each concrete cylinder was measured in accordance with ASTM C215 (ASTM, 2014a). The procedure for measuring dynamic modulus is described in Section 3.7.4.2 and not repeated here. Figure 5-2 is a photograph of the setup used to measure dynamic modulus. The weight and dynamic modulus of each cylinder were measured before inducing *damage*, after inducing *damage* and after heating. Additionally, the static modulus of elasticity was measured for cylinders of Con-4 per ASTM C469 (ASTM, 2014b) to determine the ratio of dynamic modulus to static modulus.

The cylinders were heated in an air-furnace with a capacity of 42 liters and capable of heating up to 2010°F [1100°C]. Figure 5-3 is a photograph of cylinders in the furnace. Cylinders were heated to a temperature of 212°F [100°C], 392°F [200°C] and 752°F [400°C]. The cylinders were heated to the target temperature at a ramp rate of 9°F/min [5°C/min]. The target temperature was maintained for 2 hours, after which the furnace was switched off. The hot air in the furnace escaped through a vent at the top of the furnace, and the cylinders cooled to room temperature inside the furnace. The doors to the furnace were kept shut during cooling.

The weight and dynamic modulus of each cylinder were measured within 24 hours of cooling to room temperature. The cylinders were then capped using a sulfur mortar, and their uniaxial compressive strength was measured in accordance with ASTM C39 (ASTM, 2017c) within 3 hours of measuring the dynamic modulus.

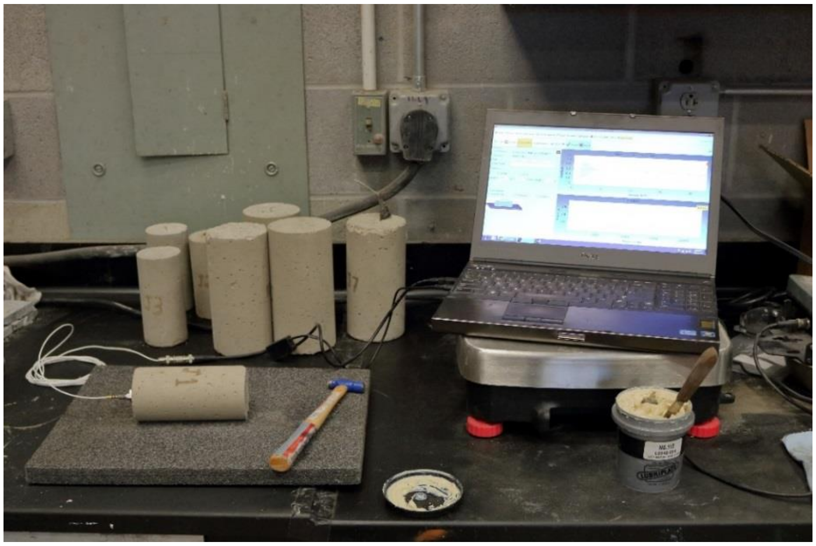

Figure 5-2. Setup for measuring dynamic modulus of elasticity of concrete cylinders

Figure 5-3. Cylinders in the furnace

5.5 Results and discussion

5.5.1 Weight

The average weights of Con-4, Con-8 and Con-9 after being subjected to elevated temperature, normalized by the corresponding value at room temperature (20°C), are plotted in Figure 5-4. The data used to calculate the average values are also plotted in Figure 5-4. The virgin Con-8 cylinders subjected to 212°F [100°C] showed a weight gain of about 4%, and the likely reason for this increase is the reabsorption of moisture from air. Weight gain was not observed for any other batch of cylinders exposed to high temperature.

The loading protocol had no effect on the change in weight with temperature. The proportion of water in the concrete materials at the time of casting was approximately 8% of the total weight, as noted in Table 5-1. The loss of weight in all three concretes at temperatures as high as 752°F [400°C] does not exceed 5%, as seen in Figure 5-4. These results are consistent with those obtained by other researchers (e.g., Naus (2010), Schneider (1988)), who noted that the reduction in weight at temperatures of 400°C and lower was due primarily to the loss of water.

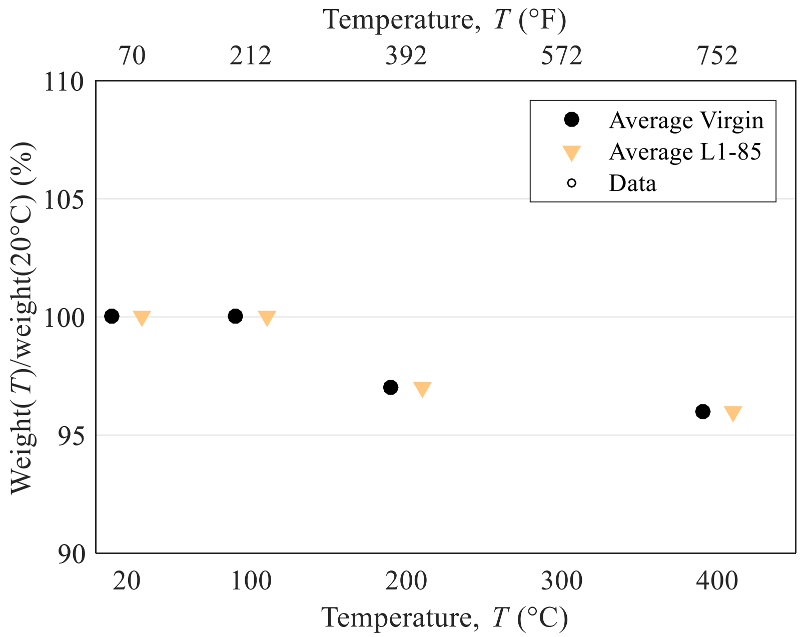

(a) Con-4

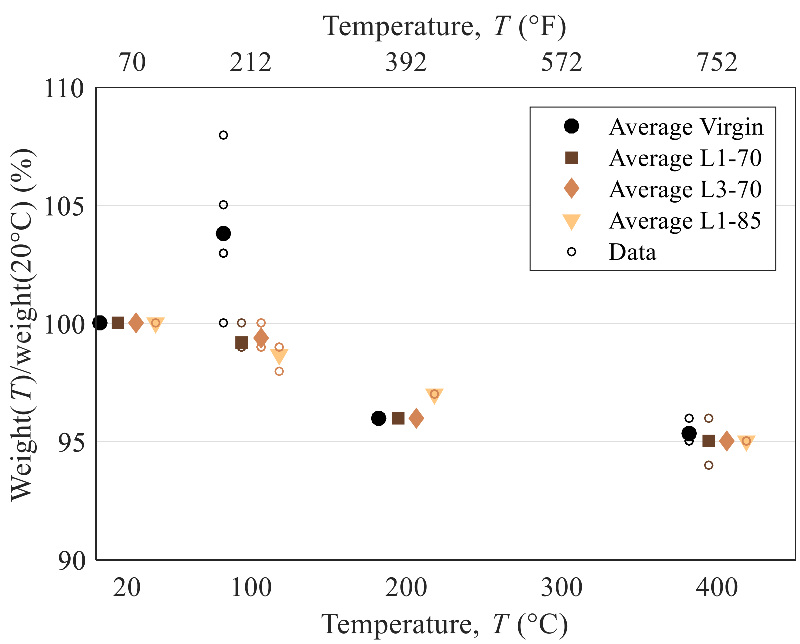

(b) Con-8

Figure 5-4. Change in weight of concrete cylinders with temperature

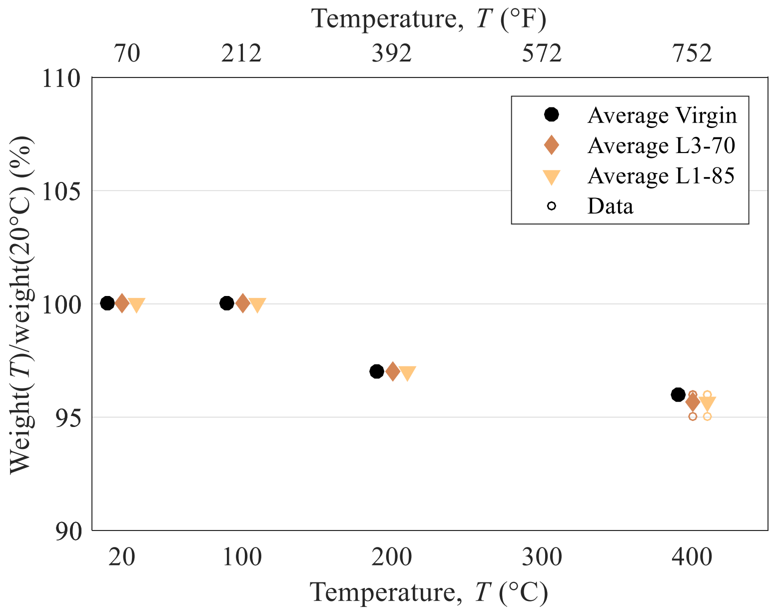

(c) Con-9

Figure 5-4 (cont.). Change in weight of concrete cylinders with temperature

5.5.2 Dynamic modulus of elasticity

The dynamic modulus of elasticity, E_{dc}, of virgin concrete cylinders for Con-4, Con-8 and Con-9, measured at room temperature was 3,500 ksi [24.1 GPa], 5,600 ksi [38.6 GPa] and 5,700 ksi [39.3 GPa], respectively, corresponding to approximately $54,700\sqrt{f_c}$ $\left[4,500\sqrt{f_c}\right]$, $62,200\sqrt{f_c}$ $\left[5,200\sqrt{f_c}\right]$ and $61,800\sqrt{f_c}$ $\left[5,100\sqrt{f_c}\right]$, respectively, where f_c is the uniaxial compressive strength of concrete measured at the time of testing in psi [MPa]. The values for the dynamic modulus are within 10% of the ACI 318-14 (ACI, 2014a) value of $57,000\sqrt{f_c}$ $\left[4,700\sqrt{f_c}\right]$ for the static modulus of elasticity.

The static modulus for Con-4, measured for cylinders tested at room temperature, was 3,100 ksi [21.4 GPa], which is approximately 15% less than the ACI 318-14 value calculated using the day-of-test uniaxial compressive strength. The dynamic modulus for Con-4 is approximately

15% greater than the static modulus. As noted in Chapter 3, the dynamic modulus is greater than the static modulus because the stress-strain relationship for concrete is nonlinear and the static modulus is traditionally measured at a stress level of approximately 40% of the ultimate compressive stress. The dynamic modulus (i.e., initial tangent modulus) is measured at an infinitesimally small stress (Mindess et al., 2003).

The average change in the dynamic modulus of Con-4, Con-8 and Con-9 with increasing temperature is presented in Figure 5-5. Results are normalized by the dynamic modulus of the corresponding cylinders in the virgin (i.e., undamaged) condition at room temperature, $E_{dc}\left(20°\text{C}\right)$. The data used to calculate the average change is also plotted in Figure 5-5. The dynamic modulus of the *damaged* cylinders at room temperature is between 5% and 15% less than the value measured before *damage*. The percentage reduction at room temperature is independent of the *damage* protocol (i.e., L1-70, L3-70 or L1-85).

The two key observations from the results presented in Figure 5-5 are: (1) the percentage reduction in the dynamic modulus due to exposure to temperature greater than 212°F [100°C] masks any reduction in the modulus due to *damage*; and (2) the percentage reduction in the normalized dynamic modulus due to exposure to temperature greater than 212°F [100°C] is independent of the compressive strength of the concrete at room temperature. The single exception to the first observation is the approximately 15% difference between the modulus of virgin and *damaged* concrete for Con-4 exposed to 212°F [100°C], which is not observed either for Con-4 exposed to higher temperatures, or for Con-8 or Con-9 at any temperature.

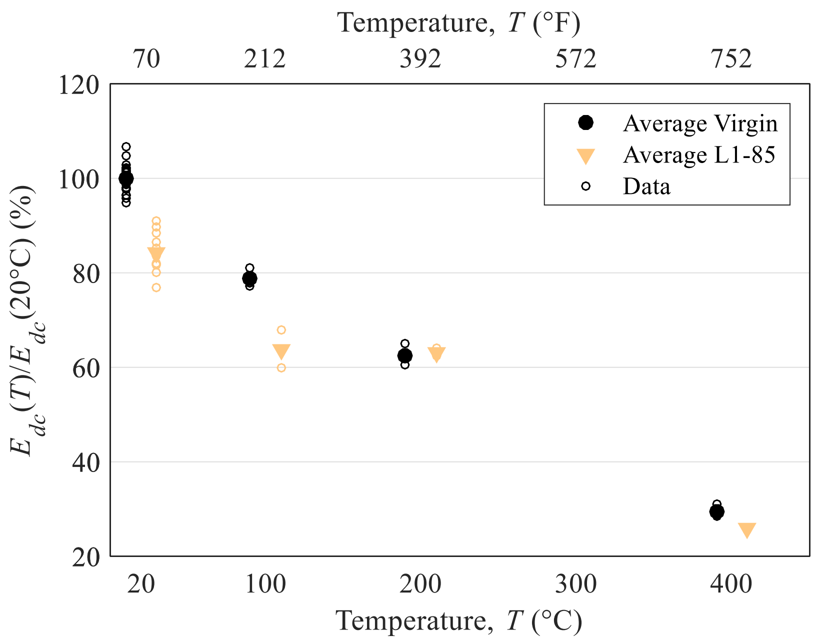

(a) Con-4

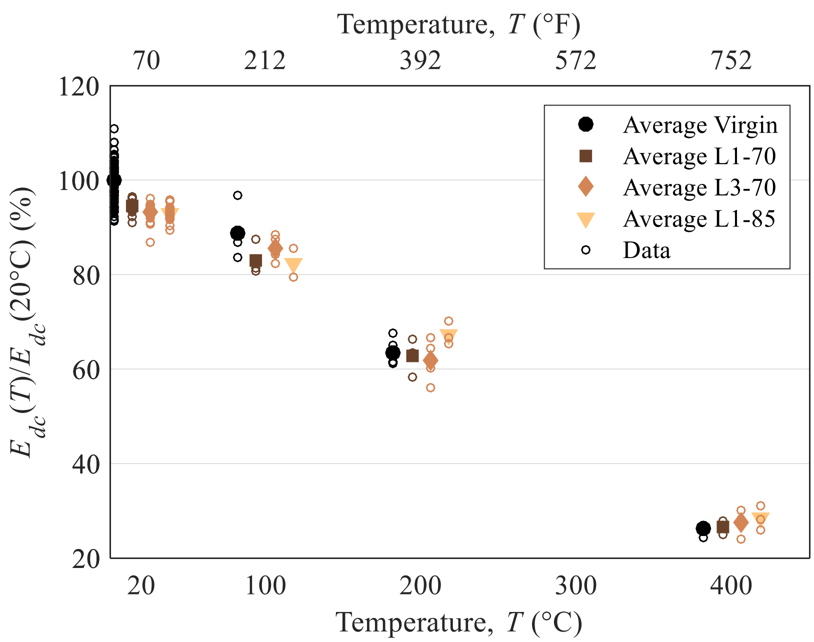

(b) Con-8

Figure 5-5. Variation in dynamic modulus of elasticity of concrete with temperature

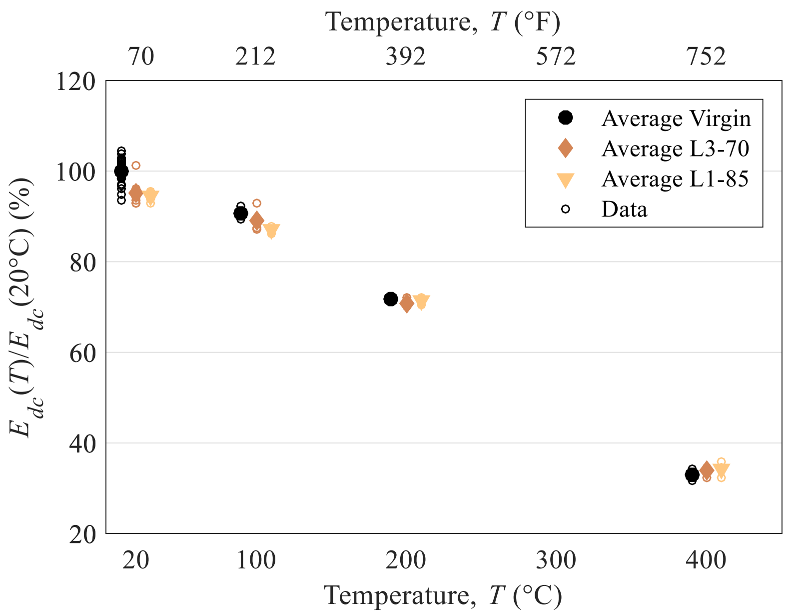

(c) Con-9

Figure 5-5 (cont.). Variation in dynamic modulus of elasticity of concrete with temperature

5.5.3 Uniaxial compressive strength

The average uniaxial compressive strength, f_c , of the virgin cylinders of Con-4, Con-8 and Con-9, measured at room temperature, at the time of testing, was 4.1 ksi [28.3 MPa], 8.1 ksi [55.8 MPa] and 8.5 ksi [58.6 MPa], respectively: benchmark values used to normalize results in this section. The average change in the uniaxial compressive strength of Con-4, Con-8 and Con-9 with increasing temperature is presented in Figure 5-6. Results are normalized by the benchmark compressive strength. The data used to calculate the average change is also plotted in Figure 5-6.

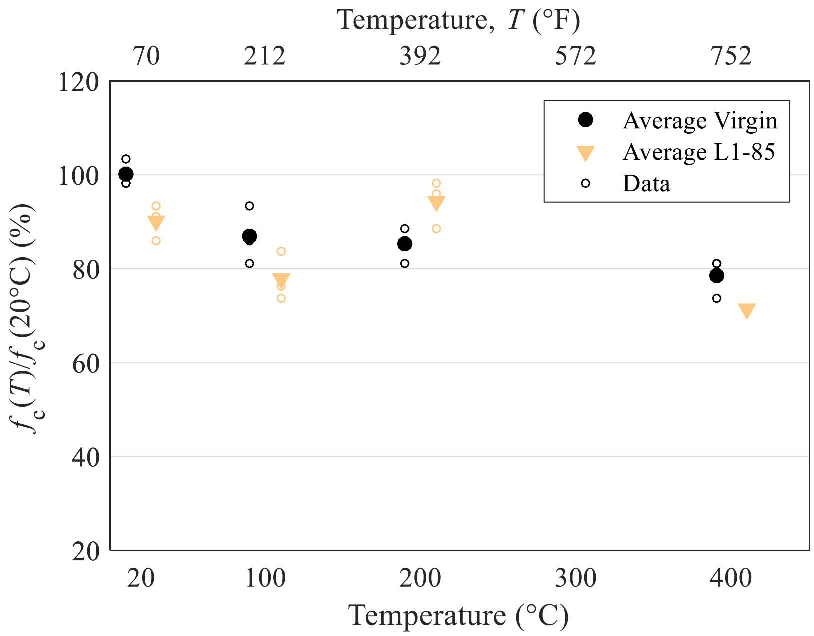

(a) Con-4

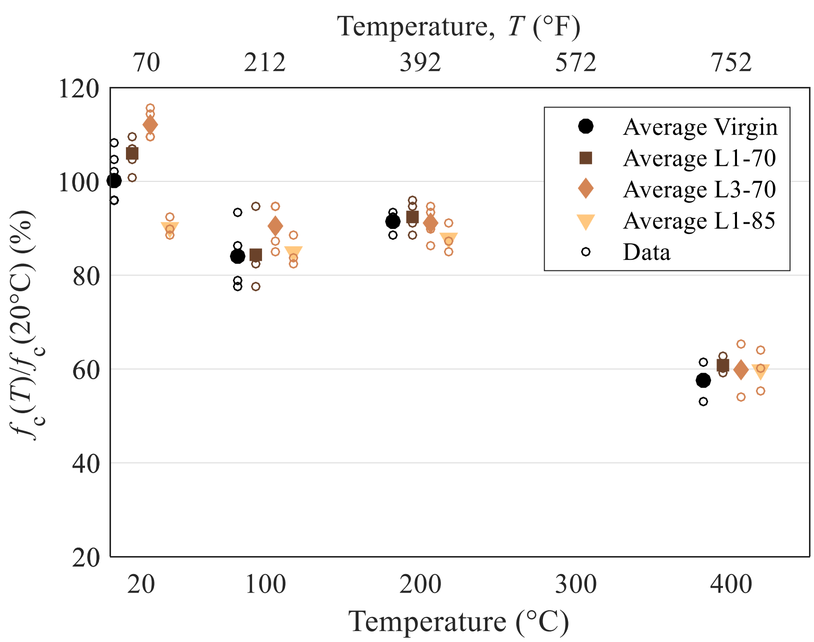

(b) Con-8

Figure 5-6. Variation of uniaxial compressive strength of concrete with temperature

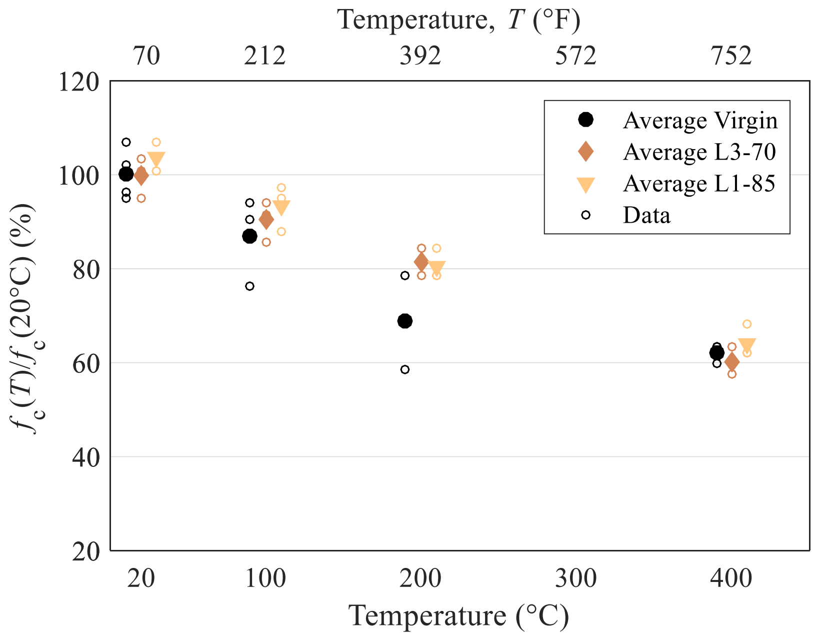

(c) Con-9

Figure 5-6 (cont.). Variation of uniaxial compressive strength of concrete with temperature

The two key observations from the data presented in Figure 5-6 are: (1) *damage*, as imposed in the experimental program, does not significantly reduce the uniaxial compressive strength of concrete after exposure to temperatures up to 752°F [400°C]; and (2) exposure to temperature greater than 212°F [100°C] reduces the uniaxial compressive strength of concrete.

CHAPTER 6
EFFECTS OF MOISTURE CONDITIONS ON CONCRETE SUBJECTED TO ELEVATED TEMPERATURE

6.1 Introduction

This chapter characterizes the behavior of concrete subjected to elevated temperature in the presence of different moisture conditions. Details of the experimental program are presented in Section 6.2. The concrete materials used in this program are described in Section 6.3. Details of the testing program are provided in Section 6.4. Results obtained from the experimental program are presented and discussed in Section 6.5.

6.2 Experimental program

The reinforced concrete walls (details and results presented in Chapters 3 and 4, respectively) were heated using radiant heater panels. The materials tests to characterize the effects of temperature on the mechanical behavior of the concrete used in the construction of the walls (reported in Chapter 3) were performed by heating concrete cylinders in an air furnace. In both cases, the generated steam, which resulted from water in the concrete undergoing a phase change, escaped the concrete during heating, as evidenced by the reduction in weight reported in Section 3.7.4.2. Researchers (e.g., Willam et al. (2009) and Naus (2010)) have described the condition in which the moisture generated by heating concrete is permitted to escape as *unsealed* heating. In *sealed* heating, the moisture (or steam) generated by heating concrete is prevented from escaping. Exposure of a concrete slab to fires is an example of unsealed heating. Exposure of a reinforced concrete wall with airtight steel liners on both surfaces (similar to a steel-plate concrete composite wall) to elevated temperatures is an example of sealed heating.

Bertero and Polivka (1972) tested a total of sixteen concrete cylinders at either elevated temperature or in the residual condition (i.e., tested at room temperature, after exposure to elevated temperature). The cylinders were either sealed and unsealed during heating, and subjected to differing numbers of heating cycles and durations. The static modulus of elasticity and uniaxial compressive strength of a cylinder heated in the sealed condition to 300°F [149°C] were approximately 15% and 30% less, respectively, than the values measured for a cylinder heated to the same temperature in the unsealed condition: the reported reductions were based on the results of tests of just two cylinders, one unsealed and one sealed. Kottas et al. (1979) tested two concretes cast using different types of aggregate to temperatures of up to 356°F [180°C] and reported reductions in uniaxial compressive strength of up to 60% for concrete heated in the sealed condition with respect to an identical test in the unsealed condition. Kottas et al. did not report the number of cylinders tested.

In the case of a steam pipe break in a nuclear power plant containment structure, the concrete elements (without a steel liner plate) will be heated by the high-pressure, high-temperature steam. This type of heating is called *steamed* heating, and its effects on the mechanical behavior of concrete are not yet known. The effects on the mechanical behavior of concrete exposed to temperatures of up to 300°F [149°C] in unsealed, sealed and steamed conditions are studied in the experimental program described in this chapter.

Three conventional concretes of different uniaxial compressive strengths were studied. The materials, designated as Con-5, Con-8 and Con-9, had uniaxial compressive strengths at the time of testing of 5.3 ksi [36.5 MPa], 8.1 ksi [55.8 MPa] and 8.5 ksi [58.6 MPa], respectively. Concrete cylinders, 3 inches [76 mm] in diameter and 6 inches [152 mm] in length, were tested. Cylinders were heated in unsealed, sealed and steamed conditions, and then cooled and tested in the residual condition (i.e., at room temperature). The properties studied in the experimental program were weight, dynamic modulus of elasticity and uniaxial compressive strength.

6.3 Materials

All cylinders for a given concrete (i.e., Con-5, Con-8 and Con-9) were cast at the same time from concrete mixed in one batch. Concrete Con-5 was used for the materials-level study reported in Chapter 3 that supported the tests reported in Chapter 4 on reinforced concrete walls. Concretes Con-8 and Con-9 were used in the *damaged concrete* study reported in Chapter 5. The mix proportions for these materials are summarized in Table 6-1, and the details of the constituents, casting and curing are provided in Chapters 3 and 5.

Table 6-1. Mix proportion (by weight) of concretes used in *moisture concrete* experimental program

Constituent	Con-5	Con-8	Con-9
Cement	1	1	1
Water	0.45	0.39	0.43
Fine aggregate	2.62	1.36	1.74
Coarse aggregate	3.28	1.93	1.83

6.4 Testing procedure

Cylinders for Con-5, Con-8 and Con-9 were tested at ages of approximately 30 days, 140 days and 170 days, respectively. The weight, dimensions and dynamic modulus of each cylinder was measured at the start of testing. The dynamic modulus was measured in accordance with ASTM C617 (ASTM, 2015). The number of cylinders tested in the experimental program (for each material in different heating conditions) is presented in Table 6-2.

Table 6-2. Number of cylinders tested for the *moisture concrete* experimental program

Temp.	Con-5			Con-8			Con-9		
	Unsealed	Sealed	Steamed	Unsealed	Sealed	Steamed	Unsealed	Sealed	Steamed
20°C	4	-	-	5	-	-	3	-	-
100°C	4	4	-	5	5	-	3	4	-
121°C	4	4	-	5	5	5	3	3	4
149°C	4	4	-	3	3	-	3	3	-

The changes in weight, dynamic modulus and uniaxial compressive strength of concrete cylinders heated in the different moisture conditions were measured after exposure to temperatures of up to 300°F [149°C] in the three moisture conditions: unsealed, sealed and steamed. Cylinders were heated in the unsealed and steamed conditions by placing them in a furnace and an autoclave, respectively. Cylinders heated in the sealed condition were placed in Schedule 40 steel pipes that were sealed at both ends and placed in a furnace. The pipes had an outside diameter of 3.5 inches [89 mm], an inside diameter of 3.07 inches [78 mm] and a length of approximately 6 inches [152 mm]. Each pipe was threaded on the outside at both ends, and steel caps were screwed on after the cylinder had been inserted. Teflon tape was attached to the threads on the pipe to ensure a tight seal. The weight of the entire assembly (i.e., pipe, concrete cylinder and caps) was measured before and after heating. No significant difference was measured before and after heating, which indicates adequate sealing. Figure 6-1 is a photograph of a cylinder, steel pipe and two steel caps, used for heating concrete in the sealed condition.

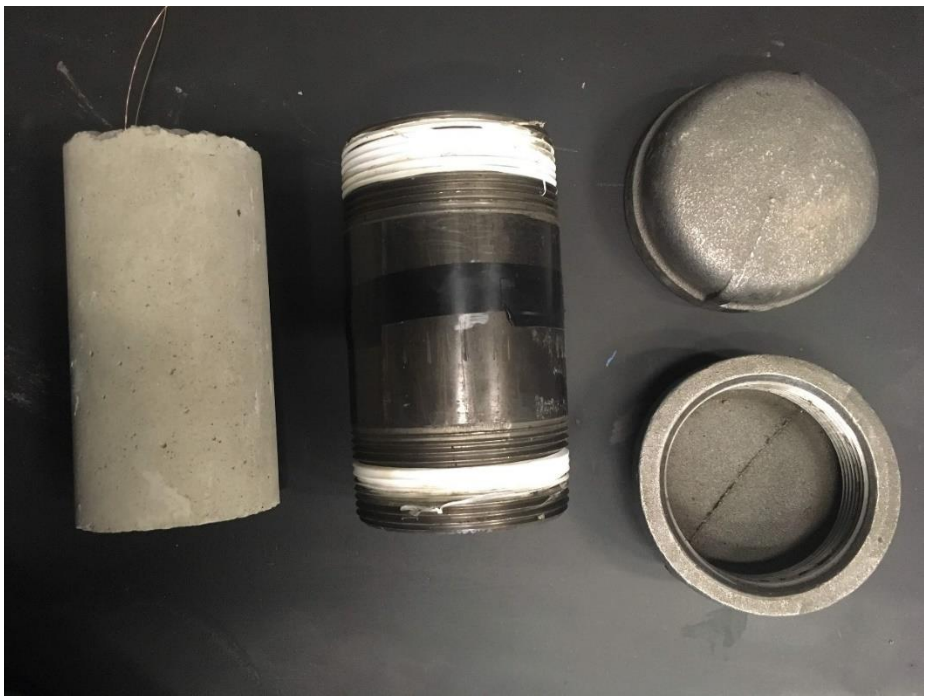

Figure 6-1. Steel pipe and steel caps used for sealed heating (concrete cylinder shown for reference)

The cylinders subjected to sealed and unsealed conditions were heated in an air furnace with a capacity of 42 liters and capable of heating up to 2100°F [1100°C]. The cylinders were heated to a temperature of 212°F [100°C], 250°F [121°C] or 300°F [149°C]. The cylinders were heated to the target temperature at a ramp rate of approximately 9°F/min [5°C/min]. The target temperature was maintained for 2 hours, after which the furnace was switched off. The hot air in the furnace escaped through a vent in the top of the furnace, and the cylinders cooled to room temperature inside the furnace. The doors to the furnace were kept shut during cooling.

A test was performed to ensure that a concrete cylinder placed in the steel pipe (for sealed heating) would be heated to approximately the same temperature as a cylinder placed directly in the furnace (unsealed heating). Temperature on the surface of the steel pipe (T2) and on the surfaces of the two concrete cylinders (T1 and T3), and air temperature inside the furnace (T4) were measured using Type-K thermocouples. Figure 6-2(a) illustrates the test setup. To accommodate the wiring for the thermocouples, the top cap was placed on top of , but not screwed to, the cylinder. Results are presented in Figure 6-2(b). The temperature histories for T1 and T3 are virtually identical. The surfaces of both concrete cylinders and the steel pipe reached approximately 212°F [100°C], which was 36°F [20°C] less than the target temperature of 250°F [121°C].

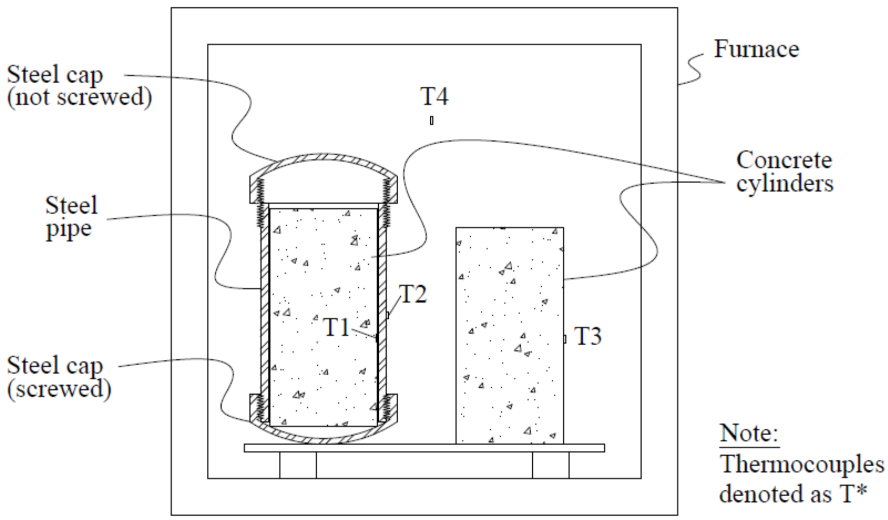

(a) Locations of thermocouples

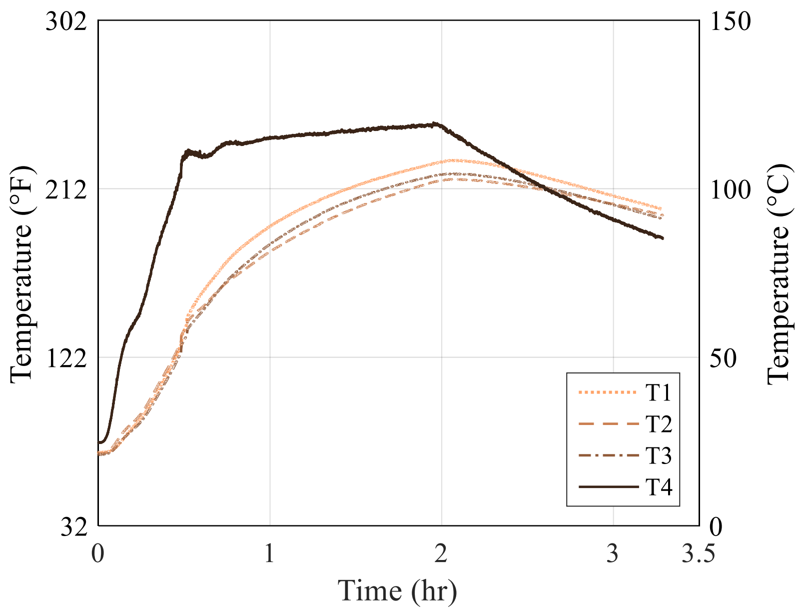

(b) Temperature histories

Figure 6-2. Thermal test setup and results

Cylinders subjected to the steamed condition were heated in an autoclave with a chamber volume of 85 liters. Figure 6-3 is a photograph of the cylinders placed in the autoclave. (In the autoclave, water is fed in to a compartment that supplies it to the autoclave chamber, and heating elements in the autoclave chamber convert the water to steam. As the autoclave chamber is sealed shut, the steam pressure increases with increasing temperature. Valves on the autoclave chamber maintain uniform pressure and temperature for the duration of a test.) The specimens were heated at a ramp rate of approximately 5°F/min [3°C/min] to a target temperature of 250°F [121°C] and steam pressure of 14 psi [97 kPa]. The target temperature and pressure were maintained for 1.5 hours, and the concrete cylinders then cooled to room temperature in the autoclave. (Heating for 2 hours per the unsealed and sealed tests introduced previously was not possible because of time settings on the autoclave.)

Figure 6-3. Placement of concrete cylinders in the autoclave

6.5 Results and discussion

6.5.1 Weight

The average weights of Con-5, Con-8 and Con-9 after being subjected to elevated temperature, normalized by the corresponding value at room temperature (20°C), are plotted in Figure 6-4. The data used to calculate the average values are also plotted in Figure 6-4.

Moisture conditions had no significant effect on the change in weight of concrete with temperature. The average loss in weight in all three concretes, subjected to temperatures of up to 300°F [149°C], in the unsealed, sealed or steamed conditions does not exceed 4%. The two outliers are the Con-8 cylinders subjected to 212°F [100°C] in the unsealed condition (weight gain of 4%) and the Con-9 cylinders subjected to 250°F [121°C] in the sealed condition (weight gain of 1%). The likely reason for the increase in weight in both outliers is the absorption of moisture from air (during heating or cooling).

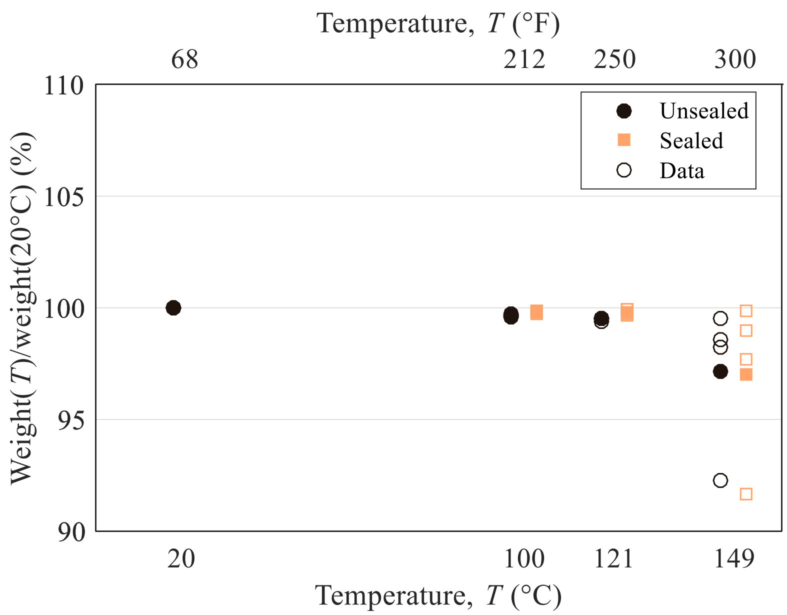

(a) Con-5

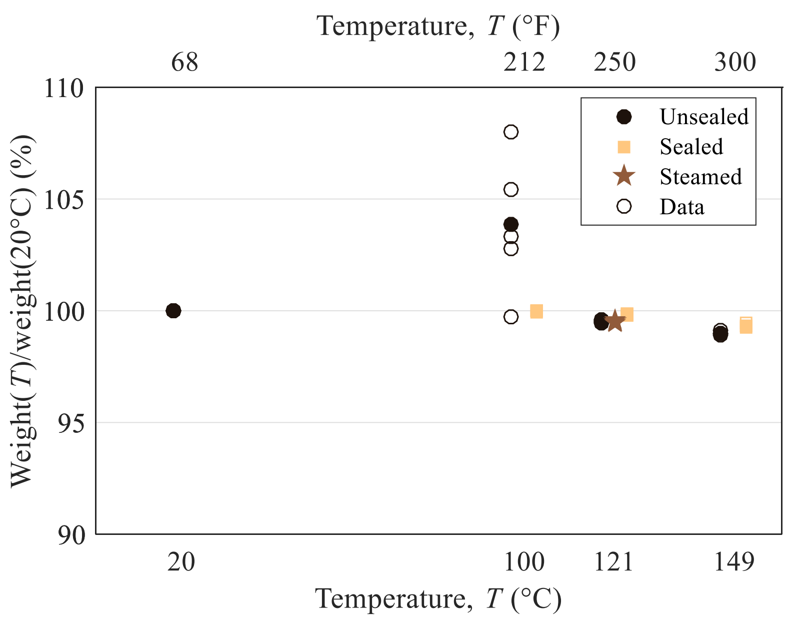

(b) Con-8

Figure 6-4. Change in weight of concrete cylinders with temperature

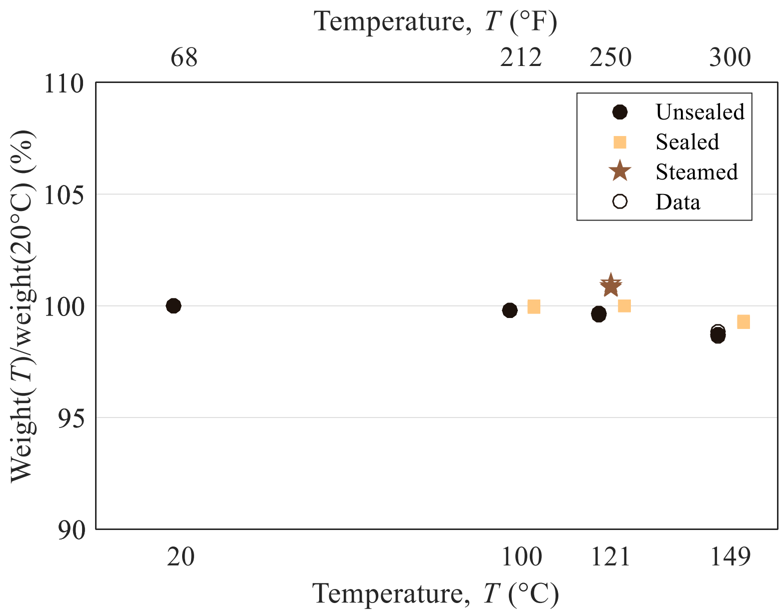

(b) Con-9

Figure 6-4 (cont.). Change in weight of concrete cylinders with temperature

6.5.2 Dynamic modulus of elasticity

The dynamic modulus of elasticity, E_{dc}, of virgin concrete cylinders for Con-5, Con-8 and Con-9, measured at room temperature (20°C) was 5,300 ksi [36.5 GPa], 5,600 ksi [38.6 GPa] and 5,700 ksi [39.3 GPa], respectively, corresponding to approximately $72,000\sqrt{f_c}$ $\left[6,000\sqrt{f_c}\right]$, $62,200\sqrt{f_c}$ $\left[5,200\sqrt{f_c}\right]$ and $61,800\sqrt{f_c}$ $\left[5,100\sqrt{f_c}\right]$, respectively, where f_c is the uniaxial compressive strength of concrete measured at the time of testing in psi [MPa]. The values for the dynamic modulus are within 25% of the ACI 318-14 (ACI, 2014a) value of $57,000\sqrt{f_c}$ $\left[4,700\sqrt{f_c}\right]$ for the static modulus of elasticity.

The average change in the dynamic modulus of Con-5, Con-8 and Con-9 with increasing temperature is presented in Figure 6-5. Results are normalized by the dynamic modulus of the corresponding cylinders at room temperature, $E_{dc}(20°\text{C})$. The data used to calculate the average change is also plotted in Figure 6-5. The two key observation from the results presented in Figure 6-5 are: (1) the percentage reduction in the dynamic modulus of concrete cylinders heated under different moisture conditions (unsealed, sealed or steamed) to the same temperature is within 10%; and (2) the percentage reduction in the normalized dynamic modulus due to exposure to temperature of up to 300°F [149°C] is essentially independent of the compressive strength of the concrete at room temperature (i.e., same percentage reductions for the three concretes at a given temperature).

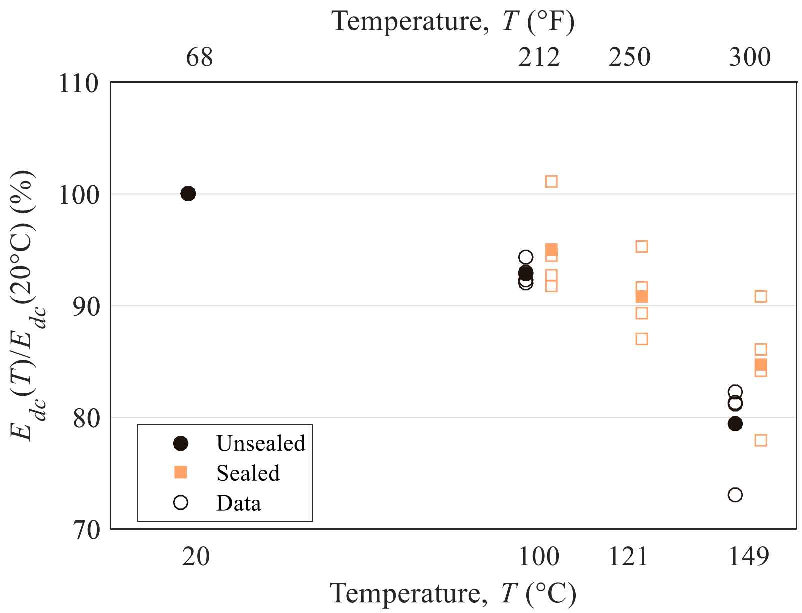

(a) Con-5

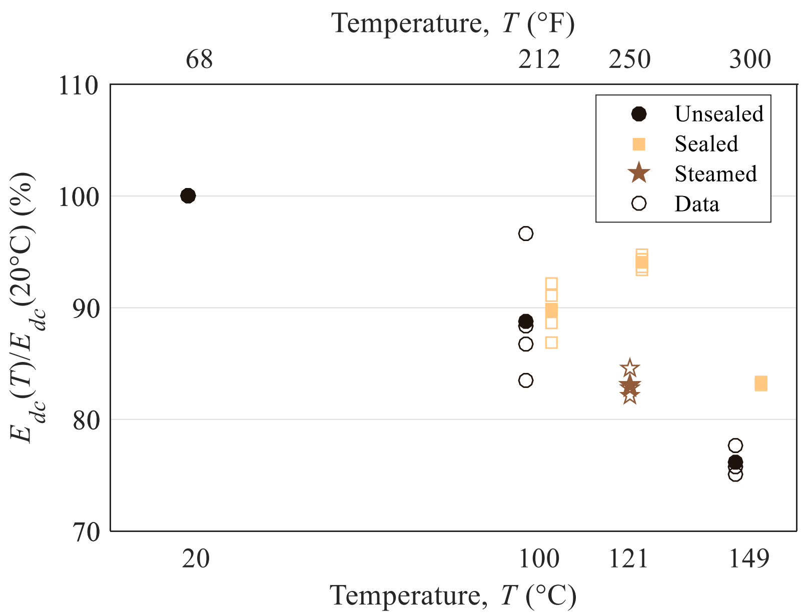

(b) Con-8

Figure 6-5. Change in dynamic modulus of elasticity of concrete with temperature

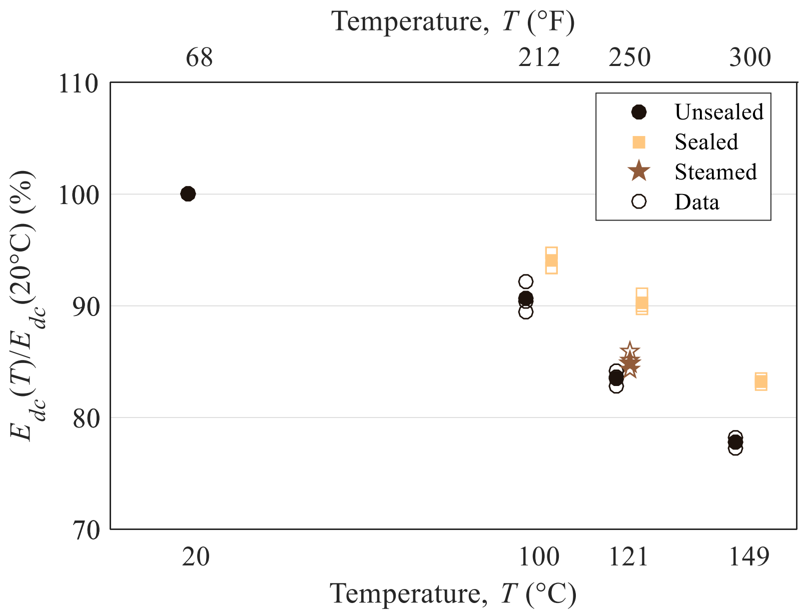

(b) Con-9

Figure 6-5 (cont.). Change in dynamic modulus of elasticity of concrete with temperature

6.5.3 Uniaxial compressive strength

The average uniaxial compressive strength, f_c, of cylinders of Con-5, Con-8 and Con-9, measured at room temperature, at the time of testing was 5.3 ksi [36.5 MPa], 8.1 ksi [55.8 MPa] and 8.5 ksi [58.6 MPa], respectively. The average change in the uniaxial compressive strength of Con-5, Con-8 and Con-9 with increasing temperature is presented in Figure 6-6. Results are normalized by the uniaxial compressive strength at room temperature, $f_c(20°C)$. The data used to calculate the average change is also plotted in Figure 6-6.

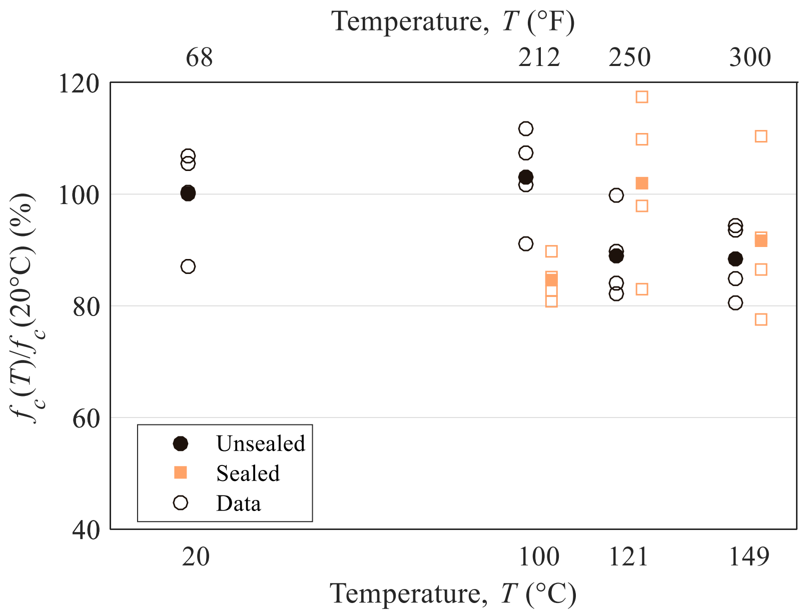

(a) Con-5

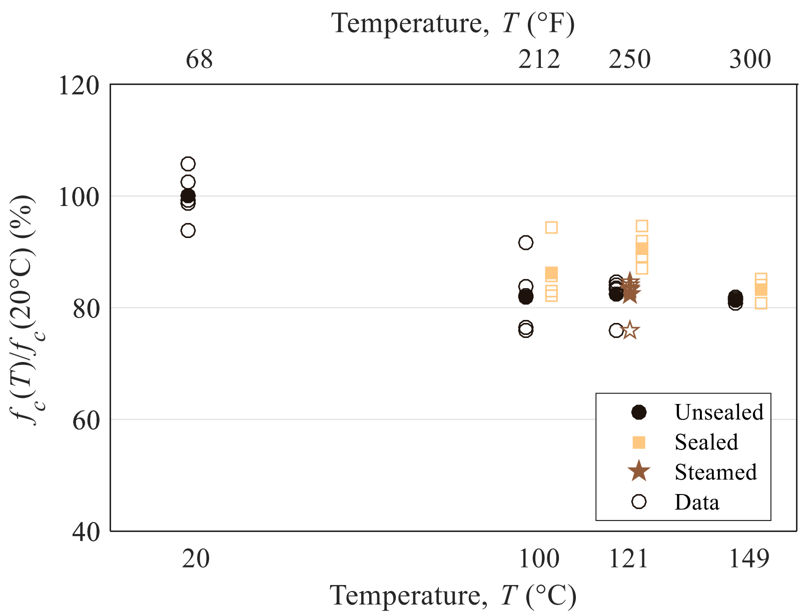

(b) Con-8

Figure 6-6. Change in uniaxial compressive strength of concrete with temperature

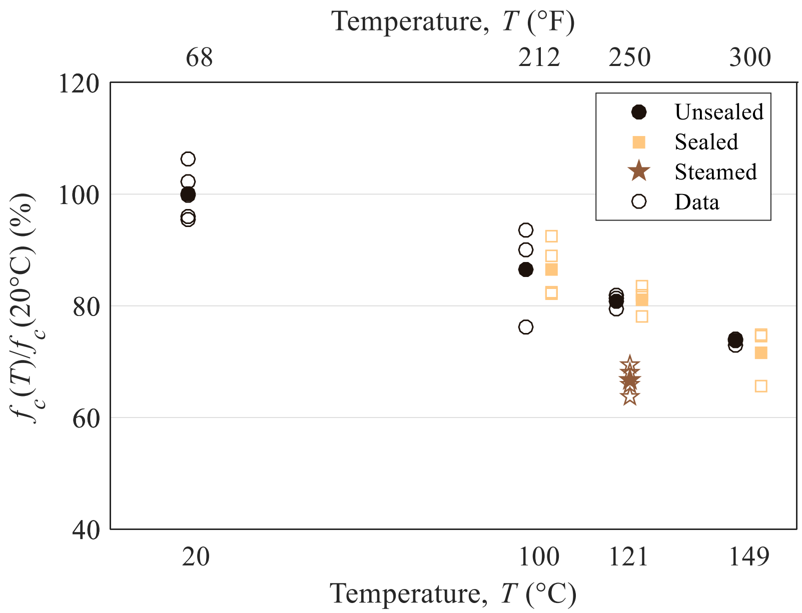

(b) Con-9

Figure 6-6 (cont.). Change in uniaxial compressive strength of concrete with temperature

The two key observations from the data presented in Figure 6-6 are: (1) exposure to temperature higher than 212°F [100°C] reduces the uniaxial compressive strength of concrete (an observation made in Chapters 3 and 5 for the unsealed condition); and (2) changing the moisture condition (unsealed or sealed) during exposure to elevated temperature of up to 300°F [149°C] for 2 hours, does not affect the percentage reduction in uniaxial compressive strength. The percentage reduction in uniaxial compressive strength for temperatures up to 300°F [149°C] in the steamed condition for 1.5 hours and in the sealed and unsealed conditions for 2 hours were similar. An exception to the second observation is the percentage reduction in compressive strength for cylinders of Con-9 heated in steamed condition at 250°F [121°C]. In this test, the autoclave lost steam pressure due to a malfunctioning seal after about 60 minutes of the scheduled 90 minutes of dwell time at the target temperature.

For concrete cylinders heated in sealed condition to 300°F [149°C], Bertero and Polivka (1972) and Kottas et al. (1979) reported reductions in uniaxial compressive strengths of approximately 30% and 60%, respectively, compared to the values measured for cylinders heated in unsealed condition to the same temperature. Two likely reasons for the differences in the observed reductions of strength in this experimental program compared to the results available in literature are: (1) smaller duration of heating used in this experimental program of 2 hours compared to approximately 4 hours and 42 days used by Bertero and Polivka (1972) and Kottas et al. (1979), respectively; and (2) small number of concrete cylinders tested by Bertero and Polivka (1972) and Kottas et al. (1979). Additional tests, perhaps repeating those by Bertero and Polivka (1972) and Kottas et al. (1979), would help reconcile the observed differences in behavior.

CHAPTER 7
SUMMARY, CONCLUSIONS AND RECOMMENDATIONS

7.1 Summary

Reinforced concrete walls are used in nuclear power plants to resist gravity and lateral forces, and some serve a containment function. Design control documents with the United States Nuclear Regulatory Commission (NRC) indicate that loss of coolant accidents in containment structures in large light water reactors can result in internal temperatures of up to 300°F [149°C].

The effects of elevated temperatures of up to 450°F [232°C] on the seismic behavior of reinforced concrete walls were investigated through an integrated series of materials tests and large-scale component experiments that were funded by the United States Department of Energy (DOE). Four rectangular, low-aspect ratio, planar walls were tested after exposure to elevated temperatures of up to 450°F [232°C] in heated and residual conditions (i.e., tested at room temperature after exposure to elevated temperature). Details of the design, construction, and instrumentation are described in this report. Materials-level tests were performed to characterize the effects of elevated temperatures on the behavior of the concrete used to cast the walls.

Materials tests were also performed on conventional, normal strength concretes to characterize the effects of elevated temperatures on the behavior of mechanically damaged concrete. Results are compared with those from tests of virgin concrete specimens heated in the same conditions. Materials tests were also performed on conventional, normal strength concretes to investigate the effects of moisture conditions during heating to temperatures of up to 300°F [149°C]. Tests were performed in the unsealed, sealed and steamed conditions, and results are reported.

7.2 Conclusions

The key conclusions from the results of materials and component tests performed in the research presented in this report are:

Concrete materials:

1. In the unsealed condition, the uniaxial compressive strength and modulus of elasticity of conventional normal strength concrete may be reduced by 10% and 30%, respectively, due to exposure to temperature of 450°F [232°C], with respect to values at room temperature (20°C).

2. The effects of exposure to elevated temperatures of up to 752°F [400°C] on dynamic modulus and uniaxial strength of mechanically *damaged* concrete are similar to those measured for *undamaged* (virgin) concrete heated to the same temperature. (Mechanical *damage*, as defined in this report, reduced the dynamic modulus of the concrete by approximately 10% compared to the values measured in the *undamaged* condition.)

3. Exposure to elevated temperature of up to 450°F [232°C] in the sealed or steamed condition for up to 1.5 hours resulted in similar reductions in weight, dynamic modulus and uniaxial compressive strength of concrete to concrete heated in unsealed condition to the same temperature and duration.

Component (wall) tests:

4. The initial in-plane stiffness of reinforced concrete walls, measured at forces corresponding to shear stress of less than $2\sqrt{f_c}$, is as low as 30% of the theoretical uncracked value calculated using strength of mechanics equations; a conclusion similar to that reached by Luna (2016).

5. The maximum reduction in in-plane lateral stiffness of walls, measured at low levels of force (smaller than 30% of peak strength), and in the absence of axial loads, due to exposure to temperature of up to 450°F [232°C], is approximately 30%. At levels of force greater than 30% of peak strength, the reduction in stiffness due to exposure to temperature of 450°F [232°C] is masked by mechanical damage, and thermal effects can be ignored. This conclusion is based on tests of walls heated in the unsealed condition.

6. For lightly reinforced concrete walls, exposure to temperature of up to 450°F [232°C] will not affect peak strength. For heavily reinforced walls, where strength is governed by

crushing of diagonal struts, exposure to temperature of 450°F [232°C] can reduce in-plane lateral strength by up to 10%, based on materials tests performed in the unsealed condition. However, given the significant variability in the peak shear strength of low aspect ratio walls, no reduction due to exposure to temperature of up to 450°F [232°C] is recommended.

7. Figure 1-8 presents the force – drift ratio cyclic backbone curve recommended by ASCE 41-17 (ASCE, 2017) for the analysis of reinforced concrete shear walls. The co-ordinates that define the piecewise linear backbone curve should be the updated values provided in Epackachi et al. (2019) and Chapter 8 of NIST GCR-17-917-45 (NIST, 2017). The recommended cyclic backbone curve for reinforced concrete shear walls exposed to 450°F [232°C] is presented in Figure 7-1.

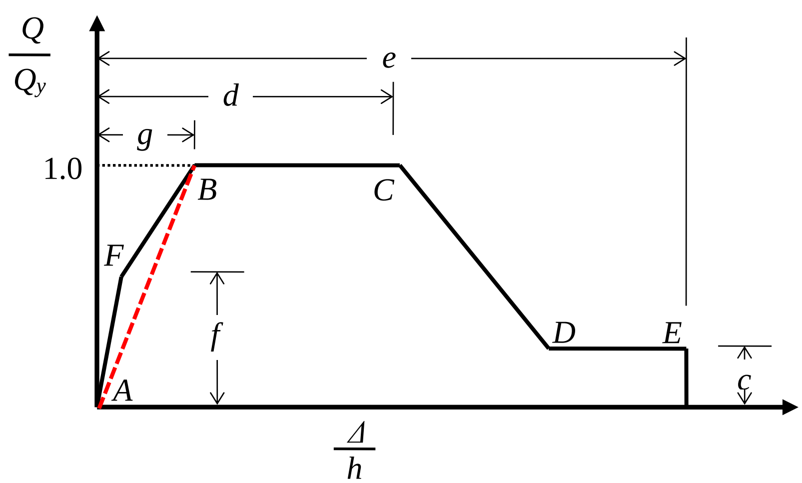

Figure 7-1: Cyclic backbone curve for reinforced concrete shear walls at 450°F [232°C]

If the goal of analysis is to predict response in the range *AF* at a temperature of 450°F [232°C], the lateral stiffness should be reduced by 30% from the updated value given in the NIST report. If the goal of analysis is to predict response in the range *AB* at a temperature of 450°F [232°C], a linear model *AB*, shown as a dashed red line in Figure 7-1, is recommended, using the updated coordinates for point *B* per the NIST report, with no additional reduction in stiffness due to thermal effects. If the goal of analysis is to predict the inelastic cyclic response, a bilinear model to point *C* (i.e., no point *F*) is recommended, using the updated coordinates per the NIST report, with no changes in stiffness or strength due to thermal effects.

8. The ACI 349-13 short-term temperature limit for concrete of 350°F [177°C] in Section E.4.2 should be increased to 450°F [232°C].

7.3 Recommendations for future research

The following recommendations are made for future research:

1. Data on effects of elevated temperature on concrete heated in sealed and steamed conditions are scarce. A comprehensive experimental program, which subjects different concretes to elevated temperatures in unsealed, sealed and steamed conditions, tested in heated and residual conditions, should be performed. By testing in well-documented, controlled conditions, the effects of each parameter (concrete mix proportions, aggregate type, maximum temperature, moisture conditions during heating) on the behavior of concrete can be better understood. The combined effects of elevated temperature and different moisture conditions on mechanical properties of concrete (e.g., tensile strength, static modulus of elasticity, and fracture energy) should be investigated further.

2. The effects of elevated temperatures on concrete should be incorporated into material models to enable analysis of the mechanical-thermal behavior of structural components.

3. The effects of elevated temperature on the seismic behavior of RC walls were measured in the unsealed condition. In nuclear power plant containment structures, steam pipe break accidents would likely result in sealed or steamed conditions. The behavior of RC walls should be investigated numerically and experimentally in the sealed and steamed conditions to further improve the understanding of the effects of thermal accidents on the seismic performance of safety-related structural components in nuclear power plants.

CHAPTER 8
REFERENCES

American Concrete Institute (ACI). (2013). "Code requirements for nuclear safety-related concrete structures (ACI 349-13) and commentary." Farmington Hills, MI.

American Concrete Institute (ACI). (2014a). "Building code requirements for structural concrete (ACI 318-14) and commentary." Farmington Hills, MI.

American Concrete Institute (ACI). (2014b). "Code requirements for determining fire resistance of concrete and masonry construction assemblies (ACI/TMS 216.1-14)." Farmington Hills, MI.

American Society of Civil Engineers (ASCE). (2017). "Seismic evaluation and retrofit of existing buildings (ASCE/SEI 41-17)." Reston, VA.

American Society for Testing and Materials (ASTM). (2014a). "Standard test method for fundamental transverse, longitudinal, and torsional resonant frequencies of concrete specimens (ASTM C215-14)." West Conshohocken, PA.

American Society for Testing and Materials (ASTM). (2014b). "Standard test method for static modulus of elasticity and Poisson’s ratio of concrete in compression (ASTM C469/C469M-14)." West Conshohocken, PA.

American Society for Testing and Materials (ASTM). (2015). "Standard practice for capping cylindrical concrete specimens (ASTM C617/C617M-15)." West Conshohocken, PA.

American Society for Testing and Materials (ASTM). (2016a). "Standard method for flexural strength of concrete (using simple beam with third point loading) (ASTM C78/C78M-16)." West Conshohocken, PA.

American Society for Testing and Materials (ASTM). (2016b). "Standard specification for deformed and plain low-alloy steel bars for concrete reinforcement (ASTM A706/A706M-16)." West Conshohocken, PA.

American Society for Testing and Materials (ASTM). (2017a). "Standard specification for Portland cement (ASTM C150 / C150M-17)." West Conshohocken, PA.

American Society for Testing and Materials (ASTM). (2017b). "Standard specification for temperature-electromotive force (emf) tables for standardized thermocouples (ASTM E230/E230M-17)." West Conshohocken, PA.

American Society for Testing and Materials (ASTM). (2017c). "Standard test method for compressive strength of cylindrical concrete specimens (ASTM C39/C39M-17b)." West Conshohocken, PA.

American Society for Testing and Materials (ASTM). (2017d). "Standard test method for splitting tensile strength of cylindrical concrete specimens (ASTM C496 / C496M - 17)." West Conshohocken, PA.

Badr, A. (2009). "Resistance of cracked concrete to fire and high temperatures." *Concrete Solutions: Proceedings of the International Conference on Concrete Solutions*, Padua, Italy.

Bazant, Z. P. and Prat, P. C. (1988). "Effect of temperature and humidity on fracture energy of concrete." *ACI Materials Journal*, 85(4), 262-271.

Bertero, V. V. and Polivka, M. (1972). "Influence of thermal exposures on mechanical characteristics of concrete (SP34-28)." American Concrete Institute (ACI). Farmington Hills, MI.

Comite Euro-international du Beton (CEB). (1991). "Fire design of concrete structures in accordance with CEB/FIP Model Code 90 (Bulletin No. 208)." Lausanne, Switzerland.

Comite Euro-international du Beton (CEB). (2008). "Fire design of concrete structures - structural behaviour and assessment. State-of-art report." Lausanne, Switzerland.

European Committee for Standardization (CEN). (2004). "Eurocode 2: Design of concrete structures. Part 1-2: General rules - Structural fire design (EN 1992-1-2:2004)." Brussels, Belgium.

Cengel, Y. A. (1998). *Heat transfer: A practical approach*. Boston, MA: WBC McGraw-Hill.

Dai, L.-C., Chen, Y.-S. and Yuann, Y.-R. (2014). "Short-term pressure and temperature MSLB response analyses for large dry containment of the Maanshan nuclear power station." *Nuclear Engineering and Design,* 280, 86-93.

Diederichs, U. and Schneider, U. (1981). "Bond strength at high temperatures." *Magazine of Concrete Research,* 33(115), 75-84.

Edwards, W. T. and Gamble, W. L. (1986). "Strength of grade 60 reinforcing bars after exposure to fire temperatures." *Concrete International,* 8(10), 17-19.

ElMohandes, F. (2013). "Advanced three-dimensional nonlinear analysis of reinforced concrete structures subjected to fire and extreme loads." PhD Dissertation, University of Toronto, Toronto, Canada.

Epackachi, S., Sharma, N., Whittaker, A., Hamburger, R. O. and Hortacsu, A. (2019). "A cyclic backbone curve for shear-critical reinforced concrete walls." *Journal of Structural Engineering*, 145(4), 4019006.

GE-Hitachi Nuclear Energy (GEH). (2014). "Design Control Document for Economic Simplified Boiling-Water Reactor (ESBWR)." Agencywide Documents Access and Management System (ADAMS) Accession Number ML14100A493. Nuclear Regulatory Commission (NRC). Washington, DC.

GE-Hitachi Nuclear Energy (GEH). (2018). https://nuclear.gepower.com/content/dam/gepower-nuclear/global/en_US/documents/product-fact-sheets/ESBWR%20Fact%20Sheet.pdf. *Accessed March 3, 2018.*

General Electric Nuclear Energy (GENE). (1997). "Design Control Document (DCD) for Advanced Boiling Water Reactor (ABWR)." Agencywide Documents Access and Management System (ADAMS) Accession Number ML11126A100. Nuclear Regulatory Commission (NRC), Washington, DC.

Gulec, C. K. and Whittaker, A. S. (2011). "Empirical equations for peak shear strength of low aspect ratio reinforced concrete walls." *ACI Structural Journal*, 108(1), 80-89.

Harada, T., Takeda, J., Yamane, S. and Furumura, F. (1972). "Strength, elasticity and thermal properties of concrete subjected to elevated temperatures." *ACI Special Publication*, 34, 377-406.

Hertz, K. (1982). "The anchorage capacity of reinforcing bars at normal and high temperatures." *Magazine of Concrete Research*, 34(121), 213-220.

Hlavička, É. L.-V. (2017). "Bond after fire." *Construction and Building Materials*, 132, 210-218.

International Atomic Energy Agency (IAEA). (2018). "Nuclear power reactors in the world." Vienna, Austria.

Khoury, G. A. (2000). "Effect of fire on concrete and concrete structures." *Progress in Structural Engineering and Materials*, 2(4), 429-447.

Klingsch, E. (2014). "Explosive spalling of concrete in fire." PhD Dissertation, Swiss Federal Institute of Technology in Zurich (ETH Zurich), Zurich, Switzerland.

Kottas, R., Seeberger, J. and Hilsdorf, H. K. (1979). "Strength characteristics of concrete in the temperature range of 20° to 200°C." *Transactions, 5th International Conference on Structural Mechanics in Reactor Technology (SMiRT 5)*, IASMiRT, Raleigh, NC.

Li, V. C. (1992). "A simplified micromechanical model of compressive strength of fiber-reinforced cementitious composites." *Cement and Concrete Composites*, 14(2), 131-141.

Livermore Software Technology Corporation (LSTC). (2016). "LS-DYNA theory manual." Livermore, CA.

Luna, B. N. (2016). "Seismic response of low aspect ratio reinforced concrete walls for buildings and safety-related nuclear applications." PhD Dissertation, State University of New York at Buffalo, Buffalo, New York, USA.

Luna, B. N., Rivera, J. P., Epackachi, S. and Whittaker, A. S. (2018). "Seismic response of low aspect ratio reinforced concrete walls for buildings and safety-related nuclear applications." Report MCEER-18-0002, Buffalo, NY.

Lv, X., Li, S., Wang, X., Wang, Y., Wang, Z., Xue, F. and Zhang, H. (2014). "Effect of thermal aging on the leak-before-break analysis of nuclear primary pipes." *Nuclear Engineering and Design*, 280, 493-500.

Maraveas, C. and Vrakas, A. A. (2014). "Design of concrete tunnel linings for fire safety." *Structural Engineering International*, 24(3), 319-329.

Mindeguia, J.-C., Pimienta, P., Noumowé, A. and Kanema, M. (2010). "Temperature, pore pressure and mass variation of concrete subjected to high temperature - experimental and numerical discussion on spalling risk." *Cement and Concrete Research*, 40(3), 477-487.

Mindess, S., Young, J. F. and Darwin, D. (2003). *Concrete*. Englewood Cliffs, NJ: Prentice Hall.

Morley, P. D. and Royles, R. (1983). "Response of the bond in reinforced concrete to high temperatures." *Magazine of Concrete Research*, 35(123), 67-74.

Naus, D. J. (2010). "A compilation of elevated temperature concrete material property data and information for use in assessments of nuclear power plant reinforced concrete structures." NUREG/CR-7031, Nuclear Regulatory Commission (NRC), Office of Nuclear Regulatory Research, Washington, DC.

National Instruments (NI). (2017). "LabVIEW user manual." Austin, TX.

National Institute of Standards and Technology (NIST). (2017). "Recommended modeling parameters and acceptance criteria for nonlinear analysis in support of seismic evaluation, retrofit, and design." NIST GCR 17-917-45, Gaithersburg, MD.

Nuclear Regulatory Commission (NRC). (2018a). https://www.nrc.gov/reactors/bwrs.html. *Accessed April 15, 2018.*

Nuclear Regulatory Commission (NRC). (2018b). https://www.nrc.gov/reactors/new-reactors/design-cert.html. *Accessed January 18, 2018.*

Nuclear Regulatory Commission (NRC). (2018c). https://www.nrc.gov/reactors/power.html. *Accessed January 18, 2018.*

Nuclear Regulatory Commission (NRC). (2018d). https://www.nrc.gov/reactors/pwrs.html. *Accessed April 15, 2018.*

Nuclear Regulatory Commission (NRC). (2018e). https://www.nrc.gov/reading-rm/basic-ref/glossary/loss-of-coolant-accident-loca.html. *Accessed January 18, 2018.*

Phan, L. T. and Carino, N. J. (2002). "Effects of test conditions and mixture proportions on behavior of high-strength concrete exposed to high temperatures." *ACI Materials Journal*, 99(1), 54-66.

Schneider, U. (1988). "Concrete at high temperatures - a general review." *Fire Safety Journal,* 13(1), 55-68.

Schneider, U., Diederichs, U. and Ehm, C. (1982). "Effect of temperature on steel and concrete for PCRV's." *Nuclear Engineering and Design,* 67(2), 245-258.

Shin, K.-Y., Kim, S.-B., Kim, J.-H., Chung, M. and Jung, P.-S. (2002). "Thermo-physical properties and transient heat transfer of concrete at elevated temperatures." *Nuclear Engineering and Design,* 212(1), 233-241.

Simonen, F. A., Khaleel, M. A., Phan, H. K., Harris, D. O., Dedhia, D. D., Kalinousky, D. N. and Shaukat, S. K. (2001). "Evaluation of environmental effects on fatigue life of piping." *Nuclear Engineering and Design,* 208(2), 143-165.

Takeuchi, M., Hiramoto, M., Kumagai, N., Yamazaki, N., Kodaira, A. and Sugiyama, K. (1993). "Material properties of concrete and steel bars at elevated temperatures." *Transactions, 12th International Conference on Structural Mechanics in Reactor Technology (SMiRT).* IASMiRT, Raleigh, NC.

Thelandersson, S. (1972). "Effect of high temperatures on tensile strength of concrete." Division of Structural Mechanics and Concrete Construction, Lund Institute of Technology, Lund, Sweden.

Westinghouse Electric Company (WEC). (2011). "Design Control Document (DCD) for Advanced Passive 1000 (AP1000) reactor." Agencywide Documents Access and Management System (ADAMS) Accession Number ML11171A303. Nuclear Regulatory Commission (NRC), Washington, DC.

Westinghouse Electric Company (WEC). (2018). http://www.westinghousenuclear.com/New-Plants/AP1000-PWR/Economic-Benefits. *Accessed March 3, 2018.*

Willam, K., Xi, Y., Lee, K. and Kim, B. (2009). "Thermal response of reinforced concrete structures in nuclear power plants." Department of Civil, Environmental, and Architectural Engineering, University of Colorado, Boulder, CO.

Wong, P., Vecchio, F. and Trommels, H. (2013). "VecTor2 and FormWorks user's manual." University of Toronto, Toronto, Canada.

Wood, S. L. (1990). "Shear strength of low-rise reinforced concrete walls." *ACI Structural Journal*, 87(1), 99-107.

APPENDIX A
THERMAL RESPONSES OF RC WALLS

A.1 Introduction

Thermal responses of RC walls subjected to pipe-break accidents in Nuclear Power Plants (NPPs) are calculated in this appendix using a verified numerical solution. Analytical and numerical solutions to the heat equation are presented in Section A.2. The experimental data reported in Chapter 4 is compared to the results calculated using the numerical solution in Section A.3. The effects of different mechanical (e.g., density) and thermodynamic (e.g., specific heat, thermal conductivity) properties on the thermal responses of RC walls in NPPs subjected to postulated thermal accidents are investigated in Section A.4.

A.2 Heat equation

The heat equation, also known as the Fourier's law for heat conduction, in one dimension is (Cengel, 2003):

$$\frac{\partial}{\partial x}\left(k\frac{\partial T}{\partial x}\right)+\dot{g}=\rho C\frac{\partial T}{\partial t} \tag{A.1}$$

where k is the thermal conductivity of the material, ρ is the density of the material, C is the specific heat capacity of the material, T is the temperature at position x and time t, and $\dot{g}$ is the rate of heat generation in the material. If no heat is generated in the material, $\dot{g}$ is equal to zero and equation (A.1) reduces to:

$$\frac{\partial}{\partial x}\left(k\frac{\partial T}{\partial x}\right)=\rho C\frac{\partial T}{\partial t} \tag{A.2}$$

If the thermal conductivity of the material, k, is considered constant with respect to location x, equation (A.2) can be rewritten as:

$$\frac{\partial T}{\partial t} = \alpha \frac{\partial^2 T}{\partial x^2} \tag{A.3}$$

where α is the thermal diffusivity of the material:

$$\alpha = \frac{k}{\rho C} \tag{A.4}$$

As discussed in Chapter 2, the density, conductivity, and specific heat capacity of concrete vary with temperature. The thermal diffusivity of a given concrete is therefore a function of temperature. However, the ranges in the values of the above properties for different concretes (e.g., mix designs, curing conditions) at room temperature are significant with respect to the change in properties of a given concrete with varying temperature. Further, the change in the above properties with temperature depend on rate and duration of heating, moisture content of concrete, and moisture conditions during heating (unsealed or sealed), which are not well quantified (Naus, 2010; Willam et al., 2009). Accordingly, density, thermal conductivity, and specific heat capacity are assumed to be independent of temperature herein. Importantly, these properties were not measured for the concrete used in the experiments that are described in the body of this report.

A.2.1 Steady state solution of heat equation

A special case of equation (A.3) is no change in temperature with respect to time at any point in the heated medium. This case can be used to determine the temperature distribution in a medium after a long time of heating. In this case, equation (A.3) reduces to

$$\alpha \frac{\partial^2 T}{\partial x^2} = 0 \tag{A.5}$$

Equation (A.5) is a second-order ordinary differential equation and its solution is:

$$T(x) = \left(1 - \frac{x}{L}\right) T_0 + \left(\frac{x}{L}\right) T_L \tag{A.6}$$

where T_0 and T_L are constant temperatures at $x = 0$ and $x = L$, respectively. Here, the temperature distribution in a heated medium in the steady-state condition can be linearly interpolated between the boundary temperatures. The temperature is independent of the material and depends only on the boundary conditions.

A.2.2 Numerical solution of heat equation

Analytical solutions for equation (A.3) exist only for idealized boundary conditions. Therefore, a numerical solution for equation (A.3) is needed to solve for the range of boundary conditions identified in Chapter 1 of this report. In this section, finite difference method is used to develop a solution for equation (A.3). A brief summary of the development of the finite difference solution is presented here; additional details can be found in the archival literature, including Cengel (2003).

Temperature, T, is a function of location, x and time, t: $T(x,t)$. In the finite difference method, the first derivative of $T(x,t)$ with respect to time, t, is approximated as:

$$\frac{\partial T(x,t)}{\partial t} \approx \frac{T(x_1,t_2)-T(x_1,t_1)}{\Delta t} \tag{A.7}$$

where t_1 and t_2 are two successive instants in time and Δt is the time step, calculated as:

$$\Delta t = t_2 - t_1 \tag{A.8}$$

Similarly, the second derivative of $T(x,t)$ with respect to position, x, is approximated as:

$$\frac{\partial^2 T(x,t)}{\partial x^2} \approx \frac{T(x_2,t_1)-2T(x_1,t_1)+T(x_0,t_1)}{(\Delta x)^2} \tag{A.9}$$

where x_0, x_1 and x_2 are successive positions in the heated medium and Δx is calculated as:

$$\Delta x = x_2 - x_1 = x_1 - x_0 \tag{A.10}$$

The finite difference solution to the heat equation in one dimension is obtained by substituting equations (A.7) and (A.9) into equation (A.3), which when simplified leads to the following expression for approximating the temperature, T, at position x_1 and time t_2 :

$$T(x_1,t_2) \approx T(x_1,t_1) + \alpha \frac{\Delta t}{(\Delta x)^2}\left[T(x_2,t_1) - 2T(x_1,t_1) + T(x_0,t_1)\right] \quad \text{(A.11)}$$

Thus, if the temperatures at a locations x_0, x_1 and x_2 are known at time t_1, then the temperature at x_1 can be calculated at time t_2. Equation (A.11) is an explicit formulation of the solution to the heat equation and is not unconditionally stable (Cengel, 2003). The value of the time step, Δt, must satisfy the stability criterion, which is (Cengel, 2003):

$$\frac{\alpha \Delta t}{(\Delta x)^2} \leq 0.5 \quad \text{(A.12)}$$

A.2.3 MATLAB script for the finite difference solution of the heat equation in one dimension

```
% MATLAB script to solve 1d heat conduction equation
% Written by    : Alok Deshpande
% Last modified : 16 Nov 2019

clear; close all; clc;

% Inputs ----------------------------------------------------

L = 10*25.4/1000;   % length in meters

% Discretize length and time
M    = 10;          % number of parts along length
delt = 1;           % time step in seconds

% Thermal properties at 20C (room temperature)
k20   = 2.5;            % Heat conduction in W/m.K
c20   = 800;            % Specific heat capacity in J/kg.K
rho20 = 2500;           % Density in kg/m3

% Input for boundary conditions
% t* is the time at which temperature is T*
t1 = 1;
T1 = 100;
t2 = 100*60;
T2 = 100;

% End of inputs----------------------------------------------

% Discretized length
delx = L/M;

% Number of time steps
```

```
N = t2/delt;

% Time steps
t = 0:delt:N*delt;

% Boundary temperature at all time steps
BoundaryTemp = min(T2,(T1/t1)*t);

% Initializing array to store temperatures at
% all locations and at all time steps
TAll = zeros(M+1,N+1);

% As per the boundary conditions,
% initialize first and last rows
% i.e., the temperature at the boundaries
TAll(1,:)   = BoundaryTemp;
TAll(M+1,:) = BoundaryTemp;

% Calculate thermal diffusivity, alpha
alpha = k20/(c20*rho20);

% Numerical solution of heat equation
% Outer loop in direction of time
% Outer loop starts at second row and goes till end
for n = 2:N+1
    % Inner for loop in direction of location
    % Inner loop only

    % Display current time
    disp(t(n))
    for m = 2:M

        % Calculation parameter
        lambda = alpha*delt/((delx)^2);

        TAll(m,n) = TAll(m,n-1)+(delt*alpha/(delx^2))*(...
                                   TAll(m+1,n-1)-...
                                   2*TAll(m,n-1)+...
                                   TAll(m-1,n-1));
    end
end

% End of script ---------------------------------------------
```

A.2.4 Verification of the numerical solution

To verify the accuracy of the numerical solution to the heat equation developed in Section A.2.2 and presented in Section A.2.3, results of numerical analysis are compared with an available analytical solution. To do so, analysis is performed of a wall of thickness L with a uniform initial temperature of T_0, subjected to boundary surface temperatures of 0°C, beginning at $t = 0$.

The temperature at an arbitrary location x at time t is given by equation (A.3) and the initial and boundary conditions given above. A solution to the partial differential equation (A.3) is:

$$T(x,t) = \left[A\sin\left(\lambda x\right) + B\cos\left(\lambda x\right)\right]e^{-\alpha\lambda^2 t} \tag{A.13}$$

where coefficients A, B and λ can be determined using the boundary conditions. The details of the calculations are not provided here but are discussed by Cengel (2003). For these boundary conditions, the analytical solution is:

$$T\left(x,t\right) = \frac{4T_0}{\pi} \sum_{n=1,3,5...} \frac{1}{n} \sin\left(\frac{n\pi x}{L}\right) e^{-\alpha\left(\frac{n\pi}{L}\right)^2 t} \tag{A.14}$$

For generating analytical and numerical solutions, T_0, L and α are assumed to be 100°C, 0.254 m [10 in.], and 1.25×10^{-6} m²/s, respectively. The thermal gradients through the wall thickness at three instants in time, calculated using the first three terms of the analytical solution of equation (A.14) and the numerical solution are plotted in Figure A-1. The numerical solutions are in good agreement with the analytical solution at the three instants in time (*t* = 600 s, 3000 s, 6000 s) and so the numerical solution is assumed to be verified for calculating temperature distributions in walls of nuclear power plants exposed to thermal accidents.

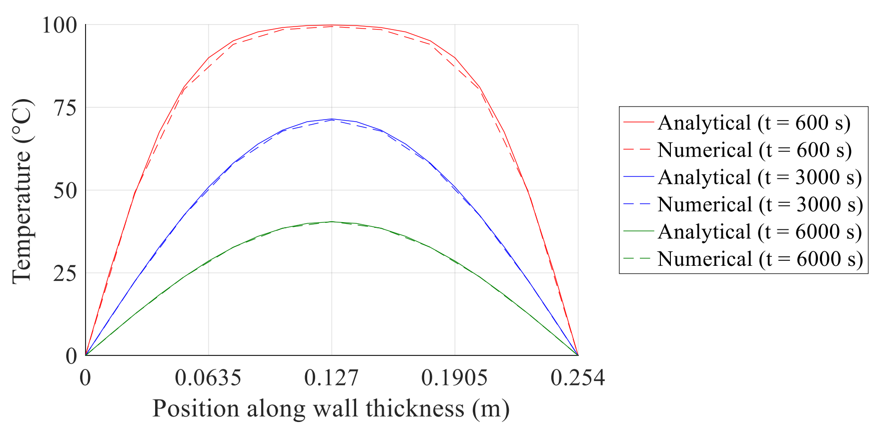

Figure A-1: Thermal gradients through a 0.254 m thick wall calculated using analytical and numerical methods

A.3 Comparison of experimental data with numerical solutions

Results of numerical analysis of the four walls tested in Chapter 4 are presented in this section. Values for the mechanical and thermodynamic properties of the concrete required to perform the numerical analysis were taken from the archival literature because they were not measured. (Values at room temperature and their variation with temperature are discussed in Chapter 2.) A density of 2500 kg/m^3, thermal conductivity of 2.5 W/m.K and specific heat capacity of 1200 J/kg.K were assumed for the numerical analysis. The temperatures measured on the wall surfaces in the experimental program were applied as boundary conditions in the numerical model. The wall was discretized into ten equal lengths through the thickness. A time step of 1 second was chosen, which is significantly smaller than the time step required to satisfy the stability criterion of equation (A.12).

The thermal gradients measured in the last heated cycle and the thermal history measured at the center of the wall are plotted together with the results of the numerical analyses for each wall in Figure A-2. There is reasonable agreement between the numerical results and the measured temperatures.

As discussed in Chapters 3 and 4, even though the same concrete mixture was specified for the four walls, the walls were tested at different ages and the duration of testing for each wall was different. Differences in the thermal properties of the concretes in the four walls at room temperature are expected. Variations in the properties with changing temperature for the concrete in a given wall are also expected. However, because these data were not measured, and representative values were assigned, differences between measured and predicted thermal histories are expected. Another source for the discrepancy between the measured and predicted results is the wall surface temperature. Four panels heated each face of the wall. Each heating panel was controlled independently and there were small differences in the heat applied by each panel. Temperature at one representative location on the wall was then assumed to represent that of the entire wall surface.

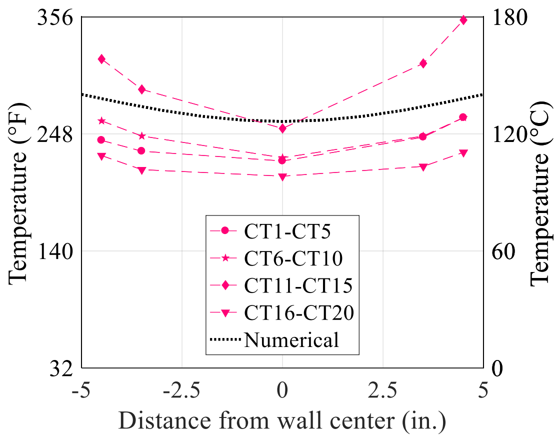

(a) Wall 1, thermal gradients, start of LC15

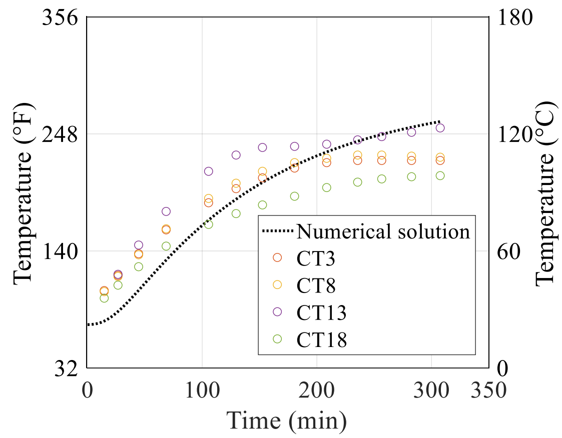

(b) Wall 1, thermal history, center of wall

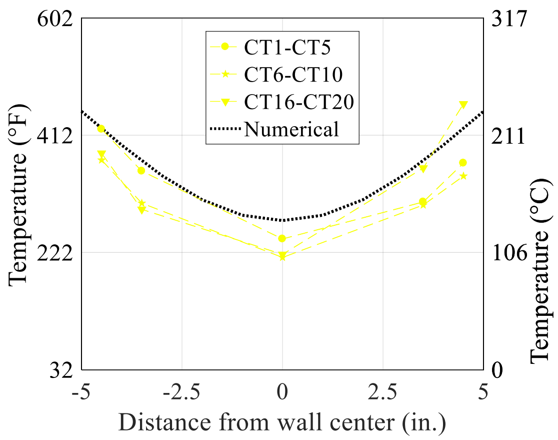

(c) Wall 2, thermal gradients, start of LC16

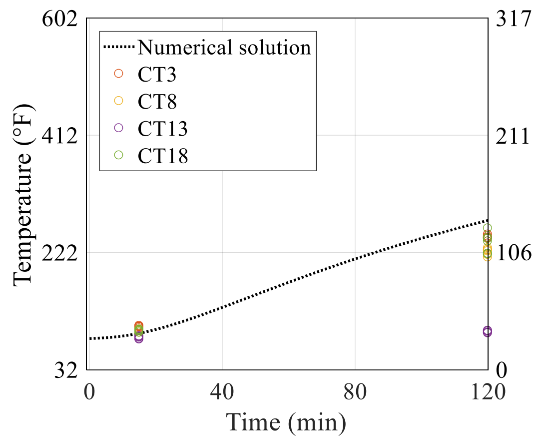

(d) Wall 2, thermal history, center of wall

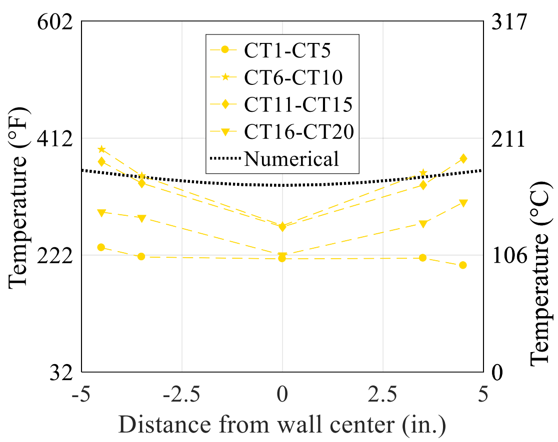

(e) Wall 3, thermal gradients, start of LC15

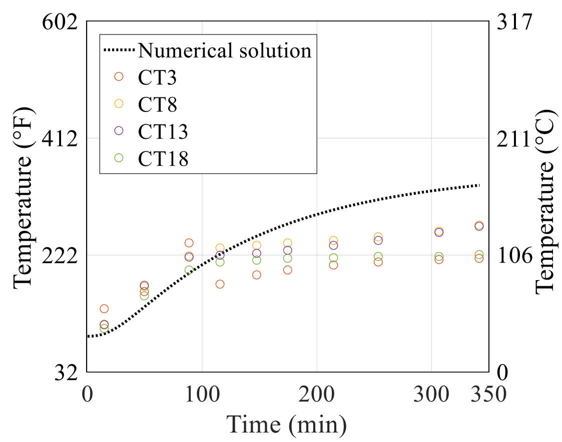

(f) Wall 3, thermal history, center of wall

Figure A-2: Temperatures measured in walls of Chapter 4 and numerical solutions

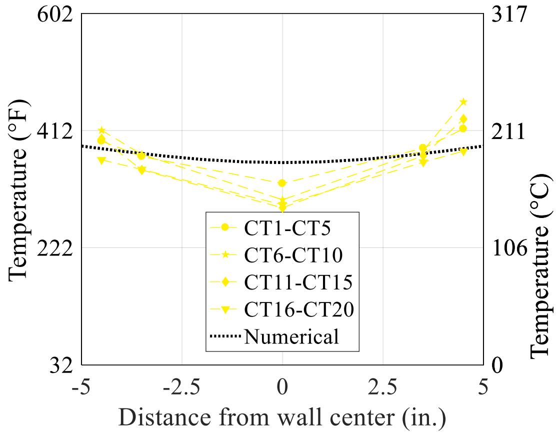

(g) Wall 4, thermal gradients, start of LC15

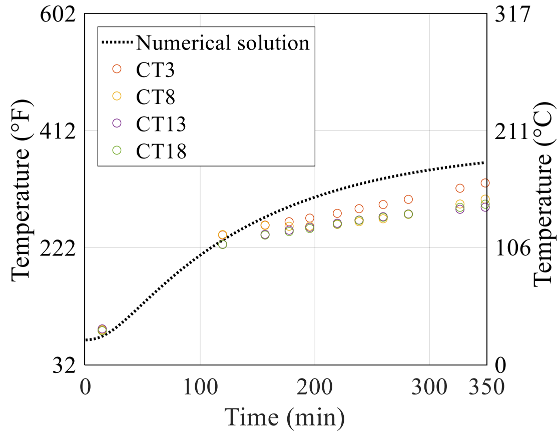

(h) Wall 4, thermal history, center of wall

Figure A-2 (cont.): Temperatures measured in walls of Chapter 4 and numerical solutions

A.4 Response of RC walls in NPPs to thermal accidents

A.4.1 Thermal histories of pipe-break accidents in NPPs

The published thermal histories from postulated pipe-break accidents in containment structures, as discussed in Chapter 1, were digitized and reproduced in Figure A-3. (Data are published for different time periods: 5 hours for ABWR, 70 hours for AP1000, 72 hours for ESBWR.) The steady-state temperatures range between 160°F [71°C] and 285°F [141°C]. An idealized temperature-time curve, with a near instantaneous rise to 300°F [149°C] between time equal to 0 and 1 minute, and constant temperature thereafter is also presented in the figure. The thermal histories are plotted at two different time scales. The digitized histories may be inaccurate for times close to $t = 0$.

The idealized temperature history envelopes the published thermal histories and the profile is similar to all except for the ESBWR wetwell. Accordingly, it is used here to study the evolution of temperatures in walls of NPPs subjected to pipe-break accidents.

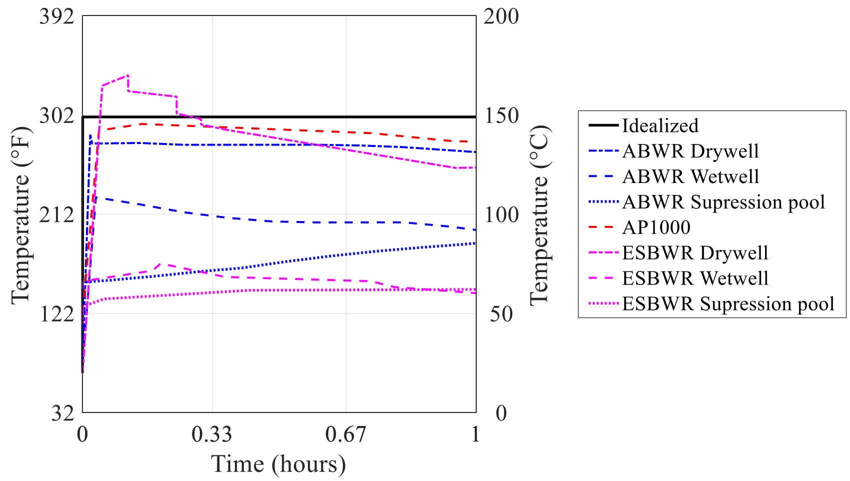

(a) 1 hour

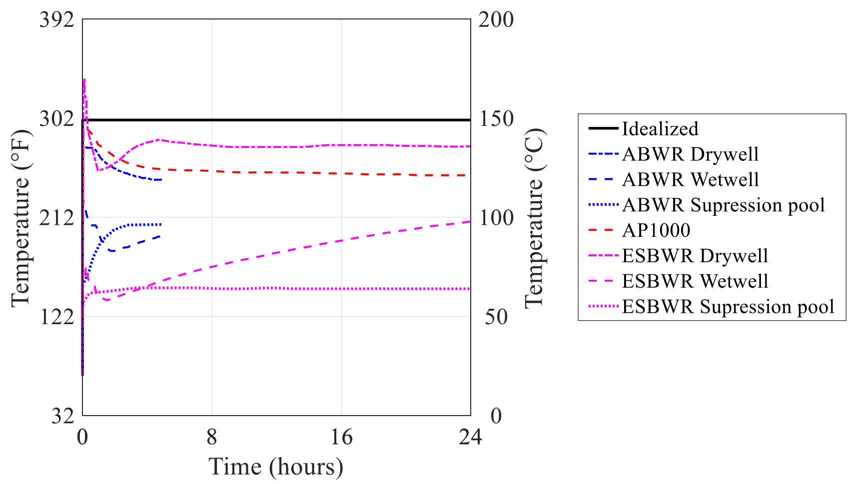

(b) 72 hours

Figure A-3: Idealized and published thermal histories for pipe-break accidents in NPPs at two time scales

A.4.2 Effects of wall thickness and time

The experiments presented in Chapter 4 were performed on 10 in. [0.254 m] thick RC walls and the maximum duration of heating was approximately six hours. In contrast, postulated thermal accidents in NPP containment structures can subject the surrounding RC walls to elevated temperature for at least 72 hours (see Figure A-3) and the walls can be 60+ in. [1.52+ m] thick. Thus, it is important to understand the effects of wall thickness and duration of heating at the test and prototype scales to ensure that the interpretation of the test results can be assumed to be appropriate at full scale.

The numerical solution developed in Section A.2.2, is applied to calculate the thermal response of concrete walls of five thicknesses subjected to the idealized temperature-time series discussed in Section A.4.1. Wall thicknesses of 10, 24, 36, 48 and 60 in. [0.25, 0.61, 0.91, 1.22 and 1.52 m] are considered. The initial (ambient) temperature of the walls is 70°F [20°C]. The density, thermal conductivity and specific heat capacity of the concrete are considered to be 2500 kg/m^3, 2.5 W/m.K and 800 J/kg.K, respectively. The wall thickness is discretized into ten equal lengths and a time step of 1 second is used. Two sets of boundary conditions are considered: heating of both faces of the wall and heating of one face only. The resulting thermal histories at the centers of the walls are presented in Figure A-4. The temperature asymptote in Figure A-4a is 302°F [150°C]. The temperature asymptote in Figure A-4b is 186°F [85°C]: the average of the two surface temperatures. The temperature asymptotes represent the steady states in both boundary conditions.

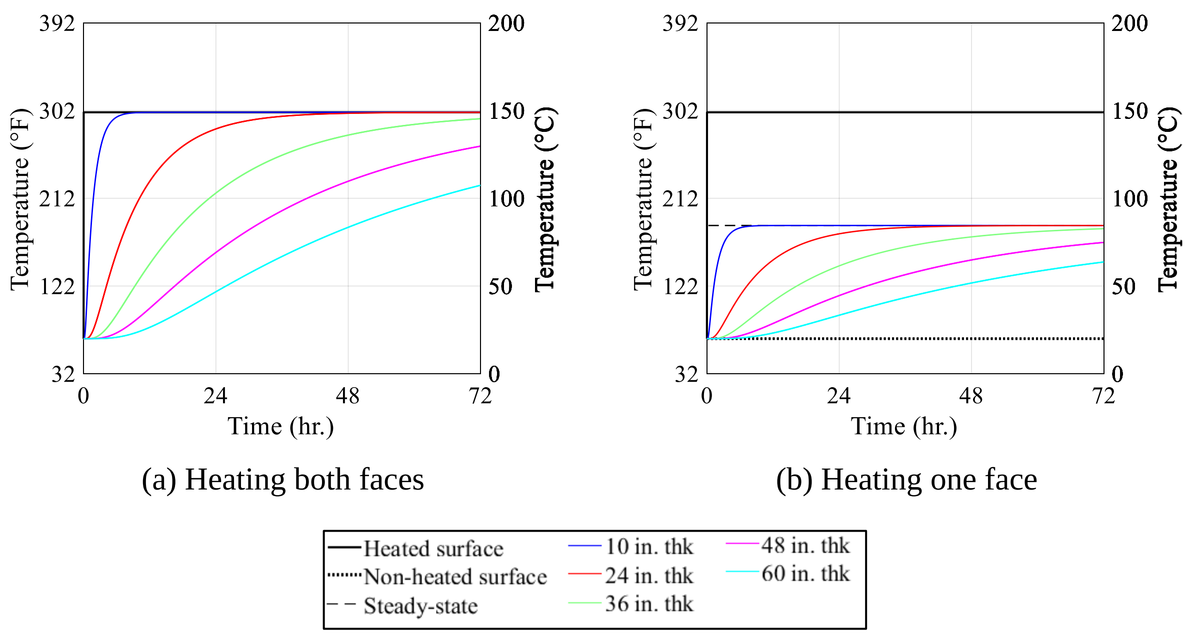

Figure A-4: Thermal histories at the centers of walls of different thicknesses

For the case of heating on one face, the temperature of the non-heated surface is held constant at room temperature (=70°F [20°C]). In the event of an accident, the temperature of non-heated face will depend on the transfer of heat from the wall to the surrounding environment through convection (air) and conduction (soil, water, concrete, steel or other media). Convection depends on environmental conditions such as the temperature and moisture content of the air, and wind speed. Conduction into the surrounding media depends on factors such as moisture content, and thickness. It is possible that the rate of heat transfer from the heated face to the non-heated face would exceed the rate of heat loss from the non-heated face to the surrounding environment. In this case, the temperature of the non-heated face would increase from the ambient value but that is not considered here. A steeper thermal gradient results from the boundary conditions assumed here than would be the case if the temperature of the non-heated face increased above ambient.

The thermal history at the center of each wall is normalized and replotted in Figure A-5. For each temperature-time series, time is normalized by dividing by the square of the wall thickness and temperature is normalized by dividing by the temperature of the heated surface(s).

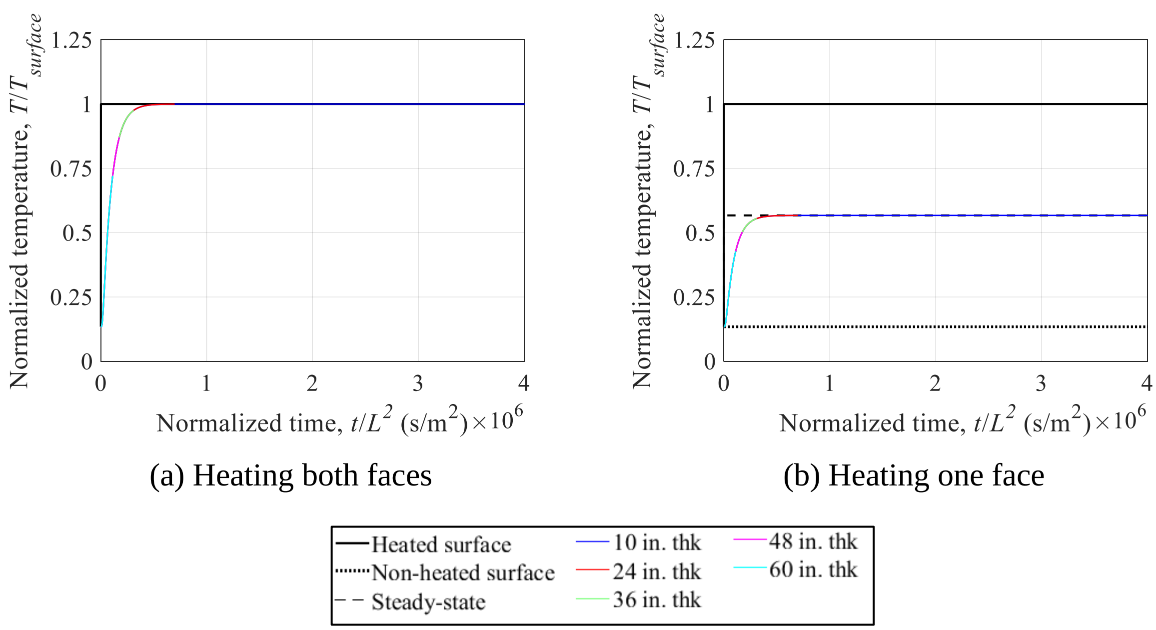

Figure A-5: Normalized thermal histories at the centers of walls of different thicknesses

The normalized temperature-time series for walls of all thicknesses in Figure A-5 *collapse* to a single curve for each heating boundary condition. For example, the temperature at the center of a 24 in. [0.61 m] thick wall after 1 hour of heating will be reached at the center of a 48 in. [1.22 m] thick wall after 4 hours of heating. Thus, the thermal gradients in the 10 in. [0.254 m] thick walls tested in the experimental program after 1 (6) hours of heating are representative of the gradients in a 24 in. [0.609 m] thick wall after 6 (34) hours of exposure and a 60 in. [1.52 m] thick wall after 36 (216) hours of exposure.

The thermal gradients for wall of different thicknesses at five time instants (= 0.5, 1, 3, 6, 12, 36 and 72 hours) are plotted in Figure A-6 and Figure A-7 for heating on both faces and one face, respectively. The center of the wall corresponds to a normalized thickness of 0. The normalizing surface temperature in both figures is 302°F [150°C]. Significant differences are observed in the evolution of the thermal profiles for walls of different thicknesses, but after 72 hours, the profiles stabilize. For the walls heated on both faces, the temperature after 72 hours is constant through the thickness for the 10-, 24- and 36-inch thick walls, and equal to the surface temperature. For the walls heated on one face only, the temperature profile through wall is linear with thickness after 72 hours for the 10-, 24- and 36-inch thick walls. The thermal gradients described at the end of the previous paragraph are confirmed by the data in the Figure A-6.

The experiments described in Chapter 4 involved 10 in. thick walls exposed for hours to elevated temperatures on both faces. The thermal profiles developed in the experimental program are not inconsistent with those expected in thicker walls in NPPs exposed to elevated temperatures for tens of hours.

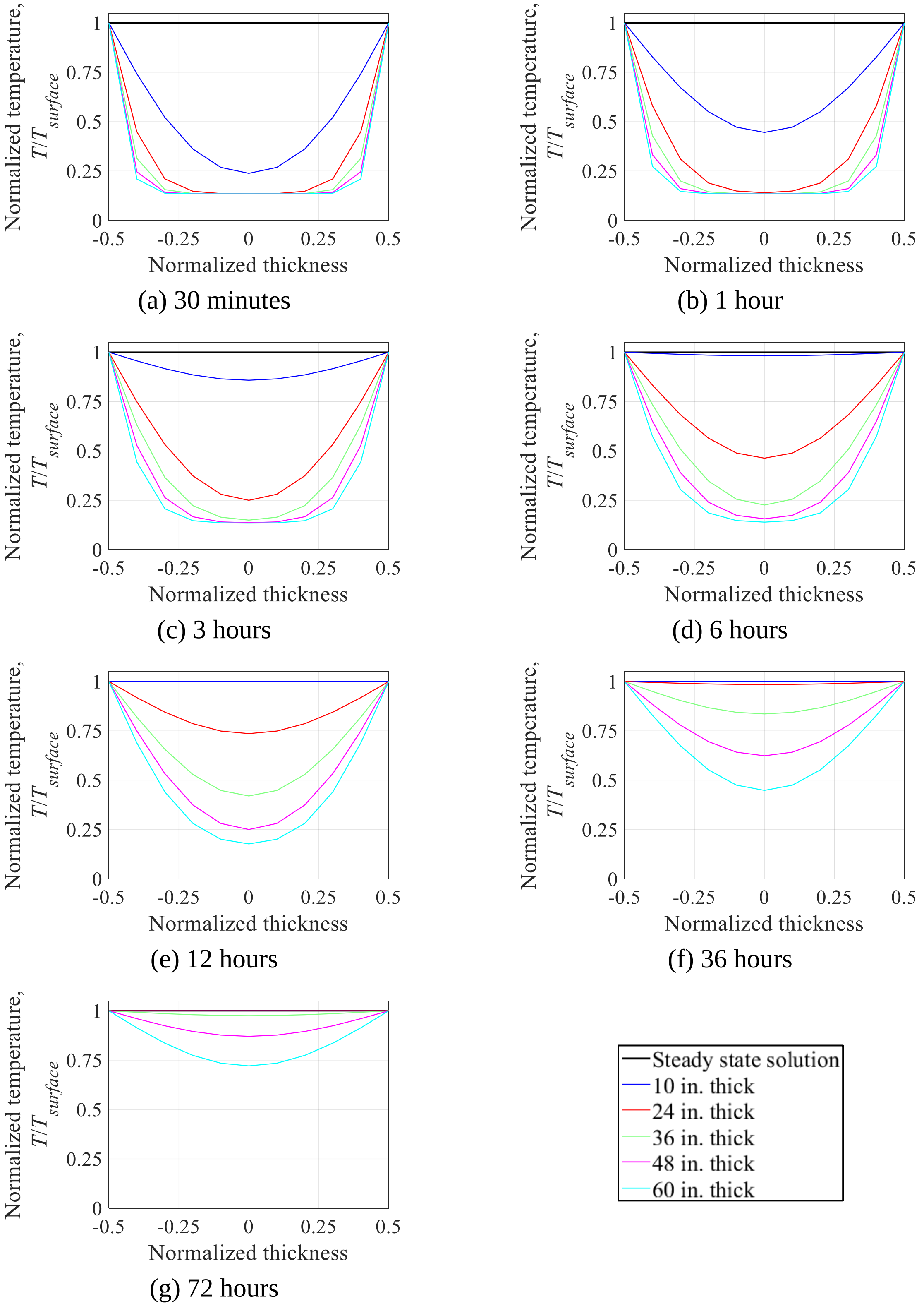

Figure A-6: Thermal gradients in walls of different thicknesses at different times, heating on both faces

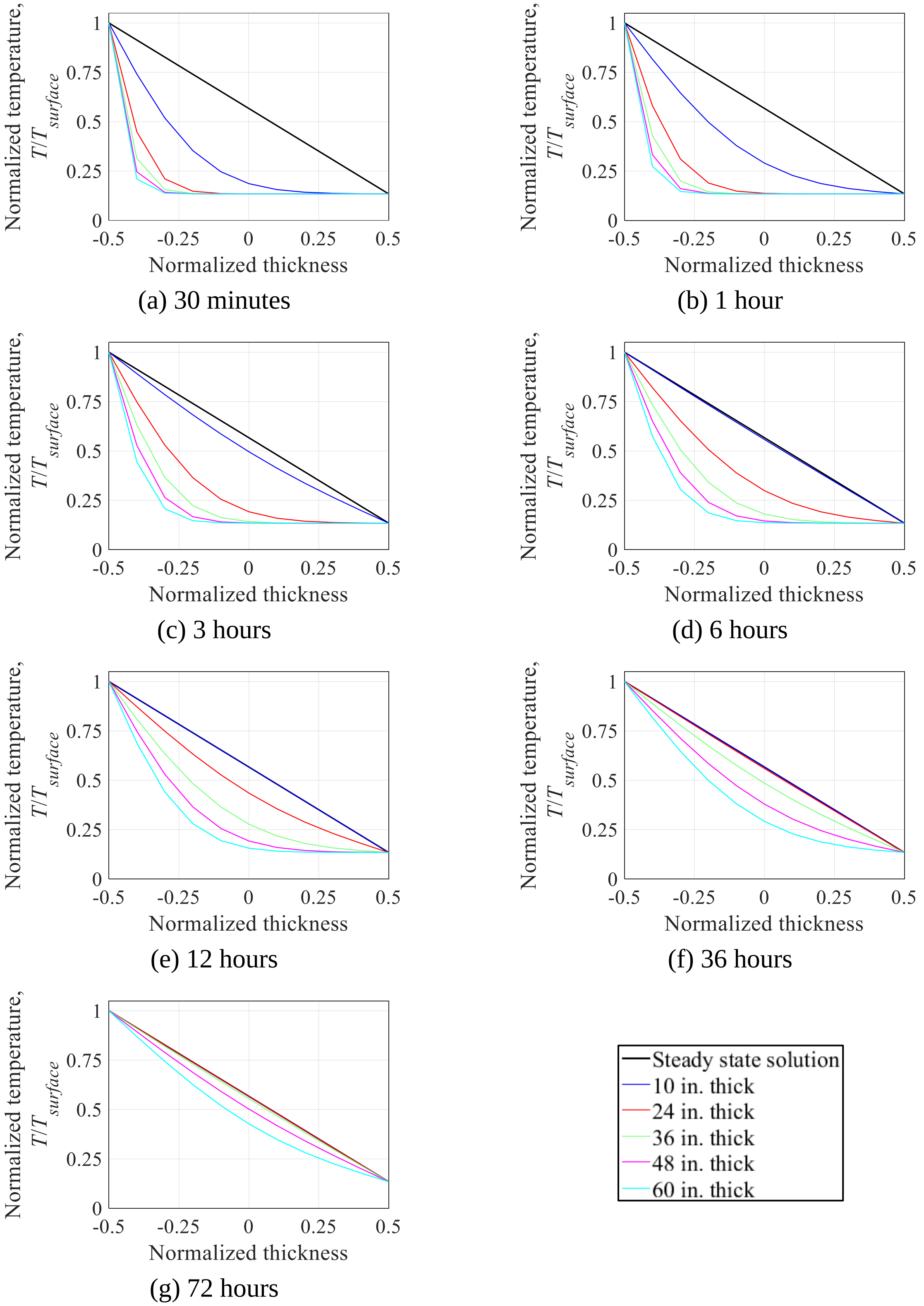

Figure A-7: Thermal gradients in walls of different thicknesses at different times, heating on one face

A.4.3 Effects of variation in thermal properties

The mechanical and thermodynamic properties of concrete affecting its thermal response are density, thermal conductivity and specific heat capacity. As discussed in Chapter 2, there is a large scatter in the values of these properties, even at room temperature, and all are temperature dependent. In the temperature range of interest here (i.e., pipe-break accidents in NPPs), density can decrease by 5%, thermal conductivity can vary between 1.2 and 2.5 W/m.K, and specific heat capacity can vary between 800 and 1200 J/kg.K (Naus, 2010). The possible range in specific heat capacity is much greater, with a maximum value of 2000 J/kgK, but this is very sensitive to moisture content. Herein, it is assumed that the concrete is mature with a low moisture content and that 1200 J/kg.K is a reasonable upper bound on specific heat capacity for temperature between ambient and 300°F [149°C].

Thermal diffusivity is calculated per equation (A.4). Conservative maximum and minimum values for the thermal diffusivity can be established by using upper and lower bounding values of density, thermal conductivity, and specific heat capacity.

An upper bound on the density of concrete is assumed to be 156 lb/ft^3 [2500 kg/m^3]; the lower bound is assumed to be 5% smaller. Upper and lower bounds for thermal conductivity and specific heat capacity are provided above. The thermal responses of a 24 in. [0.51 m] thick wall with upper, best estimate, and lower bounds on thermal diffusivity (= 1.32×10^{-6}, 0.74×10^{-6}, and 0.40×10^{-6} m^2/s, respectively), and heated on both faces and one face, are plotted in Figure A-8. There is a significant difference in the thermal histories for the upper and lower bounds on thermal diffusivities for each boundary condition. For example, the difference in temperature in the middle of the wall for the bounding values of thermal diffusivity is greater than 90°F [50°C] after 12 hours of heating.

There is a lack of information on the thermodynamic properties of concrete, which vary as a function of mix design, curing, age, and temperature. Collecting and publishing these data would be of significant value to engineers tasked with evaluating the performance of nuclear and non-nuclear reinforced concrete structures at elevated temperatures. Some advanced reactors will operate at high temperatures and such data would help avoid conservatisms in design and the associated increases in overnight capital cost. The analysis described in this section assumed that the thermodynamic properties of concrete were independent. An understanding of the dependencies would lead to tighter ranges on thermal diffusivity and improved predictions of the thermal response of reinforced concrete walls.

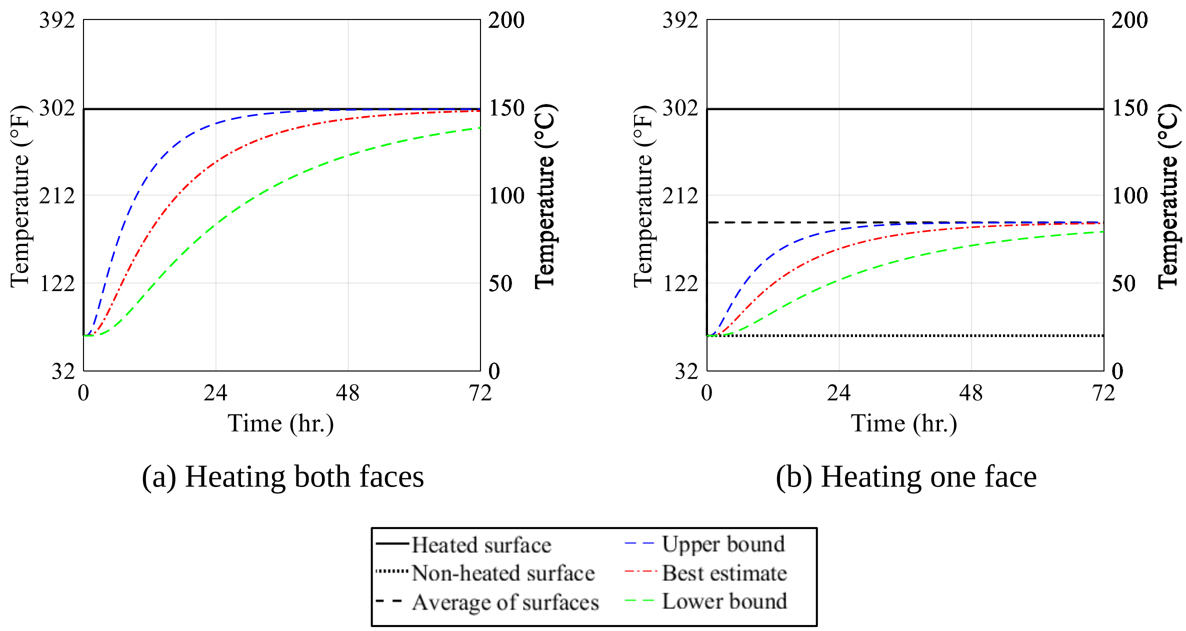

Figure A-8: Thermal histories at the center of a 24 in. thick wall in different heating conditions and bounds on thermal diffusivity

MCEER Technical Reports

MCEER publishes technical reports on a variety of subjects written by authors funded through MCEER. These reports can be downloaded from the MCEER website at http://www.buffalo.edu/mceer. They can also be requested through NTIS, P.O. Box 1425, Springfield, Virginia 22151. NTIS accession numbers are shown in parenthesis, if available.

NCEER-87-0001 "First-Year Program in Research, Education and Technology Transfer," 3/5/87, (PB88-134275, A04, MF-A01).

NCEER-87-0002 "Experimental Evaluation of Instantaneous Optimal Algorithms for Structural Control," by R.C. Lin, T.T. Soong and A.M. Reinhorn, 4/20/87, (PB88-134341, A04, MF-A01).

NCEER-87-0003 "Experimentation Using the Earthquake Simulation Facilities at University at Buffalo," by A.M. Reinhorn and R.L. Ketter, not available.

NCEER-87-0004 "The System Characteristics and Performance of a Shaking Table," by J.S. Hwang, K.C. Chang and G.C. Lee, 6/1/87, (PB88-134259, A03, MF-A01). This report is available only through NTIS (see address given above).

NCEER-87-0005 "A Finite Element Formulation for Nonlinear Viscoplastic Material Using a Q Model," by O. Gyebi and G. Dasgupta, 11/2/87, (PB88-213764, A08, MF-A01).

NCEER-87-0006 "Symbolic Manipulation Program (SMP) - Algebraic Codes for Two and Three Dimensional Finite Element Formulations," by X. Lee and G. Dasgupta, 11/9/87, (PB88-218522, A05, MF-A01).

NCEER-87-0007 "Instantaneous Optimal Control Laws for Tall Buildings Under Seismic Excitations," by J.N. Yang, A. Akbarpour and P. Ghaemmaghami, 6/10/87, (PB88-134333, A06, MF-A01). This report is only available through NTIS (see address given above).

NCEER-87-0008 "IDARC: Inelastic Damage Analysis of Reinforced Concrete Frame - Shear-Wall Structures," by Y.J. Park, A.M. Reinhorn and S.K. Kunnath, 7/20/87, (PB88-134325, A09, MF-A01). This report is only available through NTIS (see address given above).

NCEER-87-0009 "Liquefaction Potential for New York State: A Preliminary Report on Sites in Manhattan and Buffalo," by M. Budhu, V. Vijayakumar, R.F. Giese and L. Baumgras, 8/31/87, (PB88-163704, A03, MF-A01). This report is available only through NTIS (see address given above).

NCEER-87-0010 "Vertical and Torsional Vibration of Foundations in Inhomogeneous Media," by A.S. Veletsos and K.W. Dotson, 6/1/87, (PB88-134291, A03, MF-A01). This report is only available through NTIS (see address given above).

NCEER-87-0011 "Seismic Probabilistic Risk Assessment and Seismic Margins Studies for Nuclear Power Plants," by Howard H.M. Hwang, 6/15/87, (PB88-134267, A03, MF-A01). This report is only available through NTIS (see address given above).

NCEER-87-0012 "Parametric Studies of Frequency Response of Secondary Systems Under Ground-Acceleration Excitations," by Y. Yong and Y.K. Lin, 6/10/87, (PB88-134309, A03, MF-A01). This report is only available through NTIS (see address given above).

NCEER-87-0013 "Frequency Response of Secondary Systems Under Seismic Excitation," by J.A. HoLung, J. Cai and Y.K. Lin, 7/31/87, (PB88-134317, A05, MF-A01). This report is only available through NTIS (see address given above).

NCEER-87-0014 "Modelling Earthquake Ground Motions in Seismically Active Regions Using Parametric Time Series Methods," by G.W. Ellis and A.S. Cakmak, 8/25/87, (PB88-134283, A08, MF-A01). This report is only available through NTIS (see address given above).

NCEER-87-0015 "Detection and Assessment of Seismic Structural Damage," by E. DiPasquale and A.S. Cakmak, 8/25/87, (PB88-163712, A05, MF-A01). This report is only available through NTIS (see address given above).

NCEER-87-0016 "Pipeline Experiment at Parkfield, California," by J. Isenberg and E. Richardson, 9/15/87, (PB88-163720, A03, MF-A01). This report is available only through NTIS (see address given above).

NCEER-87-0017 "Digital Simulation of Seismic Ground Motion," by M. Shinozuka, G. Deodatis and T. Harada, 8/31/87, (PB88-155197, A04, MF-A01). This report is available only through NTIS (see address given above).

NCEER-87-0018 "Practical Considerations for Structural Control: System Uncertainty, System Time Delay and Truncation of Small Control Forces," J.N. Yang and A. Akbarpour, 8/10/87, (PB88-163738, A08, MF-A01). This report is only available through NTIS (see address given above).

NCEER-87-0019 "Modal Analysis of Nonclassically Damped Structural Systems Using Canonical Transformation," by J.N. Yang, S. Sarkani and F.X. Long, 9/27/87, (PB88-187851, A04, MF-A01).

NCEER-87-0020 "A Nonstationary Solution in Random Vibration Theory," by J.R. Red-Horse and P.D. Spanos, 11/3/87, (PB88-163746, A03, MF-A01).

NCEER-87-0021 "Horizontal Impedances for Radially Inhomogeneous Viscoelastic Soil Layers," by A.S. Veletsos and K.W. Dotson, 10/15/87, (PB88-150859, A04, MF-A01).

NCEER-87-0022 "Seismic Damage Assessment of Reinforced Concrete Members," by Y.S. Chung, C. Meyer and M. Shinozuka, 10/9/87, (PB88-150867, A05, MF-A01). This report is available only through NTIS (see address given above).

NCEER-87-0023 "Active Structural Control in Civil Engineering," by T.T. Soong, 11/11/87, (PB88-187778, A03, MF-A01).

NCEER-87-0024 "Vertical and Torsional Impedances for Radially Inhomogeneous Viscoelastic Soil Layers," by K.W. Dotson and A.S. Veletsos, 12/87, (PB88-187786, A03, MF-A01).

NCEER-87-0025 "Proceedings from the Symposium on Seismic Hazards, Ground Motions, Soil-Liquefaction and Engineering Practice in Eastern North America," October 20-22, 1987, edited by K.H. Jacob, 12/87, (PB88-188115, A23, MF-A01). This report is available only through NTIS (see address given above).

NCEER-87-0026 "Report on the Whittier-Narrows, California, Earthquake of October 1, 1987," by J. Pantelic and A. Reinhorn, 11/87, (PB88-187752, A03, MF-A01). This report is available only through NTIS (see address given above).

NCEER-87-0027 "Design of a Modular Program for Transient Nonlinear Analysis of Large 3-D Building Structures," by S. Srivastav and J.F. Abel, 12/30/87, (PB88-187950, A05, MF-A01). This report is only available through NTIS (see address given above).

NCEER-87-0028 "Second-Year Program in Research, Education and Technology Transfer," 3/8/88, (PB88-219480, A04, MF-A01).

NCEER-88-0001 "Workshop on Seismic Computer Analysis and Design of Buildings With Interactive Graphics," by W. McGuire, J.F. Abel and C.H. Conley, 1/18/88, (PB88-187760, A03, MF-A01). This report is only available through NTIS (see address given above).

NCEER-88-0002 "Optimal Control of Nonlinear Flexible Structures," by J.N. Yang, F.X. Long and D. Wong, 1/22/88, (PB88-213772, A06, MF-A01).

NCEER-88-0003 "Substructuring Techniques in the Time Domain for Primary-Secondary Structural Systems," by G.D. Manolis and G. Juhn, 2/10/88, (PB88-213780, A04, MF-A01).

NCEER-88-0004 "Iterative Seismic Analysis of Primary-Secondary Systems," by A. Singhal, L.D. Lutes and P.D. Spanos, 2/23/88, (PB88-213798, A04, MF-A01).

NCEER-88-0005 "Stochastic Finite Element Expansion for Random Media," by P.D. Spanos and R. Ghanem, 3/14/88, (PB88-213806, A03, MF-A01).

NCEER-88-0006 "Combining Structural Optimization and Structural Control," by F.Y. Cheng and C.P. Pantelides, 1/10/88, (PB88-213814, A05, MF-A01).

NCEER-88-0007 "Seismic Performance Assessment of Code-Designed Structures," by H.H-M. Hwang, J-W. Jaw and H-J. Shau, 3/20/88, (PB88-219423, A04, MF-A01). This report is only available through NTIS (see address given above).

NCEER-88-0008 "Reliability Analysis of Code-Designed Structures Under Natural Hazards," by H.H-M. Hwang, H. Ushiba and M. Shinozuka, 2/29/88, (PB88-229471, A07, MF-A01). This report is only available through NTIS (see address given above).

NCEER-88-0009 "Seismic Fragility Analysis of Shear Wall Structures," by J-W Jaw and H.H-M. Hwang, 4/30/88, (PB89-102867, A04, MF-A01).

NCEER-88-0010 "Base Isolation of a Multi-Story Building Under a Harmonic Ground Motion - A Comparison of Performances of Various Systems," by F-G Fan, G. Ahmadi and I.G. Tadjbakhsh, 5/18/88, (PB89-122238, A06, MF-A01). This report is only available through NTIS (see address given above).

NCEER-88-0011 "Seismic Floor Response Spectra for a Combined System by Green's Functions," by F.M. Lavelle, L.A. Bergman and P.D. Spanos, 5/1/88, (PB89-102875, A03, MF-A01).

NCEER-88-0012 "A New Solution Technique for Randomly Excited Hysteretic Structures," by G.Q. Cai and Y.K. Lin, 5/16/88, (PB89-102883, A03, MF-A01).

NCEER-88-0013 "A Study of Radiation Damping and Soil-Structure Interaction Effects in the Centrifuge," by K. Weissman, supervised by J.H. Prevost, 5/24/88, (PB89-144703, A06, MF-A01).

NCEER-88-0014 "Parameter Identification and Implementation of a Kinematic Plasticity Model for Frictional Soils," by J.H. Prevost and D.V. Griffiths, not available.

NCEER-88-0015 "Two- and Three- Dimensional Dynamic Finite Element Analyses of the Long Valley Dam," by D.V. Griffiths and J.H. Prevost, 6/17/88, (PB89-144711, A04, MF-A01).

NCEER-88-0016 "Damage Assessment of Reinforced Concrete Structures in Eastern United States," by A.M. Reinhorn, M.J. Seidel, S.K. Kunnath and Y.J. Park, 6/15/88, (PB89-122220, A04, MF-A01). This report is only available through NTIS (see address given above).

NCEER-88-0017 "Dynamic Compliance of Vertically Loaded Strip Foundations in Multilayered Viscoelastic Soils," by S. Ahmad and A.S.M. Israil, 6/17/88, (PB89-102891, A04, MF-A01).

NCEER-88-0018 "An Experimental Study of Seismic Structural Response With Added Viscoelastic Dampers," by R.C. Lin, Z. Liang, T.T. Soong and R.H. Zhang, 6/30/88, (PB89-122212, A05, MF-A01). This report is available only through NTIS (see address given above).

NCEER-88-0019 "Experimental Investigation of Primary - Secondary System Interaction," by G.D. Manolis, G. Juhn and A.M. Reinhorn, 5/27/88, (PB89-122204, A04, MF-A01).

NCEER-88-0020 "A Response Spectrum Approach For Analysis of Nonclassically Damped Structures," by J.N. Yang, S. Sarkani and F.X. Long, 4/22/88, (PB89-102909, A04, MF-A01).

NCEER-88-0021 "Seismic Interaction of Structures and Soils: Stochastic Approach," by A.S. Veletsos and A.M. Prasad, 7/21/88, (PB89-122196, A04, MF-A01). This report is only available through NTIS (see address given above).

NCEER-88-0022 "Identification of the Serviceability Limit State and Detection of Seismic Structural Damage," by E. DiPasquale and A.S. Cakmak, 6/15/88, (PB89-122188, A05, MF-A01). This report is available only through NTIS (see address given above).

NCEER-88-0023 "Multi-Hazard Risk Analysis: Case of a Simple Offshore Structure," by B.K. Bhartia and E.H. Vanmarcke, 7/21/88, (PB89-145213, A05, MF-A01).

NCEER-88-0024 "Automated Seismic Design of Reinforced Concrete Buildings," by Y.S. Chung, C. Meyer and M. Shinozuka, 7/5/88, (PB89-122170, A06, MF-A01). This report is available only through NTIS (see address given above).

NCEER-88-0025 "Experimental Study of Active Control of MDOF Structures Under Seismic Excitations," by L.L. Chung, R.C. Lin, T.T. Soong and A.M. Reinhorn, 7/10/88, (PB89-122600, A04, MF-A01).

NCEER-88-0026 "Earthquake Simulation Tests of a Low-Rise Metal Structure," by J.S. Hwang, K.C. Chang, G.C. Lee and R.L. Ketter, 8/1/88, (PB89-102917, A04, MF-A01).

NCEER-88-0027 "Systems Study of Urban Response and Reconstruction Due to Catastrophic Earthquakes," by F. Kozin and H.K. Zhou, 9/22/88, (PB90-162348, A04, MF-A01).

NCEER-88-0028 "Seismic Fragility Analysis of Plane Frame Structures," by H.H-M. Hwang and Y.K. Low, 7/31/88, (PB89-131445, A06, MF-A01).

NCEER-88-0029 "Response Analysis of Stochastic Structures," by A. Kardara, C. Bucher and M. Shinozuka, 9/22/88, (PB89-174429, A04, MF-A01).

NCEER-88-0030 "Nonnormal Accelerations Due to Yielding in a Primary Structure," by D.C.K. Chen and L.D. Lutes, 9/19/88, (PB89-131437, A04, MF-A01).

NCEER-88-0031 "Design Approaches for Soil-Structure Interaction," by A.S. Veletsos, A.M. Prasad and Y. Tang, 12/30/88, (PB89-174437, A03, MF-A01). This report is available only through NTIS (see address given above).

NCEER-88-0032 "A Re-evaluation of Design Spectra for Seismic Damage Control," by C.J. Turkstra and A.G. Tallin, 11/7/88, (PB89-145221, A05, MF-A01).

NCEER-88-0033 "The Behavior and Design of Noncontact Lap Splices Subjected to Repeated Inelastic Tensile Loading," by V.E. Sagan, P. Gergely and R.N. White, 12/8/88, (PB89-163737, A08, MF-A01).

NCEER-88-0034 "Seismic Response of Pile Foundations," by S.M. Mamoon, P.K. Banerjee and S. Ahmad, 11/1/88, (PB89-145239, A04, MF-A01).

NCEER-88-0035 "Modeling of R/C Building Structures With Flexible Floor Diaphragms (IDARC2)," by A.M. Reinhorn, S.K. Kunnath and N. Panahshahi, 9/7/88, (PB89-207153, A07, MF-A01).

NCEER-88-0036 "Solution of the Dam-Reservoir Interaction Problem Using a Combination of FEM, BEM with Particular Integrals, Modal Analysis, and Substructuring," by C-S. Tsai, G.C. Lee and R.L. Ketter, 12/31/88, (PB89-207146, A04, MF-A01).

NCEER-88-0037 "Optimal Placement of Actuators for Structural Control," by F.Y. Cheng and C.P. Pantelides, 8/15/88, (PB89-162846, A05, MF-A01).

NCEER-88-0038 "Teflon Bearings in Aseismic Base Isolation: Experimental Studies and Mathematical Modeling," by A. Mokha, M.C. Constantinou and A.M. Reinhorn, 12/5/88, (PB89-218457, A10, MF-A01). This report is available only through NTIS (see address given above).

NCEER-88-0039 "Seismic Behavior of Flat Slab High-Rise Buildings in the New York City Area," by P. Weidlinger and M. Ettouney, 10/15/88, (PB90-145681, A04, MF-A01).

NCEER-88-0040 "Evaluation of the Earthquake Resistance of Existing Buildings in New York City," by P. Weidlinger and M. Ettouney, 10/15/88, not available.

NCEER-88-0041 "Small-Scale Modeling Techniques for Reinforced Concrete Structures Subjected to Seismic Loads," by W. Kim, A. El-Attar and R.N. White, 11/22/88, (PB89-189625, A05, MF-A01).

NCEER-88-0042 "Modeling Strong Ground Motion from Multiple Event Earthquakes," by G.W. Ellis and A.S. Cakmak, 10/15/88, (PB89-174445, A03, MF-A01).

NCEER-88-0043 "Nonstationary Models of Seismic Ground Acceleration," by M. Grigoriu, S.E. Ruiz and E. Rosenblueth, 7/15/88, (PB89-189617, A04, MF-A01).

NCEER-88-0044 "SARCF User's Guide: Seismic Analysis of Reinforced Concrete Frames," by Y.S. Chung, C. Meyer and M. Shinozuka, 11/9/88, (PB89-174452, A08, MF-A01).

NCEER-88-0045 "First Expert Panel Meeting on Disaster Research and Planning," edited by J. Pantelic and J. Stoyle, 9/15/88, (PB89-174460, A05, MF-A01).

NCEER-88-0046 "Preliminary Studies of the Effect of Degrading Infill Walls on the Nonlinear Seismic Response of Steel Frames," by C.Z. Chrysostomou, P. Gergely and J.F. Abel, 12/19/88, (PB89-208383, A05, MF-A01).

NCEER-88-0047 "Reinforced Concrete Frame Component Testing Facility - Design, Construction, Instrumentation and Operation," by S.P. Pessiki, C. Conley, T. Bond, P. Gergely and R.N. White, 12/16/88, (PB89-174478, A04, MF-A01).

NCEER-89-0001 "Effects of Protective Cushion and Soil Compliancy on the Response of Equipment Within a Seismically Excited Building," by J.A. HoLung, 2/16/89, (PB89-207179, A04, MF-A01).

NCEER-89-0002 "Statistical Evaluation of Response Modification Factors for Reinforced Concrete Structures," by H.H-M. Hwang and J-W. Jaw, 2/17/89, (PB89-207187, A05, MF-A01).

NCEER-89-0003 "Hysteretic Columns Under Random Excitation," by G-Q. Cai and Y.K. Lin, 1/9/89, (PB89-196513, A03, MF-A01).

NCEER-89-0004 "Experimental Study of `Elephant Foot Bulge' Instability of Thin-Walled Metal Tanks," by Z-H. Jia and R.L. Ketter, 2/22/89, (PB89-207195, A03, MF-A01).

NCEER-89-0005 "Experiment on Performance of Buried Pipelines Across San Andreas Fault," by J. Isenberg, E. Richardson and T.D. O'Rourke, 3/10/89, (PB89-218440, A04, MF-A01). This report is available only through NTIS (see address given above).

NCEER-89-0006 "A Knowledge-Based Approach to Structural Design of Earthquake-Resistant Buildings," by M. Subramani, P. Gergely, C.H. Conley, J.F. Abel and A.H. Zaghw, 1/15/89, (PB89-218465, A06, MF-A01).

NCEER-89-0007 "Liquefaction Hazards and Their Effects on Buried Pipelines," by T.D. O'Rourke and P.A. Lane, 2/1/89, (PB89-218481, A09, MF-A01).

NCEER-89-0008 "Fundamentals of System Identification in Structural Dynamics," by H. Imai, C-B. Yun, O. Maruyama and M. Shinozuka, 1/26/89, (PB89-207211, A04, MF-A01).

NCEER-89-0009 "Effects of the 1985 Michoacan Earthquake on Water Systems and Other Buried Lifelines in Mexico," by A.G. Ayala and M.J. O'Rourke, 3/8/89, (PB89-207229, A06, MF-A01).

NCEER-89-R010 "NCEER Bibliography of Earthquake Education Materials," by K.E.K. Ross, Second Revision, 9/1/89, (PB90-125352, A05, MF-A01). This report is replaced by NCEER-92-0018.

NCEER-89-0011 "Inelastic Three-Dimensional Response Analysis of Reinforced Concrete Building Structures (IDARC-3D), Part I - Modeling," by S.K. Kunnath and A.M. Reinhorn, 4/17/89, (PB90-114612, A07, MF-A01). This report is available only through NTIS (see address given above).

NCEER-89-0012 "Recommended Modifications to ATC-14," by C.D. Poland and J.O. Malley, 4/12/89, (PB90-108648, A15, MF-A01).

NCEER-89-0013 "Repair and Strengthening of Beam-to-Column Connections Subjected to Earthquake Loading," by M. Corazao and A.J. Durrani, 2/28/89, (PB90-109885, A06, MF-A01).

NCEER-89-0014 "Program EXKAL2 for Identification of Structural Dynamic Systems," by O. Maruyama, C-B. Yun, M. Hoshiya and M. Shinozuka, 5/19/89, (PB90-109877, A09, MF-A01).

NCEER-89-0015 "Response of Frames With Bolted Semi-Rigid Connections, Part I - Experimental Study and Analytical Predictions," by P.J. DiCorso, A.M. Reinhorn, J.R. Dickerson, J.B. Radziminski and W.L. Harper, 6/1/89, not available.

NCEER-89-0016 "ARMA Monte Carlo Simulation in Probabilistic Structural Analysis," by P.D. Spanos and M.P. Mignolet, 7/10/89, (PB90-109893, A03, MF-A01).

NCEER-89-P017 "Preliminary Proceedings from the Conference on Disaster Preparedness - The Place of Earthquake Education in Our Schools," Edited by K.E.K. Ross, 6/23/89, (PB90-108606, A03, MF-A01).

NCEER-89-0017 "Proceedings from the Conference on Disaster Preparedness - The Place of Earthquake Education in Our Schools," Edited by K.E.K. Ross, 12/31/89, (PB90-207895, A012, MF-A02). This report is available only through NTIS (see address given above).

NCEER-89-0018 "Multidimensional Models of Hysteretic Material Behavior for Vibration Analysis of Shape Memory Energy Absorbing Devices, by E.J. Graesser and F.A. Cozzarelli, 6/7/89, (PB90-164146, A04, MF-A01).

NCEER-89-0019 "Nonlinear Dynamic Analysis of Three-Dimensional Base Isolated Structures (3D-BASIS)," by S. Nagarajaiah, A.M. Reinhorn and M.C. Constantinou, 8/3/89, (PB90-161936, A06, MF-A01). This report has been replaced by NCEER-93-0011.

NCEER-89-0020 "Structural Control Considering Time-Rate of Control Forces and Control Rate Constraints," by F.Y. Cheng and C.P. Pantelides, 8/3/89, (PB90-120445, A04, MF-A01).

NCEER-89-0021 "Subsurface Conditions of Memphis and Shelby County," by K.W. Ng, T-S. Chang and H-H.M. Hwang, 7/26/89, (PB90-120437, A03, MF-A01).

NCEER-89-0022 "Seismic Wave Propagation Effects on Straight Jointed Buried Pipelines," by K. Elhmadi and M.J. O'Rourke, 8/24/89, (PB90-162322, A10, MF-A02).

NCEER-89-0023 "Workshop on Serviceability Analysis of Water Delivery Systems," edited by M. Grigoriu, 3/6/89, (PB90-127424, A03, MF-A01).

NCEER-89-0024 "Shaking Table Study of a 1/5 Scale Steel Frame Composed of Tapered Members," by K.C. Chang, J.S. Hwang and G.C. Lee, 9/18/89, (PB90-160169, A04, MF-A01).

NCEER-89-0025 "DYNA1D: A Computer Program for Nonlinear Seismic Site Response Analysis - Technical Documentation," by Jean H. Prevost, 9/14/89, (PB90-161944, A07, MF-A01). This report is available only through NTIS (see address given above).

NCEER-89-0026 "1:4 Scale Model Studies of Active Tendon Systems and Active Mass Dampers for Aseismic Protection," by A.M. Reinhorn, T.T. Soong, R.C. Lin, Y.P. Yang, Y. Fukao, H. Abe and M. Nakai, 9/15/89, (PB90-173246, A10, MF-A02). This report is available only through NTIS (see address given above).

NCEER-89-0027 "Scattering of Waves by Inclusions in a Nonhomogeneous Elastic Half Space Solved by Boundary Element Methods," by P.K. Hadley, A. Askar and A.S. Cakmak, 6/15/89, (PB90-145699, A07, MF-A01).

NCEER-89-0028 "Statistical Evaluation of Deflection Amplification Factors for Reinforced Concrete Structures," by H.H.M. Hwang, J-W. Jaw and A.L. Ch'ng, 8/31/89, (PB90-164633, A05, MF-A01).

NCEER-89-0029 "Bedrock Accelerations in Memphis Area Due to Large New Madrid Earthquakes," by H.H.M. Hwang, C.H.S. Chen and G. Yu, 11/7/89, (PB90-162330, A04, MF-A01).

NCEER-89-0030 "Seismic Behavior and Response Sensitivity of Secondary Structural Systems," by Y.Q. Chen and T.T. Soong, 10/23/89, (PB90-164658, A08, MF-A01).

NCEER-89-0031 "Random Vibration and Reliability Analysis of Primary-Secondary Structural Systems," by Y. Ibrahim, M. Grigoriu and T.T. Soong, 11/10/89, (PB90-161951, A04, MF-A01).

NCEER-89-0032 "Proceedings from the Second U.S. - Japan Workshop on Liquefaction, Large Ground Deformation and Their Effects on Lifelines, September 26-29, 1989," Edited by T.D. O'Rourke and M. Hamada, 12/1/89, (PB90-209388, A22, MF-A03).

NCEER-89-0033 "Deterministic Model for Seismic Damage Evaluation of Reinforced Concrete Structures," by J.M. Bracci, A.M. Reinhorn, J.B. Mander and S.K. Kunnath, 9/27/89, (PB91-108803, A06, MF-A01).

NCEER-89-0034 "On the Relation Between Local and Global Damage Indices," by E. DiPasquale and A.S. Cakmak, 8/15/89, (PB90-173865, A05, MF-A01).

NCEER-89-0035 "Cyclic Undrained Behavior of Nonplastic and Low Plasticity Silts," by A.J. Walker and H.E. Stewart, 7/26/89, (PB90-183518, A10, MF-A01).

NCEER-89-0036 "Liquefaction Potential of Surficial Deposits in the City of Buffalo, New York," by M. Budhu, R. Giese and L. Baumgrass, 1/17/89, (PB90-208455, A04, MF-A01).

NCEER-89-0037 "A Deterministic Assessment of Effects of Ground Motion Incoherence," by A.S. Veletsos and Y. Tang, 7/15/89, (PB90-164294, A03, MF-A01).

NCEER-89-0038 "Workshop on Ground Motion Parameters for Seismic Hazard Mapping," July 17-18, 1989, edited by R.V. Whitman, 12/1/89, (PB90-173923, A04, MF-A01).

NCEER-89-0039 "Seismic Effects on Elevated Transit Lines of the New York City Transit Authority," by C.J. Costantino, C.A. Miller and E. Heymsfield, 12/26/89, (PB90-207887, A06, MF-A01).

NCEER-89-0040 "Centrifugal Modeling of Dynamic Soil-Structure Interaction," by K. Weissman, Supervised by J.H. Prevost, 5/10/89, (PB90-207879, A07, MF-A01).

NCEER-89-0041 "Linearized Identification of Buildings With Cores for Seismic Vulnerability Assessment," by I-K. Ho and A.E. Aktan, 11/1/89, (PB90-251943, A07, MF-A01).

NCEER-90-0001 "Geotechnical and Lifeline Aspects of the October 17, 1989 Loma Prieta Earthquake in San Francisco," by T.D. O'Rourke, H.E. Stewart, F.T. Blackburn and T.S. Dickerman, 1/90, (PB90-208596, A05, MF-A01).

NCEER-90-0002 "Nonnormal Secondary Response Due to Yielding in a Primary Structure," by D.C.K. Chen and L.D. Lutes, 2/28/90, (PB90-251976, A07, MF-A01).

NCEER-90-0003 "Earthquake Education Materials for Grades K-12," by K.E.K. Ross, 4/16/90, (PB91-251984, A05, MF-A05). This report has been replaced by NCEER-92-0018.

NCEER-90-0004 "Catalog of Strong Motion Stations in Eastern North America," by R.W. Busby, 4/3/90, (PB90-251984, A05, MF-A01).

NCEER-90-0005 "NCEER Strong-Motion Data Base: A User Manual for the GeoBase Release (Version 1.0 for the Sun3)," by P. Friberg and K. Jacob, 3/31/90 (PB90-258062, A04, MF-A01).

NCEER-90-0006 "Seismic Hazard Along a Crude Oil Pipeline in the Event of an 1811-1812 Type New Madrid Earthquake," by H.H.M. Hwang and C-H.S. Chen, 4/16/90, (PB90-258054, A04, MF-A01).

NCEER-90-0007 "Site-Specific Response Spectra for Memphis Sheahan Pumping Station," by H.H.M. Hwang and C.S. Lee, 5/15/90, (PB91-108811, A05, MF-A01).

NCEER-90-0008 "Pilot Study on Seismic Vulnerability of Crude Oil Transmission Systems," by T. Ariman, R. Dobry, M. Grigoriu, F. Kozin, M. O'Rourke, T. O'Rourke and M. Shinozuka, 5/25/90, (PB91-108837, A06, MF-A01).

NCEER-90-0009 "A Program to Generate Site Dependent Time Histories: EQGEN," by G.W. Ellis, M. Srinivasan and A.S. Cakmak, 1/30/90, (PB91-108829, A04, MF-A01).

NCEER-90-0010 "Active Isolation for Seismic Protection of Operating Rooms," by M.E. Talbott, Supervised by M. Shinozuka, 6/8/9, (PB91-110205, A05, MF-A01).

NCEER-90-0011 "Program LINEARID for Identification of Linear Structural Dynamic Systems," by C-B. Yun and M. Shinozuka, 6/25/90, (PB91-110312, A08, MF-A01).

NCEER-90-0012 "Two-Dimensional Two-Phase Elasto-Plastic Seismic Response of Earth Dams," by A.N. Yiagos, Supervised by J.H. Prevost, 6/20/90, (PB91-110197, A13, MF-A02).

NCEER-90-0013 "Secondary Systems in Base-Isolated Structures: Experimental Investigation, Stochastic Response and Stochastic Sensitivity," by G.D. Manolis, G. Juhn, M.C. Constantinou and A.M. Reinhorn, 7/1/90, (PB91-110320, A08, MF-A01).

NCEER-90-0014 "Seismic Behavior of Lightly-Reinforced Concrete Column and Beam-Column Joint Details," by S.P. Pessiki, C.H. Conley, P. Gergely and R.N. White, 8/22/90, (PB91-108795, A11, MF-A02).

NCEER-90-0015 "Two Hybrid Control Systems for Building Structures Under Strong Earthquakes," by J.N. Yang and A. Danielians, 6/29/90, (PB91-125393, A04, MF-A01).

NCEER-90-0016 "Instantaneous Optimal Control with Acceleration and Velocity Feedback," by J.N. Yang and Z. Li, 6/29/90, (PB91-125401, A03, MF-A01).

NCEER-90-0017 "Reconnaissance Report on the Northern Iran Earthquake of June 21, 1990," by M. Mehrain, 10/4/90, (PB91-125377, A03, MF-A01).

NCEER-90-0018 "Evaluation of Liquefaction Potential in Memphis and Shelby County," by T.S. Chang, P.S. Tang, C.S. Lee and H. Hwang, 8/10/90, (PB91-125427, A09, MF-A01).

NCEER-90-0019 "Experimental and Analytical Study of a Combined Sliding Disc Bearing and Helical Steel Spring Isolation System," by M.C. Constantinou, A.S. Mokha and A.M. Reinhorn, 10/4/90, (PB91-125385, A06, MF-A01). This report is available only through NTIS (see address given above).

NCEER-90-0020 "Experimental Study and Analytical Prediction of Earthquake Response of a Sliding Isolation System with a Spherical Surface," by A.S. Mokha, M.C. Constantinou and A.M. Reinhorn, 10/11/90, (PB91-125419, A05, MF-A01).

NCEER-90-0021 "Dynamic Interaction Factors for Floating Pile Groups," by G. Gazetas, K. Fan, A. Kaynia and E. Kausel, 9/10/90, (PB91-170381, A05, MF-A01).

NCEER-90-0022 "Evaluation of Seismic Damage Indices for Reinforced Concrete Structures," by S. Rodriguez-Gomez and A.S. Cakmak, 9/30/90, PB91-171322, A06, MF-A01).

NCEER-90-0023 "Study of Site Response at a Selected Memphis Site," by H. Desai, S. Ahmad, E.S. Gazetas and M.R. Oh, 10/11/90, (PB91-196857, A03, MF-A01).

NCEER-90-0024 "A User's Guide to Strongmo: Version 1.0 of NCEER's Strong-Motion Data Access Tool for PCs and Terminals," by P.A. Friberg and C.A.T. Susch, 11/15/90, (PB91-171272, A03, MF-A01).

NCEER-90-0025 "A Three-Dimensional Analytical Study of Spatial Variability of Seismic Ground Motions," by L-L. Hong and A.H.-S. Ang, 10/30/90, (PB91-170399, A09, MF-A01).

NCEER-90-0026 "MUMOID User's Guide - A Program for the Identification of Modal Parameters," by S. Rodriguez-Gomez and E. DiPasquale, 9/30/90, (PB91-171298, A04, MF-A01).

NCEER-90-0027 "SARCF-II User's Guide - Seismic Analysis of Reinforced Concrete Frames," by S. Rodriguez-Gomez, Y.S. Chung and C. Meyer, 9/30/90, (PB91-171280, A05, MF-A01).

NCEER-90-0028 "Viscous Dampers: Testing, Modeling and Application in Vibration and Seismic Isolation," by N. Makris and M.C. Constantinou, 12/20/90 (PB91-190561, A06, MF-A01).

NCEER-90-0029 "Soil Effects on Earthquake Ground Motions in the Memphis Area," by H. Hwang, C.S. Lee, K.W. Ng and T.S. Chang, 8/2/90, (PB91-190751, A05, MF-A01).

NCEER-91-0001 "Proceedings from the Third Japan-U.S. Workshop on Earthquake Resistant Design of Lifeline Facilities and Countermeasures for Soil Liquefaction, December 17-19, 1990," edited by T.D. O'Rourke and M. Hamada, 2/1/91, (PB91-179259, A99, MF-A04).

NCEER-91-0002 "Physical Space Solutions of Non-Proportionally Damped Systems," by M. Tong, Z. Liang and G.C. Lee, 1/15/91, (PB91-179242, A04, MF-A01).

NCEER-91-0003 "Seismic Response of Single Piles and Pile Groups," by K. Fan and G. Gazetas, 1/10/91, (PB92-174994, A04, MF-A01).

NCEER-91-0004 "Damping of Structures: Part 1 - Theory of Complex Damping," by Z. Liang and G. Lee, 10/10/91, (PB92-197235, A12, MF-A03).

NCEER-91-0005 "3D-BASIS - Nonlinear Dynamic Analysis of Three Dimensional Base Isolated Structures: Part II," by S. Nagarajaiah, A.M. Reinhorn and M.C. Constantinou, 2/28/91, (PB91-190553, A07, MF-A01). This report has been replaced by NCEER-93-0011.

NCEER-91-0006 "A Multidimensional Hysteretic Model for Plasticity Deforming Metals in Energy Absorbing Devices," by E.J. Graesser and F.A. Cozzarelli, 4/9/91, (PB92-108364, A04, MF-A01).

NCEER-91-0007 "A Framework for Customizable Knowledge-Based Expert Systems with an Application to a KBES for Evaluating the Seismic Resistance of Existing Buildings," by E.G. Ibarra-Anaya and S.J. Fenves, 4/9/91, (PB91-210930, A08, MF-A01).

NCEER-91-0008 "Nonlinear Analysis of Steel Frames with Semi-Rigid Connections Using the Capacity Spectrum Method," by G.G. Deierlein, S-H. Hsieh, Y-J. Shen and J.F. Abel, 7/2/91, (PB92-113828, A05, MF-A01).

NCEER-91-0009 "Earthquake Education Materials for Grades K-12," by K.E.K. Ross, 4/30/91, (PB91-212142, A06, MF-A01). This report has been replaced by NCEER-92-0018.

NCEER-91-0010 "Phase Wave Velocities and Displacement Phase Differences in a Harmonically Oscillating Pile," by N. Makris and G. Gazetas, 7/8/91, (PB92-108356, A04, MF-A01).

NCEER-91-0011 "Dynamic Characteristics of a Full-Size Five-Story Steel Structure and a 2/5 Scale Model," by K.C. Chang, G.C. Yao, G.C. Lee, D.S. Hao and Y.C. Yeh," 7/2/91, (PB93-116648, A06, MF-A02).

NCEER-91-0012 "Seismic Response of a 2/5 Scale Steel Structure with Added Viscoelastic Dampers," by K.C. Chang, T.T. Soong, S-T. Oh and M.L. Lai, 5/17/91, (PB92-110816, A05, MF-A01).

NCEER-91-0013 "Earthquake Response of Retaining Walls; Full-Scale Testing and Computational Modeling," by S. Alampalli and A-W.M. Elgamal, 6/20/91, not available.

NCEER-91-0014 "3D-BASIS-M: Nonlinear Dynamic Analysis of Multiple Building Base Isolated Structures," by P.C. Tsopelas, S. Nagarajaiah, M.C. Constantinou and A.M. Reinhorn, 5/28/91, (PB92-113885, A09, MF-A02).

NCEER-91-0015 "Evaluation of SEAOC Design Requirements for Sliding Isolated Structures," by D. Theodossiou and M.C. Constantinou, 6/10/91, (PB92-114602, A11, MF-A03).

NCEER-91-0016 "Closed-Loop Modal Testing of a 27-Story Reinforced Concrete Flat Plate-Core Building," by H.R. Somaprasad, T. Toksoy, H. Yoshiyuki and A.E. Aktan, 7/15/91, (PB92-129980, A07, MF-A02).

NCEER-91-0017 "Shake Table Test of a 1/6 Scale Two-Story Lightly Reinforced Concrete Building," by A.G. El-Attar, R.N. White and P. Gergely, 2/28/91, (PB92-222447, A06, MF-A02).

NCEER-91-0018 "Shake Table Test of a 1/8 Scale Three-Story Lightly Reinforced Concrete Building," by A.G. El-Attar, R.N. White and P. Gergely, 2/28/91, (PB93-116630, A08, MF-A02).

NCEER-91-0019 "Transfer Functions for Rigid Rectangular Foundations," by A.S. Veletsos, A.M. Prasad and W.H. Wu, 7/31/91, not available.

NCEER-91-0020 "Hybrid Control of Seismic-Excited Nonlinear and Inelastic Structural Systems," by J.N. Yang, Z. Li and A. Danielians, 8/1/91, (PB92-143171, A06, MF-A02).

NCEER-91-0021 "The NCEER-91 Earthquake Catalog: Improved Intensity-Based Magnitudes and Recurrence Relations for U.S. Earthquakes East of New Madrid," by L. Seeber and J.G. Armbruster, 8/28/91, (PB92-176742, A06, MF-A02).

NCEER-91-0022 "Proceedings from the Implementation of Earthquake Planning and Education in Schools: The Need for Change - The Roles of the Changemakers," by K.E.K. Ross and F. Winslow, 7/23/91, (PB92-129998, A12, MF-A03).

NCEER-91-0023 "A Study of Reliability-Based Criteria for Seismic Design of Reinforced Concrete Frame Buildings," by H.H.M. Hwang and H-M. Hsu, 8/10/91, (PB92-140235, A09, MF-A02).

NCEER-91-0024 "Experimental Verification of a Number of Structural System Identification Algorithms," by R.G. Ghanem, H. Gavin and M. Shinozuka, 9/18/91, (PB92-176577, A18, MF-A04).

NCEER-91-0025 "Probabilistic Evaluation of Liquefaction Potential," by H.H.M. Hwang and C.S. Lee," 11/25/91, (PB92-143429, A05, MF-A01).

NCEER-91-0026 "Instantaneous Optimal Control for Linear, Nonlinear and Hysteretic Structures - Stable Controllers," by J.N. Yang and Z. Li, 11/15/91, (PB92-163807, A04, MF-A01).

NCEER-91-0027 "Experimental and Theoretical Study of a Sliding Isolation System for Bridges," by M.C. Constantinou, A. Kartoum, A.M. Reinhorn and P. Bradford, 11/15/91, (PB92-176973, A10, MF-A03).

NCEER-92-0001 "Case Studies of Liquefaction and Lifeline Performance During Past Earthquakes, Volume 1: Japanese Case Studies," Edited by M. Hamada and T. O'Rourke, 2/17/92, (PB92-197243, A18, MF-A04).

NCEER-92-0002 "Case Studies of Liquefaction and Lifeline Performance During Past Earthquakes, Volume 2: United States Case Studies," Edited by T. O'Rourke and M. Hamada, 2/17/92, (PB92-197250, A20, MF-A04).

NCEER-92-0003 "Issues in Earthquake Education," Edited by K. Ross, 2/3/92, (PB92-222389, A07, MF-A02).

NCEER-92-0004 "Proceedings from the First U.S. - Japan Workshop on Earthquake Protective Systems for Bridges," Edited by I.G. Buckle, 2/4/92, (PB94-142239, A99, MF-A06).

NCEER-92-0005 "Seismic Ground Motion from a Haskell-Type Source in a Multiple-Layered Half-Space," A.P. Theoharis, G. Deodatis and M. Shinozuka, 1/2/92, not available.

NCEER-92-0006 "Proceedings from the Site Effects Workshop," Edited by R. Whitman, 2/29/92, (PB92-197201, A04, MF-A01).

NCEER-92-0007 "Engineering Evaluation of Permanent Ground Deformations Due to Seismically-Induced Liquefaction," by M.H. Baziar, R. Dobry and A-W.M. Elgamal, 3/24/92, (PB92-222421, A13, MF-A03).

NCEER-92-0008 "A Procedure for the Seismic Evaluation of Buildings in the Central and Eastern United States," by C.D. Poland and J.O. Malley, 4/2/92, (PB92-222439, A20, MF-A04).

NCEER-92-0009 "Experimental and Analytical Study of a Hybrid Isolation System Using Friction Controllable Sliding Bearings," by M.Q. Feng, S. Fujii and M. Shinozuka, 5/15/92, (PB93-150282, A06, MF-A02).

NCEER-92-0010 "Seismic Resistance of Slab-Column Connections in Existing Non-Ductile Flat-Plate Buildings," by A.J. Durrani and Y. Du, 5/18/92, (PB93-116812, A06, MF-A02).

NCEER-92-0011 "The Hysteretic and Dynamic Behavior of Brick Masonry Walls Upgraded by Ferrocement Coatings Under Cyclic Loading and Strong Simulated Ground Motion," by H. Lee and S.P. Prawel, 5/11/92, not available.

NCEER-92-0012 "Study of Wire Rope Systems for Seismic Protection of Equipment in Buildings," by G.F. Demetriades, M.C. Constantinou and A.M. Reinhorn, 5/20/92, (PB93-116655, A08, MF-A02).

NCEER-92-0013 "Shape Memory Structural Dampers: Material Properties, Design and Seismic Testing," by P.R. Witting and F.A. Cozzarelli, 5/26/92, (PB93-116663, A05, MF-A01).

NCEER-92-0014 "Longitudinal Permanent Ground Deformation Effects on Buried Continuous Pipelines," by M.J. O'Rourke, and C. Nordberg, 6/15/92, (PB93-116671, A08, MF-A02).

NCEER-92-0015 "A Simulation Method for Stationary Gaussian Random Functions Based on the Sampling Theorem," by M. Grigoriu and S. Balopoulou, 6/11/92, (PB93-127496, A05, MF-A01).

NCEER-92-0016 "Gravity-Load-Designed Reinforced Concrete Buildings: Seismic Evaluation of Existing Construction and Detailing Strategies for Improved Seismic Resistance," by G.W. Hoffmann, S.K. Kunnath, A.M. Reinhorn and J.B. Mander, 7/15/92, (PB94-142007, A08, MF-A02).

NCEER-92-0017 "Observations on Water System and Pipeline Performance in the Limón Area of Costa Rica Due to the April 22, 1991 Earthquake," by M. O'Rourke and D. Ballantyne, 6/30/92, (PB93-126811, A06, MF-A02).

NCEER-92-0018 "Fourth Edition of Earthquake Education Materials for Grades K-12," Edited by K.E.K. Ross, 8/10/92, (PB93-114023, A07, MF-A02).

NCEER-92-0019 "Proceedings from the Fourth Japan-U.S. Workshop on Earthquake Resistant Design of Lifeline Facilities and Countermeasures for Soil Liquefaction," Edited by M. Hamada and T.D. O'Rourke, 8/12/92, (PB93-163939, A99, MF-E11).

NCEER-92-0020 "Active Bracing System: A Full Scale Implementation of Active Control," by A.M. Reinhorn, T.T. Soong, R.C. Lin, M.A. Riley, Y.P. Wang, S. Aizawa and M. Higashino, 8/14/92, (PB93-127512, A06, MF-A02).

NCEER-92-0021 "Empirical Analysis of Horizontal Ground Displacement Generated by Liquefaction-Induced Lateral Spreads," by S.F. Bartlett and T.L. Youd, 8/17/92, (PB93-188241, A06, MF-A02).

NCEER-92-0022 "IDARC Version 3.0: Inelastic Damage Analysis of Reinforced Concrete Structures," by S.K. Kunnath, A.M. Reinhorn and R.F. Lobo, 8/31/92, (PB93-227502, A07, MF-A02).

NCEER-92-0023 "A Semi-Empirical Analysis of Strong-Motion Peaks in Terms of Seismic Source, Propagation Path and Local Site Conditions, by M. Kamiyama, M.J. O'Rourke and R. Flores-Berrones, 9/9/92, (PB93-150266, A08, MF-A02).

NCEER-92-0024 "Seismic Behavior of Reinforced Concrete Frame Structures with Nonductile Details, Part I: Summary of Experimental Findings of Full Scale Beam-Column Joint Tests," by A. Beres, R.N. White and P. Gergely, 9/30/92, (PB93-227783, A05, MF-A01).

NCEER-92-0025 "Experimental Results of Repaired and Retrofitted Beam-Column Joint Tests in Lightly Reinforced Concrete Frame Buildings," by A. Beres, S. El-Borgi, R.N. White and P. Gergely, 10/29/92, (PB93-227791, A05, MF-A01).

NCEER-92-0026 "A Generalization of Optimal Control Theory: Linear and Nonlinear Structures," by J.N. Yang, Z. Li and S. Vongchavalitkul, 11/2/92, (PB93-188621, A05, MF-A01).

NCEER-92-0027 "Seismic Resistance of Reinforced Concrete Frame Structures Designed Only for Gravity Loads: Part I - Design and Properties of a One-Third Scale Model Structure," by J.M. Bracci, A.M. Reinhorn and J.B. Mander, 12/1/92, (PB94-104502, A08, MF-A02).

NCEER-92-0028 "Seismic Resistance of Reinforced Concrete Frame Structures Designed Only for Gravity Loads: Part II - Experimental Performance of Subassemblages," by L.E. Aycardi, J.B. Mander and A.M. Reinhorn, 12/1/92, (PB94-104510, A08, MF-A02).

NCEER-92-0029 "Seismic Resistance of Reinforced Concrete Frame Structures Designed Only for Gravity Loads: Part III - Experimental Performance and Analytical Study of a Structural Model," by J.M. Bracci, A.M. Reinhorn and J.B. Mander, 12/1/92, (PB93-227528, A09, MF-A01).

NCEER-92-0030 "Evaluation of Seismic Retrofit of Reinforced Concrete Frame Structures: Part I - Experimental Performance of Retrofitted Subassemblages," by D. Choudhuri, J.B. Mander and A.M. Reinhorn, 12/8/92, (PB93-198307, A07, MF-A02).

NCEER-92-0031 "Evaluation of Seismic Retrofit of Reinforced Concrete Frame Structures: Part II - Experimental Performance and Analytical Study of a Retrofitted Structural Model," by J.M. Bracci, A.M. Reinhorn and J.B. Mander, 12/8/92, (PB93-198315, A09, MF-A03).

NCEER-92-0032 "Experimental and Analytical Investigation of Seismic Response of Structures with Supplemental Fluid Viscous Dampers," by M.C. Constantinou and M.D. Symans, 12/21/92, (PB93-191435, A10, MF-A03). This report is available only through NTIS (see address given above).

NCEER-92-0033 "Reconnaissance Report on the Cairo, Egypt Earthquake of October 12, 1992," by M. Khater, 12/23/92, (PB93-188621, A03, MF-A01).

NCEER-92-0034 "Low-Level Dynamic Characteristics of Four Tall Flat-Plate Buildings in New York City," by H. Gavin, S. Yuan, J. Grossman, E. Pekelis and K. Jacob, 12/28/92, (PB93-188217, A07, MF-A02).

NCEER-93-0001 "An Experimental Study on the Seismic Performance of Brick-Infilled Steel Frames With and Without Retrofit," by J.B. Mander, B. Nair, K. Wojtkowski and J. Ma, 1/29/93, (PB93-227510, A07, MF-A02).

NCEER-93-0002 "Social Accounting for Disaster Preparedness and Recovery Planning," by S. Cole, E. Pantoja and V. Razak, 2/22/93, (PB94-142114, A12, MF-A03).

NCEER-93-0003 "Assessment of 1991 NEHRP Provisions for Nonstructural Components and Recommended Revisions," by T.T. Soong, G. Chen, Z. Wu, R-H. Zhang and M. Grigoriu, 3/1/93, (PB93-188639, A06, MF-A02).

NCEER-93-0004 "Evaluation of Static and Response Spectrum Analysis Procedures of SEAOC/UBC for Seismic Isolated Structures," by C.W. Winters and M.C. Constantinou, 3/23/93, (PB93-198299, A10, MF-A03).

NCEER-93-0005 "Earthquakes in the Northeast - Are We Ignoring the Hazard? A Workshop on Earthquake Science and Safety for Educators," edited by K.E.K. Ross, 4/2/93, (PB94-103066, A09, MF-A02).

NCEER-93-0006 "Inelastic Response of Reinforced Concrete Structures with Viscoelastic Braces," by R.F. Lobo, J.M. Bracci, K.L. Shen, A.M. Reinhorn and T.T. Soong, 4/5/93, (PB93-227486, A05, MF-A02).

NCEER-93-0007 "Seismic Testing of Installation Methods for Computers and Data Processing Equipment," by K. Kosar, T.T. Soong, K.L. Shen, J.A. HoLung and Y.K. Lin, 4/12/93, (PB93-198299, A07, MF-A02).

NCEER-93-0008 "Retrofit of Reinforced Concrete Frames Using Added Dampers," by A. Reinhorn, M. Constantinou and C. Li, not available.

NCEER-93-0009 "Seismic Behavior and Design Guidelines for Steel Frame Structures with Added Viscoelastic Dampers," by K.C. Chang, M.L. Lai, T.T. Soong, D.S. Hao and Y.C. Yeh, 5/1/93, (PB94-141959, A07, MF-A02).

NCEER-93-0010 "Seismic Performance of Shear-Critical Reinforced Concrete Bridge Piers," by J.B. Mander, S.M. Waheed, M.T.A. Chaudhary and S.S. Chen, 5/12/93, (PB93-227494, A08, MF-A02).

NCEER-93-0011 "3D-BASIS-TABS: Computer Program for Nonlinear Dynamic Analysis of Three Dimensional Base Isolated Structures," by S. Nagarajaiah, C. Li, A.M. Reinhorn and M.C. Constantinou, 8/2/93, (PB94-141819, A09, MF-A02).

NCEER-93-0012 "Effects of Hydrocarbon Spills from an Oil Pipeline Break on Ground Water," by O.J. Helweg and H.H.M. Hwang, 8/3/93, (PB94-141942, A06, MF-A02).

NCEER-93-0013 "Simplified Procedures for Seismic Design of Nonstructural Components and Assessment of Current Code Provisions," by M.P. Singh, L.E. Suarez, E.E. Matheu and G.O. Maldonado, 8/4/93, (PB94-141827, A09, MF-A02).

NCEER-93-0014 "An Energy Approach to Seismic Analysis and Design of Secondary Systems," by G. Chen and T.T. Soong, 8/6/93, (PB94-142767, A11, MF-A03).

NCEER-93-0015 "Proceedings from School Sites: Becoming Prepared for Earthquakes - Commemorating the Third Anniversary of the Loma Prieta Earthquake," Edited by F.E. Winslow and K.E.K. Ross, 8/16/93, (PB94-154275, A16, MF-A02).

NCEER-93-0016 "Reconnaissance Report of Damage to Historic Monuments in Cairo, Egypt Following the October 12, 1992 Dahshur Earthquake," by D. Sykora, D. Look, G. Croci, E. Karaesmen and E. Karaesmen, 8/19/93, (PB94-142221, A08, MF-A02).

NCEER-93-0017 "The Island of Guam Earthquake of August 8, 1993," by S.W. Swan and S.K. Harris, 9/30/93, (PB94-141843, A04, MF-A01).

NCEER-93-0018 "Engineering Aspects of the October 12, 1992 Egyptian Earthquake," by A.W. Elgamal, M. Amer, K. Adalier and A. Abul-Fadl, 10/7/93, (PB94-141983, A05, MF-A01).

NCEER-93-0019 "Development of an Earthquake Motion Simulator and its Application in Dynamic Centrifuge Testing," by I. Krstelj, Supervised by J.H. Prevost, 10/23/93, (PB94-181773, A-10, MF-A03).

NCEER-93-0020 "NCEER-Taisei Corporation Research Program on Sliding Seismic Isolation Systems for Bridges: Experimental and Analytical Study of a Friction Pendulum System (FPS)," by M.C. Constantinou, P. Tsopelas, Y-S. Kim and S. Okamoto, 11/1/93, (PB94-142775, A08, MF-A02).

NCEER-93-0021 "Finite Element Modeling of Elastomeric Seismic Isolation Bearings," by L.J. Billings, Supervised by R. Shepherd, 11/8/93, not available.

NCEER-93-0022 "Seismic Vulnerability of Equipment in Critical Facilities: Life-Safety and Operational Consequences," by K. Porter, G.S. Johnson, M.M. Zadeh, C. Scawthorn and S. Eder, 11/24/93, (PB94-181765, A16, MF-A03).

NCEER-93-0023 "Hokkaido Nansei-oki, Japan Earthquake of July 12, 1993, by P.I. Yanev and C.R. Scawthorn, 12/23/93, (PB94-181500, A07, MF-A01).

NCEER-94-0001 "An Evaluation of Seismic Serviceability of Water Supply Networks with Application to the San Francisco Auxiliary Water Supply System," by I. Markov, Supervised by M. Grigoriu and T. O'Rourke, 1/21/94, (PB94-204013, A07, MF-A02).

NCEER-94-0002 "NCEER-Taisei Corporation Research Program on Sliding Seismic Isolation Systems for Bridges: Experimental and Analytical Study of Systems Consisting of Sliding Bearings, Rubber Restoring Force Devices and Fluid Dampers," Volumes I and II, by P. Tsopelas, S. Okamoto, M.C. Constantinou, D. Ozaki and S. Fujii, 2/4/94, (PB94-181740, A09, MF-A02 and PB94-181757, A12, MF-A03).

NCEER-94-0003 "A Markov Model for Local and Global Damage Indices in Seismic Analysis," by S. Rahman and M. Grigoriu, 2/18/94, (PB94-206000, A12, MF-A03).

NCEER-94-0004 "Proceedings from the NCEER Workshop on Seismic Response of Masonry Infills," edited by D.P. Abrams, 3/1/94, (PB94-180783, A07, MF-A02).

NCEER-94-0005 "The Northridge, California Earthquake of January 17, 1994: General Reconnaissance Report," edited by J.D. Goltz, 3/11/94, (PB94-193943, A10, MF-A03).

NCEER-94-0006 "Seismic Energy Based Fatigue Damage Analysis of Bridge Columns: Part I - Evaluation of Seismic Capacity," by G.A. Chang and J.B. Mander, 3/14/94, (PB94-219185, A11, MF-A03).

NCEER-94-0007 "Seismic Isolation of Multi-Story Frame Structures Using Spherical Sliding Isolation Systems," by T.M. Al-Hussaini, V.A. Zayas and M.C. Constantinou, 3/17/94, (PB94-193745, A09, MF-A02).

NCEER-94-0008 "The Northridge, California Earthquake of January 17, 1994: Performance of Highway Bridges," edited by I.G. Buckle, 3/24/94, (PB94-193851, A06, MF-A02).

NCEER-94-0009 "Proceedings of the Third U.S.-Japan Workshop on Earthquake Protective Systems for Bridges," edited by I.G. Buckle and I. Friedland, 3/31/94, (PB94-195815, A99, MF-A06).

NCEER-94-0010 "3D-BASIS-ME: Computer Program for Nonlinear Dynamic Analysis of Seismically Isolated Single and Multiple Structures and Liquid Storage Tanks," by P.C. Tsopelas, M.C. Constantinou and A.M. Reinhorn, 4/12/94, (PB94-204922, A09, MF-A02).

NCEER-94-0011 "The Northridge, California Earthquake of January 17, 1994: Performance of Gas Transmission Pipelines," by T.D. O'Rourke and M.C. Palmer, 5/16/94, (PB94-204989, A05, MF-A01).

NCEER-94-0012 "Feasibility Study of Replacement Procedures and Earthquake Performance Related to Gas Transmission Pipelines," by T.D. O'Rourke and M.C. Palmer, 5/25/94, (PB94-206638, A09, MF-A02).

NCEER-94-0013 "Seismic Energy Based Fatigue Damage Analysis of Bridge Columns: Part II - Evaluation of Seismic Demand," by G.A. Chang and J.B. Mander, 6/1/94, (PB95-18106, A08, MF-A02).

NCEER-94-0014 "NCEER-Taisei Corporation Research Program on Sliding Seismic Isolation Systems for Bridges: Experimental and Analytical Study of a System Consisting of Sliding Bearings and Fluid Restoring Force/Damping Devices," by P. Tsopelas and M.C. Constantinou, 6/13/94, (PB94-219144, A10, MF-A03).

NCEER-94-0015 "Generation of Hazard-Consistent Fragility Curves for Seismic Loss Estimation Studies," by H. Hwang and J-R. Huo, 6/14/94, (PB95-181996, A09, MF-A02).

NCEER-94-0016 "Seismic Study of Building Frames with Added Energy-Absorbing Devices," by W.S. Pong, C.S. Tsai and G.C. Lee, 6/20/94, (PB94-219136, A10, A03).

NCEER-94-0017 "Sliding Mode Control for Seismic-Excited Linear and Nonlinear Civil Engineering Structures," by J. Yang, J. Wu, A. Agrawal and Z. Li, 6/21/94, (PB95-138483, A06, MF-A02).

NCEER-94-0018 "3D-BASIS-TABS Version 2.0: Computer Program for Nonlinear Dynamic Analysis of Three Dimensional Base Isolated Structures," by A.M. Reinhorn, S. Nagarajaiah, M.C. Constantinou, P. Tsopelas and R. Li, 6/22/94, (PB95-182176, A08, MF-A02).

NCEER-94-0019 "Proceedings of the International Workshop on Civil Infrastructure Systems: Application of Intelligent Systems and Advanced Materials on Bridge Systems," Edited by G.C. Lee and K.C. Chang, 7/18/94, (PB95-252474, A20, MF-A04).

NCEER-94-0020 "Study of Seismic Isolation Systems for Computer Floors," by V. Lambrou and M.C. Constantinou, 7/19/94, (PB95-138533, A10, MF-A03).

NCEER-94-0021 "Proceedings of the U.S.-Italian Workshop on Guidelines for Seismic Evaluation and Rehabilitation of Unreinforced Masonry Buildings," Edited by D.P. Abrams and G.M. Calvi, 7/20/94, (PB95-138749, A13, MF-A03).

NCEER-94-0022 "NCEER-Taisei Corporation Research Program on Sliding Seismic Isolation Systems for Bridges: Experimental and Analytical Study of a System Consisting of Lubricated PTFE Sliding Bearings and Mild Steel Dampers," by P. Tsopelas and M.C. Constantinou, 7/22/94, (PB95-182184, A08, MF-A02).

NCEER-94-0023 “Development of Reliability-Based Design Criteria for Buildings Under Seismic Load,” by Y.K. Wen, H. Hwang and M. Shinozuka, 8/1/94, (PB95-211934, A08, MF-A02).

NCEER-94-0024 “Experimental Verification of Acceleration Feedback Control Strategies for an Active Tendon System,” by S.J. Dyke, B.F. Spencer, Jr., P. Quast, M.K. Sain, D.C. Kaspari, Jr. and T.T. Soong, 8/29/94, (PB95-212320, A05, MF-A01).

NCEER-94-0025 “Seismic Retrofitting Manual for Highway Bridges,” Edited by I.G. Buckle and I.F. Friedland, published by the Federal Highway Administration (PB95-212676, A15, MF-A03).

NCEER-94-0026 “Proceedings from the Fifth U.S.-Japan Workshop on Earthquake Resistant Design of Lifeline Facilities and Countermeasures Against Soil Liquefaction,” Edited by T.D. O’Rourke and M. Hamada, 11/7/94, (PB95-220802, A99, MF-E08).

NCEER-95-0001 "Experimental and Analytical Investigation of Seismic Retrofit of Structures with Supplemental Damping: Part 1 - Fluid Viscous Damping Devices," by A.M. Reinhorn, C. Li and M.C. Constantinou, 1/3/95, (PB95-266599, A09, MF-A02).

NCEER-95-0002 "Experimental and Analytical Study of Low-Cycle Fatigue Behavior of Semi-Rigid Top-And-Seat Angle Connections," by G. Pekcan, J.B. Mander and S.S. Chen, 1/5/95, (PB95-220042, A07, MF-A02).

NCEER-95-0003 "NCEER-ATC Joint Study on Fragility of Buildings," by T. Anagnos, C. Rojahn and A.S. Kiremidjian, 1/20/95, (PB95-220026, A06, MF-A02).

NCEER-95-0004 "Nonlinear Control Algorithms for Peak Response Reduction," by Z. Wu, T.T. Soong, V. Gattulli and R.C. Lin, 2/16/95, (PB95-220349, A05, MF-A01).

NCEER-95-0005 "Pipeline Replacement Feasibility Study: A Methodology for Minimizing Seismic and Corrosion Risks to Underground Natural Gas Pipelines," by R.T. Eguchi, H.A. Seligson and D.G. Honegger, 3/2/95, (PB95-252326, A06, MF-A02).

NCEER-95-0006 "Evaluation of Seismic Performance of an 11-Story Frame Building During the 1994 Northridge Earthquake," by F. Naeim, R. DiSulio, K. Benuska, A. Reinhorn and C. Li, not available.

NCEER-95-0007 "Prioritization of Bridges for Seismic Retrofitting," by N. Basöz and A.S. Kiremidjian, 4/24/95, (PB95-252300, A08, MF-A02).

NCEER-95-0008 "Method for Developing Motion Damage Relationships for Reinforced Concrete Frames," by A. Singhal and A.S. Kiremidjian, 5/11/95, (PB95-266607, A06, MF-A02).

NCEER-95-0009 "Experimental and Analytical Investigation of Seismic Retrofit of Structures with Supplemental Damping: Part II - Friction Devices," by C. Li and A.M. Reinhorn, 7/6/95, (PB96-128087, A11, MF-A03).

NCEER-95-0010 "Experimental Performance and Analytical Study of a Non-Ductile Reinforced Concrete Frame Structure Retrofitted with Elastomeric Spring Dampers," by G. Pekcan, J.B. Mander and S.S. Chen, 7/14/95, (PB96-137161, A08, MF-A02).

NCEER-95-0011 "Development and Experimental Study of Semi-Active Fluid Damping Devices for Seismic Protection of Structures," by M.D. Symans and M.C. Constantinou, 8/3/95, (PB96-136940, A23, MF-A04).

NCEER-95-0012 "Real-Time Structural Parameter Modification (RSPM): Development of Innervated Structures," by Z. Liang, M. Tong and G.C. Lee, 4/11/95, (PB96-137153, A06, MF-A01).

NCEER-95-0013 "Experimental and Analytical Investigation of Seismic Retrofit of Structures with Supplemental Damping: Part III - Viscous Damping Walls," by A.M. Reinhorn and C. Li, 10/1/95, (PB96-176409, A11, MF-A03).

NCEER-95-0014 "Seismic Fragility Analysis of Equipment and Structures in a Memphis Electric Substation," by J-R. Huo and H.H.M. Hwang, 8/10/95, (PB96-128087, A09, MF-A02).

NCEER-95-0015 "The Hanshin-Awaji Earthquake of January 17, 1995: Performance of Lifelines," Edited by M. Shinozuka, 11/3/95, (PB96-176383, A15, MF-A03).

NCEER-95-0016 "Highway Culvert Performance During Earthquakes," by T.L. Youd and C.J. Beckman, available as NCEER-96-0015.

NCEER-95-0017 "The Hanshin-Awaji Earthquake of January 17, 1995: Performance of Highway Bridges," Edited by I.G. Buckle, 12/1/95, not available.

NCEER-95-0018 "Modeling of Masonry Infill Panels for Structural Analysis," by A.M. Reinhorn, A. Madan, R.E. Valles, Y. Reichmann and J.B. Mander, 12/8/95, (PB97-110886, MF-A01, A06).

NCEER-95-0019 "Optimal Polynomial Control for Linear and Nonlinear Structures," by A.K. Agrawal and J.N. Yang, 12/11/95, (PB96-168737, A07, MF-A02).

NCEER-95-0020 "Retrofit of Non-Ductile Reinforced Concrete Frames Using Friction Dampers," by R.S. Rao, P. Gergely and R.N. White, 12/22/95, (PB97-133508, A10, MF-A02).

NCEER-95-0021 "Parametric Results for Seismic Response of Pile-Supported Bridge Bents," by G. Mylonakis, A. Nikolaou and G. Gazetas, 12/22/95, (PB97-100242, A12, MF-A03).

NCEER-95-0022 "Kinematic Bending Moments in Seismically Stressed Piles," by A. Nikolaou, G. Mylonakis and G. Gazetas, 12/23/95, (PB97-113914, MF-A03, A13).

NCEER-96-0001 "Dynamic Response of Unreinforced Masonry Buildings with Flexible Diaphragms," by A.C. Costley and D.P. Abrams," 10/10/96, (PB97-133573, MF-A03, A15).

NCEER-96-0002 "State of the Art Review: Foundations and Retaining Structures," by I. Po Lam, not available.

NCEER-96-0003 "Ductility of Rectangular Reinforced Concrete Bridge Columns with Moderate Confinement," by N. Wehbe, M. Saiidi, D. Sanders and B. Douglas, 11/7/96, (PB97-133557, A06, MF-A02).

NCEER-96-0004 "Proceedings of the Long-Span Bridge Seismic Research Workshop," edited by I.G. Buckle and I.M. Friedland, not available.

NCEER-96-0005 "Establish Representative Pier Types for Comprehensive Study: Eastern United States," by J. Kulicki and Z. Prucz, 5/28/96, (PB98-119217, A07, MF-A02).

NCEER-96-0006 "Establish Representative Pier Types for Comprehensive Study: Western United States," by R. Imbsen, R.A. Schamber and T.A. Osterkamp, 5/28/96, (PB98-118607, A07, MF-A02).

NCEER-96-0007 "Nonlinear Control Techniques for Dynamical Systems with Uncertain Parameters," by R.G. Ghanem and M.I. Bujakov, 5/27/96, (PB97-100259, A17, MF-A03).

NCEER-96-0008 "Seismic Evaluation of a 30-Year Old Non-Ductile Highway Bridge Pier and Its Retrofit," by J.B. Mander, B. Mahmoodzadegan, S. Bhadra and S.S. Chen, 5/31/96, (PB97-110902, MF-A03, A10).

NCEER-96-0009 "Seismic Performance of a Model Reinforced Concrete Bridge Pier Before and After Retrofit," by J.B. Mander, J.H. Kim and C.A. Ligozio, 5/31/96, (PB97-110910, MF-A02, A10).

NCEER-96-0010 "IDARC2D Version 4.0: A Computer Program for the Inelastic Damage Analysis of Buildings," by R.E. Valles, A.M. Reinhorn, S.K. Kunnath, C. Li and A. Madan, 6/3/96, (PB97-100234, A17, MF-A03).

NCEER-96-0011 "Estimation of the Economic Impact of Multiple Lifeline Disruption: Memphis Light, Gas and Water Division Case Study," by S.E. Chang, H.A. Seligson and R.T. Eguchi, 8/16/96, (PB97-133490, A11, MF-A03).

NCEER-96-0012 "Proceedings from the Sixth Japan-U.S. Workshop on Earthquake Resistant Design of Lifeline Facilities and Countermeasures Against Soil Liquefaction, Edited by M. Hamada and T. O'Rourke, 9/11/96, (PB97-133581, A99, MF-A06).

NCEER-96-0013 "Chemical Hazards, Mitigation and Preparedness in Areas of High Seismic Risk: A Methodology for Estimating the Risk of Post-Earthquake Hazardous Materials Release," by H.A. Seligson, R.T. Eguchi, K.J. Tierney and K. Richmond, 11/7/96, (PB97-133565, MF-A02, A08).

NCEER-96-0014 "Response of Steel Bridge Bearings to Reversed Cyclic Loading," by J.B. Mander, D-K. Kim, S.S. Chen and G.J. Premus, 11/13/96, (PB97-140735, A12, MF-A03).

NCEER-96-0015 "Highway Culvert Performance During Past Earthquakes," by T.L. Youd and C.J. Beckman, 11/25/96, (PB97-133532, A06, MF-A01).

NCEER-97-0001 "Evaluation, Prevention and Mitigation of Pounding Effects in Building Structures," by R.E. Valles and A.M. Reinhorn, 2/20/97, (PB97-159552, A14, MF-A03).

NCEER-97-0002 "Seismic Design Criteria for Bridges and Other Highway Structures," by C. Rojahn, R. Mayes, D.G. Anderson, J. Clark, J.H. Hom, R.V. Nutt and M.J. O'Rourke, 4/30/97, (PB97-194658, A06, MF-A03).

NCEER-97-0003 “Proceedings of the U.S.-Italian Workshop on Seismic Evaluation and Retrofit,” Edited by D.P. Abrams and G.M. Calvi, 3/19/97, (PB97-194666, A13, MF-A03).

NCEER-97-0004 "Investigation of Seismic Response of Buildings with Linear and Nonlinear Fluid Viscous Dampers," by A.A. Seleemah and M.C. Constantinou, 5/21/97, (PB98-109002, A15, MF-A03).

NCEER-97-0005 "Proceedings of the Workshop on Earthquake Engineering Frontiers in Transportation Facilities," edited by G.C. Lee and I.M. Friedland, 8/29/97, (PB98-128911, A25, MR-A04).

NCEER-97-0006 "Cumulative Seismic Damage of Reinforced Concrete Bridge Piers," by S.K. Kunnath, A. El-Bahy, A. Taylor and W. Stone, 9/2/97, (PB98-108814, A11, MF-A03).

NCEER-97-0007 "Structural Details to Accommodate Seismic Movements of Highway Bridges and Retaining Walls," by R.A. Imbsen, R.A. Schamber, E. Thorkildsen, A. Kartoum, B.T. Martin, T.N. Rosser and J.M. Kulicki, 9/3/97, (PB98-108996, A09, MF-A02).

NCEER-97-0008 "A Method for Earthquake Motion-Damage Relationships with Application to Reinforced Concrete Frames," by A. Singhal and A.S. Kiremidjian, 9/10/97, (PB98-108988, A13, MF-A03).

NCEER-97-0009 "Seismic Analysis and Design of Bridge Abutments Considering Sliding and Rotation," by K. Fishman and R. Richards, Jr., 9/15/97, (PB98-108897, A06, MF-A02).

NCEER-97-0010 "Proceedings of the FHWA/NCEER Workshop on the National Representation of Seismic Ground Motion for New and Existing Highway Facilities," edited by I.M. Friedland, M.S. Power and R.L. Mayes, 9/22/97, (PB98-128903, A21, MF-A04).

NCEER-97-0011 "Seismic Analysis for Design or Retrofit of Gravity Bridge Abutments," by K.L. Fishman, R. Richards, Jr. and R.C. Divito, 10/2/97, (PB98-128937, A08, MF-A02).

NCEER-97-0012 "Evaluation of Simplified Methods of Analysis for Yielding Structures," by P. Tsopelas, M.C. Constantinou, C.A. Kircher and A.S. Whittaker, 10/31/97, (PB98-128929, A10, MF-A03).

NCEER-97-0013 "Seismic Design of Bridge Columns Based on Control and Repairability of Damage," by C-T. Cheng and J.B. Mander, 12/8/97, (PB98-144249, A11, MF-A03).

NCEER-97-0014 "Seismic Resistance of Bridge Piers Based on Damage Avoidance Design," by J.B. Mander and C-T. Cheng, 12/10/97, (PB98-144223, A09, MF-A02).

NCEER-97-0015 “Seismic Response of Nominally Symmetric Systems with Strength Uncertainty,” by S. Balopoulou and M. Grigoriu, 12/23/97, (PB98-153422, A11, MF-A03).

NCEER-97-0016 “Evaluation of Seismic Retrofit Methods for Reinforced Concrete Bridge Columns,” by T.J. Wipf, F.W. Klaiber and F.M. Russo, 12/28/97, (PB98-144215, A12, MF-A03).

NCEER-97-0017 “Seismic Fragility of Existing Conventional Reinforced Concrete Highway Bridges,” by C.L. Mullen and A.S. Cakmak, 12/30/97, (PB98-153406, A08, MF-A02).

NCEER-97-0018 “Loss Asssessment of Memphis Buildings,” edited by D.P. Abrams and M. Shinozuka, 12/31/97, (PB98-144231, A13, MF-A03).

NCEER-97-0019 “Seismic Evaluation of Frames with Infill Walls Using Quasi-static Experiments,” by K.M. Mosalam, R.N. White and P. Gergely, 12/31/97, (PB98-153455, A07, MF-A02).

NCEER-97-0020 “Seismic Evaluation of Frames with Infill Walls Using Pseudo-dynamic Experiments,” by K.M. Mosalam, R.N. White and P. Gergely, 12/31/97, (PB98-153430, A07, MF-A02).

NCEER-97-0021 “Computational Strategies for Frames with Infill Walls: Discrete and Smeared Crack Analyses and Seismic Fragility,” by K.M. Mosalam, R.N. White and P. Gergely, 12/31/97, (PB98-153414, A10, MF-A02).

NCEER-97-0022 "Proceedings of the NCEER Workshop on Evaluation of Liquefaction Resistance of Soils," edited by T.L. Youd and I.M. Idriss, 12/31/97, (PB98-155617, A15, MF-A03).

MCEER-98-0001 "Extraction of Nonlinear Hysteretic Properties of Seismically Isolated Bridges from Quick-Release Field Tests," by Q. Chen, B.M. Douglas, E.M. Maragakis and I.G. Buckle, 5/26/98, (PB99-118838, A06, MF-A01).

MCEER-98-0002 "Methodologies for Evaluating the Importance of Highway Bridges," by A. Thomas, S. Eshenaur and J. Kulicki, 5/29/98, (PB99-118846, A10, MF-A02).

MCEER-98-0003 "Capacity Design of Bridge Piers and the Analysis of Overstrength," by J.B. Mander, A. Dutta and P. Goel, 6/1/98, (PB99-118853, A09, MF-A02).

MCEER-98-0004 "Evaluation of Bridge Damage Data from the Loma Prieta and Northridge, California Earthquakes," by N. Basoz and A. Kiremidjian, 6/2/98, (PB99-118861, A15, MF-A03).

MCEER-98-0005 "Screening Guide for Rapid Assessment of Liquefaction Hazard at Highway Bridge Sites," by T. L. Youd, 6/16/98, (PB99-118879, A06, not available on microfiche).

MCEER-98-0006 "Structural Steel and Steel/Concrete Interface Details for Bridges," by P. Ritchie, N. Kauhl and J. Kulicki, 7/13/98, (PB99-118945, A06, MF-A01).

MCEER-98-0007 "Capacity Design and Fatigue Analysis of Confined Concrete Columns," by A. Dutta and J.B. Mander, 7/14/98, (PB99-118960, A14, MF-A03).

MCEER-98-0008 "Proceedings of the Workshop on Performance Criteria for Telecommunication Services Under Earthquake Conditions," edited by A.J. Schiff, 7/15/98, (PB99-118952, A08, MF-A02).

MCEER-98-0009 "Fatigue Analysis of Unconfined Concrete Columns," by J.B. Mander, A. Dutta and J.H. Kim, 9/12/98, (PB99-123655, A10, MF-A02).

MCEER-98-0010 "Centrifuge Modeling of Cyclic Lateral Response of Pile-Cap Systems and Seat-Type Abutments in Dry Sands," by A.D. Gadre and R. Dobry, 10/2/98, (PB99-123606, A13, MF-A03).

MCEER-98-0011 "IDARC-BRIDGE: A Computational Platform for Seismic Damage Assessment of Bridge Structures," by A.M. Reinhorn, V. Simeonov, G. Mylonakis and Y. Reichman, 10/2/98, (PB99-162919, A15, MF-A03).

MCEER-98-0012 "Experimental Investigation of the Dynamic Response of Two Bridges Before and After Retrofitting with Elastomeric Bearings," by D.A. Wendichansky, S.S. Chen and J.B. Mander, 10/2/98, (PB99-162927, A15, MF-A03).

MCEER-98-0013 "Design Procedures for Hinge Restrainers and Hinge Sear Width for Multiple-Frame Bridges," by R. Des Roches and G.L. Fenves, 11/3/98, (PB99-140477, A13, MF-A03).

MCEER-98-0014 "Response Modification Factors for Seismically Isolated Bridges," by M.C. Constantinou and J.K. Quarshie, 11/3/98, (PB99-140485, A14, MF-A03).

MCEER-98-0015 "Proceedings of the U.S.-Italy Workshop on Seismic Protective Systems for Bridges," edited by I.M. Friedland and M.C. Constantinou, 11/3/98, (PB2000-101711, A22, MF-A04).

MCEER-98-0016 "Appropriate Seismic Reliability for Critical Equipment Systems: Recommendations Based on Regional Analysis of Financial and Life Loss," by K. Porter, C. Scawthorn, C. Taylor and N. Blais, 11/10/98, (PB99-157265, A08, MF-A02).

MCEER-98-0017 "Proceedings of the U.S. Japan Joint Seminar on Civil Infrastructure Systems Research," edited by M. Shinozuka and A. Rose, 11/12/98, (PB99-156713, A16, MF-A03).

MCEER-98-0018 "Modeling of Pile Footings and Drilled Shafts for Seismic Design," by I. PoLam, M. Kapuskar and D. Chaudhuri, 12/21/98, (PB99-157257, A09, MF-A02).

MCEER-99-0001 "Seismic Evaluation of a Masonry Infilled Reinforced Concrete Frame by Pseudodynamic Testing," by S.G. Buonopane and R.N. White, 2/16/99, (PB99-162851, A09, MF-A02).

MCEER-99-0002 "Response History Analysis of Structures with Seismic Isolation and Energy Dissipation Systems: Verification Examples for Program SAP2000," by J. Scheller and M.C. Constantinou, 2/22/99, (PB99-162869, A08, MF-A02).

MCEER-99-0003 "Experimental Study on the Seismic Design and Retrofit of Bridge Columns Including Axial Load Effects," by A. Dutta, T. Kokorina and J.B. Mander, 2/22/99, (PB99-162877, A09, MF-A02).

MCEER-99-0004 "Experimental Study of Bridge Elastomeric and Other Isolation and Energy Dissipation Systems with Emphasis on Uplift Prevention and High Velocity Near-source Seismic Excitation," by A. Kasalanati and M. C. Constantinou, 2/26/99, (PB99-162885, A12, MF-A03).

MCEER-99-0005 "Truss Modeling of Reinforced Concrete Shear-flexure Behavior," by J.H. Kim and J.B. Mander, 3/8/99, (PB99-163693, A12, MF-A03).

MCEER-99-0006 "Experimental Investigation and Computational Modeling of Seismic Response of a 1:4 Scale Model Steel Structure with a Load Balancing Supplemental Damping System," by G. Pekcan, J.B. Mander and S.S. Chen, 4/2/99, (PB99-162893, A11, MF-A03).

MCEER-99-0007 "Effect of Vertical Ground Motions on the Structural Response of Highway Bridges," by M.R. Button, C.J. Cronin and R.L. Mayes, 4/10/99, (PB2000-101411, A10, MF-A03).

MCEER-99-0008 "Seismic Reliability Assessment of Critical Facilities: A Handbook, Supporting Documentation, and Model Code Provisions," by G.S. Johnson, R.E. Sheppard, M.D. Quilici, S.J. Eder and C.R. Scawthorn, 4/12/99, (PB2000-101701, A18, MF-A04).

MCEER-99-0009 "Impact Assessment of Selected MCEER Highway Project Research on the Seismic Design of Highway Structures," by C. Rojahn, R. Mayes, D.G. Anderson, J.H. Clark, D'Appolonia Engineering, S. Gloyd and R.V. Nutt, 4/14/99, (PB99-162901, A10, MF-A02).

MCEER-99-0010 "Site Factors and Site Categories in Seismic Codes," by R. Dobry, R. Ramos and M.S. Power, 7/19/99, (PB2000-101705, A08, MF-A02).

MCEER-99-0011 "Restrainer Design Procedures for Multi-Span Simply-Supported Bridges," by M.J. Randall, M. Saiidi, E. Maragakis and T. Isakovic, 7/20/99, (PB2000-101702, A10, MF-A02).

MCEER-99-0012 "Property Modification Factors for Seismic Isolation Bearings," by M.C. Constantinou, P. Tsopelas, A. Kasalanati and E. Wolff, 7/20/99, (PB2000-103387, A11, MF-A03).

MCEER-99-0013 "Critical Seismic Issues for Existing Steel Bridges," by P. Ritchie, N. Kauhl and J. Kulicki, 7/20/99, (PB2000-101697, A09, MF-A02).

MCEER-99-0014 "Nonstructural Damage Database," by A. Kao, T.T. Soong and A. Vender, 7/24/99, (PB2000-101407, A06, MF-A01).

MCEER-99-0015 "Guide to Remedial Measures for Liquefaction Mitigation at Existing Highway Bridge Sites," by H.G. Cooke and J. K. Mitchell, 7/26/99, (PB2000-101703, A11, MF-A03).

MCEER-99-0016 "Proceedings of the MCEER Workshop on Ground Motion Methodologies for the Eastern United States," edited by N. Abrahamson and A. Becker, 8/11/99, (PB2000-103385, A07, MF-A02).

MCEER-99-0017 "Quindío, Colombia Earthquake of January 25, 1999: Reconnaissance Report," by A.P. Asfura and P.J. Flores, 10/4/99, (PB2000-106893, A06, MF-A01).

MCEER-99-0018 "Hysteretic Models for Cyclic Behavior of Deteriorating Inelastic Structures," by M.V. Sivaselvan and A.M. Reinhorn, 11/5/99, (PB2000-103386, A08, MF-A02).

MCEER-99-0019 "Proceedings of the 7th U.S.- Japan Workshop on Earthquake Resistant Design of Lifeline Facilities and Countermeasures Against Soil Liquefaction," edited by T.D. O'Rourke, J.P. Bardet and M. Hamada, 11/19/99, (PB2000-103354, A99, MF-A06).

MCEER-99-0020 "Development of Measurement Capability for Micro-Vibration Evaluations with Application to Chip Fabrication Facilities," by G.C. Lee, Z. Liang, J.W. Song, J.D. Shen and W.C. Liu, 12/1/99, (PB2000-105993, A08, MF-A02).

MCEER-99-0021 "Design and Retrofit Methodology for Building Structures with Supplemental Energy Dissipating Systems," by G. Pekcan, J.B. Mander and S.S. Chen, 12/31/99, (PB2000-105994, A11, MF-A03).

MCEER-00-0001 "The Marmara, Turkey Earthquake of August 17, 1999: Reconnaissance Report," edited by C. Scawthorn; with major contributions by M. Bruneau, R. Eguchi, T. Holzer, G. Johnson, J. Mander, J. Mitchell, W. Mitchell, A. Papageorgiou, C. Scaethorn, and G. Webb, 3/23/00, (PB2000-106200, A11, MF-A03).

MCEER-00-0002 "Proceedings of the MCEER Workshop for Seismic Hazard Mitigation of Health Care Facilities," edited by G.C. Lee, M. Ettouney, M. Grigoriu, J. Hauer and J. Nigg, 3/29/00, (PB2000-106892, A08, MF-A02).

MCEER-00-0003 "The Chi-Chi, Taiwan Earthquake of September 21, 1999: Reconnaissance Report," edited by G.C. Lee and C.H. Loh, with major contributions by G.C. Lee, M. Bruneau, I.G. Buckle, S.E. Chang, P.J. Flores, T.D. O'Rourke, M. Shinozuka, T.T. Soong, C-H. Loh, K-C. Chang, Z-J. Chen, J-S. Hwang, M-L. Lin, G-Y. Liu, K-C. Tsai, G.C. Yao and C-L. Yen, 4/30/00, (PB2001-100980, A10, MF-A02).

MCEER-00-0004 "Seismic Retrofit of End-Sway Frames of Steel Deck-Truss Bridges with a Supplemental Tendon System: Experimental and Analytical Investigation," by G. Pekcan, J.B. Mander and S.S. Chen, 7/1/00, (PB2001-100982, A10, MF-A02).

MCEER-00-0005 "Sliding Fragility of Unrestrained Equipment in Critical Facilities," by W.H. Chong and T.T. Soong, 7/5/00, (PB2001-100983, A08, MF-A02).

MCEER-00-0006 "Seismic Response of Reinforced Concrete Bridge Pier Walls in the Weak Direction," by N. Abo-Shadi, M. Saiidi and D. Sanders, 7/17/00, (PB2001-100981, A17, MF-A03).

MCEER-00-0007 "Low-Cycle Fatigue Behavior of Longitudinal Reinforcement in Reinforced Concrete Bridge Columns," by J. Brown and S.K. Kunnath, 7/23/00, (PB2001-104392, A08, MF-A02).

MCEER-00-0008 "Soil Structure Interaction of Bridges for Seismic Analysis," I. PoLam and H. Law, 9/25/00, (PB2001-105397, A08, MF-A02).

MCEER-00-0009 "Proceedings of the First MCEER Workshop on Mitigation of Earthquake Disaster by Advanced Technologies (MEDAT-1), edited by M. Shinozuka, D.J. Inman and T.D. O'Rourke, 11/10/00, (PB2001-105399, A14, MF-A03).

MCEER-00-0010 "Development and Evaluation of Simplified Procedures for Analysis and Design of Buildings with Passive Energy Dissipation Systems, Revision 01," by O.M. Ramirez, M.C. Constantinou, C.A. Kircher, A.S. Whittaker, M.W. Johnson, J.D. Gomez and C. Chrysostomou, 11/16/01, (PB2001-105523, A23, MF-A04).

MCEER-00-0011 "Dynamic Soil-Foundation-Structure Interaction Analyses of Large Caissons," by C-Y. Chang, C-M. Mok, Z-L. Wang, R. Settgast, F. Waggoner, M.A. Ketchum, H.M. Gonnermann and C-C. Chin, 12/30/00, (PB2001-104373, A07, MF-A02).

MCEER-00-0012 "Experimental Evaluation of Seismic Performance of Bridge Restrainers," by A.G. Vlassis, E.M. Maragakis and M. Saiid Saiidi, 12/30/00, (PB2001-104354, A09, MF-A02).

MCEER-00-0013 "Effect of Spatial Variation of Ground Motion on Highway Structures," by M. Shinozuka, V. Saxena and G. Deodatis, 12/31/00, (PB2001-108755, A13, MF-A03).

MCEER-00-0014 "A Risk-Based Methodology for Assessing the Seismic Performance of Highway Systems," by S.D. Werner, C.E. Taylor, J.E. Moore, II, J.S. Walton and S. Cho, 12/31/00, (PB2001-108756, A14, MF-A03).

MCEER-01-0001 "Experimental Investigation of P-Delta Effects to Collapse During Earthquakes," by D. Vian and M. Bruneau, 6/25/01, (PB2002-100534, A17, MF-A03).

MCEER-01-0002 "Proceedings of the Second MCEER Workshop on Mitigation of Earthquake Disaster by Advanced Technologies (MEDAT-2)," edited by M. Bruneau and D.J. Inman, 7/23/01, (PB2002-100434, A16, MF-A03).

MCEER-01-0003 "Sensitivity Analysis of Dynamic Systems Subjected to Seismic Loads," by C. Roth and M. Grigoriu, 9/18/01, (PB2003-100884, A12, MF-A03).

MCEER-01-0004 "Overcoming Obstacles to Implementing Earthquake Hazard Mitigation Policies: Stage 1 Report," by D.J. Alesch and W.J. Petak, 12/17/01, (PB2002-107949, A07, MF-A02).

MCEER-01-0005 "Updating Real-Time Earthquake Loss Estimates: Methods, Problems and Insights," by C.E. Taylor, S.E. Chang and R.T. Eguchi, 12/17/01, (PB2002-107948, A05, MF-A01).

MCEER-01-0006 "Experimental Investigation and Retrofit of Steel Pile Foundations and Pile Bents Under Cyclic Lateral Loadings," by A. Shama, J. Mander, B. Blabac and S. Chen, 12/31/01, (PB2002-107950, A13, MF-A03).

MCEER-02-0001 "Assessment of Performance of Bolu Viaduct in the 1999 Duzce Earthquake in Turkey" by P.C. Roussis, M.C. Constantinou, M. Erdik, E. Durukal and M. Dicleli, 5/8/02, (PB2003-100883, A08, MF-A02).

MCEER-02-0002 "Seismic Behavior of Rail Counterweight Systems of Elevators in Buildings," by M.P. Singh, Rildova and L.E. Suarez, 5/27/02. (PB2003-100882, A11, MF-A03).

MCEER-02-0003 "Development of Analysis and Design Procedures for Spread Footings," by G. Mylonakis, G. Gazetas, S. Nikolaou and A. Chauncey, 10/02/02, (PB2004-101636, A13, MF-A03, CD-A13).

MCEER-02-0004 "Bare-Earth Algorithms for Use with SAR and LIDAR Digital Elevation Models," by C.K. Huyck, R.T. Eguchi and B. Houshmand, 10/16/02, (PB2004-101637, A07, CD-A07).

MCEER-02-0005 "Review of Energy Dissipation of Compression Members in Concentrically Braced Frames," by K.Lee and M. Bruneau, 10/18/02, (PB2004-101638, A10, CD-A10).

MCEER-03-0001 "Experimental Investigation of Light-Gauge Steel Plate Shear Walls for the Seismic Retrofit of Buildings" by J. Berman and M. Bruneau, 5/2/03, (PB2004-101622, A10, MF-A03, CD-A10).

MCEER-03-0002 "Statistical Analysis of Fragility Curves," by M. Shinozuka, M.Q. Feng, H. Kim, T. Uzawa and T. Ueda, 6/16/03, (PB2004-101849, A09, CD-A09).

MCEER-03-0003 "Proceedings of the Eighth U.S.-Japan Workshop on Earthquake Resistant Design f Lifeline Facilities and Countermeasures Against Liquefaction," edited by M. Hamada, J.P. Bardet and T.D. O'Rourke, 6/30/03, (PB2004-104386, A99, CD-A99).

MCEER-03-0004 "Proceedings of the PRC-US Workshop on Seismic Analysis and Design of Special Bridges," edited by L.C. Fan and G.C. Lee, 7/15/03, (PB2004-104387, A14, CD-A14).

MCEER-03-0005 "Urban Disaster Recovery: A Framework and Simulation Model," by S.B. Miles and S.E. Chang, 7/25/03, (PB2004-104388, A07, CD-A07).

MCEER-03-0006 "Behavior of Underground Piping Joints Due to Static and Dynamic Loading," by R.D. Meis, M. Maragakis and R. Siddharthan, 11/17/03, (PB2005-102194, A13, MF-A03, CD-A00).

MCEER-04-0001 "Experimental Study of Seismic Isolation Systems with Emphasis on Secondary System Response and Verification of Accuracy of Dynamic Response History Analysis Methods," by E. Wolff and M. Constantinou, 1/16/04 (PB2005-102195, A99, MF-E08, CD-A00).

MCEER-04-0002 "Tension, Compression and Cyclic Testing of Engineered Cementitious Composite Materials," by K. Kesner and S.L. Billington, 3/1/04, (PB2005-102196, A08, CD-A08).

MCEER-04-0003 "Cyclic Testing of Braces Laterally Restrained by Steel Studs to Enhance Performance During Earthquakes," by O.C. Celik, J.W. Berman and M. Bruneau, 3/16/04, (PB2005-102197, A13, MF-A03, CD-A00).

MCEER-04-0004 "Methodologies for Post Earthquake Building Damage Detection Using SAR and Optical Remote Sensing: Application to the August 17, 1999 Marmara, Turkey Earthquake," by C.K. Huyck, B.J. Adams, S. Cho, R.T. Eguchi, B. Mansouri and B. Houshmand, 6/15/04, (PB2005-104888, A10, CD-A00).

MCEER-04-0005 "Nonlinear Structural Analysis Towards Collapse Simulation: A Dynamical Systems Approach," by M.V. Sivaselvan and A.M. Reinhorn, 6/16/04, (PB2005-104889, A11, MF-A03, CD-A00).

MCEER-04-0006 "Proceedings of the Second PRC-US Workshop on Seismic Analysis and Design of Special Bridges," edited by G.C. Lee and L.C. Fan, 6/25/04, (PB2005-104890, A16, CD-A00).

MCEER-04-0007 "Seismic Vulnerability Evaluation of Axially Loaded Steel Built-up Laced Members," by K. Lee and M. Bruneau, 6/30/04, (PB2005-104891, A16, CD-A00).

MCEER-04-0008 "Evaluation of Accuracy of Simplified Methods of Analysis and Design of Buildings with Damping Systems for Near-Fault and for Soft-Soil Seismic Motions," by E.A. Pavlou and M.C. Constantinou, 8/16/04, (PB2005-104892, A08, MF-A02, CD-A00).

MCEER-04-0009 "Assessment of Geotechnical Issues in Acute Care Facilities in California," by M. Lew, T.D. O'Rourke, R. Dobry and M. Koch, 9/15/04, (PB2005-104893, A08, CD-A00).

MCEER-04-0010 "Scissor-Jack-Damper Energy Dissipation System," by A.N. Sigaher-Boyle and M.C. Constantinou, 12/1/04 (PB2005-108221).

MCEER-04-0011 "Seismic Retrofit of Bridge Steel Truss Piers Using a Controlled Rocking Approach," by M. Pollino and M. Bruneau, 12/20/04 (PB2006-105795).

MCEER-05-0001 "Experimental and Analytical Studies of Structures Seismically Isolated with an Uplift-Restraint Isolation System," by P.C. Roussis and M.C. Constantinou, 1/10/05 (PB2005-108222).

MCEER-05-0002 "A Versatile Experimentation Model for Study of Structures Near Collapse Applied to Seismic Evaluation of Irregular Structures," by D. Kusumastuti, A.M. Reinhorn and A. Rutenberg, 3/31/05 (PB2006-101523).

MCEER-05-0003 "Proceedings of the Third PRC-US Workshop on Seismic Analysis and Design of Special Bridges," edited by L.C. Fan and G.C. Lee, 4/20/05, (PB2006-105796).

MCEER-05-0004 "Approaches for the Seismic Retrofit of Braced Steel Bridge Piers and Proof-of-Concept Testing of an Eccentrically Braced Frame with Tubular Link," by J.W. Berman and M. Bruneau, 4/21/05 (PB2006-101524).

MCEER-05-0005 "Simulation of Strong Ground Motions for Seismic Fragility Evaluation of Nonstructural Components in Hospitals," by A. Wanitkorkul and A. Filiatrault, 5/26/05 (PB2006-500027).

MCEER-05-0006 "Seismic Safety in California Hospitals: Assessing an Attempt to Accelerate the Replacement or Seismic Retrofit of Older Hospital Facilities," by D.J. Alesch, L.A. Arendt and W.J. Petak, 6/6/05 (PB2006-105794).

MCEER-05-0007 "Development of Seismic Strengthening and Retrofit Strategies for Critical Facilities Using Engineered Cementitious Composite Materials," by K. Kesner and S.L. Billington, 8/29/05 (PB2006-111701).

MCEER-05-0008 "Experimental and Analytical Studies of Base Isolation Systems for Seismic Protection of Power Transformers," by N. Murota, M.Q. Feng and G-Y. Liu, 9/30/05 (PB2006-111702).

MCEER-05-0009 "3D-BASIS-ME-MB: Computer Program for Nonlinear Dynamic Analysis of Seismically Isolated Structures," by P.C. Tsopelas, P.C. Roussis, M.C. Constantinou, R. Buchanan and A.M. Reinhorn, 10/3/05 (PB2006-111703).

MCEER-05-0010 "Steel Plate Shear Walls for Seismic Design and Retrofit of Building Structures," by D. Vian and M. Bruneau, 12/15/05 (PB2006-111704).

MCEER-05-0011 "The Performance-Based Design Paradigm," by M.J. Astrella and A. Whittaker, 12/15/05 (PB2006-111705).

MCEER-06-0001 "Seismic Fragility of Suspended Ceiling Systems," H. Badillo-Almaraz, A.S. Whittaker, A.M. Reinhorn and G.P. Cimellaro, 2/4/06 (PB2006-111706).

MCEER-06-0002 "Multi-Dimensional Fragility of Structures," by G.P. Cimellaro, A.M. Reinhorn and M. Bruneau, 3/1/06 (PB2007-106974, A09, MF-A02, CD A00).

MCEER-06-0003 "Built-Up Shear Links as Energy Dissipators for Seismic Protection of Bridges," by P. Dusicka, A.M. Itani and I.G. Buckle, 3/15/06 (PB2006-111708).

MCEER-06-0004 "Analytical Investigation of the Structural Fuse Concept," by R.E. Vargas and M. Bruneau, 3/16/06 (PB2006-111709).

MCEER-06-0005 "Experimental Investigation of the Structural Fuse Concept," by R.E. Vargas and M. Bruneau, 3/17/06 (PB2006-111710).

MCEER-06-0006 "Further Development of Tubular Eccentrically Braced Frame Links for the Seismic Retrofit of Braced Steel Truss Bridge Piers," by J.W. Berman and M. Bruneau, 3/27/06 (PB2007-105147).

MCEER-06-0007 "REDARS Validation Report," by S. Cho, C.K. Huyck, S. Ghosh and R.T. Eguchi, 8/8/06 (PB2007-106983).

MCEER-06-0008 "Review of Current NDE Technologies for Post-Earthquake Assessment of Retrofitted Bridge Columns," by J.W. Song, Z. Liang and G.C. Lee, 8/21/06 (PB2007-106984).

MCEER-06-0009 "Liquefaction Remediation in Silty Soils Using Dynamic Compaction and Stone Columns," by S. Thevanayagam, G.R. Martin, R. Nashed, T. Shenthan, T. Kanagalingam and N. Ecemis, 8/28/06 (PB2007-106985).

MCEER-06-0010 "Conceptual Design and Experimental Investigation of Polymer Matrix Composite Infill Panels for Seismic Retrofitting," by W. Jung, M. Chiewanichakorn and A.J. Aref, 9/21/06 (PB2007-106986).

MCEER-06-0011 "A Study of the Coupled Horizontal-Vertical Behavior of Elastomeric and Lead-Rubber Seismic Isolation Bearings," by G.P. Warn and A.S. Whittaker, 9/22/06 (PB2007-108679).

MCEER-06-0012 "Proceedings of the Fourth PRC-US Workshop on Seismic Analysis and Design of Special Bridges: Advancing Bridge Technologies in Research, Design, Construction and Preservation," Edited by L.C. Fan, G.C. Lee and L. Ziang, 10/12/06 (PB2007-109042).

MCEER-06-0013 "Cyclic Response and Low Cycle Fatigue Characteristics of Plate Steels," by P. Dusicka, A.M. Itani and I.G. Buckle, 11/1/06 06 (PB2007-106987).

MCEER-06-0014 "Proceedings of the Second US-Taiwan Bridge Engineering Workshop," edited by W.P. Yen, J. Shen, J-Y. Chen and M. Wang, 11/15/06 (PB2008-500041).

MCEER-06-0015 "User Manual and Technical Documentation for the REDARS^{TM} Import Wizard," by S. Cho, S. Ghosh, C.K. Huyck and S.D. Werner, 11/30/06 (PB2007-114766).

MCEER-06-0016 "Hazard Mitigation Strategy and Monitoring Technologies for Urban and Infrastructure Public Buildings: Proceedings of the China-US Workshops," edited by X.Y. Zhou, A.L. Zhang, G.C. Lee and M. Tong, 12/12/06 (PB2008-500018).

MCEER-07-0001 "Static and Kinetic Coefficients of Friction for Rigid Blocks," by C. Kafali, S. Fathali, M. Grigoriu and A.S. Whittaker, 3/20/07 (PB2007-114767).

MCEER-07-0002 "Hazard Mitigation Investment Decision Making: Organizational Response to Legislative Mandate," by L.A. Arendt, D.J. Alesch and W.J. Petak, 4/9/07 (PB2007-114768).

MCEER-07-0003 "Seismic Behavior of Bidirectional-Resistant Ductile End Diaphragms with Unbonded Braces in Straight or Skewed Steel Bridges," by O. Celik and M. Bruneau, 4/11/07 (PB2008-105141).

MCEER-07-0004 "Modeling Pile Behavior in Large Pile Groups Under Lateral Loading," by A.M. Dodds and G.R. Martin, 4/16/07(PB2008-105142).

MCEER-07-0005 "Experimental Investigation of Blast Performance of Seismically Resistant Concrete-Filled Steel Tube Bridge Piers," by S. Fujikura, M. Bruneau and D. Lopez-Garcia, 4/20/07 (PB2008-105143).

MCEER-07-0006 "Seismic Analysis of Conventional and Isolated Liquefied Natural Gas Tanks Using Mechanical Analogs," by I.P. Christovasilis and A.S. Whittaker, 5/1/07, not available.

MCEER-07-0007 "Experimental Seismic Performance Evaluation of Isolation/Restraint Systems for Mechanical Equipment – Part 1: Heavy Equipment Study," by S. Fathali and A. Filiatrault, 6/6/07 (PB2008-105144).

MCEER-07-0008 "Seismic Vulnerability of Timber Bridges and Timber Substructures," by A.A. Sharma, J.B. Mander, I.M. Friedland and D.R. Allicock, 6/7/07 (PB2008-105145).

MCEER-07-0009 "Experimental and Analytical Study of the XY-Friction Pendulum (XY-FP) Bearing for Bridge Applications," by C.C. Marin-Artieda, A.S. Whittaker and M.C. Constantinou, 6/7/07 (PB2008-105191).

MCEER-07-0010 "Proceedings of the PRC-US Earthquake Engineering Forum for Young Researchers," Edited by G.C. Lee and X.Z. Qi, 6/8/07 (PB2008-500058).

MCEER-07-0011 "Design Recommendations for Perforated Steel Plate Shear Walls," by R. Purba and M. Bruneau, 6/18/07, (PB2008-105192).

MCEER-07-0012 "Performance of Seismic Isolation Hardware Under Service and Seismic Loading," by M.C. Constantinou, A.S. Whittaker, Y. Kalpakidis, D.M. Fenz and G.P. Warn, 8/27/07, (PB2008-105193).

MCEER-07-0013 "Experimental Evaluation of the Seismic Performance of Hospital Piping Subassemblies," by E.R. Goodwin, E. Maragakis and A.M. Itani, 9/4/07, (PB2008-105194).

MCEER-07-0014 "A Simulation Model of Urban Disaster Recovery and Resilience: Implementation for the 1994 Northridge Earthquake," by S. Miles and S.E. Chang, 9/7/07, (PB2008-106426).

MCEER-07-0015 "Statistical and Mechanistic Fragility Analysis of Concrete Bridges," by M. Shinozuka, S. Banerjee and S-H. Kim, 9/10/07, (PB2008-106427).

MCEER-07-0016 "Three-Dimensional Modeling of Inelastic Buckling in Frame Structures," by M. Schachter and AM. Reinhorn, 9/13/07, (PB2008-108125).

MCEER-07-0017 "Modeling of Seismic Wave Scattering on Pile Groups and Caissons," by I. Po Lam, H. Law and C.T. Yang, 9/17/07 (PB2008-108150).

MCEER-07-0018 "Bridge Foundations: Modeling Large Pile Groups and Caissons for Seismic Design," by I. Po Lam, H. Law and G.R. Martin (Coordinating Author), 12/1/07 (PB2008-111190).

MCEER-07-0019 "Principles and Performance of Roller Seismic Isolation Bearings for Highway Bridges," by G.C. Lee, Y.C. Ou, Z. Liang, T.C. Niu and J. Song, 12/10/07 (PB2009-110466).

MCEER-07-0020 "Centrifuge Modeling of Permeability and Pinning Reinforcement Effects on Pile Response to Lateral Spreading," by L.L Gonzalez-Lagos, T. Abdoun and R. Dobry, 12/10/07 (PB2008-111191).

MCEER-07-0021 "Damage to the Highway System from the Pisco, Perú Earthquake of August 15, 2007," by J.S. O'Connor, L. Mesa and M. Nykamp, 12/10/07, (PB2008-108126).

MCEER-07-0022 "Experimental Seismic Performance Evaluation of Isolation/Restraint Systems for Mechanical Equipment – Part 2: Light Equipment Study," by S. Fathali and A. Filiatrault, 12/13/07 (PB2008-111192).

MCEER-07-0023 "Fragility Considerations in Highway Bridge Design," by M. Shinozuka, S. Banerjee and S.H. Kim, 12/14/07 (PB2008-111193).

MCEER-07-0024 "Performance Estimates for Seismically Isolated Bridges," by G.P. Warn and A.S. Whittaker, 12/30/07 (PB2008-112230).

MCEER-08-0001 "Seismic Performance of Steel Girder Bridge Superstructures with Conventional Cross Frames," by L.P. Carden, A.M. Itani and I.G. Buckle, 1/7/08, (PB2008-112231).

MCEER-08-0002 "Seismic Performance of Steel Girder Bridge Superstructures with Ductile End Cross Frames with Seismic Isolators," by L.P. Carden, A.M. Itani and I.G. Buckle, 1/7/08 (PB2008-112232).

MCEER-08-0003 "Analytical and Experimental Investigation of a Controlled Rocking Approach for Seismic Protection of Bridge Steel Truss Piers," by M. Pollino and M. Bruneau, 1/21/08 (PB2008-112233).

MCEER-08-0004 "Linking Lifeline Infrastructure Performance and Community Disaster Resilience: Models and Multi-Stakeholder Processes," by S.E. Chang, C. Pasion, K. Tatebe and R. Ahmad, 3/3/08 (PB2008-112234).

MCEER-08-0005 "Modal Analysis of Generally Damped Linear Structures Subjected to Seismic Excitations," by J. Song, Y-L. Chu, Z. Liang and G.C. Lee, 3/4/08 (PB2009-102311).

MCEER-08-0006 "System Performance Under Multi-Hazard Environments," by C. Kafali and M. Grigoriu, 3/4/08 (PB2008-112235).

MCEER-08-0007 "Mechanical Behavior of Multi-Spherical Sliding Bearings," by D.M. Fenz and M.C. Constantinou, 3/6/08 (PB2008-112236).

MCEER-08-0008 "Post-Earthquake Restoration of the Los Angeles Water Supply System," by T.H.P. Tabucchi and R.A. Davidson, 3/7/08 (PB2008-112237).

MCEER-08-0009 "Fragility Analysis of Water Supply Systems," by A. Jacobson and M. Grigoriu, 3/10/08 (PB2009-105545).

MCEER-08-0010 "Experimental Investigation of Full-Scale Two-Story Steel Plate Shear Walls with Reduced Beam Section Connections," by B. Qu, M. Bruneau, C-H. Lin and K-C. Tsai, 3/17/08 (PB2009-106368).

MCEER-08-0011 "Seismic Evaluation and Rehabilitation of Critical Components of Electrical Power Systems," S. Ersoy, B. Feizi, A. Ashrafi and M. Ala Saadeghvaziri, 3/17/08 (PB2009-105546).

MCEER-08-0012 "Seismic Behavior and Design of Boundary Frame Members of Steel Plate Shear Walls," by B. Qu and M. Bruneau, 4/26/08 . (PB2009-106744).

MCEER-08-0013 "Development and Appraisal of a Numerical Cyclic Loading Protocol for Quantifying Building System Performance," by A. Filiatrault, A. Wanitkorkul and M. Constantinou, 4/27/08 (PB2009-107906).

MCEER-08-0014 "Structural and Nonstructural Earthquake Design: The Challenge of Integrating Specialty Areas in Designing Complex, Critical Facilities," by W.J. Petak and D.J. Alesch, 4/30/08 (PB2009-107907).

MCEER-08-0015 "Seismic Performance Evaluation of Water Systems," by Y. Wang and T.D. O'Rourke, 5/5/08 (PB2009-107908).

MCEER-08-0016 "Seismic Response Modeling of Water Supply Systems," by P. Shi and T.D. O'Rourke, 5/5/08 (PB2009-107910).

MCEER-08-0017 "Numerical and Experimental Studies of Self-Centering Post-Tensioned Steel Frames," by D. Wang and A. Filiatrault, 5/12/08 (PB2009-110479).

MCEER-08-0018 "Development, Implementation and Verification of Dynamic Analysis Models for Multi-Spherical Sliding Bearings," by D.M. Fenz and M.C. Constantinou, 8/15/08 (PB2009-107911).

MCEER-08-0019 "Performance Assessment of Conventional and Base Isolated Nuclear Power Plants for Earthquake Blast Loadings," by Y.N. Huang, A.S. Whittaker and N. Luco, 10/28/08 (PB2009-107912).

MCEER-08-0020 "Remote Sensing for Resilient Multi-Hazard Disaster Response – Volume I: Introduction to Damage Assessment Methodologies," by B.J. Adams and R.T. Eguchi, 11/17/08 (PB2010-102695).

MCEER-08-0021 "Remote Sensing for Resilient Multi-Hazard Disaster Response – Volume II: Counting the Number of Collapsed Buildings Using an Object-Oriented Analysis: Case Study of the 2003 Bam Earthquake," by L. Gusella, C.K. Huyck and B.J. Adams, 11/17/08 (PB2010-100925).

MCEER-08-0022 "Remote Sensing for Resilient Multi-Hazard Disaster Response – Volume III: Multi-Sensor Image Fusion Techniques for Robust Neighborhood-Scale Urban Damage Assessment," by B.J. Adams and A. McMillan, 11/17/08 (PB2010-100926).

MCEER-08-0023 "Remote Sensing for Resilient Multi-Hazard Disaster Response – Volume IV: A Study of Multi-Temporal and Multi-Resolution SAR Imagery for Post-Katrina Flood Monitoring in New Orleans," by A. McMillan, J.G. Morley, B.J. Adams and S. Chesworth, 11/17/08 (PB2010-100927).

MCEER-08-0024 "Remote Sensing for Resilient Multi-Hazard Disaster Response – Volume V: Integration of Remote Sensing Imagery and VIEWS^{TM} Field Data for Post-Hurricane Charley Building Damage Assessment," by J.A. Womble, K. Mehta and B.J. Adams, 11/17/08 (PB2009-115532).

MCEER-08-0025 "Building Inventory Compilation for Disaster Management: Application of Remote Sensing and Statistical Modeling," by P. Sarabandi, A.S. Kiremidjian, R.T. Eguchi and B. J. Adams, 11/20/08 (PB2009-110484).

MCEER-08-0026 "New Experimental Capabilities and Loading Protocols for Seismic Qualification and Fragility Assessment of Nonstructural Systems," by R. Retamales, G. Mosqueda, A. Filiatrault and A. Reinhorn, 11/24/08 (PB2009-110485).

MCEER-08-0027 "Effects of Heating and Load History on the Behavior of Lead-Rubber Bearings," by I.V. Kalpakidis and M.C. Constantinou, 12/1/08 (PB2009-115533).

MCEER-08-0028 "Experimental and Analytical Investigation of Blast Performance of Seismically Resistant Bridge Piers," by S.Fujikura and M. Bruneau, 12/8/08 (PB2009-115534).

MCEER-08-0029 "Evolutionary Methodology for Aseismic Decision Support," by Y. Hu and G. Dargush, 12/15/08.

MCEER-08-0030 "Development of a Steel Plate Shear Wall Bridge Pier System Conceived from a Multi-Hazard Perspective," by D. Keller and M. Bruneau, 12/19/08 (PB2010-102696).

MCEER-09-0001 "Modal Analysis of Arbitrarily Damped Three-Dimensional Linear Structures Subjected to Seismic Excitations," by Y.L. Chu, J. Song and G.C. Lee, 1/31/09 (PB2010-100922).

MCEER-09-0002 "Air-Blast Effects on Structural Shapes," by G. Ballantyne, A.S. Whittaker, A.J. Aref and G.F. Dargush, 2/2/09 (PB2010-102697).

MCEER-09-0003 "Water Supply Performance During Earthquakes and Extreme Events," by A.L. Bonneau and T.D. O'Rourke, 2/16/09 (PB2010-100923).

MCEER-09-0004 "Generalized Linear (Mixed) Models of Post-Earthquake Ignitions," by R.A. Davidson, 7/20/09 (PB2010-102698).

MCEER-09-0005 "Seismic Testing of a Full-Scale Two-Story Light-Frame Wood Building: NEESWood Benchmark Test," by I.P. Christovasilis, A. Filiatrault and A. Wanitkorkul, 7/22/09 (PB2012-102401).

MCEER-09-0006 "IDARC2D Version 7.0: A Program for the Inelastic Damage Analysis of Structures," by A.M. Reinhorn, H. Roh, M. Sivaselvan, S.K. Kunnath, R.E. Valles, A. Madan, C. Li, R. Lobo and Y.J. Park, 7/28/09 (PB2010-103199).

MCEER-09-0007 "Enhancements to Hospital Resiliency: Improving Emergency Planning for and Response to Hurricanes," by D.B. Hess and L.A. Arendt, 7/30/09 (PB2010-100924).

MCEER-09-0008 “Assessment of Base-Isolated Nuclear Structures for Design and Beyond-Design Basis Earthquake Shaking,” by Y.N. Huang, A.S. Whittaker, R.P. Kennedy and R.L. Mayes, 8/20/09 (PB2010-102699).

MCEER-09-0009 “Quantification of Disaster Resilience of Health Care Facilities,” by G.P. Cimellaro, C. Fumo, A.M Reinhorn and M. Bruneau, 9/14/09 (PB2010-105384).

MCEER-09-0010 “Performance-Based Assessment and Design of Squat Reinforced Concrete Shear Walls,” by C.K. Gulec and A.S. Whittaker, 9/15/09 (PB2010-102700).

MCEER-09-0011 “Proceedings of the Fourth US-Taiwan Bridge Engineering Workshop,” edited by W.P. Yen, J.J. Shen, T.M. Lee and R.B. Zheng, 10/27/09 (PB2010-500009).

MCEER-09-0012 “Proceedings of the Special International Workshop on Seismic Connection Details for Segmental Bridge Construction,” edited by W. Phillip Yen and George C. Lee, 12/21/09 (PB2012-102402).

MCEER-10-0001 “Direct Displacement Procedure for Performance-Based Seismic Design of Multistory Woodframe Structures,” by W. Pang and D. Rosowsky, 4/26/10 (PB2012-102403).

MCEER-10-0002 “Simplified Direct Displacement Design of Six-Story NEESWood Capstone Building and Pre-Test Seismic Performance Assessment,” by W. Pang, D. Rosowsky, J. van de Lindt and S. Pei, 5/28/10 (PB2012-102404).

MCEER-10-0003 “Integration of Seismic Protection Systems in Performance-Based Seismic Design of Woodframed Structures,” by J.K. Shinde and M.D. Symans, 6/18/10 (PB2012-102405).

MCEER-10-0004 “Modeling and Seismic Evaluation of Nonstructural Components: Testing Frame for Experimental Evaluation of Suspended Ceiling Systems,” by A.M. Reinhorn, K.P. Ryu and G. Maddaloni, 6/30/10 (PB2012-102406).

MCEER-10-0005 “Analytical Development and Experimental Validation of a Structural-Fuse Bridge Pier Concept,” by S. El-Bahey and M. Bruneau, 10/1/10 (PB2012-102407).

MCEER-10-0006 “A Framework for Defining and Measuring Resilience at the Community Scale: The PEOPLES Resilience Framework,” by C.S. Renschler, A.E. Frazier, L.A. Arendt, G.P. Cimellaro, A.M. Reinhorn and M. Bruneau, 10/8/10 (PB2012-102408).

MCEER-10-0007 “Impact of Horizontal Boundary Elements Design on Seismic Behavior of Steel Plate Shear Walls,” by R. Purba and M. Bruneau, 11/14/10 (PB2012-102409).

MCEER-10-0008 “Seismic Testing of a Full-Scale Mid-Rise Building: The NEESWood Capstone Test,” by S. Pei, J.W. van de Lindt, S.E. Pryor, H. Shimizu, H. Isoda and D.R. Rammer, 12/1/10 (PB2012-102410).

MCEER-10-0009 “Modeling the Effects of Detonations of High Explosives to Inform Blast-Resistant Design,” by P. Sherkar, A.S. Whittaker and A.J. Aref, 12/1/10 (PB2012-102411).

MCEER-10-0010 “L’Aquila Earthquake of April 6, 2009 in Italy: Rebuilding a Resilient City to Withstand Multiple Hazards,” by G.P. Cimellaro, I.P. Christovasilis, A.M. Reinhorn, A. De Stefano and T. Kirova, 12/29/10.

MCEER-11-0001 “Numerical and Experimental Investigation of the Seismic Response of Light-Frame Wood Structures,” by I.P. Christovasilis and A. Filiatrault, 8/8/11 (PB2012-102412).

MCEER-11-0002 “Seismic Design and Analysis of a Precast Segmental Concrete Bridge Model,” by M. Anagnostopoulou, A. Filiatrault and A. Aref, 9/15/11.

MCEER-11-0003 ‘Proceedings of the Workshop on Improving Earthquake Response of Substation Equipment,” Edited by A.M. Reinhorn, 9/19/11 (PB2012-102413).

MCEER-11-0004 “LRFD-Based Analysis and Design Procedures for Bridge Bearings and Seismic Isolators,” by M.C. Constantinou, I. Kalpakidis, A. Filiatrault and R.A. Ecker Lay, 9/26/11.

MCEER-11-0005 “Experimental Seismic Evaluation, Model Parameterization, and Effects of Cold-Formed Steel-Framed Gypsum Partition Walls on the Seismic Performance of an Essential Facility,” by R. Davies, R. Retamales, G. Mosqueda and A. Filiatrault, 10/12/11.

MCEER-11-0006 “Modeling and Seismic Performance Evaluation of High Voltage Transformers and Bushings,” by A.M. Reinhorn, K. Oikonomou, H. Roh, A. Schiff and L. Kempner, Jr., 10/3/11.

MCEER-11-0007 “Extreme Load Combinations: A Survey of State Bridge Engineers,” by G.C. Lee, Z. Liang, J.J. Shen and J.S. O’Connor, 10/14/11.

MCEER-12-0001 “Simplified Analysis Procedures in Support of Performance Based Seismic Design,” by Y.N. Huang and A.S. Whittaker.

MCEER-12-0002 “Seismic Protection of Electrical Transformer Bushing Systems by Stiffening Techniques,” by M. Koliou, A. Filiatrault, A.M. Reinhorn and N. Oliveto, 6/1/12.

MCEER-12-0003 “Post-Earthquake Bridge Inspection Guidelines,” by J.S. O’Connor and S. Alampalli, 6/8/12.

MCEER-12-0004 “Integrated Design Methodology for Isolated Floor Systems in Single-Degree-of-Freedom Structural Fuse Systems,” by S. Cui, M. Bruneau and M.C. Constantinou, 6/13/12.

MCEER-12-0005 “Characterizing the Rotational Components of Earthquake Ground Motion,” by D. Basu, A.S. Whittaker and M.C. Constantinou, 6/15/12.

MCEER-12-0006 “Bayesian Fragility for Nonstructural Systems,” by C.H. Lee and M.D. Grigoriu, 9/12/12.

MCEER-12-0007 “A Numerical Model for Capturing the In-Plane Seismic Response of Interior Metal Stud Partition Walls,” by R.L. Wood and T.C. Hutchinson, 9/12/12.

MCEER-12-0008 “Assessment of Floor Accelerations in Yielding Buildings,” by J.D. Wieser, G. Pekcan, A.E. Zaghi, A.M. Itani and E. Maragakis, 10/5/12.

MCEER-13-0001 “Experimental Seismic Study of Pressurized Fire Sprinkler Piping Systems,” by Y. Tian, A. Filiatrault and G. Mosqueda, 4/8/13.

MCEER-13-0002 “Enhancing Resource Coordination for Multi-Modal Evacuation Planning,” by D.B. Hess, B.W. Conley and C.M. Farrell, 2/8/13.

MCEER-13-0003 “Seismic Response of Base Isolated Buildings Considering Pounding to Moat Walls,” by A. Masroor and G. Mosqueda, 2/26/13.

MCEER-13-0004 “Seismic Response Control of Structures Using a Novel Adaptive Passive Negative Stiffness Device,” by D.T.R. Pasala, A.A. Sarlis, S. Nagarajaiah, A.M. Reinhorn, M.C. Constantinou and D.P. Taylor, 6/10/13.

MCEER-13-0005 “Negative Stiffness Device for Seismic Protection of Structures,” by A.A. Sarlis, D.T.R. Pasala, M.C. Constantinou, A.M. Reinhorn, S. Nagarajaiah and D.P. Taylor, 6/12/13.

MCEER-13-0006 “Emilia Earthquake of May 20, 2012 in Northern Italy: Rebuilding a Resilient Community to Withstand Multiple Hazards,” by G.P. Cimellaro, M. Chiriatti, A.M. Reinhorn and L. Tirca, June 30, 2013.

MCEER-13-0007 “Precast Concrete Segmental Components and Systems for Accelerated Bridge Construction in Seismic Regions,” by A.J. Aref, G.C. Lee, Y.C. Ou and P. Sideris, with contributions from K.C. Chang, S. Chen, A. Filiatrault and Y. Zhou, June 13, 2013.

MCEER-13-0008 “A Study of U.S. Bridge Failures (1980-2012),” by G.C. Lee, S.B. Mohan, C. Huang and B.N. Fard, June 15, 2013.

MCEER-13-0009 “Development of a Database Framework for Modeling Damaged Bridges,” by G.C. Lee, J.C. Qi and C. Huang, June 16, 2013.

MCEER-13-0010 "Model of Triple Friction Pendulum Bearing for General Geometric and Frictional Parameters and for Uplift Conditions," by A.A. Sarlis and M.C. Constantinou, July 1, 2013.

MCEER-13-0011 "Shake Table Testing of Triple Friction Pendulum Isolators under Extreme Conditions," by A.A. Sarlis, M.C. Constantinou and A.M. Reinhorn, July 2, 2013.

MCEER-13-0012 "Theoretical Framework for the Development of MH-LRFD," by G.C. Lee (coordinating author), H.A Capers, Jr., C. Huang, J.M. Kulicki, Z. Liang, T. Murphy, J.J.D. Shen, M. Shinozuka and P.W.H. Yen, July 31, 2013.

MCEER-13-0013 "Seismic Protection of Highway Bridges with Negative Stiffness Devices," by N.K.A. Attary, M.D. Symans, S. Nagarajaiah, A.M. Reinhorn, M.C. Constantinou, A.A. Sarlis, D.T.R. Pasala, and D.P. Taylor, September 3, 2014.

MCEER-14-0001 "Simplified Seismic Collapse Capacity-Based Evaluation and Design of Frame Buildings with and without Supplemental Damping Systems," by M. Hamidia, A. Filiatrault, and A. Aref, May 19, 2014.

MCEER-14-0002 "Comprehensive Analytical Seismic Fragility of Fire Sprinkler Piping Systems," by Siavash Soroushian, Emmanuel "Manos" Maragakis, Arash E. Zaghi, Alicia Echevarria, Yuan Tian and Andre Filiatrault, August 26, 2014.

MCEER-14-0003 "Hybrid Simulation of the Seismic Response of a Steel Moment Frame Building Structure through Collapse," by M. Del Carpio Ramos, G. Mosqueda and D.G. Lignos, October 30, 2014.

MCEER-14-0004 "Blast and Seismic Resistant Concrete-Filled Double Skin Tubes and Modified Steel Jacketed Bridge Columns," by P.P. Fouche and M. Bruneau, June 30, 2015.

MCEER-14-0005 "Seismic Performance of Steel Plate Shear Walls Considering Various Design Approaches," by R. Purba and M. Bruneau, October 31, 2014.

MCEER-14-0006 "Air-Blast Effects on Civil Structures," by Jinwon Shin, Andrew S. Whittaker, Amjad J. Aref and David Cormie, October 30, 2014.

MCEER-14-0007 "Seismic Performance Evaluation of Precast Girders with Field-Cast Ultra High Performance Concrete (UHPC) Connections," by G.C. Lee, C. Huang, J. Song, and J. S. O'Connor, July 31, 2014.

MCEER-14-0008 "Post-Earthquake Fire Resistance of Ductile Concrete-Filled Double-Skin Tube Columns," by Reza Imani, Gilberto Mosqueda and Michel Bruneau, December 1, 2014.

MCEER-14-0009 "Cyclic Inelastic Behavior of Concrete Filled Sandwich Panel Walls Subjected to In-Plane Flexure," by Y. Alzeni and M. Bruneau, December 19, 2014.

MCEER-14-0010 "Analytical and Experimental Investigation of Self-Centering Steel Plate Shear Walls," by D.M. Dowden and M. Bruneau, December 19, 2014.

MCEER-15-0001 "Seismic Analysis of Multi-story Unreinforced Masonry Buildings with Flexible Diaphragms," by J. Aleman, G. Mosqueda and A.S. Whittaker, June 12, 2015.

MCEER-15-0002 "Site Response, Soil-Structure Interaction and Structure-Soil-Structure Interaction for Performance Assessment of Buildings and Nuclear Structures," by C. Bolisetti and A.S. Whittaker, June 15, 2015.

MCEER-15-0003 "Stress Wave Attenuation in Solids for Mitigating Impulsive Loadings," by R. Rafiee-Dehkharghani, A.J. Aref and G. Dargush, August 15, 2015.

MCEER-15-0004 "Computational, Analytical, and Experimental Modeling of Masonry Structures," by K.M. Dolatshahi and A.J. Aref, November 16, 2015.

MCEER-15-0005 "Property Modification Factors for Seismic Isolators: Design Guidance for Buildings," by W.J. McVitty and M.C. Constantinou, June 30, 2015.

MCEER-15-0006 "Seismic Isolation of Nuclear Power Plants using Sliding Bearings," by Manish Kumar, Andrew S. Whittaker and Michael C. Constantinou, December 27, 2015.

MCEER-15-0007 "Quintuple Friction Pendulum Isolator Behavior, Modeling and Validation," by Donghun Lee and Michael C. Constantinou, December 28, 2015.

MCEER-15-0008 "Seismic Isolation of Nuclear Power Plants using Elastomeric Bearings," by Manish Kumar, Andrew S. Whittaker and Michael C. Constantinou, December 29, 2015.

MCEER-16-0001 "Experimental, Numerical and Analytical Studies on the Seismic Response of Steel-Plate Concrete (SC) Composite Shear Walls," by Siamak Epackachi and Andrew S. Whittaker, June 15, 2016.

MCEER-16-0002 "Seismic Demand in Columns of Steel Frames," by Lisa Shrestha and Michel Bruneau, June 17, 2016.

MCEER-16-0003 "Development and Evaluation of Procedures for Analysis and Design of Buildings with Fluidic Self-Centering Systems" by Shoma Kitayama and Michael C. Constantinou, July 21, 2016.

MCEER-16-0004 "Real Time Control of Shake Tables for Nonlinear Hysteretic Systems," by Ki Pung Ryu and Andrei M. Reinhorn, October 22, 2016.

MCEER-16-0006 "Seismic Isolation of High Voltage Electrical Power Transformers," by Kostis Oikonomou, Michael C. Constantinou, Andrei M. Reinhorn and Leon Kemper, Jr., November 2, 2016.

MCEER-16-0007 "Open Space Damping System Theory and Experimental Validation," by Erkan Polat and Michael C. Constantinou, December 13, 2016.

MCEER-16-0008 "Seismic Response of Low Aspect Ratio Reinforced Concrete Walls for Buildings and Safety-Related Nuclear Applications," by Bismarck N. Luna and Andrew S. Whittaker.

MCEER-16-0009 "Buckling Restrained Braces Applications for Superstructure and Substructure Protection in Bridges," by Xiaone Wei and Michel Bruneau, December 28, 2016.

MCEER-16-0010 "Procedures and Results of Assessment of Seismic Performance of Seismically Isolated Electrical Transformers with Due Consideration for Vertical Isolation and Vertical Ground Motion Effects," by Shoma Kitayama, Michael C. Constantinou and Donghun Lee, December 31, 2016.

MCEER-17-0001 "Diagonal Tension Field Inclination Angle in Steel Plate Shear Walls," by Yushan Fu, Fangbo Wang and Michel Bruneau, February 10, 2017.

MCEER-17-0002 "Behavior of Steel Plate Shear Walls Subjected to Long Duration Earthquakes," by Ramla Qureshi and Michel Bruneau, September 1, 2017.

MCEER-17-0003 "Response of Steel-plate Concrete (SC) Wall Piers to Combined In-plane and Out-of-plane Seismic Loadings," by Brian Terranova, Andrew S. Whittaker, Siamak Epackachi and Nebojsa Orbovic, July 17, 2017.

MCEER-17-0004 "Design of Reinforced Concrete Panels for Wind-borne Missile Impact," by Brian Terranova, Andrew S. Whittaker and Len Schwer, July 18, 2017.

MCEER-17-0005 "A Simple Strategy for Dynamic Substructuring and its Application to Soil-Foundation-Structure Interaction," by Aikaterini Stefanaki and Metttupalayam V. Sivaselvan, December 15, 2017.

MCEER-17-0006 "Dynamics of Cable Structures: Modeling and Applications," by Nicholas D. Oliveto and Mettupalayam V. Sivaselvan, December 1, 2017.

MCEER-17-0007 "Development and Validation of a Combined Horizontal-Vertical Seismic Isolation System for High-Voltage-Power Transformers," by Donghun Lee and Michael C. Constantinou, November 3, 2017.

MCEER-18-0001 "Reduction of Seismic Acceleration Parameters for Temporary Bridge Design," by Conor Stucki and Michel Bruneau, March 22, 2018.

MCEER-18-0002 "Seismic Response of Low Aspect Ratio Reinforced Concrete Walls," by Bismarck N. Luna, Jonathan P. Rivera, Siamak Epackachi and Andrew S. Whittaker, April 21, 2018.

MCEER-18-0003 "Seismic Damage Assessment of Low Aspect Ratio Reinforced Concrete Shear Walls," by Jonathan P. Rivera, Bismarck N. Luna and Andrew S. Whittaker, April 16, 2018.

MCEER-18-0004 "Seismic Performance Assessment of Seismically Isolated Buildings Designed by the Procedures of ASCE/SEI 7," by Shoma Kitayama and Michael C. Constantinou, April 14, 2018.

MCEER-19-0001 MCEER-19-0001 "Development and Validation of a Seismic Isolation System for Lightweight Residential Construction," by Huseyin Cisalar and Michael C. Constantinou, March 24, 2019.

MCEER-20-0001 "A Multiscale Study of Reinforced Concrete Shear Walls Subjected to Elevated Temperatures," Alok Deshpande and Andrew S. Whittaker, June 26, 2020.

University at Buffalo
The State University of New York

MCEER: Earthquake Engineering to Extreme Events

University at Buffalo, The State University of New York
133A Ketter Hall | Buffalo, NY 14260
mceer@buffalo.edu; buffalo.edu/mceer

ISSN 1520-295X